SSC–346

FATIGUE CHARACTERIZATION OF FABRICATED SHIP DETAILS
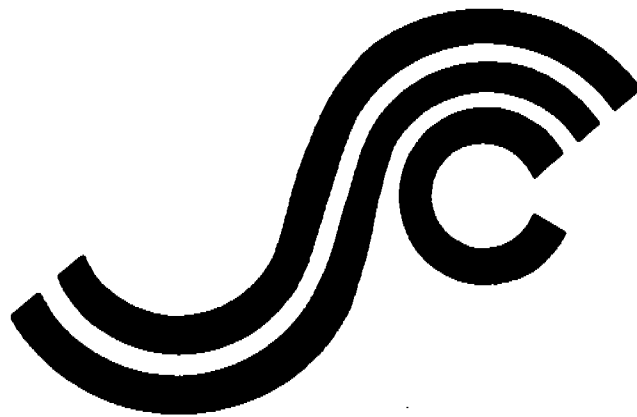
(Phase 2)

SHIP STRUCTURE COMMITTEE

1990

SHIP STRUCTURE COMMITTEE

The SHIP STRUCTURE COMMITTEE is constituted to prosecute a research program to improve the hull structures of ships and other marine structures by an extension of knowledge pertaining to design, materials, and methods of construction.

RADM J. D. Sipes, USCG, (Chairman)
Chief, Office of Marine Safety, Security
  and Environmental Protection
U. S. Coast Guard

Mr. Alexander Malakhoff
Director, Structural Integrity
  Subgroup (SEA 55Y)
Naval Sea Systems Command

Dr. Donald Liu
Senior Vice President
American Bureau of Shipping

Mr. H. T. Haller
Associate Administrator for Ship–
  building and Ship Operations
Maritime Administration

Mr. Thomas W. Allen
Engineering Officer (N7)
Military Sealift Command

CDR Michael K. Parmelee, USCG,
Secretary, Ship Structure Committee
U. S. Coast Guard

CONTRACTING OFFICER TECHNICAL REPRESENTATIVES

Mr. William J. Siekierka
SEA 55Y3
Naval Sea Systems Command

Mr. Greg D. Woods
SEA 55Y3
Naval Sea Systems Command

SHIP STRUCTURE SUBCOMMITTEE

The SHIP STRUCTURE SUBCOMMITTEE acts for the Ship Structure Committee on technical matters by providing technical coordination for determinating the goals and objectives of the program and by evaluating and interpreting the results in terms of structural design, construction, and operation.

AMERICAN BUREAU OF SHIPPING

Mr. Stephen G. Arntson (Chairman)
Mr. John F. Conlon
Mr. William Hanzalek
Mr. Philip G. Rynn

MILITARY SEALIFT COMMAND

Mr. Albert J. Attermeyer
Mr. Michael W. Touma
Mr. Jeffery E. Beach

MARITIME ADMINISTRATION

Mr. Frederick Seibold
Mr. Norman O. Hammer
Mr. Chao H. Lin
Dr. Walter M. Maclean

NAVAL SEA SYSTEMS COMMAND

Mr. Robert A. Sielski
Mr. Charles L. Null
Mr. W. Thomas Packard
Mr. Allen H. Engle

U. S. COAST GUARD

CAPT T. E. Thompson
CAPT Donald S. Jensen
CDR Mark E. Noll

SHIP STRUCTURE SUBCOMMITTEE LIAISON MEMBERS

U. S. COAST GUARD ACADEMY

LT Bruce Mustain

U. S. MERCHANT MARINE ACADEMY

Dr. C. B. Kim

U. S. NAVAL ACADEMY

Dr. Ramswar Bhattacharyya

STATE UNIVERSITY OF NEW YORK MARITIME COLLEGE

Dr. W. R. Porter

WELDING RESEARCH COUNCIL

Dr. Martin Prager

NATIONAL ACADEMY OF SCIENCES – MARINE BOARD

Mr. Alexander B. Stavovy

NATIONAL ACADEMY OF SCIENCES – COMMITTEE ON MARINE STRUCTURES

Mr. Stanley G. Stiansen

SOCIETY OF NAVAL ARCHITECTS AND MARINE ENGINEERS – HYDRODYNAMICS COMMITTEE

Dr. William Sandberg

AMERICAN IRON AND STEEL INSTITUTE

Mr. Alexander D. Wilson

Ship
Structure
Committee

An Interagency Advisory Committee
Dedicated to the Improvement of Marine Structures

SSC-346
SR-1298

December 3, 1990

FATIGUE CHARACTERIZATION OF FABRICATED
SHIP DETAILS (PHASE 2)

A basic understanding of fatigue characteristics of fabricated details is necessary to ensure the continued reliability and safety of ship structures. Phase 1 of this study (SSC-318) provided a fatigue design procedure for selecting and evaluating these details. In this second phase, an extensive series of fatigue tests were carried on structural details using variable loads to simulate a vessel's service history. This report contains the test results as well as fatigue predictions obtained from available analytical models.

J. D. SIPES
Rear Admiral, U.S. Coast Guard
Chairman, Ship Structure Committee

1. Report No.	2. Government Accession No.	3. Recipient's Catalog No.
SSC-346		

4. Title and Subtitle	5. Report Date
Fatigue Characterization of Fabricated Ship Details for Design - Phase II	May 1988
	6. Performing Organization Code
	Ship Structure Committee

7. Author's)	8. Performing Organization Report No.
S. K. Park and F. V. Lawrence	SR-1298

9. Performing Organization Name and Address	10. Work Unit No. (TRAIS)
Department of Civil Engineering University of Illinois at Urbana-Champaign 205 N. Mathews Avenue Urbana, IL 61801	
	11. Contract or Grant No.
	DTCG 23-84-C-20018
	13. Type of Report and Period Covered

12. Sponsoring Agency Name and Address	
U. S. Coast Guard 2100 2nd Street S.W. Washington, DC 20593	Final Technical Report
	14. Sponsoring Agency Code
	G-M

15. Supplementary Notes

The U.S.C.G. acts as the contracting office for the Ship Structure Committee.

16. Abstract

The available analytical models for predicting the fatigue behavior of weldments under variable amplitude load histories were compared using test results for weldments subjected to the SAE bracket and transmission variable load amplitude histories. Models based on detail S-N diagrams such as the Munse Fatigue Design Procedure (MFDP) were found to perform well except when the history had a significant average mean stress. Models based on fatigue crack propagation alone were generally conservative, while a model based upon estimates of both fatigue crack initiation and propagation (the I-P Model) performed the best.

An extensive series of fatigue tests was carried out on welded structural details commonly encountered in ship construction using a variable load history which simulated the service history of a ship. The results from this study showed that linear cumulative damage concepts predicted the test results, but the importance of small stress range events was not studied because events smaller than 68 MPa (10 ksi) stress range were deleted from the developed ship history to reduce the time required for testing. An appreciable effect of mean stress was observed, but the results did not verify the existence of a specimen-size effect.

Baseline constant-amplitude S-N diagrams were developed for five complex ship details not commonly studied in the past.

17. Key Words	18. Distribution Statement
Fatigue, Ship Structure Details, Design, Reliability, Loading History, Variable Load Histories	Document is available to the U.S. public, the National Technical Information Service, Springfield, VA 22151

19. Security Classif. (of this report)	20. Security Classif. (of this page)	21. No. of Pages	22. Price
Unclassified	Unclassified	201	

Form DOT F 1700.7 (8-72)　　　Reproduction of completed page authorized

METRIC CONVERSION FACTORS

Approximate Conversions to Metric Measures

Symbol	When You Know	Multiply by	To Find	Symbol
LENGTH				
in	inches	*2.5	centimeters	cm
ft	feet	30	centimeters	cm
yd	yards	0.9	meters	m
mi	miles	1.6	kilometers	km
AREA				
in²	square inches	6.5	square centimeters	cm²
ft²	square feet	0.09	square meters	m²
yd²	square yards	0.8	square meters	m²
mi²	square miles	2.6	square kilometers	km²
	acres	0.4	hectares	ha
MASS (weight)				
oz	ounces	28	grams	g
lb	pounds	0.45	kilograms	kg
	short tons (2000 lb)	0.9	tonnes	t
VOLUME				
tsp	teaspoons	5	milliliters	ml
Tbsp	tablespoons	15	milliliters	ml
fl oz	fluid ounces	30	milliliters	ml
c	cups	0.24	liters	l
pt	pints	0.47	liters	l
qt	quarts	0.95	liters	l
gal	gallons	3.8	liters	l
ft³	cubic feet	0.03	cubic meters	m³
yd³	cubic yards	0.76	cubic meters	m³
TEMPERATURE (exact)				
°F	Fahrenheit temperature	5/9 (after subtracting 32)	Celsius temperature	°C

*1 in = 2.54 (exactly). For other exact conversions and more detailed tables, see NBS Misc. Publ. 286, Units of Weights and Measures, Price $2.25, SD Catalog No. C13.10:286.

Approximate Conversions from Metric Measures

Symbol	When You Know	Multiply by	To Find	Symbol
LENGTH				
mm	millimeters	0.04	inches	in
cm	centimeters	0.4	inches	in
m	meters	3.3	feet	ft
m	meters	1.1	yards	yd
km	kilometers	0.6	miles	mi
AREA				
cm²	square centimeters	0.16	square inches	in²
m²	square meters	1.2	square yards	yd²
km²	square kilometers	0.4	square miles	mi²
ha	hectares (10,000 m²)	2.5	acres	
MASS (weight)				
g	grams	0.035	ounces	oz
kg	kilograms	2.2	pounds	lb
t	tonnes (1000 kg)	1.1	short tons	
VOLUME				
ml	milliliters	0.03	fluid ounces	fl oz
l	liters	2.1	pints	pt
l	liters	1.06	quarts	qt
l	liters	0.26	gallons	gal
m³	cubic meters	35	cubic feet	ft³
m³	cubic meters	1.3	cubic yards	yd³
TEMPERATURE (exact)				
°C	Celsius temperature	9/5 (then add 32)	Fahrenheit temperature	°F

```
°F   -40    0      32      98.6           212
      |  |  |  |  |  |  |  |  |  |  |  |  |  |
     -40      0      40    80   120   160  200
      |  |  |  |  |  |  |  |  |  |  |  |  |  |
°C   -40   -20     0      20    37 40   60   80   100
```

TABLE OF CONTENTS

EXECUTIVE SUMMARY

This study is a continuation of a research effort at the University of Illinois at Urbana-Champaign (UIUC) to characterize the fatigue behavior of fabricated ship details. The current study evaluated the Munse Fatigue Design Procedure and performed further tests on ship details.

The available analytical models for predicting the fatigue behavior of weldments under variable amplitude load histories were compared using test results for weldments subjected to the SAE bracket and transmission variable load amplitude histories. Models based on detail S-N diagrams such as the Munse Fatigue Design Procedure (MFDP) were found to perform well except when the history had a significant average mean stress. Models based on fatigue crack propagation alone were generally conservative, while a model based upon estimates of both fatigue crack initiation and propagation (the I-P Model) performed the best.

An extensive series of fatigue tests was carried out on welded structural details commonly encountered in ship construction using a variable load history which simulated the service history of a ship. The results from this study showed that linear cumulative damage concepts predicted the test results, but the importance of small stress range events was not studied because events smaller than 68 MPa (10 ksi) stress range were deleted from the developed ship history to reduce the time required for testing. An appreciable effect of mean stress was observed, but the results did not verify the existence of a specimen-size effect.

Both the Munse Fatigue Design Procedure (MFDP) and the I-P Model were used to predict the test results. The MFDP predicted the mean fatigue life reasonably well. Improved life predictions were obtained when the effect of mean stress was included in the MFDP. Mean stress and detail size corrections were suggested for the Munse Fatigue Design Procedure.

Generally good results were obtained using the I-P Model, but the predictions for the smallest size weldments were very unconservative. The I-P model was used to develop a stochastic model for weldment fatigue behavior based on the observed random variations in specimen geometry and induced secondary stresses resulting from distortions produced by welding. Design aids based on the I-P model are presented.

Baseline constant-amplitude S-N diagrams were developed for five complex ship details not commonly studied in the past.

LIST OF SYMBOLS

a, a_i, a_f	crack length, initial crack length, final crack length
b	fatigue strength exponent
C	fatigue crack growth coefficient; also, S-N curve coefficient
c	fatigue ductility exponent; also, original half length of incomplete joint penetration and length of major axis of elliptical crack
D_i, D_{block}	fatigue damage per cycle and per block, respectively
E	Young's Modulus
F	function of residual stress distribution
IJP	incomplete joint penetration
K'	cyclic strength coefficient
K_f, K_{fmax}	fatigue notch factor and maximum fatigue notch factor
K_t	elastic stress concentration factor
K_{max}^{rms}, K_{min}^{rms}	maximum and minimum root mean square stress intensity factor
K_r	stress intensity factor due to residual stress
ΔK	stress intensity factor range
ΔK_{rms}	root mean square stress intensity factor range
k	the Weibull scale or shape parameter
L1	leg length of weld perpendicular to the IJP
L2	S-N curve slope parallel to the IJP
M_s, M_t, M_k	magnification factor for free surface, width and stress gradient
m	reciprocal slope of the S-N diagram
N_f	cycles to failure
$2N_{fi}$	reversals to failure
N_i, N_{fi}	cycles to failure at ith amplitude
N_T, N_I, N_p	total, initiation and propagation fatigue life

n	fatigue crack growth exponent; also, thickness effect exponent
n'	cyclic strain hardening exponent
n_i	cycles at ith amplitude
R	stress ratio
R_F	reliability factor
r	notch root radius
S, S_a	remote stress range, amplitude of remote stress
S_a^A	remote axial stress amplitude
S_a^B	remote bending stress amplitude
S_{max}^{rms}, S_{min}^{rms}	stress and root mean square of maximum and minimum stress
S_a^T	total remote stress amplitude
S_m	applied average axial mean stress
S_m^B	gripping bending stress
S_u	ultimate tensile stress
t	plate thickness; also, time
w	specimen width
x	ratio of remote bending stress amplitude to total remote stress amplitude
X	ratio of K_{max}^B to K_{max}^A
Y	geometry factor on stress intensity factor
$y(t)$	stress (strain) spectral ordinate for random time load history
z	ratio of bending stress to axial stress
α, β, λ	geometry coefficients for elastic stress concentration factor
Δ_f	possible error in fatigue model
δ_f	coefficient of variation in fatigue life
ΔS_D	maximum allowable design stress range expected once during the entire life of a structure

ΔS_{Dm}	maximum allowable design stress range expected once during the entire life of a structure with allowance for baseline data and applied history mean stress
ΔS_N	average constant amplitude fatigue strength at the desired design life
$\Delta S_{N(R)}$	average constant amplitude fatigue strength at the desired design life from baseline testing conditions under stress ratio (R) = R
$\Delta S_{N(-1)}$	average constant amplitude fatigue strength at the desired design life from R = -1 baseline testing conditions
ε, $\Delta\varepsilon$	local strain and local strain range
ε'_f	fatigue ductility coefficient
ε_n	strain normal to the crack
ψ_i	spectral ordinates output from the FFT analyzer (in volts)
ϕ_i	random phase angle sampled from a uniform distribution, $0\sim 2\pi$
σ, $\Delta\sigma$, σ_a	local stress, local stress range, local stress amplitude
σ_o, σ_r	mean stress and residual stress
σ_a^P	local maximum principal stress amplitude
σ_r^E	effective residual stress amplitude
σ'_f	fatigue strength coefficient
θ	flank angle of welds
ξ	random load factor
Ω_c	uncertainty in the mean intercept of the S-N repression line
Ω_f	uncertainty in the fatigue data life
Ω_n	total uncertainty

1. INTRODUCTION AND BACKGROUND

1.1 The Fatigue Structural Weldments

Ships, like most other welded steel structures which are subjected to fluctuating loads, are prone to metallic fatigue. While fatigue can occur in any metal component, weldments are of particular concern because of their wide use, because they provide the stress concentrators and, because they are, therefore, likely sites for fatigue to occur. It is for these reasons that the fatigue of weldments has been so exhaustively studied. However, despite 100 years of research and thousands of studies of weldment fatigue, there seems to be only slow progress in putting this problem to rest. This slow progress is probably due to the following:

There is a nearly infinite variety of welded joints.

Weldments of the same joint type are usually not exactly alike.

The behavior of even simple weldments can be exceedingly complex.

The stresses in a weldment are usually imprecisely known.

The variety and complexity of the more common structural weldments are evident in Fig 1-1 which shows the structural details covered in the AISC fatigue provisions [1-1].

1.2 The Fatigue Design of Weldments

There are three main approaches to the fatigue design of weldments:

S-N diagrams: Weldments may be designed using the S-N curves for the particular detail. The behavior of weldments under constant amplitude loading has been reported in the literature for hundreds of different joint geometries. Attempts to collect the available information and develop a weldment fatigue data base have been undertaken at the University of Illinois by Munse [1-2] and by The Welding Institute [1-3]. A typical collection of weldment fatigue data from the University of Illinois Data Bank is shown in Fig. 1-2 in which it is evident that the fatigue resistance of low stress concentration fatigue-efficient weldments is less than plain plate and is characterized by a great deal of scatter. Munse [1-4] proposed a fatigue design procedure which uses the "baseline" S-N diagram information (Fig. 1-3) to establish a fatigue design stress and which takes into account

1

both the desired level of reliability and the variable nature of the applied loads (Fig. 1-4). A short description of the Munse Fatigue Design Procedure is given in Section 1-5.

Fracture Mechanics: Because fatigue is a process which begins at stress concentrations (notches), several analytical methods of weldment fatigue design have recently been developed which are based on mechanics analyses of fatigue crack initiation and fatigue crack growth at the critical locations in the structure. Such design methods or analyses involve sophisticated, complex models (see Fig. 1-4). Models based on both fatigue crack initiation and growth have been proposed by Lawrence et al. [1-5]: see Appendix A. Models based on fatigue crack growth alone have been suggested by Maddox [1-6] and Shilling, et al. [1-7].

Structural Tests: A third alternative for the fatigue design of structures is to base the design on full-scale tests or observations of service history. While such observations are closest to reality, full-scale tests are usually prohibitively expensive and time consuming. Moreover, it is sometimes difficult to apply results from one structure to another. In the case of ships, such tests may require a 20 year study.

1.3 Factors Influencing the Fatigue Life of Weldments

There are four attributes of weldments which, together with the magnitude of the fluctuating stresses applied, determine the slope and intercept of their S-N diagram: the ratio of the applied or self-induced axial and bending stresses; the severity of the discontinuity or notch which is an inherent property of the geometry of the joint; the notch-root residual stresses which result from fabrication and subsequent use of the weldment, and the mechanical properties of the material in which fatigue crack initiation and propagation take place. Of these four, the mechanical properties are probably the least influential.

In most engineering design situations involving as-welded weldments of a given material, the permissible design stresses are governed by: the joint geometry, the desired level of reliability, the variable nature of the applied load and the applied mean stress. Figure 1-5 provides a general

2

indication of the sensitivity of the fatigue design stress to these design variables. The design stress varies greatly with detail geometry, desired level of reliability and the nature of the variable load. Mean stress has only a modest influence.

1.4 Purpose of the Current Study

This report summarizes a research program sponsored by the U.S. Coast Guard at the University of Illinois at Champaign-Urbana on the "Fatigue Characterization of Fabricated Ship Details, Phase II" (contract DTCG 23-84-C-20018). This program is a continuation of one begun at the University of Illinois under the direction of Professor W. H. Munse [1-4]. The second phase had as its principal objectives:

* To evaluate the Munse Fatigue Design Procedure developed and discussed under Phase I of the project;

* To carry out laboratory fatigue tests of fabricated ship details;

* And to perform further tests on ship details.

The tasks of this study are summarized in Table 1-1.

Seven tasks were originally proposed, and they may be broken into four categories: The first category, **Task 1** was a comparison of the Munse Fatigue Design Procedure (MFDP) predictions with the predictions resulting from other methods of estimating the fatigue life of weldments and an assessment of the accuracy of the Munse Fatigue Design Procedure in general. The results of this comparison are summarized in Section 2.

In the second category, **Tasks 2-4** involved long-life testing, mean stress effects, and size effects. Each of these three tasks address a separate issue of concern affecting our ability to predict the fatigue life of weldments. For example, there is concern whether linear cumulative damage is accurate in the long-life regime. Also, mean stress effects are not generally dealt with, and there is concern that neglecting mean stress introduces a considerable inaccuracy in the fatigue life prediction methods. Lastly, one generally ignores the influence of the absolute size of weldments, and there is increasing evidence that there is an effect of size on the fatigue life of weldments. These phenomena were studied experimentally, and the results are summarized in Section 3.

3

The third category was the application of the I-P Model for total fatigue life prediction to the ship details considered in this program. The I-P model was proposed as a basis for fatigue rating of ship details, but this task (Task 5) was deleted at the outset of the program. The I-P model in its current state of development is summarized in Appendix A. Section 4 compares the predictions made using the Munse Fatigue Design Procedure and the I-P Model with the experimental test results (Task 6).

The fourth category (Task 7) was a program of fatigue testing of selected ship details for which inadequate fatigue test data currently exists. The results of constant amplitude testing of the selected ship details is summarized in Section 5.

1.5 The Munse Fatigue Design Procedure (MFDP)

The Munse Fatigue Design Procedure MFDP [1-4] is an effective method of design against structural fatigue and deals with the complex geometries, the variable load histories, and the variability in these and other factors encountered in the fatigue design of weldments.

Figure 1-2 shows the output from the University of Illinois Fatigue Data Bank for a mild steel double-V butt weld. The Munse method fits such data with the basic S-N relationship shown in Fig. 1-3. When stress histories other than constant-amplitude are used, different S-N diagrams result if the test results are plotted against the maximum stress: see Fig. 1-6. The Munse method accounts for this effect by introducing a term ξ which when multiplied by the constant amplitude fatigue strength at a given life will predict the fatigue strength for the variable load history at the same number of cycles: see Fig. 1-7.

Similarly, the natural scatter in fatigue data shown in Fig. 1-8 together with the uncertainties in fabrication and stress analysis are dealt with by the MFDP through the concept of total uncertainty.

$$\Omega_n^2 \approx \Omega_f^2 + m^2 \, \Omega_s^2 + \Omega_c^2 \qquad (1\text{-}1)$$

where, Ω_n = the _total_ uncertainty in fatigue life.

Ω_f = the uncertainty in the fatigue data life.

4

$\Omega_f = \sqrt{\sigma_f^2 + \Delta_f^2}$; in which σ_f is the coefficient of variation in the fatigue life data about the S-N regression lines; and Δ_f is the error in the fatigue model (the S-N equation, including such effects as mean stress), and the imperfections in the use of the linear damage rule (Miner) and the Weibull distribution approximations.

Ω_c = the uncertainty in the mean intercept of the S-N regression lines, and includes in particular the effects of workmanship and fabrication. A model for this uncertainty is suggested in Section 4.3.

Ω_s = measure of total uncertainty in mean stress range, including the effects of impact and error of stress analysis and stress determination.

Of the above mentioned sources of uncertainty, those which are best estimated are probably the smallest (Ω_f). Those which are the largest are probably the least easy to estimate (Ω_s). In modern fatigue analysis, it is commonly believed that the greatest uncertainty is an exact knowledge of the loads to which a structure or vehicle will be subjected in service. Often the service history bears little resemblance to that which the designer contemplates. This difficulty with application of the Munse method as with all other design methods will require extensive field observations and measurements.

Having estimated the total uncertainty in fatigue life Ω_n, the reliability factor R_f is estimated after assuming an appropriate distribution to characterize the load history and after specifying a desired level of reliability.

The MFDP estimates the maximum allowable design stress range ΔS_D from the weldment S-N diagram by determining the average fatigue strength at the desired design life ΔS_N and multiplying this value by the random load correction factor ξ and the reliability factor (R_F):

$$\Delta S_D = \Delta S_N \, (\xi) \, (R_F) \qquad\qquad (1-2)$$

5

The Munse method takes all uncertainties into account and provides a rational framework for designing structural details to a desired level of reliability: see Fig. 1-9.

1.6 References

1-1. AISC. "Specification for the Design, Fabrication and Erection of Structural Steel for Buildings," American Institute of Steel Construction, Nov. 1, 1978.

1-2. Radziminski, J.B., Srinivasan, R., Moore, D., Thrasher, C. and Munse, W.H. "Fatigue Data Bank and Data Analysis Investigation," Structural Research Series No. 405, Civil Engineering Studies, University of Illinois at Urbana-Champaign, June, 1973.

1-3. The Welding Institute, Proceedings of the Conference on Fatigue of Welded Structures," July 6-9, 1970, The Welding Institute, Cambridge, England, 1971.

1-4. Munse, W.H., Wilbur, T.W., Tellalian, M.L., Nicoll, K. and Wilson, K., "Fatigue Characterization of Fabricated Ship Details for Design," Ship Structure Committee, SSC-318, 1983.

1-5. Ho, N.-J. and Lawrence, F.V., Jr., "The Fatigue of Weldments Subjected to Complex Loadings," FCP Report No. 45, College of Engineering, University of Illinois at Urbana-Champaign, Jan. 1983.

1-6. Maddox, S.J., "A Fracture Mechanics Approach to Service Load Fatigue in Welded Structures," Welding Research International, Vol. 4, No. 2, 1974.

1-7. Schilling, C.G., Klippstein, K.H., Barsom, J.M. and Blake, G.T., "Fatigue of Welded Steel Bridge Members under Variable Amplitude Loadings," NCHRP Project Final Report 12-12, August 1975.

Table 1.1

Program Summary

Task	Description
1. Comparison of MFC Prediction	Compare prediction of Munse Criterion with other predictive methods.
2. Long Life Testing	Perform long life variable load history fatigue tests on structural details.
3. Mean Stress Effects	Check the influence of average mean stress on fatigue resistance under variable load history.
4. Size Effect	Check the influence of plate thickness and weld size on fatigue resistance.
5. Fatigue Rating	Deleted.
6. I-P Model Application	Predict long life of ship structure through I-P Model application.
7. Fatigue Testing of Ship Structural Details	Selected structural details will be fatigue tested to determine base line fatigue resistance.
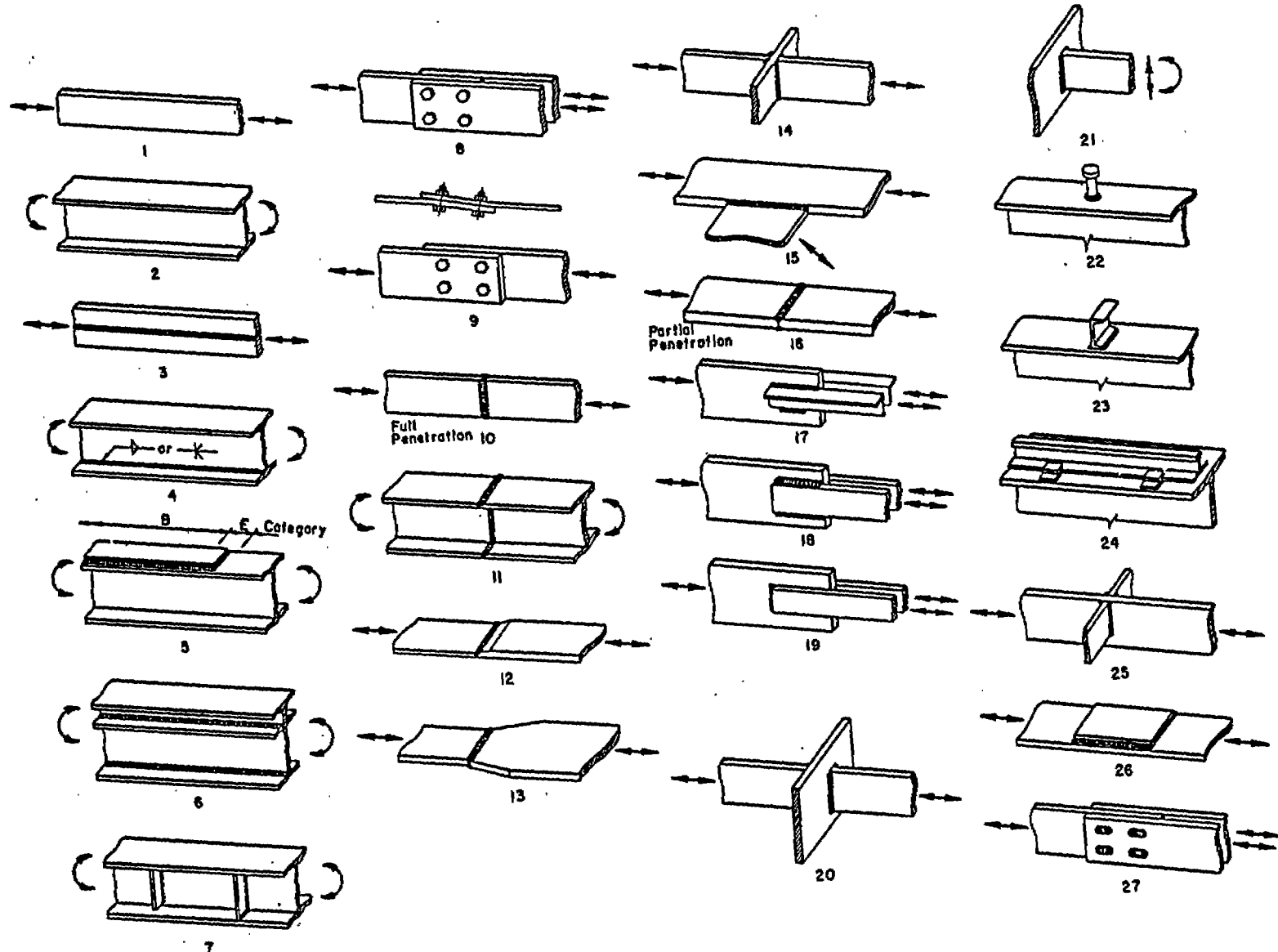
Fig. 1-1 Structural details provided in AISC fatigue provision [1-1].
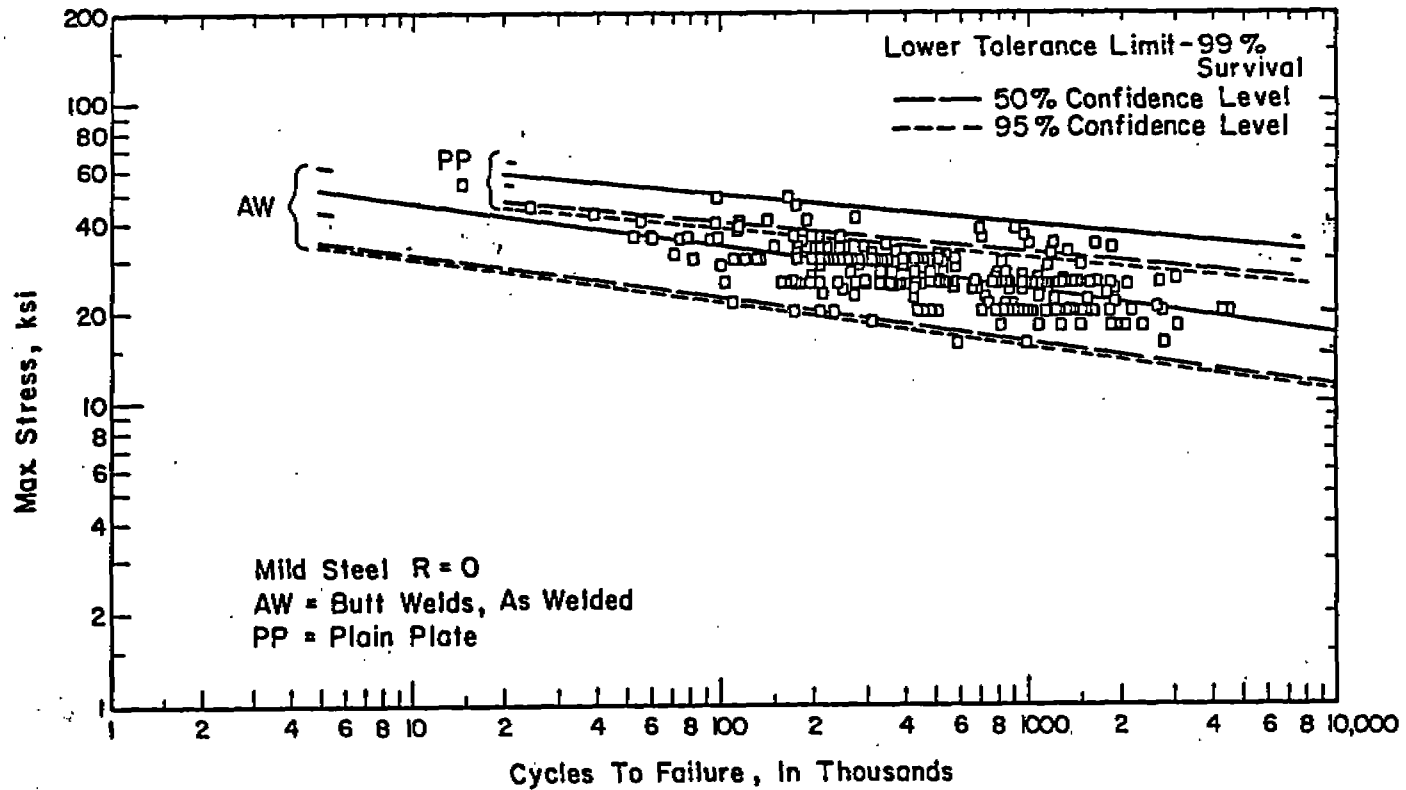
Fig. 1-2 Stress range versus cycle to failure for mild steel butt welds subjected to zero to tension loading. The fatigue resistance of as-welded butt weld is generally less than the fatigue resistance of plain plate which is also indicated in this figure [1-2].

$$\bar{n} = \frac{C}{S^m}$$

Log S

$$\text{Log } \bar{n} = \text{Log } C - m \text{ Log } S$$

Log $\bar{n}$
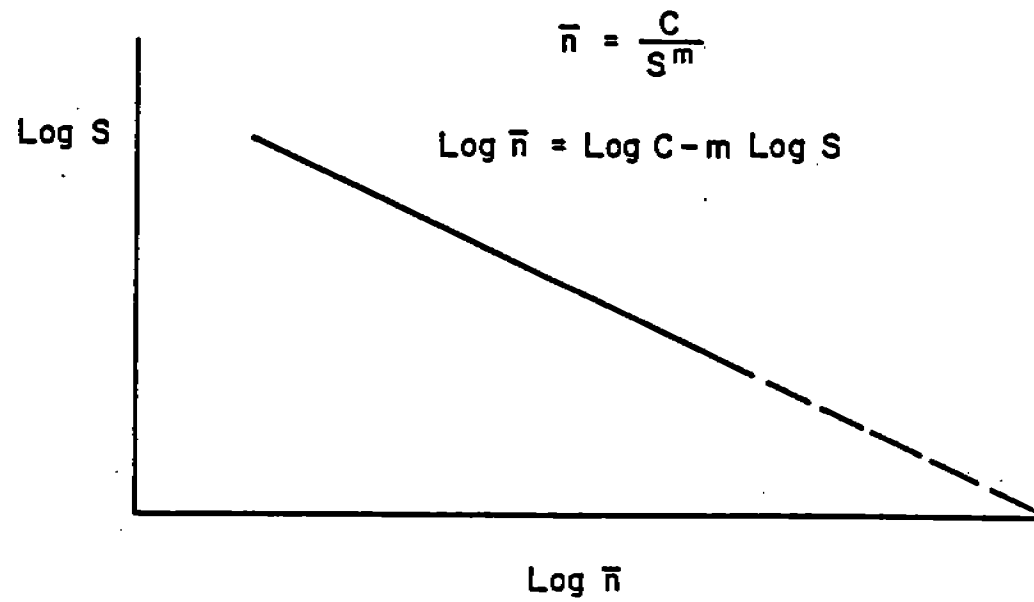
Fig. 1-3 Basic S-N relationship for fatigue [1-4].
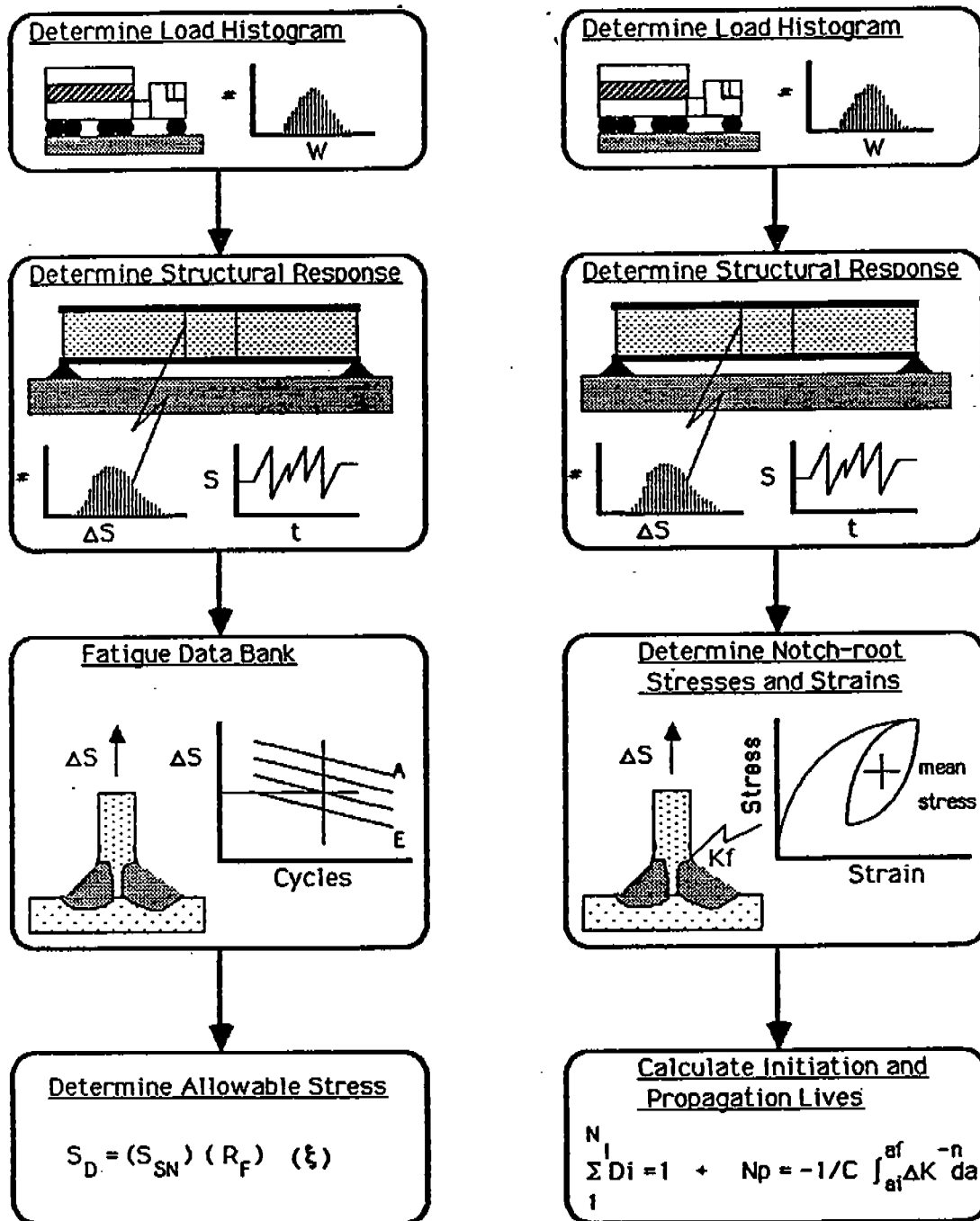
Fig. 1-4 Fatigue design method. Fatigue design method based on detail
S-N diagrams (left) such as the Munse approach compute the
design stress S_D based on corrections to constant amplitude
fatigue resistance for the effects of variable load history
( ) and the desired reliability (R_F). Fracture mechanics based
design methods (right) deal with the local strain events at
the critical locations and provide estimates of the fatigue
crack initiation life (N_I), fatigue crack propagation life (N_P)
or the total fatigue life ($N_I + N_P$).

Variation in $S_{50\%}$ due to detail geometry		$N = 10^5$	$N = 10^6$
	$S_{50\%} =$	69.4 ksi. (100%)	31.1 ksi. (100%)
	$S_{50\%} =$	20.3 ksi. (29%)	6.5 ksi. (21%)
	$S_{50\%} =$	21.5 ksi. (31%)	5.8 ksi. (19%)
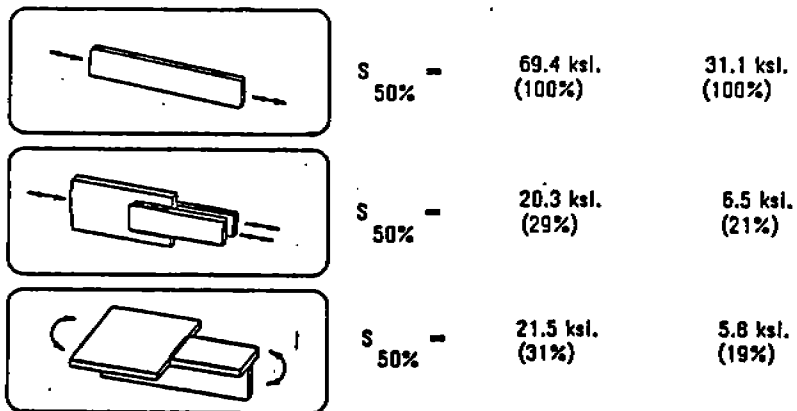
Sensitivity of S_D to variable load history factor: (VLH)

constant amplitude $S_D = 1.00 \, S_{50\%}$

Beta (q=3, p=7) $S_D = 2.83 \, S_{50\%}$

Weibull (k=1) $S_D = 9.10 \, S_{50\%}$

Beta (q=7, p=7) $S_D = 1.89 \, S_{50\%}$

Weibull (k=2) $S_D = 3.75 \, S_{50\%}$

Beta (q=7, p=3) $S_D = 1.38 \, S_{50\%}$
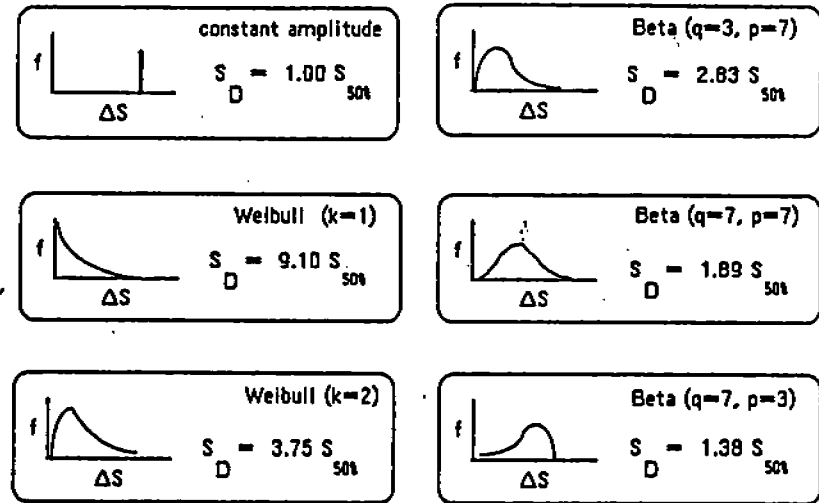
Sensitivity of S_D to level of reliability (Rel)

log stress range (ΔS) vs log cycles (N)

50% reliability = $1.00 \, S_{50\%}$

90% reliability = $0.70 \, S_{50\%}$

95% reliability = $0.60 \, S_{50\%}$

99% reliability = $0.45 \, S_{50\%}$
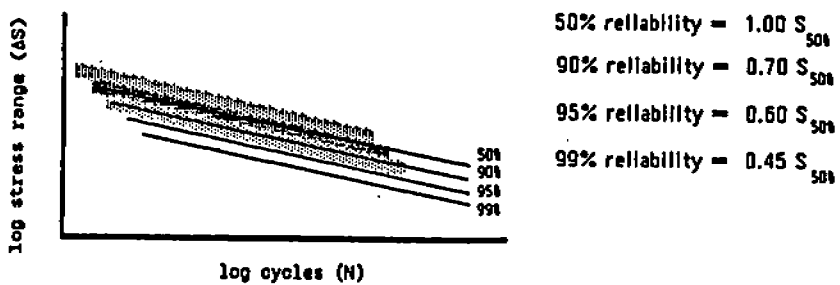
Variation in $S_{50\%}$ due to mean stress

$$S_{50\%}_{R=R} = (1 - 0.25\,R)\, S_{50\%}_{R=0}$$
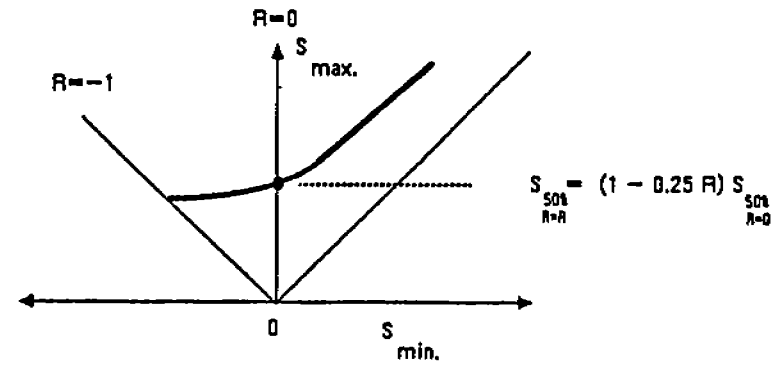
Fig. 1-5 A general indication of the sensitivity of the fatigue design stress to the design variables of the joint geometry, the variable nature of the applied load, the desired level of reliability and the applied mean stress.

Shape of the
Amplitude
Distribution

Characteristic Stress Amplitude $\overline{S}_a$(log) N/mm²

400

200

100

50

P—— ——P
Welded Specimen St 37/St52

10³ 10⁴ 10⁵ 10⁶ 10⁷ 10⁸ 10⁹

No. of Cycles $\overline{N}$

25
20
16
12
10
8
6
5
4

Ton / in²
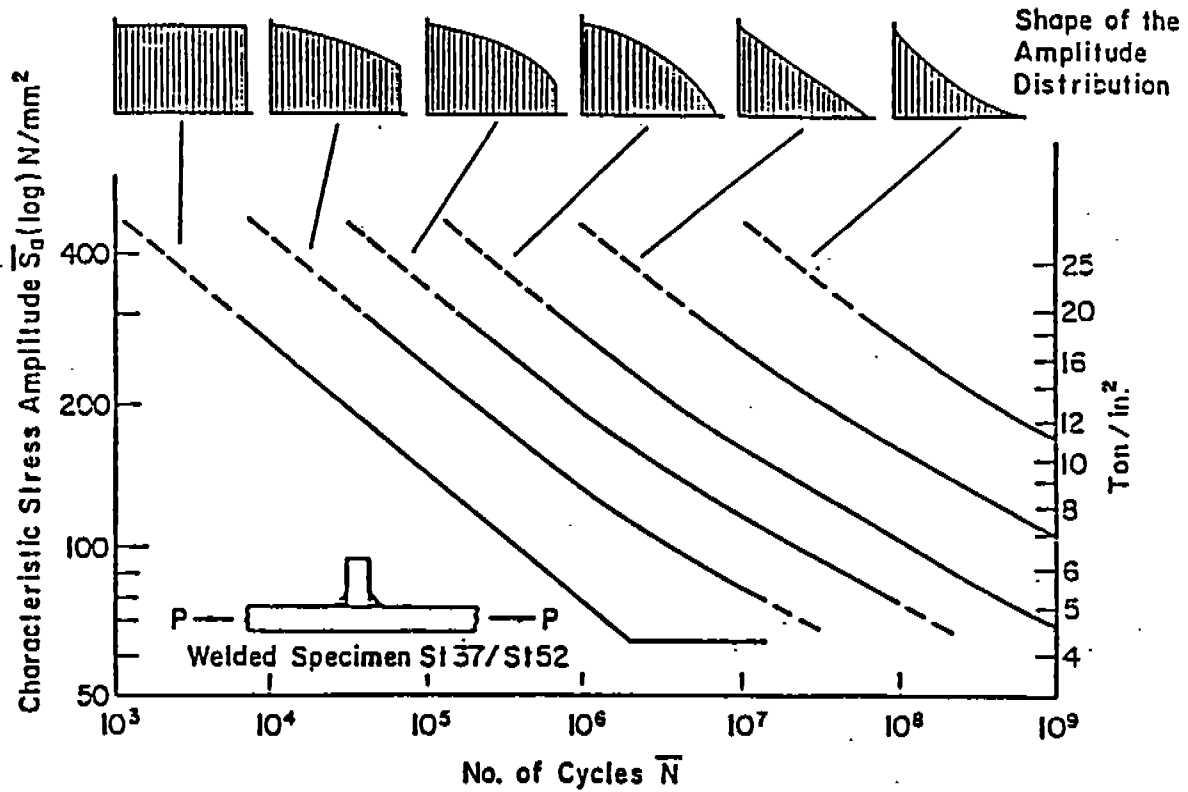
Fig. 1-6 Fatigue resistance of a weldment subjected to variable
         loadings [1- 2].

$S_e = S_c \cdot \xi$

Log S

S_e

S_c

Random Loading

Constant-Cycle

$\overline{n}$

Log n
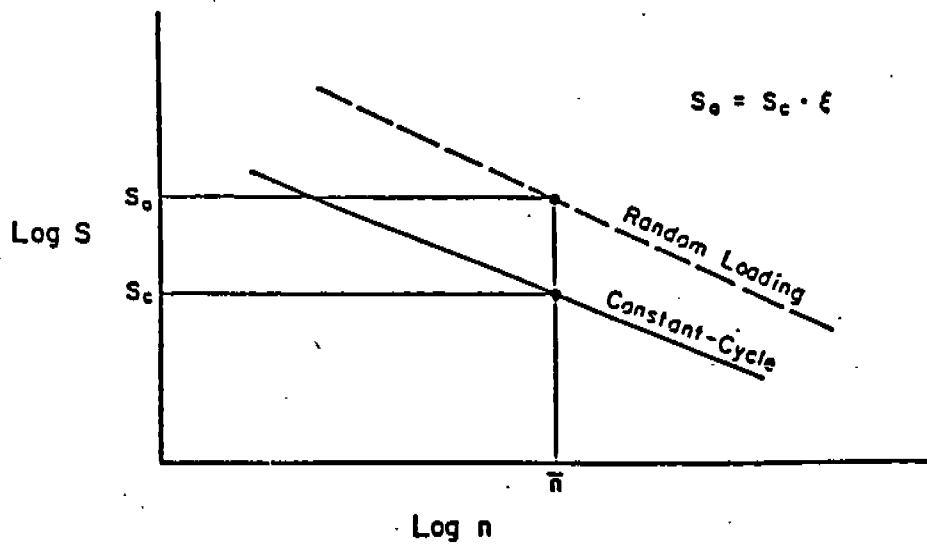
Fig. 1-7 Relationship between maximum stress range of variable
         (random) loading and equivalent constant-cycle stress
         range [1-4].

13

Constant Cycle Fatigue
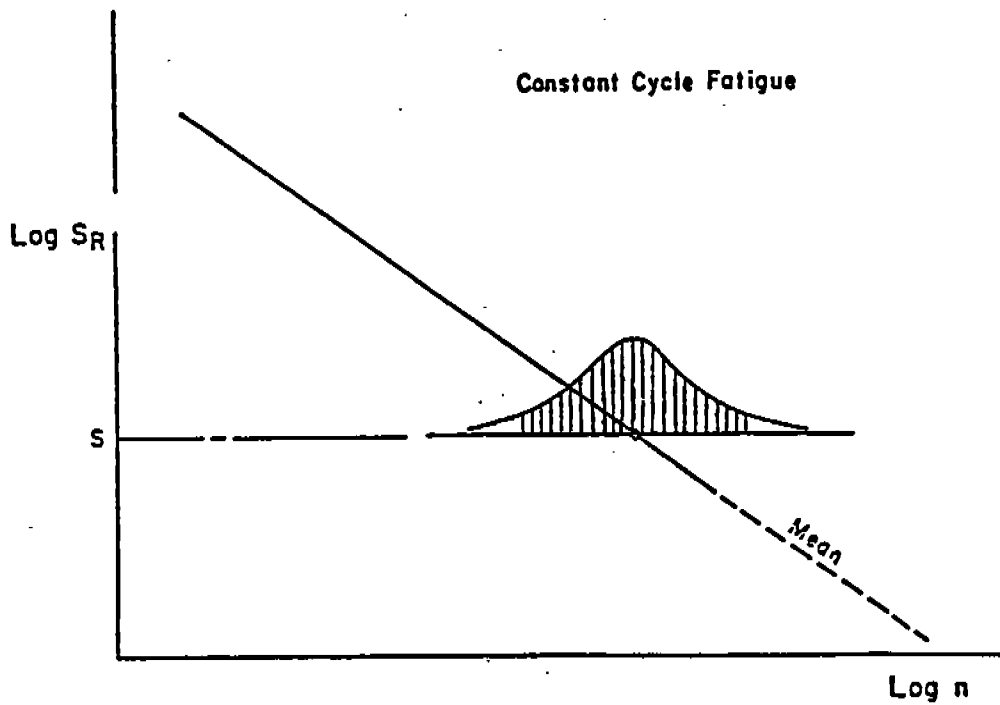
Fig. 1-8 Distribution of fatigue life at a given stress level [1-4].

Constant Cycle

$$\bar{n} = \frac{C}{S^m}$$

$$\bar{n} = n \cdot \gamma_L$$

$$S_o = S \times R_F = S \times \left(\frac{1}{\gamma_L}\right)^{1/m}$$

n
Useful
Life At
L(n)

$\bar{n}$
Mean Life
For Design
Stress
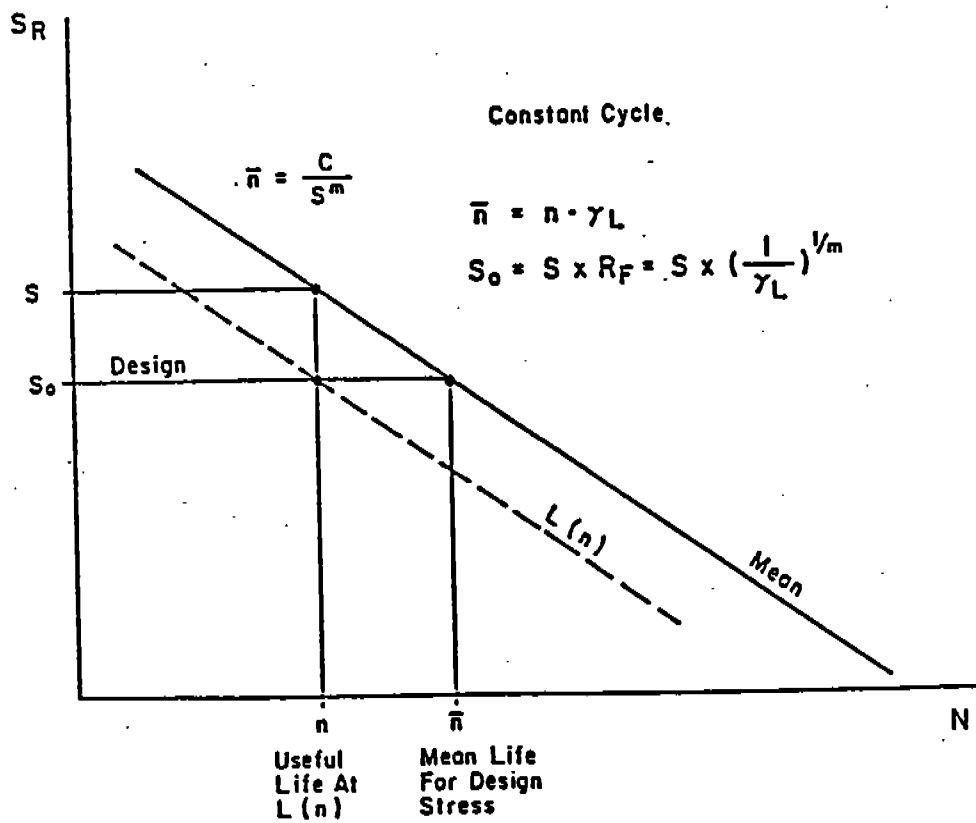
Fig. 1-9 Application of reliability factor to mean fatigue resistance [1-4].

2. COMPARISON OF THE AVAILABLE FATIGUE LIFE PREDICTION METHODS (TASK 1)

The effect of variable loadings on the fatigue performance of welds is generally accounted for by using cumulative damage rules. These rules attempt to relate fatigue behavior under a variable loading history to the behavior under constant amplitude loading. The Palmgren-Miner linear cumulative damage rule (or commonly, "Miner's rule") is widely used in many current standards and design codes. Several models for predicting weldment fatigue life have been proposed based on the S-N curve for weld details and Miner's rule.

There are essentially two types of prediction models reported, and these are summarized in Table 2.1. The first type is based on the S-N diagrams for the actual weld details, and the Munse Fatigue Design Procedure is in this category. The second type is based on the fracture mechanics and the fatigue properties of laboratory specimens, and the I-P model is in this category.

2.1 Models Based on S-N Diagrams

The S-N diagram approach is conventionally used in current practice. Miner's rule is used for the cumulative damage calculations:

$$\sum \frac{n_i}{N_i} = 1 \tag{2-1}$$

where n_i is the number of cycles applied at stress range ΔS_i in the variable loading history and N_i is the constant amplitude fatigue life corresponding to ΔS_i. While Miner's rule usually gives slightly conservative life predictions, it has been found to give unconservative life predictions for certain types of variable loading history [2-1]. Two better methods of damage accumulation have been proposed to predict the fatigue strength of weldments.

The first method uses the Miner's rule but modifies the fatigue limit of the constant amplitude S-N curve for the welded detail. Figure 2-1 shows two typical ways of modifying the S-N curve. One way is to extend the sloped line to the region below the fatigue limit, i.e., no cut-off. For

15

example, Schilling and Klippstein [2-2] have employed an equivalent stress range of constant amplitude that produces the same fatigue damage at the variable amplitude stress range history it replaces. As the negative reciprocal slope of S-N curve is about three for structural steel and structural details, Schilling et al. suggested the use of the "root-mean-cube (RMC) stress range" for welded bridge details subjected to variable amplitude loading history.

The other way suggested in BS 5400 [2-3] is changing the S-N curve from a slope of -1/m to -1/(m+2) at 10^7 cycles.

The second method for improving damage accumulation is to introduce a nonlinear damage rule. In the Joehnk and Zwerneman's nonlinear damage model [2-4], the ratio of damage to stress range increases nonlinearly as the stress range decreases. Effective stress ranges were defined for subcycles first, then Miner's rule was employed to calculate the damage of subcycles.

Two fatigue prediction models have been proposed to predict the fatigue resistance of welds subjected to variable loading history using constant amplitude S-N diagram and will be discussed below: one uses Miner's rule and an extended S-N curve, the Munse Fatigue Design Procedure, and the other uses and empirical relationship based on test results, Gurney's model.

Munse's Fatigue Design Procedure

The Munse Fatigue Design Procedure was reviewed in Section 1.5 and can be used as a prediction method if one considers the variation in the random variables to approach zero. Three factors are considered in Munse Fatigue Design Procedure [1-4]: (a) the mean fatigue resistance of the weld details, (b) a "random load factor" (ξ) that is a function of variable amplitude loading history and slope of the mean S-N curve, and (c) a "reliability factor" (R_F) (roughly the inverse of the safety factor) that is a function of the slope of the mean S-N curve, level of reliability, and a coefficient of variation here taken to be 1.

The maximum allowable fatigue stress range ΔS_D for welds subjected to variable loading history is obtained from the following equation:

$$\Delta S_D = \Delta S_N \ (\xi) \ (R_F) \qquad\qquad (1-2)$$

16

where ΔS_N is the constant amplitude stress range at fatigue life of N cycles. For welds subjected to a constant amplitude stress-range (ΔS_N), the mean fatigue life N is given by the relationship:

$$N = \frac{C}{(\Delta S_N)^m} \qquad (2\text{-}2)$$

where C and m are empirical constants obtained from a least-squares analysis of S-N diagram data. Munse's procedure uses the extended straight S-N line at the stress ratio R=0 as its basis (see Fig. 2-1) and neglects the effects of mean stress, material properties, and residual stress.

After cycle counting, the variable load history is plotted in a stress range histogram. Mean stress level and sequence effects are regarded as secondary effects. Since random loadings for weld details usually cannot be determined exactly, Munse's procedure uses probability distribution functions to represent the weld fatigue loading. Six probability distribution functions are employed to represent different common variable loading histories: beta, lognormal, Weibull, exponential, Rayleigh and a shifted exponential distribution function. It is necessary to determine which distribution or distributions provides the best fit to a given loading history. The random load factor in Munse's procedure are for a desired life and are tabulated in [1-4]. Table 7.5 in [1-4] gives coefficients to adjust values of ξ to other design lines. In this study, the values of random load factor have been derived for any arbitrary fatigue life and are shown in Table 2-2.

The reliability factor is given by:

$$R_f = \left\{ \frac{[P_F(N)]\Omega_N^{1.08}}{\Gamma(1 + \Omega_N^{1.08})} \right\}^{1/m} \qquad (2\text{-}3)$$

where $P_F(N)$ is the probability of failure, Ω_N is the total uncertainty for fatigue life of N cycles and Γ is the gamma function.

In Ref. 1-3 it is suggested that this relationship can be represented by the following approximate values.

17

50% Reliability	$R_F = 1.00$
90% Reliability	$R_F = 0.70$
95% Reliability	$R_F = 0.60$
99% Reliability	$R_F = 0.45$

Gurney's Model

Gurney [2-5] performed fatigue tests on fillet welded joints using simple variable loading history. It was found that the logarithm of number of blocks to failure varied linearly with the ratio of the subcycle's stress range to the maximum stress range in the history:

$$N_b = N_c \left\{ \left[\prod_2^n \frac{N_i - 1}{N_i} \right]^{p_i} \right\} \qquad (2-4)$$

where N_b = the fatigue life in blocks

N_c = the fatigue life in cycles at maximum stress range in the block history

N_i = number of cycles per block equal or exceeding p_i times the maximum stress range in the block history

n = total number of cycles in a block

The parameter contained within the braces is the random load factor.

2.2 Methods Based upon Fracture Mechanics

Methods based upon fracture mechanics ignore the fatigue crack initiation phase and calculate the fatigue crack propagation life only. Maddox [1-6] used linear fracture mechanics and Miner's rule to predict the fatigue life of welds subjected to variable loading history. Miner's rule was found to be accurate for welds under loading histories without stress interaction.

Barsom [1-6] used a single stress intensity factor parameter, root-mean-square stress intensity factor, to define the crack growth rate under both constant and variable amplitude loadings. The root-mean-square stress intensity factor, ΔK_{rms}, is characteristic of the load distribution and is independent of the order of the cyclic load fluctuations. Hudson [2-6] applied the root-mean-square (RMS) method for random loading history with variable minimum load. This simple RMS approach has been shown applicable

18

for loading history with random sequences. The root-mean-square stresses are defined as:

$$S_{max}^{rms} = \left[\frac{1}{N}\sum_{n=1}^{N}(S_{max}^n)^2\right]^{1/2} \tag{2-5}$$

and

$$S_{min}^{rms} = \left[\frac{1}{N}\sum_{n=1}^{N}(S_{min}^n)^2\right]^{1/2} \tag{2-6}$$

where S_{max} and S_{min} are the maximum and minimum stress for each cycle respectively, and N is the total number of cycles for the random loading history.

The root-mean-square stress intensity factor range is calculated from

$$\Delta K_{rms} = K_{max}^{rms} - K_{min}^{rms} \tag{2-7}$$

Calculation of fatigue crack propagation life is through the substitution of Eq. 2-7 into the fatigue crack propagation model, Eq. A-18.

A deterministic model for estimating the total fatigue life of welds has been developed by the authors and is presented in Appendix A. This model is termed the initiation-propagation (I-P) or total life model and assumes that the total fatigue life of a weld (N_T) is composed of a fatigue crack initiation (N_I) and a fatigue crack propagation period (N_P) such that:

$$N_T = N_I + N_P \tag{2-8}$$

The initiation portion of life may be estimated using the fatigue data from strain-controlled fatigue tests on smooth specimens. The initiation life so estimated includes a portion of life which is devoted to the development and growth of very small cracks. The fatigue crack propagation portion of life may be estimated using fatigue crack propagation data and an arbitrarily assumed initiated crack length (a_i) of 0.01-in. in the instances in which the initial crack length is not obvious. A second alternative is to assume that a_i is equal to a_{th} the threshold crack length. In most cases, the arbitrary 0.01-in. assumption permits a prediction of total life

19

within a factor of 2 [1-5]. Naturally, for welds containing crack-life defects, N_I may be very short. However, for other internal defects having low values of K_t such as slag or porosity, N_I may be appreciable; and neglecting N_I may be overly conservative. This is particularly the case for welds containing no discontinuities other than the weld toe. In this case and particularly for the long life region, it is believed that the fatigue crack initiation portion life (as defined) is very important. A detailed discussion of the I-P model is given in Appendix A.

2.3 Comparisons of Predictions with Test Results

Table 2.1 summarizes the prediction models discussed above. Several of these models were used to predict the "mean fatigue lives" of welds tested in this and other studies [2-7]. Figures 2-2 to 2-10 compare the predictions made by the Munse Fatigue Design Procedure, Miner's rule, Gurney's model, the RMS method, and the I-P model with actual test data for several histories. The Munse Fatigue Design Procedure (MFDP) and the Miner's Rule predictions in these figures differ only in that the MFDP uses a continuous probability distribution function to model the load history while the Miner's rule sums the actual history. The "Rainflow" counting method was used in these comparisons. In these comparisons, the maximum stress in the load history (S_{min}^A or S_{max}^A) is plotted against the predicted life. The effects of bending stresses were taken into account.

The Munse Fatigue Design Procedure (MFDP) provided good mean fatigue life predictions for welds subjected to the SAE bracket history (See Appendix C) as shown in Figs. 2-2, 2-3, and 2-5. For welds tested under the SAE transmission history (See Appendix C), unconservative predictions were made by the MFDP (Fig. 2-4). This discrepancy might be due to means stress effects because the transmission history has a tensile mean stress while the bracket history has only a small average mean stress. The root-mean-square method (fatigue crack propagation life only) gave conservative predictions for all cases. It is interesting to note that the predictions made based on S-N curves without cutoff and Miner's rule are similar to the predictions of the MFDP. Predictions resulting from the Total Fatigue Life (I-P) model seem to agree well with the test results. Table 2-3 is a statistical sum-

mary of the departures of predicted lives from the test data as in Fig. 2-6 to Fig. 2-10.

While the agreement between the prediction methods discussed above and the two variable load histories employed in the comparison are quite good, there are histories for which all predictions methods based on linear cumulative damage fall short even when the very conservative assumption of an extended S-N diagram is used [2-8]. These histories are typically very long histories in which most of the damaging cycles are near the constant amplitude S-N diagram endurance limit. Neither the SAE bracket or transmission histories nor the edited history discussed in the next section fall into this category; consequently, this serious problem in fatigue life prediction is not addressed by the comparison of this section nor the experimental study of the next section.

2.4 References

2-1. Fash, J.W., "Fatigue Life Prediction for Long Load Histories," Digital Techniques in Fatigue, S.E.E. Int. Conf., City University of London, England, March 28-30, 1983, pp. 243-255.

2-2. Schilling, C.G. and K.H. Klippstein, "Fatigue of Steel Beams by Simulated Bridge Traffic," Journal of Structural Division, Proceedings of ASCE, Vol. 103, No. ST8, August, 1977.

2-3. BS5400: Part 10: 1982, "Steel Concrete and Composite Bridges, Code of Practice of Fatigue."

2-4. Zwerneman, F.J., "Influence of the Stress Level of Minor Cycles on Fatigue Life of Steel Weldments," Dept. of Civil Engineering, The University of Texas at Austin, Master Thesis, May 1983.

2-5. Gurney, T.R., "Some Fatigue Tests on Fillet Welded Joints under Simple Variable Amplitude Loading," The Welding Institute, May 1981.

2-6. Hudson, C.M., "A Root-Mean-Square Approach for Predicting Fatigue Crack Growth under Random Loading," ASTM STP 748, 1981, pp. 41-52.

2-7. Yung, J.-Y. and Lawrence, "A Comparison of Methods for Predicting Weldment Fatigue Life under Variable Load Histories," FCP Report No. 117, University of Illinois at Urbana-Champaign, Feb., 1975,

2-8. Gurney, T.R., "Fatigue Test on Fillet Welded Joints to Assess the Validity of Miner's Cumulative Damage Rule," Proc. Roy. Soc., A386, 1983, pp. 393-408.

2-9. Miner, M.A., "Cumalative Damage in Fatigue," Journal of Applied Mechanics, Vol. 12, Trans. of ASME, Vol. 67, 1945, pp. A159-A164.

Table 2.1

Summary of Fatigue Life Prediction Models
For Weldments Subjected to Variable Loadings

Basis	Proposed by	Model
S-N curve	Miner [2-9]	$\sum (n_i/N_i) = 1$ n_i : no. of cycles applied at ΔS_i N_i : no. of cycles to failure at ΔS_i linear damage accumulation
	Zwerneman [2-4] Joehnk	$\Delta S_{eff} = \Delta S_i (\Delta S_{max}/\Delta S_i)^a$ ΔS_{eff} : effective stress range at ΔS_{max} ΔS_i : stress range of subcyles ΔS_{max} : maximum stress range a : varies with loading history nonlinear cumulative damage
	Gurney [2-5]	$N_b = N_c [\prod_{2}^{n} (N_{ei-1}/N_{ei})^{p_i}]$ N_b : no. of blocks to failure N_c : no. of cycles to failure at ΔS_{max} N_{ei}: no. of cycles per block equal to or exceeding p_i times the maximum stress in one block
	Munse [1-4]	$S_D = S_N * \xi * R_F$ S_D : allowable maximum stress range S_N : maximum stress range in life N ξ : probabilistic random load factor R_F : reliability factor
fracture mechanics	Barsom [1-7]	$\Delta K_{rms} = [(\sum \Delta K_i)^2/n]^{1/2}$ ΔK_{rms} : root mean square stress intensity factor range fatigue crack propagation life only
	Lawrence [1-5] Ho	$N_T = N_I + N_p$ N_T : total fatigue life N_I : fatigue crack initiation life N_p : fatigue crack propagation life

Table 2.2

Random Load Factors for Distribution Functions [1-4]

Distribution Function	Random Load Factor, ξ
beta	$\{[\Gamma(q)\Gamma(m+q+r)]/[\Gamma(m+q)\Gamma(q+r)]\}^{1/m}$
Weibull	$(\ell nN)^{1/k}[\Gamma(1+m/k)]^{-1/m}$
exponential	$(\ell nN)[\Gamma(1+m)]^{-1/m}$
Rayleigh	$(\ell nN)^{1/2}[\Gamma(1+m/2)]^{-1/m}$
lognormal	$(1+\delta_s^2)^{-m/2}\exp\{\gamma[\ell n(1+\delta_s)]^{1/2}\}$ $\delta_s = \sigma_s/\mu_s$ $\gamma = \Phi^{-1}(1-N^{-1})$
shifted exponential	$[\sum_{n=0}^{m} m!/(m-n)!(\ell nN)^{-n}(1-\alpha)^n\alpha^{m-n}]^{-1/m}$ $\alpha = a/[a+\mu_s(\ell nN_b)]$

Table 2.3

Statistical Summary of the Departures of
Predicted Lives from Fatigue Test Data

	Munse's (Fig. 2-6)	Miner's (Fig. 2-7)	Gurney's (Fig. 2-8)	RMS Method (Fig. 2-9)	I-P Model (Fig. 2-10)
No. of Cases	29	29	29	13	29
$\overline{F}_p$	1.061	1.015	0.894	0.906	1.016
Ω_{F_p}	0.124	0.093	0.081	0.052	0.067

$\overline{F}_p$: Mean value of F_p; $F_p = \dfrac{\log_{10}(N_{prediction})}{\log_{10}(N_{Test})}$, a unity of F_p value represents the perfect agreement between the prediction and fatigue data.

Ω_{F_p} : Coefficient of Variation of F_p.

24
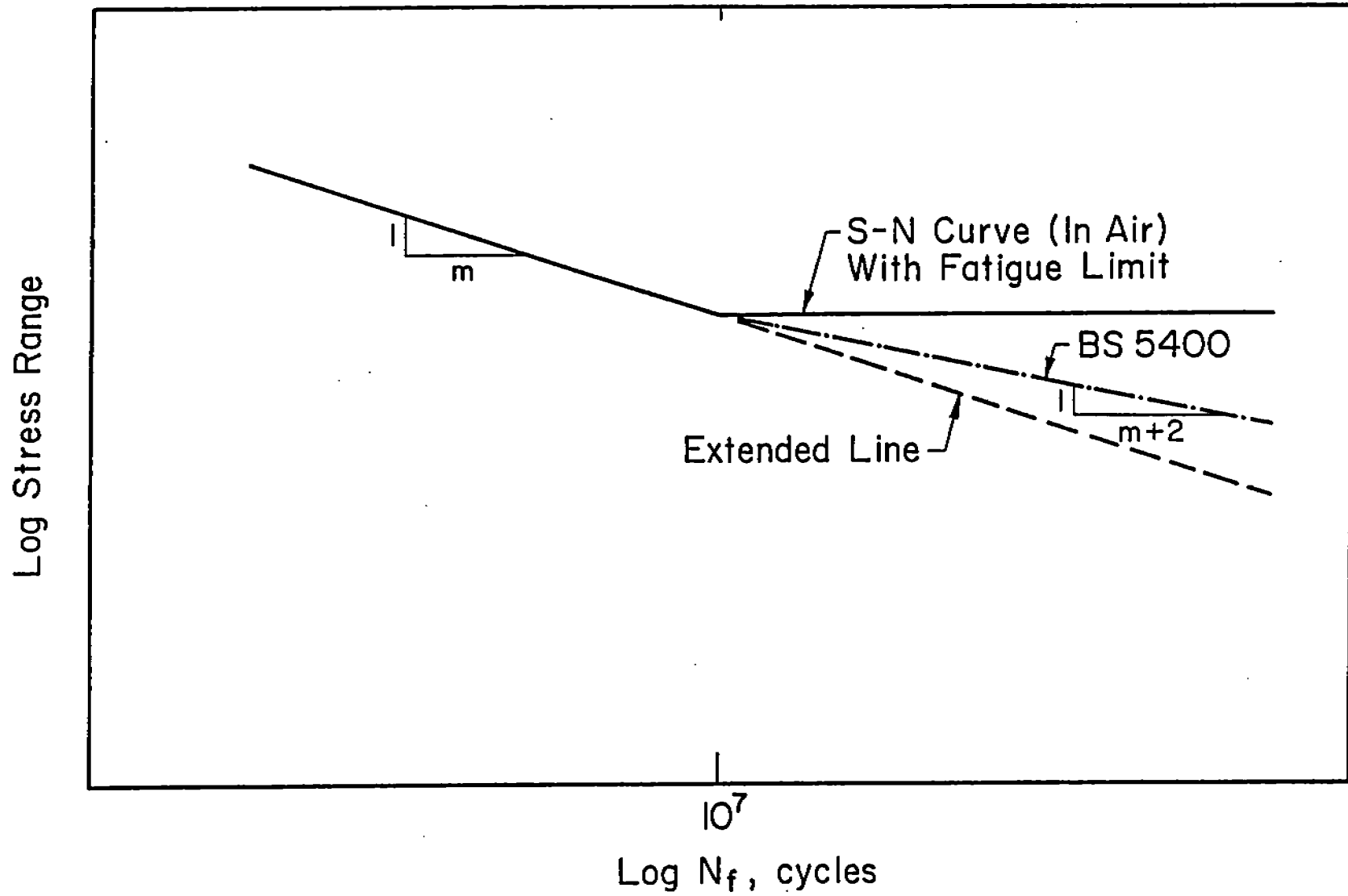
Fig. 2-1 Modification of S-N diagram.

10^2

$-S^A_{min}$, ksi

10^1

GM MS4361 Steel
Fillet Welds
SAE Bracket History
IJP Failure

● : Test Results
—— : I-P Model
— — : Munse's Beta (S-N)
—·— : Miner's Rule (S-N)
—··— : RMS Method

$-S^A_{min}$, MPa

10^2

10^1

10^1 10^2 10^3 10^4

N_T, blocks
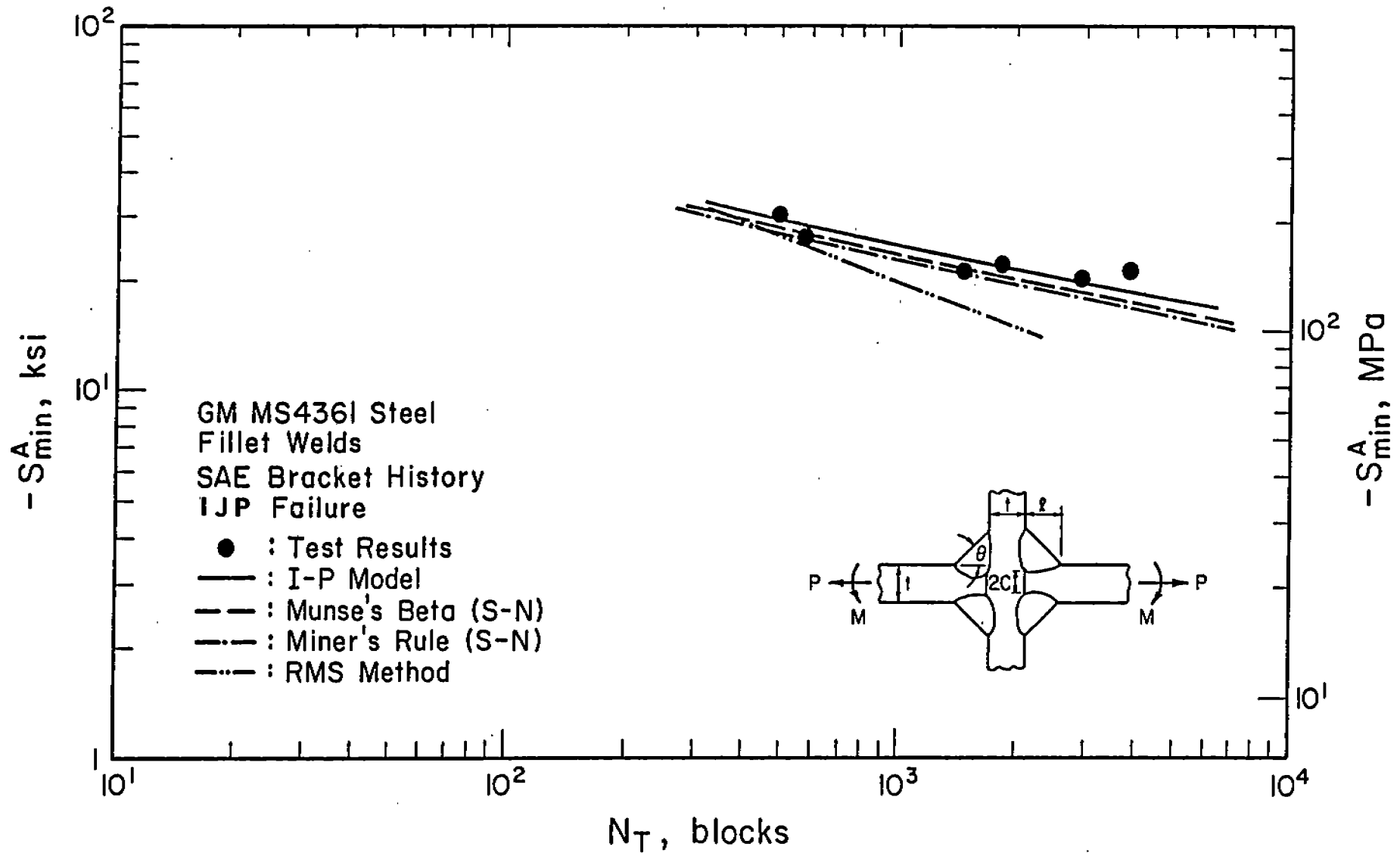
Fig. 2-2 Fatigue test results and predictions for GM MS4361 Fillet welded cruciform joints
subjected to SAE Bracket history. S^A_{min} is the minimum stress in the load history.
The Incomplete Joint penetration (IJP) is indicated by 2C.
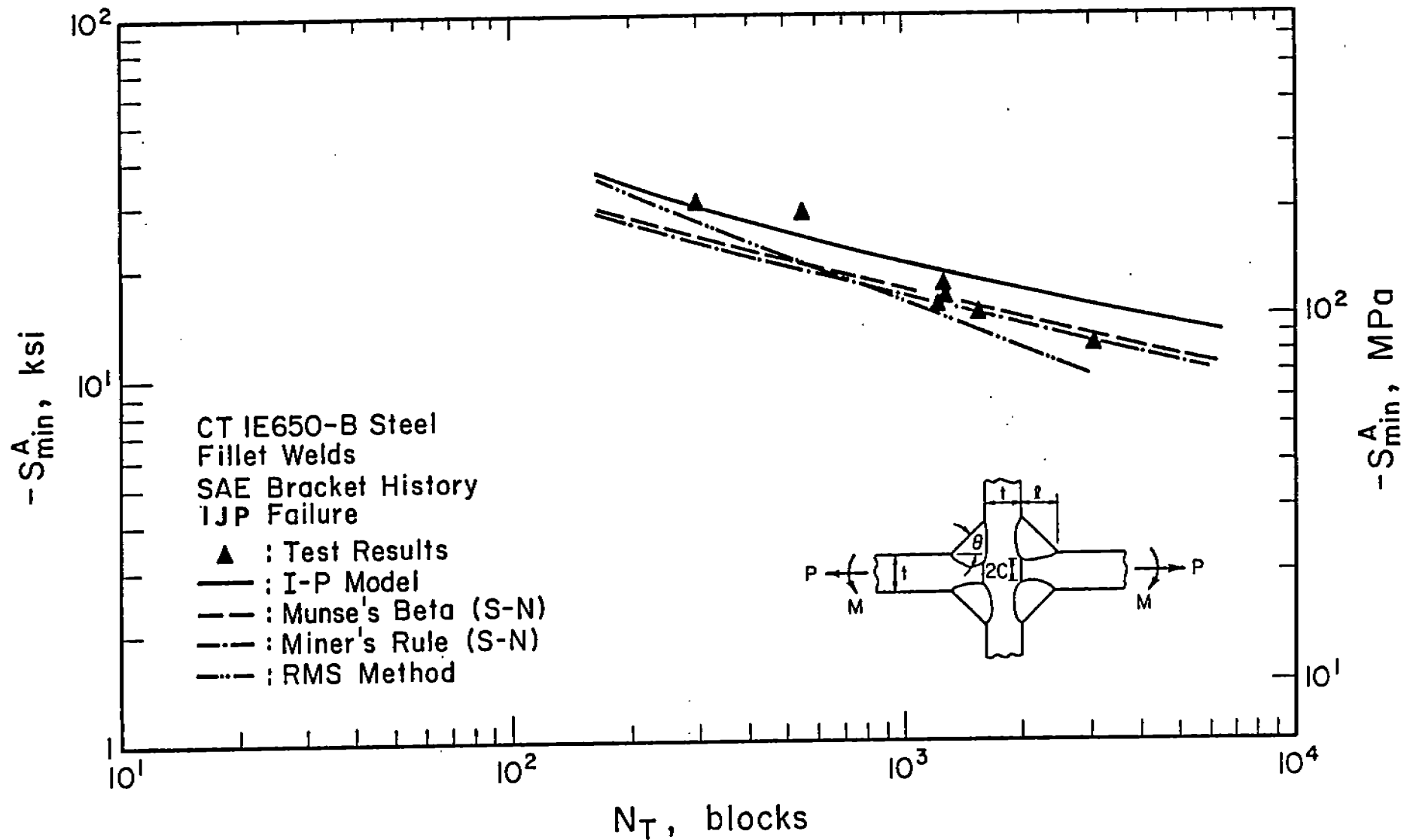
Fig. 2-3 Fatigue test results and predictions for CT 1E650-B fillet welded cruciform joints subjected to SAE Bracket history. S_{min}^A is the minimum stress in the load history. The Incomplete Joint penetration (IJP) is indicated by 2C.
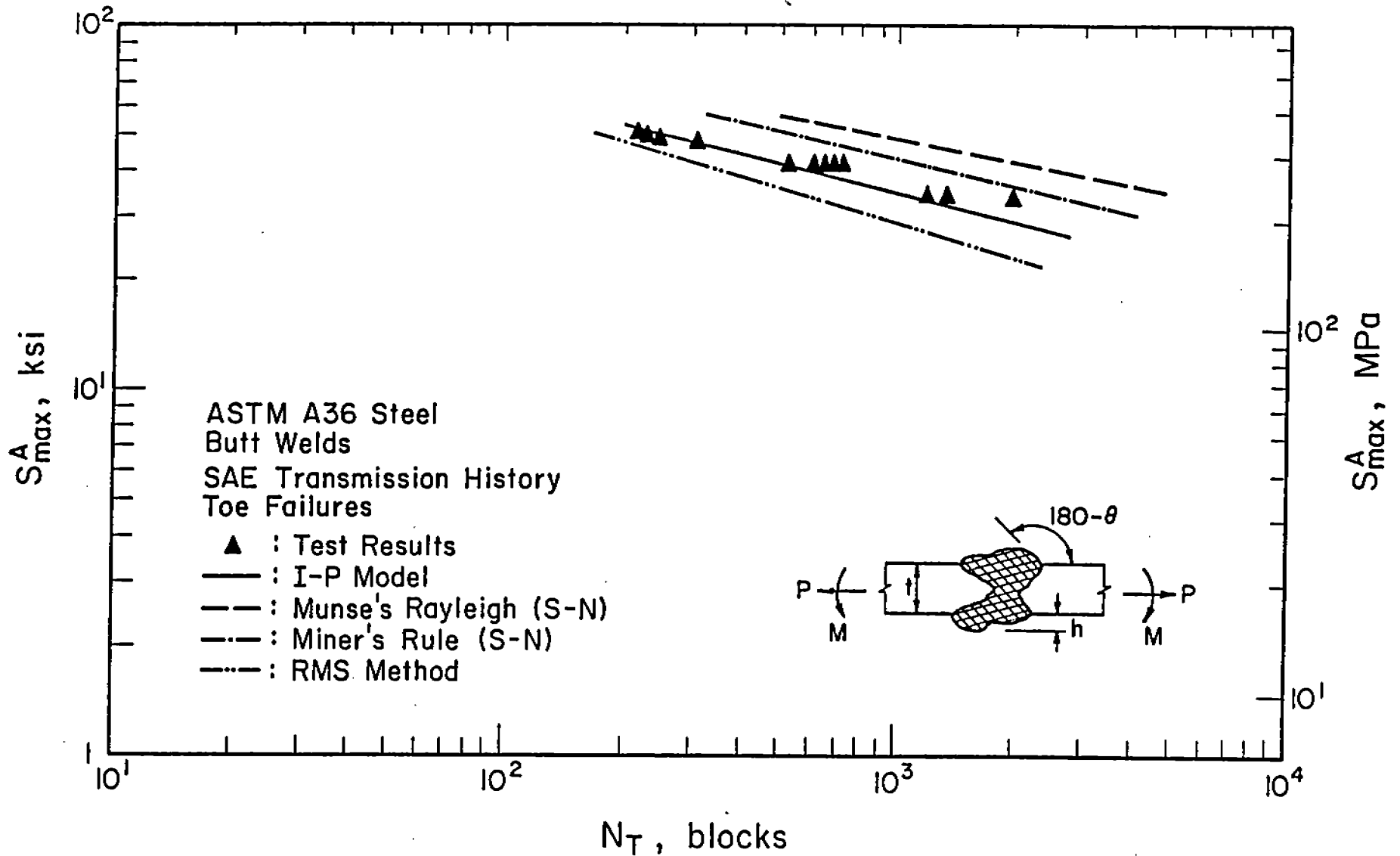
Fig. 2-4 Fatigue test results and predictions for ASTM A 36 butt welds subjected to SAE transmission history. S_{min}^A is the maximum stress in the load history.
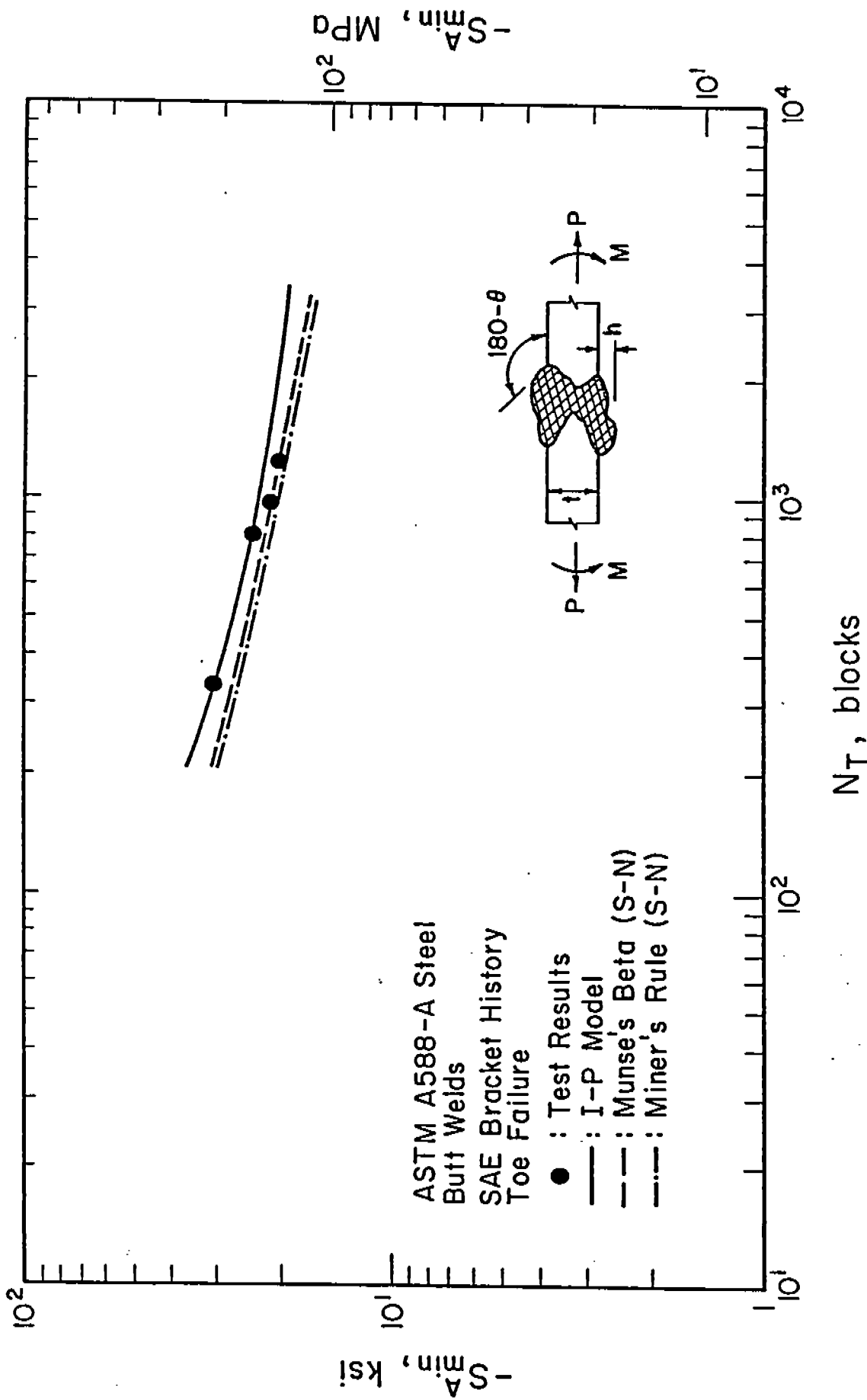
Fig. 2-5 Fatigue test results and predictions for ASTM A588-A butt welds subjected to SAE Bracket history. S_{min}^A is the minimum stress in the load history.
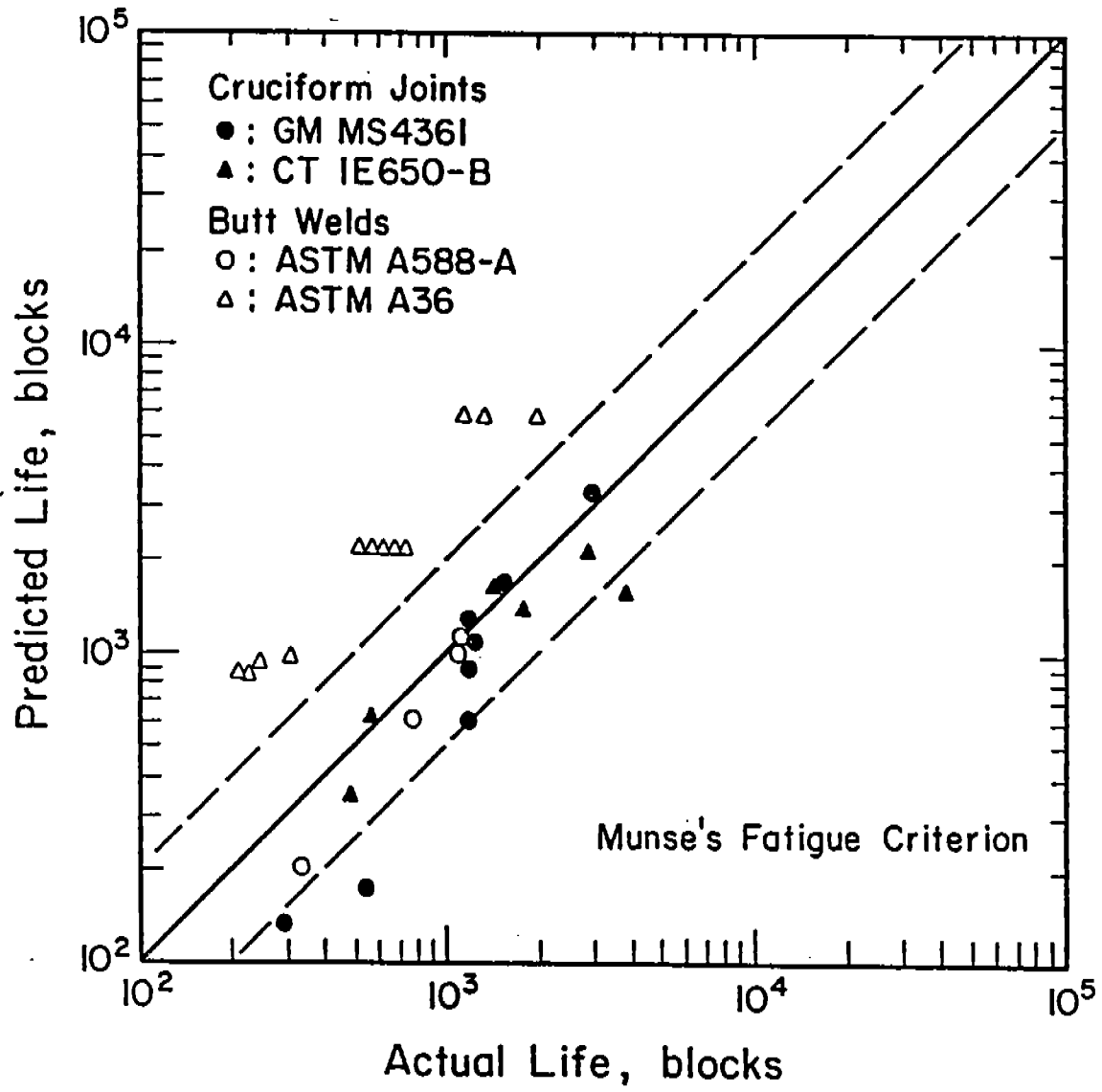
Fig. 2-6 Comparison of actual and predicted fatigue life using Munse's
Fatigue Criterion (Extended S-N Curve). The dashed lines
represented factors of two departures from perfect agreement.
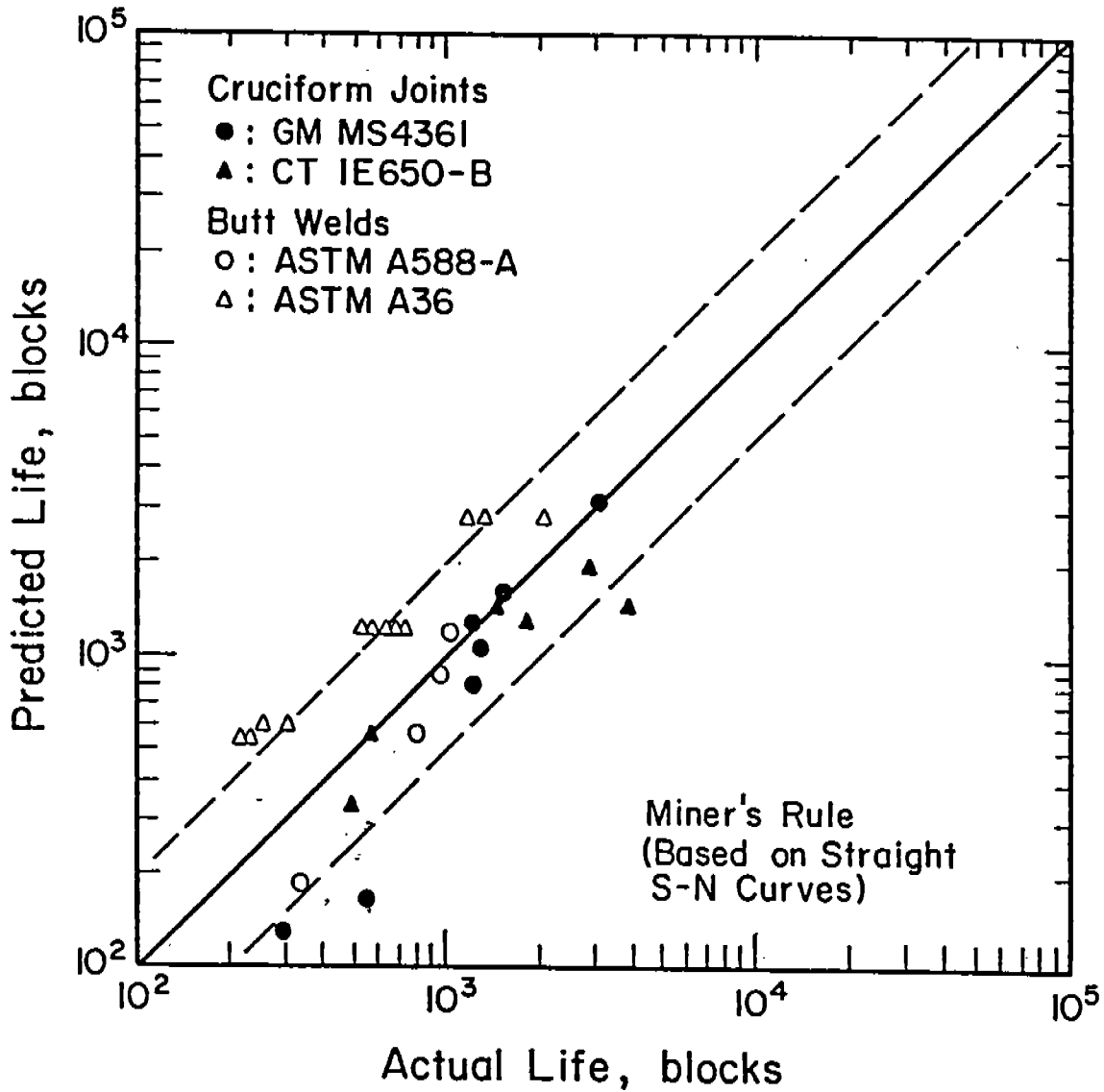
Fig. 2-7 Comparison of actual and predicted fatigue life using Miner's
Rule and the Extended S-N Curve. The dashed lines represented
factors of two departures from perfect agreement.
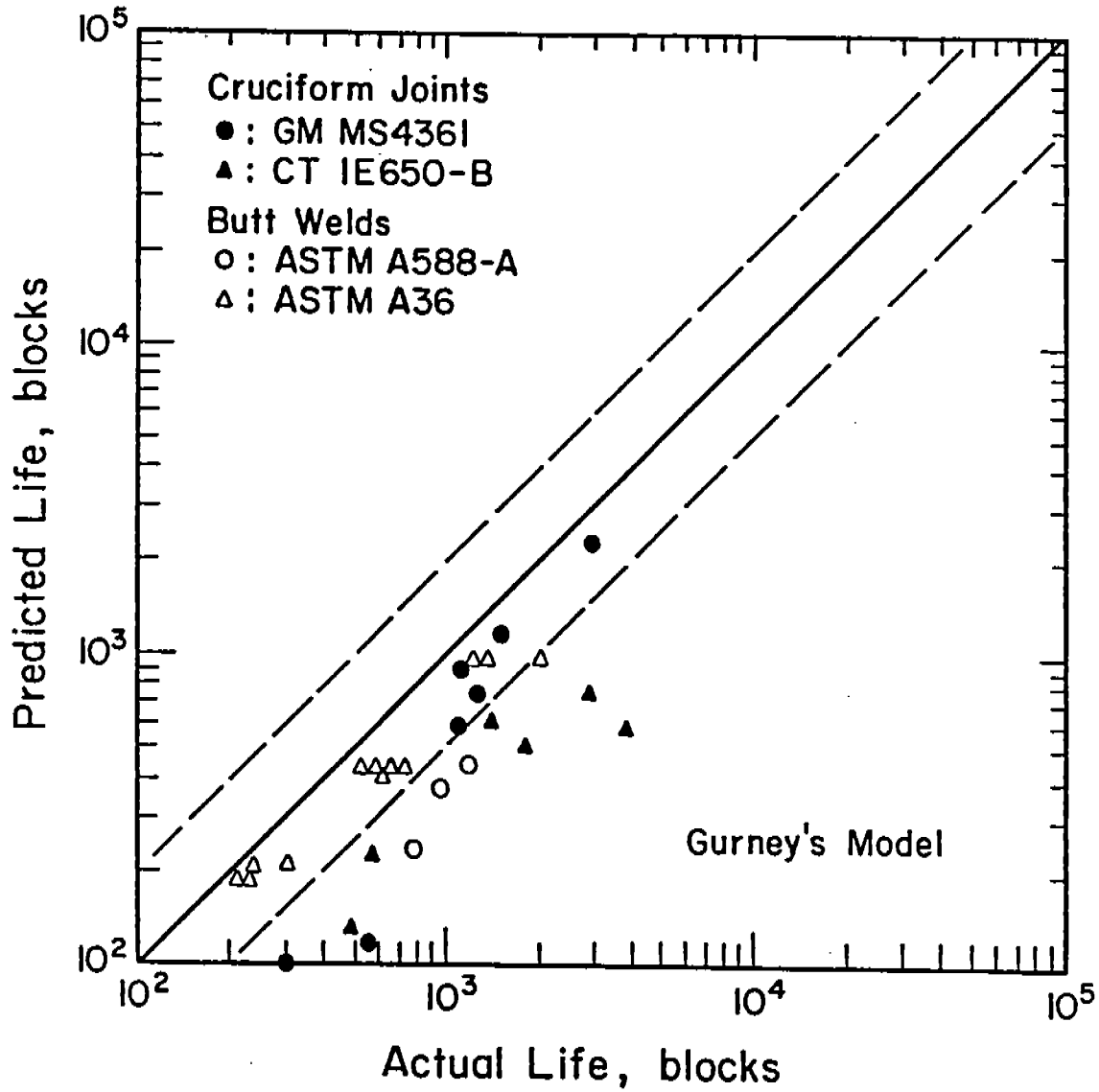
Fig. 2-8 Comparison of actual and predicted fatigue life using Gurney's Model. The dashed lines represented factors of two departures from perfect agreement.
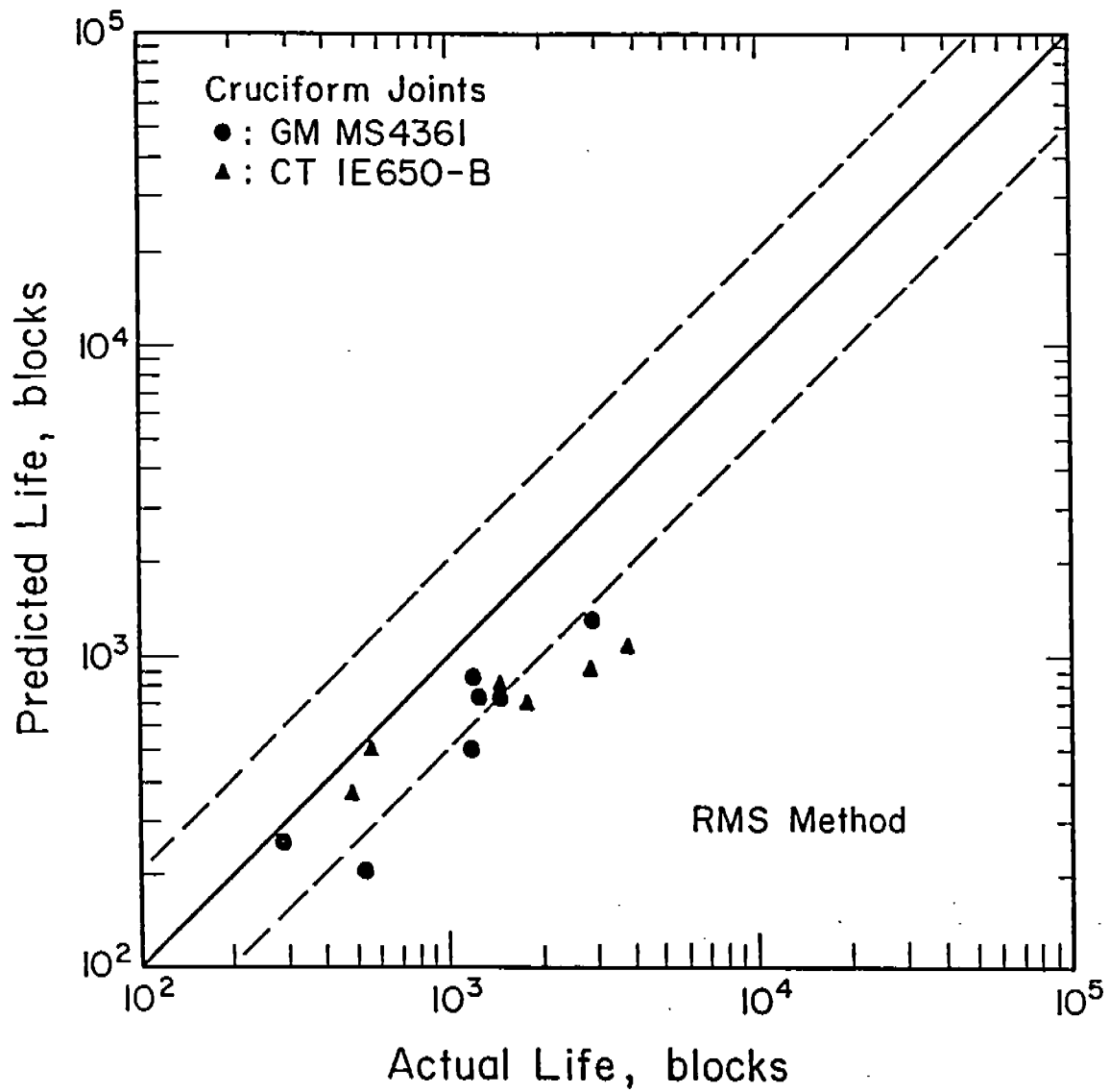
Fig. 2-9 Comparison of actual and predicted fatigue life using the
RMS Method. The dashed lines represented factors of two
departures from perfect agreement.

33
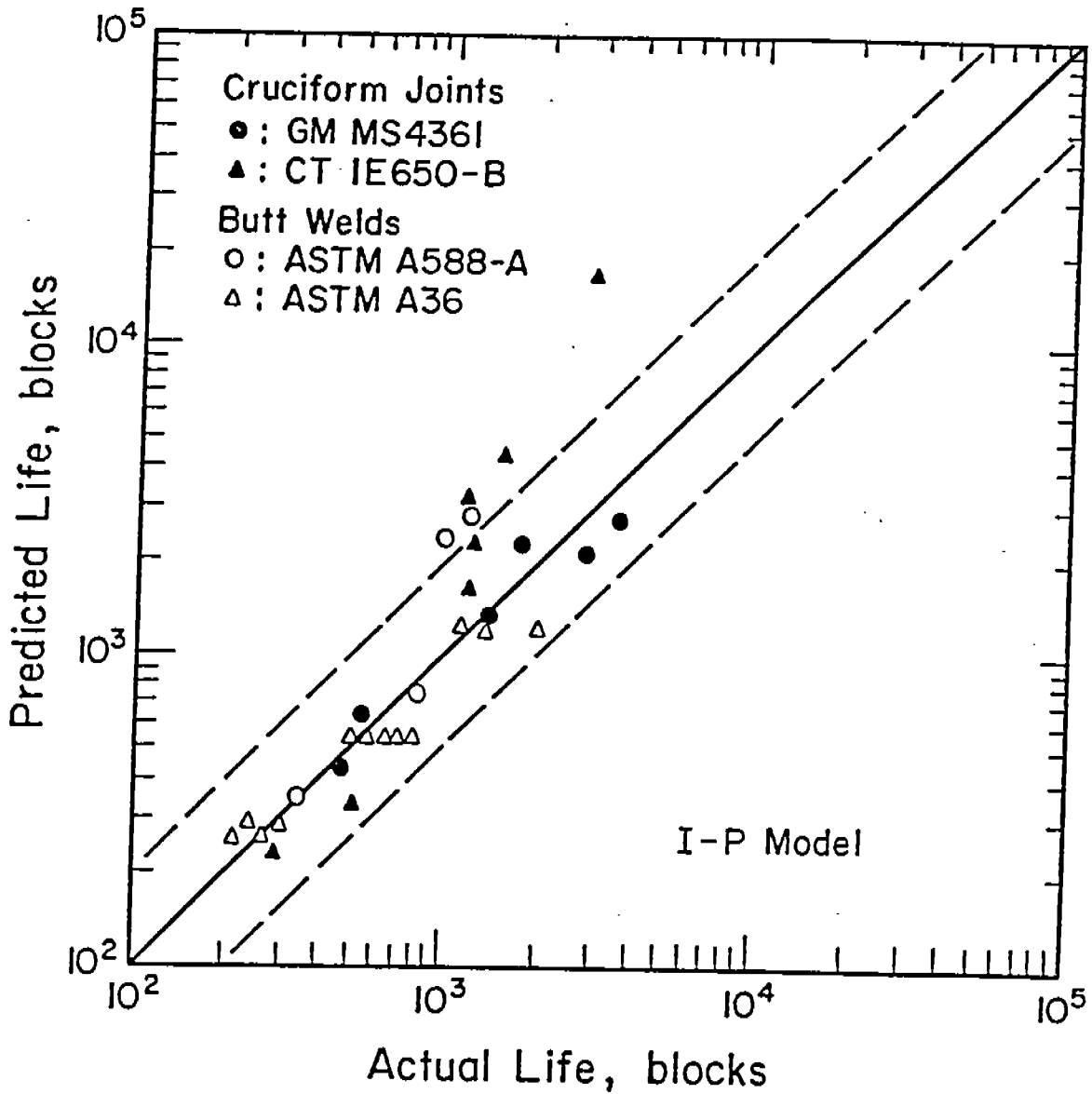
Fig. 2-10 Comparison of actual and predicted fatigue life using the
I-P model. The dashed lines represented factors of two
departures from perfect agreement.

3. FATIGUE TESTING OF SELECTED SHIP STRUCTURAL DETAIL UNDER A VARIABLE SHIP BLOCK LOAD HISTORY (TASKS 2-4)

The experimental portions of this study can be divided into two parts: The first and major effort of this study was to test a selected structural detail under a variable load history which simulated a ship history. This part encompassed Long Life Variable Load Testing (Task 2), Mean Stress Effects (Task 3), and Thickness Effects (Task 4). The results of the first part of the experimental program are discussed in this section. The second part of the experimental program (Task 7) was the collection of baseline constant amplitude fatigue data for selected ship structural details. The results of this latter study are summarized in Section 5.

A major technical difficulty at the outset of this part of the experimental program was obtaining a variable load history which simulated the typical service history experienced by ships. Since no standard ship history was available, the first major task for the experiments described in this section was to develop a reasonable variable load history block which simulated the load history of a ship. This task was further complicated by the fact that typical ship histories have occasional large overloads which cannot be contained in every block or repetition of a short history and by the large number of small cycles which contribute little to the accumulation of fatigue damage but which enormously increase the time required for testing and consequently determine whether or not the laboratory testing can be completed in a reasonable time.

3.1 Determination of The Variable Block Load History.

The Weibull distribution was demonstrated to be an appropriate probability distribution for long-term histories through comparison with actual data such as the SL-7 container ship history [3-1]: see Fig. 3-1.

Munse [1-4] used the 36,011 scratch SL-7 gauge measurements or records taken over four-hour periods shown in Fig. 3-1. Each measurement or short history contained 1,920 cycles. The biggest "grand cycle" of each history was termed an occurrence, and the 36,011 occurrences were assembled into the histogram shown in Fig. 3-2 and fitted with a Weibull distribution (k = 1.2, w = 4.674). This Weibull distribution was assumed to represent the

35

histogram for the entire history composed of 52,000 short histories containing 1,920 cycles each, or 10^8 cycles. Using the fitted Weibull distribution, Munse estimated the maximum stress range expected during the ship life of 10^8 cycles ($S_{10^{-8}}$) by assuming that the probability associated with this stress range would be $1/10^8$, that is, equal to that for the largest occurrence. From this argument and the fitted Weibull distribution, a maximum stress range of 235 MPa (34.11 ksi) was calculated as the maximum stress in the 20 year ship life history for the location at which the stress history was recorded.

The SL-7 history and Munse's Weibull distribution representation of it was adopted for use in this study. The next problem was to create a typical history, that is a sequence of stress ranges which represented the typical ship experience (period of normal sea state interdispersed with storm episodes), which conformed to the overall Weibull distribution. Furthermore, to permit long-life fatigue testing, the history had to be edited to remove cycles which caused little fatigue damage but needlessly extended the required testing time. It was decided to edit the history so that one "block" would contain only 5,047 cycles and yet contain the most damaging events in a typical one month (345,600 cycle) ship history (see Fig. 3-6).

The first step was to decide which of the events in the SL-7 history were the most damaging and which were the least damaging and could therefore be omitted. The damage calculated for a given interval of stress range of the SL-7 history depends upon three things: the method of summing damage (linear accumulative damage or Miner's rule was used); the assessment of damage caused by a given stress range (we used the I-P model [1-5] rather than the extended S-N approach of Munse and this makes a big difference in what can be omitted); and the degree of stress concentration by the weld defects to be studied (we assumed a maximum fatigue notch factor (K_{fmax}) typical for Detail No. 20 as $K_{fmax} = 4.9$).

The justification for adhering to the predictions of our I-P model is that it has given reasonable estimates of weldment fatigue life under variable load histories in laboratory air [2-6]: see Fig. 2-10. A major difference between the I-P model and Munse's approach is the anticipated behavior of the weldments in the long-life region. Fig. 3-3 shows the extended line used in the Munse Fatigue Design Procedure (MFDP). Use of the extended line

exaggerates the importance of the smaller stress ranges and leads to the conclusion that they can not be deleted. The I-P model predicts that the S-N curve has a slope of about 1:10 in the long life region and consequently, predicts a lesser importance for the smaller stress ranges: see Fig. 3-4.

We used the following strategy for editing the SL-7 history. If each cycle had an average period of 7.5 seconds as reported, a one month ship history would consist of 345,600 cycles [3-1]. Keeping only those stress ranges which contributed 92.8% of the total damage (estimated using the I-P model and Miner's rule, see Figs. 3-4 and 3-5) leads to the elimination of stress range less than 68.9 MPa (10 ksi) and greater than 152 MPa (22 ksi). This decision would permit a reduction in length of the one month history from 345,600 (total) cycles to 5,047 cycles. Fig. 3-6 shows the developed "one-month history" which starts with a period of low stress range, 75.8 MPa (11 ksi), and gradually increases to a maximum of 145 MPa (21 ksi) during the central storm period after which the amplitude decreased to the original 11 ksi. At a testing frequency of 5 Hz, a block required about 17 minutes. Since a 5,047 cycle block represents 345,600 cycles in service, 290 blocks or 3.5 days of testing at 5 Hz or 10 to 15 days at lower testing frequencies are equivalent to a 10^8 cycle service history or 24 years of service.

The ship block load history shown in Fig. 3-6 was read into the memory of a function generator which controlled a 100 kip MTS fatigue testing machine.

3.2 Development of a "Random" Ship Load History

At the suggestion of the advisory committee, an alternative "random" time history was generated using a method employed by Wirsching [3-2]. To simulate a stress history from a given spectral density function, the spectral density must be discretized. This operation was accomplished by defining n random frequency intervals, Δf_i, in the region of definition of f. The value of Δf_i must be random to insure that the simulated process is a nonperiodic function. f_i is the midpoint of Δf_i. The simulation is constructed by adding the n harmonic components:

$$y(t) = \sum_{i=1}^{n} \sqrt{2} \, \hat{\psi}_i \, \cos \, (2\pi f_i t + \phi_i)$$ (3-1)

where y(t) = stress (strain) spectral ordinates

$\hat{\psi}_i$ = spectral ordinates output from the FFT analyzer (in volts)

t = time

ϕ_i = random phase angle sampled from a uniform distribution, 0 ~ 2π

Table 3-1 and Fig. 3-7 show the $\hat{\psi}_i$ provided by the American Bureau of Shipping [3-3] for a given seastate. A sample simulation of y(t) is shown in Fig. 3-8. The length of the second random time history developed was ~ 5,000 cycles. This history, while developed, was not used during this testing program due to limitations in time and funds.

3.3 Choice of Detail No. 20 and Specimen Design

Structural Detail No. 20 (see Fig. 5-1) was elected for testing because of its relative simple geometry and because of its common use in ship construction. As seen in Table 3-2, this structural detail was highly ranked as a troublesome, fatigue-failure-prone geometry.

Detail No. 20 consists of a center plate and two loading plates welded to the center plate by all-around fillet welds: see Fig. 3-9. Three sizes of specimens with three different thickness, 6.35 mm (1/4-in.), 12.7 mm (1/2-in.) and 25.4 mm (1-in.), of loading plate were prepared. Figure 3-9 shows the dimension and geometry of the basic specimen which had 12.7 mm (1/2-in.) thick loading plates. The 12.7 mm (1/2-in.) loading plates were welded to the 15.9 mm (5/8-in.) thick center plate. The leg size of the fillet weld was designed to be 9.5 mm (3/8-in.).

Two other sizes of specimens with 6.35 mm (1/4-in.) and 25.4 mm (1-in.) thick loading plates, 7.9 mm (5/16-in.) and 31.8 mm (1-1/4-in.) center plates were used. Accordingly, the fillet weld leg sizes were nominally 4.76 mm (3/16-in.) and 19.1 mm (3/4-in.), respectively, to maintain the geometric similitude. Figure 3-10 shows a comparison of the three sizes of specimens.

3.4 Materials and Specimen Fabrication

ASTM A-36 steel plates were used as base metals for all the specimens of Detail No. 20, and Table 3-3 lists the mechanical and chemical properties

of the steel plates. These material properties also meet the specifications for A131 Grade A ship plate. All specimens were welded using the Shielded Metal Arc Welding (SMAW) process and E7018 electrodes, and the estimated fatigue properties of weld metal and heat affected zone are listed in Table 3-5. The welding parameters were 17 to 22 volts, 125 to 230 amperes; no preheat or interpass temperatures were used. The horizontal welding position was used. The potential sites of fatigue crack initiation are labeled in Fig. 3-11. Each weldment had four possible weld toe and two incomplete joint penetration (IJP) sites for fatigue crack initiation. Several test pieces were machined to eliminate the wrap-around welds as shown in Fig. 3-12.

In addition to the above specimens, a series of cruciform weldments was prepared using the semi-automatic Gas Metal Arc Welding (GMAW) process to achieve better consistency in distortion and local weld geometry. 12.7 mm (1/2-in.) plate of ASTM A441 Grade 50 steel (which is compatible to the ASTM A131 AH-36 Grade ship steel) was used as the base metal, and ER70S-3 wire was used as filler metal. Figure 3-13 shows the geometry of this series of cruciform joints. Table 3-4 shows the welding parameters and material properties used in the specimen preparation, and Table 3-6 shows the estimated fatigue properties of weld metal and heat affected zone. For this group of specimens, the amplitude of block load history was doubled to reduce the testing time. However, the maximum nominal stress remained within the elastic limit of the base material.

3.5 Testing Procedures

Prior to testing, each specimen had several strain gauges mounted near the weld toes. Strain gauges were mounted in pairs on either side of the specimens so that both the axial and bending components of both the applied and induced stresses could be measured. Specimens were mounted in a 100 kip MTS frame and gripped using self-aligning hydraulic grips: see Fig. 3-14. The stresses generated during the gripping of each specimen were minimized by the self-aligning feature of the grips, but some bending stresses were induced which were measured with the strain gauges and recorded.

Each test was begun by applying one cycle of the largest stress cycle of the variable ship block history. During this first cycle, the (induced)

39

cyclic bending stresses were measured and recorded. Generally, both the gripping and induced cyclic bending stresses were quite large because Detail No. 20 inevitably experienced welding distortions during fabrication due to the nature of the joint and because of the welding procedure used. These inevitable variations in geometry and the differences in resulting stress state due to the differing amounts of induced gripping (mean stress) and cyclic bending stresses requires one to think of each test as being unique despite the intended similarity of the testpieces and despite the fact that they were all subjected to identical applied stress histories.

Following the initial static application of the largest cycle of the block, the block shown in Fig. 3-6 was repeated over and over until the specimen failed or until 1,500 blocks had been applied. Despite the elimination of the stress ranges less than 68.9 MPa (10 ksi) and the inclusion of all cycles up to 152 MPa (22 ksi), that is 92.8% of the damage inferred by the I-P model, most specimens of Detail No. 20 (K_{fmax} – 4-5) endured between 150 and 1,500 blocks of the history or an equivalent service life of 12.5 to 125 years. Except for the cruciform weldments, we did not alter the amplifier gain settings to increase the stress range of each cycle of the block since this change would have altered the nature of the history and effectively "re-edited" the history. Likewise, using a weldment with a higher stress concentration would also have altered the (effective) notch-root stress history. Thus, to avoid any change in the notch-root history during the program, neither the amplitudes of the block loading nor the severity of the stress concentrator were altered. (In fact, the histories experienced by the different thickness specimens of this study were probably not identical because of differing levels of stress concentration resulting from differences in size.) The entire program, therefore, involved rather long term tests (1.7 to 17 days at 5 Hz.). It was questionable at first whether or not the block history would fail the specimens in a manageable length of time or, indeed, at all.

Tests were terminated when the specimens exhibited excessive deformations or after the application of 1,500 blocks. The mean stress was zero for most tests, but several levels of tensile mean stress were applied to study the effect of mean stress on the specimen fatigue life. Because of the very long lives exhibited by the zero mean stress specimens, it was not

40

possible to run tests using compressive mean stresses without altering the testing conditions or further lengthening the tests, as discussed above. Thirty-two specimens were tested.

Following testing, each specimen was sectioned to measure the dimensions of the IJP and to study the pattern of fatigue initiation and propagation. Figures 3-15 and 3-16 show the patterns of failure observed. The presence of the IJP greatly complicated the failure pattern because there was almost simultaneous initiation and growth from both the weld toe and the IJP. There were two basic patterns of failure: IJP domination and toe domination.

In the rare cases in which the induced gripping and cyclic bending stresses were small, failure initiated at the most serious stress concentrator, the IJP; and a reasonably easy to interpret series of events occurred. The fatigue crack initiated at both sides of the IJP and propagated to failure as shown in the upper photo of Fig. 3-15 and in the sketch of Fig. 3-16.

When the induced bending stresses were larger, fatigue cracks initiated at both the weld toe having the greatest applied bending stress and at both the IJP notches. Because there is an interaction between the toes and the IJP resulting in a higher stress concentration at each, initiation and growth at both the toe and nearest IJP tip accelerated growth at both sites. However, continued fatigue crack growth at the active toe ultimately reduced the stresses at the nearest IJP tip causing fatigue crack growth there to cease. Because of changes in the directions of the principal stresses or because of inclusions in the steel or the presence of the large IJP (or both) the toe crack inevitably did not progress directly across the plate thickness toward the opposing toe but curved "downward" toward the IJP and, just before intersecting the IJP, a small limit-load failure occurred linking the toe crack with the IJP. At this point, the fatigue crack growth at the opposite IJP tip was greatly accelerated; and failure occurred soon after (see Fig. 3-15 (bottom) and Fig. 3-17).

3.6 Test Results and Discussion

The test results are listed in Table 3-7 through 3-11. Table 3-7 contains the test results for the three 25.4 mm (1-in.) thick specimens of Detail No. 20. Table 3-8 contains the test results for the thirteen 12.7 mm (1/2-in.) thick specimens of Detail No. 20. Table 3-9 contains the test results for the eight 6.35 mm (1/4-in.) specimens of Detail No. 20. Table 3-10 contains the results for the six specimens of Detail No. 20 (25.4 mm, 12.7 mm and 6.35 mm thicknesses) which were modified by machining off the wrap-around portion of the weldment to convert these specimens to a cruciform weldment (see Fig. 3-13). Table 3-11 lists the results for the five additional cruciform weldments fabricated using GMAW welding process and in the manner sketched in Fig. 3-12. Each table contains the blocks to failure, the location(s) on the specimen at which failure originated (F) or at which a fatigue crack was observed to initiate but not propagate to failure (I). As sketched in Fig. 3-11, there were six possible fatigue crack initiation sites for Detail No. 20: four weld toes (TOE 1-4) and two incomplete joint penetrations (IJP 1-3 and IJP 2-4). The dimensions of the weld toes and the length of the IJPs are listed for each as well as the applied mean stress, induced gripping stress and the bending factor x (the ratio of the induced cyclic bending stress range to the total cyclic stress range measured on the surface of the plate near the weld toe).

3.7 Task 2 - Long Life Variable Load History

Inasmuch as the life which the specimens lasted was not controlled or altered except by the imposition of a mean stress and because more than half of the specimens tested lasted longer than the 20 year design life (290 blocks), all of the specimens tested have been used to assess the ability of the prediction methods to estimate the long life behavior of weldments under a variable load ship history at long lives. This topic is dealt with in Section 4.

3.8 Task 3 - Mean Stress Effects

This task presented the first technical problem. Because of the long life sustained by most specimens, it was not feasible to determine the in-

fluence of compressive mean stresses because they would have further lengthened the already long fatigue life observed under zero applied mean stress. As a consequence, only tensile mean stresses were used, and these had to be limited to a maximum value of 145 MPa (21 ksi) to avoid general yielding of the testpieces.

During this study it was realized that all aspects of the geometry of Detail No. 20 (which contained an IJP) were in fact not completely defined for the purpose of Task 3. If the gap height of the IJP was greater than zero as a result of a root gap, then the IJP would be fully effective as a stress concentrator for load histories having zero and compressive minimum loads. If on the other hand, the IJP had zero height due to perfect fit-up, then the IJP would behave differently for load histories having tensile rather than zero or compressive minimum loads. In effect, if the IJP contributed to or controlled the fatigue behavior of the Detail No. 20, the nature of the Detail No. 20 would vary with testing conditions unless the fit-up was greater than zero or unless the IJP was eliminated. To avoid this uncertainty, the welding fabrication procedures were altered to ensure IJP with a definite height. This practice lead to other problems: increased joint distortion; and variable IJP width (2c), see Fig. 3-11, due to varying penetration or incomplete fusion in the areas of the tack welds (which were welded over and not ground out).

Despite the mentioned difficulties, a definite effect of mean stress was observed. Figure 3-18 shows the observed total fatigue lives as a function of applied mean stress for all (unmodified) 12.7 mm (1/2-in.) and 6.35 mm (1/4-in.) specimens of Detail No. 20. While there is some scatter, it is clear that applied tensile mean stresses reduce the expected fatigue life. The largest effect seen in Fig. 3-18 is about a factor of three.

The applied mean stress is by no means a complete representation of the mean stresses experienced by the fatigue crack initiation sites in a weldment. In addition to the applied mean stresses are the bending mean stresses induced by gripping the specimens. As seen in Table 3-7 to 3-11, the gripping stresses were often larger than the applied mean stresses. Consequently, a more rational approach to the effect of mean stresses is to consider the combined effect of the applied tensile mean stress and the bending mean stresses induced by gripping and bending of the specimens. The

43

value of the local mean stresses resulting from the applied and gripping mean stresses after the first application of the largest stress range was determined using a "set-up cycle" analysis similar to that described in Appendix A (Section A-3), and the values resulting from this analysis for both the critical toe and IJP of each specimen are plotted in Fig. 3-19. Only the values for failure sites with the highest mean stress are plotted in Fig. 3-20. The local mean stresses can be higher than the static yield because of work hardening resulting from notch-root plasticity during the set-up cycle. These two figures show a strong correlation between the level of local (notch-root) mean stress and total fatigue life.

Of course, the above analysis neglects the fact that in addition to the constant induced mean stresses, specimens differ from one another by the fact that each has a different level of induced cyclic bending stress. (Differences in geometry between specimens are presumably taken into account by the individual K_{fmax} values calculated from the actual specimen geometry.) To provide the best possible comparison of the combined effects of mean stress and the applied and induced cyclic stresses, the Smith-Watson-Topper (SWT) parameter [3-4] was calculated from the set-up cycle analysis mentioned above using the applied and induced cyclic stresses for the most damaging stress range (see Figs. 3-5and A-10). SWT parameter reflects the combined effects of maximum real stress level (σ_{max}) and total strain amplitude ($\Delta\varepsilon/2$) as:

$$\{\sigma_{max} \cdot \Delta\varepsilon/2 \cdot E\}^{1/2} \qquad \text{(SWT)} \qquad (3-2)$$

Values of the SWT are plotted for each of the potential toe and IJP fatigue crack initiation sites in Fig. 3-21. Only the locations giving the highest values of SWT are plotted in Fig. 3-22. A good correlation between the SWT and the total fatigue life is seen confirming the essential validity of the local strain approach in dealing with this complex phenomenon.

3.9 Task 4 - Thickness Effects

Predictions of fatigue life based both on fatigue crack propagation and fatigue crack initiation suggest that smaller weldments should give longer lives than larger weldments. This difference is caused by the stress grad-

ients which are smaller in the larger specimens relative to the fatigue process itself which is not scale dependent. Recent tests on large weldments have also confirmed this effect particularly for the very large weldments used in offshore construction [3-5].

Gurney [3-6] recently quantified the thickness effect based on experimental results by the relationships:

$$S = S_B (\frac{32}{t})^{1/4} \qquad \text{for tubular joints} \qquad (3-3)$$

$$S = S_B (\frac{22}{t})^{1/4} \qquad \text{for non-tubular joints} \qquad (3-4)$$

Where S is the design stress for a thickness t (in mm), S_B is the fatigue strength read from the relevant basic design curve.

Smith [3-7] calculated the fatigue crack propagation lives of three welds using linear fracture mechanics and made predictions of the thickness effect on the fatigue strength. For geometrically similar joints, Smith expressed the variation in fatigue strength with plate thickness as:

$$\frac{S_1}{S_2} = (\frac{t_1}{t_2})^n \qquad (3-5)$$

where S_1 is the predicted fatigue strength for thickness t_1 and S_2 is the predicted fatigue strength for thickness t_2. Smith indicates the value n for t < 22 mm appears to be less than that for t > 22 mm.

The total fatigue life model can be used to predict the relative fatigue strength for different joints. Assuming that the total life is essentially equal to the initiation life in the high cycle regime, the predicted effect of weldment size should be estimated by the expression below for constant amplitude loading conditions.

$$\frac{S_1}{S_2} = (\frac{K_{fmax1}}{K_{fmax2}}) \qquad (3-6)$$

45

where S_1 is the predicted fatigue strength for K_{fmax1} of thickness t_1 and S_2 is the predicted fatigue strength for K_{fmax2} of thickness t_2. As discussed in Section A-2.5, the factor $K_{f\ max}$ is a function of plate thickness, loading mode, type of joints and material properties of HAZ. Therefore, the relative fatigue strength depends on these four parameters too, i.e., $S_1/S_2 = f(t, \alpha, S_u)$.

The predictions of thickness effect made using Eq. 3-6 have been compared with Gurney's experimental results [3-6] and plotted in Figs. 3-23 and 3-24. Predictions made using Eq. 3-6 agree with Gurney's experimental results for t < 50 mm. More test results are needed to verify the predictions for t > 50 mm. In Fig. 3-23 predictions for full penetration butt weld and cruciform joints made using K_{fmax} factor and Eq. 3-6 have also been compared with Smith's predictions [3-7] and Gurney's relationship, Eqs. 3-3, 3-4 and 3-5. Generally, predictions made by the I-P model agree with Gurney's formula. Smith's results are at variance with Gurney's experimentally derived slope of n = 1/4. The above comparisons are for welds subjected to constant amplitude loading conditions. For weldments subjected to variable amplitude loading, fatigue crack propagation will become dominant, and Smith's predictions of thickness effect on fatigue strength might be better.

Smith [3-7] has also shown that the relative attachment size has an effect on the fatigue strength of full penetration welds: increasing total attachment size and length decreases fatigue strength at constant plate thickness, and this effect depends upon the joint and its loading mode. The larger the relative attachment size, the bigger is the K_t at the weld toe. This effect will increase the K_{fmax} value and reduce the fatigue strength. The relative fatigue strength of any set of weld details will depend on the competing "thickness" and "attachment" effects. Usually weld size does not increase proportionally to the plate thickness for thick welds, and the two effects may offset each other. For load carrying fillet welds, size of lack of penetration and the relative weld leg length instead of attachment size will become important.

To confirm the thickneses effect for Detail No. 20, three different thickness specimens were fabricated having geometrically similar proportions: see Fig. 3-10. One problem in maintaining strict similitude resulted from the maintenance of constant plate width (76 mm - see Fig. 3-9)

and the wrap-around weld. This condition violated exact similtude require-
ments for a fully valid comparison of the 25.4 mm (1-in.), 12.7 mm (1/2-
in.), and 6.35 mm (1/4-in.) plate thickness testpieces. This error was
corrected by machining the wrap-around welds off several of the Detail No.
20 specimens: see Fig. 3-12. These specimens are termed modified Detail
No. 20, and their test results are listed in Table 3-10. The results of
this study are plotted in Fig. 3-25. If one confines one's attention to the
cruciform weldments for which similtude is maintained, there seems to be a
slight size effect. However the data is unconvincing, and the effect is
smaller than anticipated by the I-P model which predicts that there should
be a much stronger effect.

3.10 References

3-1   Fain, R.A. and Booth, E. T., "Results of the First Five Data Years of
      Extreme Scratch Gauge Data Collected Aboard Sea Land's SL-7/s," SSC-
      286, Ship Structure Committee, March 1979.

3-2   Wirsching, P.H., "Digital Simulation of Fatigue Damage in Offshore
      Structures," presented at the 1980 ASME Winter Annual Meeting and
      published in the Symposium Proceedings, Computational Method for Off-
      shore Structure, ASME, 1980.

3-3   Quarterly Progress Report of SSC 512-1297, "Fatigue Prediction Analy-
      sis Validation from SL-7 Hatch-Corner Strain Data," American Bureau of
      Shipping, 1984.

3-4   Smith, K.N., Watson, P., and Topper, T.H., "A Stress-Strain Function
      for the Fatigue of Metals," Journal of Materials, JMLSA, Vol. 5, No.
      4, Dec. 1970, pp. 767-778.

3-5   Hicks, J.G., "Modified Design Rules for Fatigue Performance of
      Offshore Structures," Welding in Energy Related Projects, Welding
      Institute of Canada, Pergamon Press, 1984, pp. 467-475.

3-6   Gurney, T.R., "Revised Fatigue Design Rules," Metal Construction, Vol.
      15, No. 1, 1983, pp. 37-44.

3-7   Smith, I.J., "The Effect of Geometry Change upon the Predicted Fatigue
      Strength of Welded Joints," Proceedings of the 3rd International Con-
      ference on Numerical Methods in Fracture Mechanics, Pineridge Press,
      1984, pp. 561-574.

5.17673492431E-02	3.22058902168E-02	1.57721527306E-02	3.23509173047E-02
3.74662703404E-02	1.89246268702E-02	3.68536876702E-02	3.00927238029E-02
0.019807517951000	0.019761346905000	7.44424451444E-02	1.52456813275E-02
1.62834288305E-02	4.46823403496E-02	7.10674926784E-02	4.07290599555E-02
1.34468521037E-02	3.05874437251E-02	3.06786354967E-02	1.84655604724E-02
2.58427957198E-02	2.15202162837E-02	1.29474725255E-02	1.73265105765E-02
3.70424463217E-02	3.43541396905E-02	0.031437691886000	2.37226916175E-02
2.27676434551E-02	3.30124875812E-02	2.67509629733E-02	1.23441798512E-02
1.51804873044E-02	2.49440464768E-02	1.34019161525E-02	1.93333877062E-02
1.49198681709E-02	1.05650198229E-02	1.14994444552E-02	2.09251469318E-02
1.03975250314E-02	1.98022591372E-02	3.37054926773E-02	2.52680994611E-02
1.82231169029E-02	3.14604290933E-02	2.21440662747E-02	0.033809801317000
5.74272558506E-02	5.38969723932E-02	0.104321726308000	8.69690624085E-02
8.36295273292E-03	6.50614528806E-02	8.34987892481E-02	6.18186062167E-02
9.95815140972E-03	2.57123660992E-02	1.24588293013E-02	2.07800617231E-02
2.07475076377E-02	0.049956192555000	3.24697908397E-02	1.66681148664E-02
8.42570144844E-02	0.103612513964000	1.95608856931E-02	4.02673838814E-02
4.15096393058E-02	1.33494447936E-02	0.019575880280000	3.69816800334E-02
2.91372749027E-02	5.71040813804E-03	1.16630372836E-02	2.39670586768E-02
3.95242418401E-02	6.08087870905E-02	4.44028561052E-02	1.86249409196E-02
0.019011370819000	3.05223579839E-02	1.51874112626E-02	1.67272770001E-02
1.96097610434E-02	2.13350691468E-02	0.038574789328000	3.48534305327E-02
2.03773847595E-02	1.92169410198E-02	3.43206173918E-03	2.49348268544E-02
2.01998396087E-02	8.98757976537E-03	1.88548283434E-02	1.65593407151E-02
1.79855536506E-03	3.94377159310E-03	0.026383664864000	3.24478230138E-02
2.11080074099E-02	2.16143639601E-02	2.42137959457E-02	1.18094673259E-02
0.011592754538000	1.84368044318E-02	2.01192882379E-02	6.62485760888E-04
2.27900362961E-02	2.32772902361E-02	1.28073654683E-02	0.011933388874000
9.06058159637E-03	4.34738439397E-03	9.85035465545E-03	9.67517113154E-03
2.90191083219E-03	8.48833961713E-03	1.20584728651E-02	9.35162249726E-03
8.46434906093E-03	8.42716931577E-03	9.73653184998E-03	4.95064638056E-03
5.40684680195E-03	3.16056215376E-03	2.94342010793E-03	8.11421976878E-03
1.13566438405E-02	1.17603520738E-02	4.01833635578E-03	7.34789518295E-03
1.62856432436E-02	2.10826953537E-02	1.16506113504E-02	7.35073196145E-03
8.06713561201E-03	4.75529212036E-03	1.38854980472E-03	6.68277599638E-03
5.43251565820E-03	3.46853000877E-03	8.08328286375E-03	4.03657331222E-03
8.96969748239E-03	1.55032158651E-02	1.56170874666E-02	4.60619630256E-03
2.11837434379E-03	3.93038332011E-03	7.18809441194E-03	1.31844606905E-02
9.32200639007E-03	5.73352659393E-03	7.46283837027E-03	7.20299699601E-03
1.07520820662E-02	1.13195107517E-02	0.012866924460000	6.61388217329E-03
4.48493584141E-03	3.25539923551E-03	6.00988302936E-03	7.43924676607E-03
7.01100755446E-03	5.96621465002E-03	1.74179698386E-03	3.69819492944E-03
3.92596107099E-03	0.004289347575000	4.78803015548E-03	1.02082973918E-02
1.28936241452E-02	9.25427395288E-03	6.27878275924E-03	8.71081505703E-03
3.16986242884E-03	3.61904513779E-03	6.78447635436E-03	3.61952711237E-03
4.72427078819E-03	2.99495880903E-03	3.05513329450E-03	1.22676078385E-03
4.32008696933E-03	6.62408148565E-03	6.99614737925E-03	3.32722154203E-03
6.12772194635E-03	4.62959662733E-03	2.85478585126E-04	6.92621190286E-03
8.91359106615E-03	5.49297597351E-03	6.72499996734E-03	4.34714337656E-03
6.87819709165E-03	5.30783871846E-03	2.01379730375E-03	3.47522898880E-03
2.57764566420E-03	1.84336354656E-03	3.66934419282E-03	3.73785869262E-03
2.59447725174E-03	1.65792378214E-03	1.51223873657E-03	4.20741589349E-03

Table 3-1

Spectral Ordinates from FFT Analyzer (in Volts) [3-3].

1.04017832923E-04	2.72500258212E-03	2.24014062366E-03	4.772381 81 877E-03
3.74462248404E-03	3.84251949421E-03	2.57238728270E-03	2.36495117738E-03
3.06043137590E-03	3.73249170429E-03	4.12509276499E-03	5.57571477737E-03
7.02311572014E-03	3.36975448218E-03	1.27112632385E-03	2.66478940946E-03
5.77691348796E-03	5.66972334563E-03	2.48950922191E-03	2.55528015219E-03
4.30237143542E-03	2.70251947223E-03	1.22787068219E-03	3.75496833837E-03
3.92027556937E-03	4.09058483141E-03	2.34696921877E-03	2.85478006420E-03
4.53769584280E-03	5.68407929448E-03	1.74878387927E-03	1.47277978435E-03
1.27940287806E-03	2.94630746433E-03	3.20871897918E-03	4.20257339421E-03
4.09577506140E-03	2.20414251159E-03	1.82322177789E-03	2.18892979453E-03
2.15573855126E-03	3.55800317386E-03	2.22023169606E-03	8.04476151210E-04
1.03499281920E-03	1.38445331297E-03	1.03048073587E-03	4.13772459496E-03

Table 3-2

Fatigue Cracked Structural Details
Ordered by Incidence of Reported Cracks

Detail No.*	Total No. of Detail Classifications at Cracks	Fatigue Data Available	Evaluation of Fatigue Data A, B, C, D	Suggested Priority of Fatigue Tests
21	1300	Yes	D	10
51	687	Yes	C	
30A	672	Yes	B	
36	600	Yes	B	
37	462	No		1
20	318	Yes	B	
7	272	Yes	A	
28F	222	Yes	D	11
28	208	Yes	A	
26	155	Yes	C	
52	105	Yes	C	
* 43	75	No		2
21S	54	Yes	C	
19	42	Yes	B	
19S	40	Yes	C	
33	36	Yes	B	
* 47	29	No		3
* 34	23	No		4
33S	20	Yes		5
34S	17	No		6
* 44	14	No		7
41	11	No		8
29	9	No		9
38	8	Yes	D	
53	8	No		
9	7	Yes	A	
14	7	Yes	B	
29F	7	No		
42	7	Yes	A	

*: indicates a weld detail tested in this program.

Table 3-3

Material Properties of the ASTM A36 Steel
Used for the Specimens of Ship Structural Details under Constant
As Meeting ASTM A131 Grade A

Material Description	Plate Thickness (mm)	Yield Strength MPa (ksi)	Tensile Strength MPa (ksi)	C,(a)	Chemistry (%) Mn	P	S
ASTM A131 Gr. A Specifications		234 Min. (34)	400 to 489 (58 to 71)	.23,(b) Max.	(c)	.05 Max.	.05 Max.
Actual properties of	6.4	332 (48.2)	450 (65.3)	.086	.971	.024	.017
ASTM A-36 material	7.9	335 (48.6)	460 (66.7)	.153	.531	.016	.010
used in this study	12.7	310 (45.0)	488 (70.8)	.24	.69	.021	.011
as meeting ASTM 131	15.9	304 (44.1)	441 (64.0)	.14	.94	.026	.018
Grade A	25.4	285 (41.3)	441 (64.0)	.14	.94	.026	.018
	31.8	294 (42.6)	455 (66.0)	.17	.89	.014	.024

(a) ; For all ordinary strength grades, the carbon content plus 1/6 of Mn content shall not exceed 0.40 %.
(b) ; A maximum carbon content of 0.26 % is acceptable for Grade A plates equal to or less than 12.7 mm.
(c) ; Grade A plates over 12.7 mm thick shall have a minimum Mn content not less than 2.5 times the carbon content.

Table 3-4

Welding Parameters and Material Properties of ASTM A441 Gr. 50 Plate
Used For Specimen Preparation of the Cruciform Joints

Welding Parameters

Voltage:	31 V.
Current:	300 AMP.
Wire Speed:	255 in./min.
Travel Speed:	12 in./min.
Filler Wire:	1/16 in. Dia. E70 wire
Shielding Gas:	Argon with 2% Oxygen

Mechanical Properties

Material	Yield Strength ksi	Ultimate Tensile Strength ksi	Elongation %
ASTM A131 Gr. AH36 Specifications	51 min.	71 - 90	19.0 min.
ASTM A441 Gr. 50 Used	62	83	21.0 - 203

Chemical Analysis (%)

Material	C	Mn	P	S	Si	Va	Cu
A131 Gr. AH36 Specification	.18 max.	.9 - 1.6	.04 max.	.04 max.	.1 - .5	.10 max.	.35 max.
A441 Gr. 50 Used	.15	1.10	.01	.019	.231	.029	.216

Table 3-5

Estimated Fatigue Properties of 25.4 mm (1-in.),
12.7 mm (1/2-in.) and 6.35 mm (1/4-in.) Thick
Specimens of Detail No. 20

| Material Property | 25.4 mm | | 12.7 mm | | 6.35 mm | |
	W.M.	HAZ.	W.M.	HAZ.	W.M.	HAZ.
Ultimate Strength, ksi, S_u	94.5	111.7	113.4	123.2	113.0	113.8
Cyclic Yield Strength, ksi, σ'_y	57.5	67.9	68.9	74.9	68.7	69.2
Fatigue Strength Exponent, b	-.0908	-.862	-.0858	-.0840	-.0859	-.0857
Fatigue Ductility Exponent, c	-.60	-.60	-.60	-.60	-.60	-.60
Cyclic Hardening Exponent, n'	.151	.144	.143	.140	.143	.143
Cyclic Strength Coefficient, ksi, K'	145.9	172.5	175.1	190.3	174.5	175.8
Fatigue Strength Coefficient, ksi, σ'_f	144.2	161.7	162.3	171.7	161.9	162.7
Residual Stress, ksi, σ_r	42.0	42.0	45.0	45.0	48.2	48.2

Table 3-6

Estimated Fatigue Properties of 12.7 mm (1/2-in.) Thick Specimens of Cruciform Joints by GMAW Process

Material Property	W.M.	HAZ.
Ultimate Strength, ksi, S_u	122.5	125.0
Cyclic Yield Strength, ksi, σ'_y	74.6	76.1
Fatigue Strength Exponent, b	-.0839	-.0834
Fatigue Ductility Exponent, c	-.60	-.60
Cyclic Hardening Exponent, n'	.140	.139
Cyclic Strength Coefficient, ksi, K'	189.5	193.3
Fatigue Strength Coefficient, ksi, σ'_f	172.5	175.0
Residual Stress, ksi, σ_r	53.6	53.6

Table 3-7

Loading Condition and Weld Geometry for 25.4mm (1-in.)
Specimens of Structural Detail No. 20.

Spec. No.	Site	Applied Mean Stress (ksi)	Induced Grip Stress (ksi)	Bending Factor (x)	Geometry[+] L1	L2	c (in.)	Failure Sites[*]	Fatigue Life (Blocks)
T-1	IJP 1-3	0.0	0.0	-0.39	.675	.727	.500		304
	TOE 1	0.0	0.0	-0.39	.675	.727	.500		
	TOE 3	0.0	0.4	0.54	.686	.815	.500		
	IJP 2-4	0.0	1.2	0.54	.742	.705	.500		
	TOE 2	0.0	-1.9	-0.44	.879	.819	.500		
	TOE 4	0.0	1.2	0.54	.742	.705	.500	F	
T-2	IJP 1-3	0.0	30.0	0.12	.824	.810	.500		1118
	TOE 1	0.0	30.0	0.12	.824	.810	.500		(Stopped)
	TOE 3	0.0	-29.7	0.00	.730	.812	.500		
	IJP 2-4	0.0	-25.2	-0.02	.798	.846	.500	I	
	TOE 2	0.0	26.7	0.01	.750	.888	.500		
	TOE 4	0.0	-25.2	-0.02	.798	.846	.500		
T-3	IJP 1-3	0.0	2.90	0.44	.650	.717	.500		1203
	TOE 1	0.0	-2.80	-0.35	.765	.750	.500		
	TOE 3	0.0	-2.90	0.44	.650	.717	.500		
	IJP 2-4	0.0	-3.60	-0.43	.853	.718	.500	F	
	TOE 2	0.0	-3.60	-0.43	.853	.718	.500		
	TOE 4	0.0	3.70	0.37	.646	.829	.500	F	

+ See Fig. 3-11.

* F denotes a site causing fatigue failure.
  I denotes a site initiating a fatigue crack but not involved in the final fatigue failure.

Table 3-8

Loading Condition and Weldment Geometry for 12.7 mm (1/2-in.)
Specimens of Structural Detail No. 20

Spec. No.	Site	Applied Mean Stress (ksi)	Induced Grip Stress (ksi)	Bending Factor (x)	Geometry[+] L1	L2 (in.)	c	Failure Sites[*]	Fatigue Life (Blocks)
H-1	IJP 1-3	0.00	2.06	0.02	.304	.404	.250	F	926
	TOE 1	0.00	2.06	0.02	.304	.404	.250		
	TOE 3	0.00	-1.60	0.06	.369	.436	.250		
	IJP 2-4	0.00	0.67	0.14	.400	.408	.238		
	TOE 2	0.00	0.67	0.14	.400	.408	.238		
	TOE 4	0.00	-0.30	-0.13	.412	.445	.238		
H-2	IJP 1-3	0.00	3.70	0.14	.330	.370	.250		769
	TOE 1	0.00	3.70	0.14	.330	.370	.250		
	TOE 3	0.00	-5.4	0.02	.348	.375	.250		
	IJP 2-4	0.00	5.6	-0.25	.453	.411	.241	F	
	TOE 2	0.00	5.6	-0.25	.453	.411	.241		
	TOE 4	0.00	-5.4	-0.34	.357	.409	.241		
H-3	IJP 1-3	0.00	6.2	0.19	.365	.398	.245	F	1291
	TOE 1	0.00	-5.7	-0.10	.455	.439	.245		
	TOE 3	0.00	6.2	0.19	.365	.398	.245		
	IJP 2-4	0.00	-4.5	-0.03	.461	.425	.250		
	TOE 2	0.00	-4.5	-0.03	.461	.425	.250		
	TOE 4	0.00	5.4	-0.01	.355	.450	.250		
H-4	IJP 1-3	0.00	6.3	-0.03	.350	.434	.246		1414
	TOE 1	0.00	6.3	-0.03	.350	.434	.246		
	TOE 3	0.00	-0.2	-0.30	.342	.450	.246		
	IJP 2-4	0.00	-1.9	0.01	.375	.368	.234	F	
	TOE 2	0.00	2.1	0.06	.391	.393	.234		
	TOE 4	0.00	-1.9	0.01	.375	.393	.234		
H-5	IJP 1-3	0.00	-18.7	0.0	.367	.453	.250	I	416
	TOE 1	0.00	-18.7	0.0	.367	.453	.250		
	TOE 3	0.00	17.7	0.16	.378	.472	.250		
	IJP 2-4	0.00	-14.9	0.0	.350	.433	.250	I	
	TOE 2	0.00	-14.9	0.0	.350	.433	.250		
	TOE 4	0.00	14.8	0.13	.369	.492	.250	F	

+ See Fig. 3-11.

* F denotes a site causing fatigue failure.
  I denotes a site initiating a fatigue crack but not involved in the final fatigue failure.

Table 3-8 (continued)

Spec. No.	Site	Applied Mean Stress (ksi)	Induced Grip Stress (ksi)	Bending Factor (x)	Geometry[+] L1	L2	c (in.)	Failure Sites[*]	Fatigue Life (Blocks)
H-6	IJP 1-3	0.00	29.5	0.23	.370	.413	.250		303
	TOE 1	0.00	29.5	0.23	.370	.413	.250		
	TOE 3	0.00	-28.4	-0.06	.351	.472	.250		
	IJP 2-4	0.00	-27.5	-0.01	.265	.433	.250	F	
	TOE 2	0.00	27.0	0.14	.353	.531	.250	F	
	TOE 4	0.00	-27.5	-0.01	.265	.433	.250		
H-7	IJP 1-3	10.5	-0.8	-0.08	.480	.421	.223	F	269
	TOE 1	10.5	2.3	0.15	.335	.400	.223	F	
	TOE 3	10.5	-0.8	-0.08	.480	.421	.223		
	IJP 2-4	10.5	2.0	0.12	.463	.448	.234	I	
	TOE 2	10.5	2.0	0.12	.463	.448	.234		
	TOE 4	10.5	-0.6	-0.08	.384	.450	.234		
H-8	IJP 1-3	10.5	17.1	-0.05	.405	.406	.230	I	207
	TOE 1	10.5	-14.8	0.22	.345	.446	.230		
	TOE 3	10.5	17.1	-0.05	.405	.406	.230		
	IJP 2-4	10.5	-16.3	0.07	.439	.429	.214	F	
	TOE 2	10.5	-16.3	0.07	.439	.429	.214		
	TOE 4	10.5	20.5	0.39	.353	.450	.214	F	
H-9	IJP 1-3	10.5	-2.9	0.07	.339	.438	.250	F	678
	TOE 1	10.5	5.2	-0.22	.333	.473	.250		
	TOE 3	10.5	-2.9	0.07	.339	.483	.250	F	
	IJP 2-4	10.5	-4.4	-0.07	.402	.434	.233		
	TOE 2	10.5	4.4	0.08	.378	.467	.233		
	TOE 4	10.5	-4.4	-0.07	.402	.467	.233		
H-10	IJP 1-3	10.5	-5.6	0.08	.428	.467	.234	F	211
	TOE 1	10.5	-5.6	0.08	.428	.467	.234		
	TOE 3	10.5	5.9	-0.04	.346	.483	.234	F	
	IJP 2-4	10.5	-9.3	0.01	.334	.386	.246	I	
	TOE 2	10.5	-9.3	0.01	.334	.386	.246		
	TOE 4	10.5	9.8	0.05	.360	.510	.246		
H-11	IJP 1-3	21.0	3.3	0.12	.355	.381	.245	F	232
	TOE 1	21.0	3.3	0.12	.355	.381	.245	F	
	TOE 3	21.0	-1.5	-0.04	.375	.387	.245		
	IJP 2-4	21.0	1.0	0.05	.365	.404	.248	I	
	TOE 2	21.0	1.0	0.05	.365	.404	.248	I	
	TOE 4	21.0	1.7	-0.09	.325	.420	.248		

+ See Fig. 3-11.

* F denotes a site causing fatigue failure.
 I denotes a site initiating a fatigue crack but not involved in the final fatigue failure.

Table 3-8 (continued)

Spec. No.	Site	Applied Mean Stress (ksi)	Induced Grip Stress (ksi)	Bending Factor (x)	Geometry[+] L1	L2 (in.)	c	Failure Sites[*]	Fatigue Life (Blocks)
H-12	IJP 1-3	21.0	-13.4	0.12	.425	.410	.244	F	184
	TOE 1	21.0	14.8	-0.07	.356	.460	.244	F	
	TOE 3	21.0	-13.4	0.12	.425	.410	.244		
	IJP 2-4	21.0	-7.87	0.14	.451	.388	.250	F	
	TOE 2	21.0	8.8	0.01	.412	.412	.250		
	TOE 4	21.0	-7.87	0.14	.451	.388	.250		
H-13	IJP 1-3	21.0	15.4	0.08	.350	.401	.233	F	173
	TOE 1	21.0	-12.9	0.17	.336	.463	.233		
	TOE 3	21.0	15.4	0.08	.350	.401	.233	I	
	IJP 2-4	21.0	-4.73	0.28	.396	.431	.232		
	TOE 2	21.0	-4.73	0.28	.396	.431	.232		
	TOE 4	21.0	8.77	0.12	.328	.459	.232		

+ See Fig. 3-11.

* F denotes a site causing fatigue failure.
I denotes a site initiating a fatigue crack but not involved in the final fatigue failure.

Table 3-9

Loading Condition and Weldment Geometry for 6.35 mm (1/2-in.)
Specimens of Structural Detail No. 20

Spec. No.	Site	Applied Mean Stress (ksi)	Induced Grip Stress (ksi)	Bending Factor (x)	Geometry[+] L1	L2 (in.)	c	Failure Sites[*]	Fatigue Life (Blocks)
Q-1	IJP 1-3	10.5	-12.8	0.09	.184	.188	.125	F	306
	TOE 1	10.5	15.3	0.21	.139	.234	.125	F	
	TOE 3	10.5	-12.8	0.09	.184	.188	.125		
	IJP 2-4	10.5	13.0	0.16	.182	.172	.125		
	TOE 2	10.5	13.0	0.16	.182	.172	.125		
	TOE 4	10.5	-10.6	0.17	.183	.203	.125		
Q-2	IJP 1-3	10.5	30.6	0.17	.160	.219	.177	F	292
	TOE 1	10.5	-31.0	-0.12	.213	.234	.177		
	TOE 3	10.5	30.6	0.17	.160	.219	.177	F	
	IJP 2-4	10.5	-24.8	-0.06	.150	.234	.125		
	TOE 2	10.5	-24.8	-0.06	.150	.234	.125		
	TOE 4	10.5	24.1	0.12	.159	.266	.125		
Q-3	IJP 1-3	0.0	10.2	0.13	.168	.172	.125		787
	TOE 1	0.0	10.2	0.13	.168	.172	.125		
	TOE 3	0.0	-10.3	0.12	.163	.203	.125		
	IJP 2-4	0.0	-7.4	0.00	.196	.172	.125	F	
	TOE 2	0.0	7.2	0.21	.185	.188	.125		
	TOE 4	0.0	-7.4	0.00	.196	.172	.125		
Q-4	IJP 1-3	0.0	-7.2	0.03	.168	.172	.125	F	415
	TOE 1	0.0	-7.2	0.03	.168	.172	.125		
	TOE 3	0.0	6.2	0.28	.162	.203	.125	F	
	IJP 2-4	0.0	-8.2	0.18	.192	.188	.125		
	TOE 2	0.0	-8.2	0.18	.192	.188	.125		
	TOE 4	0.0	7.1	0.32	.200	.234	.125		
Q-5	IJP 1-3	0.0	9.7	0.23	.198	.188	.125		708
	TOE 1	0.0	9.7	0.23	.198	.188	.125	F	
	TOE 3	0.0	-9.2	0.00	.163	.203	.125		
	IJP 2-4	0.0	11.4	0.12	.200	.203	.125		
	TOE 2	0.0	11.4	0.12	.200	.203	.125		
	TOE 4	0.0	-10.9	0.00	.157	.219	.125		

+ See Fig. 3-11.

* F denotes a site causing fatigue failure.
   I denotes a site initiating a fatigue crack but not involved in the
   final fatigue failure.

Table 3-9 (continued)

Spec. No.	Site	Applied Mean Stress (ksi)	Induced Grip Stress (ksi)	Bending Factor (x)	Geometry[+] L1	L2 (in.)	c	Failure Sites[*]	Fatigue Life (Blocks)
Q-6	IJP 1-3	0.0	13.6	0.04	.217	.219	.125		369
	TOE 1	0.0	-13.0	0.14	.153	.219	.125		
	TOE 3	0.0	13.6	0.04	.217	.219	.125		
	IJP 2-4	0.0	7.57	0.23	.199	.216	.167	F	
	TOE 2	0.0	-6.97	-0.19	.151	.250	.167		
	TOE 4	0.0	7.57	0.23	.199	.216	.167	F	
Q-7	IJP 1-3	0.0	-7.7	-0.07	.179	.177	.125		267
	TOE 1	0.0	6.8	0.10	.200	.217	.125		
	TOE 3	0.0	-7.7	-0.07	.179	.177	.125		
	IJP 2-4	0.0	10.2	0.19	.206	.177	.125	F	
	TOE 2	0.0	10.2	0.19	.206	.177	.125	F	
	TOE 4	0.0	-10.6	-0.03	.160	.177	.125		
Q-8	IJP 1-3	0.0	-8.3	-0.07	.190	.203	.125	F	506
	TOE 1	0.0	8.0	0.19	.195	.219	.125	F	
	TOE 3	0.0	-8.3	-0.07	.190	.203	.125		
	IJP 2-4	0.0	4.2	0.12	.189	.211	.125		
	TOE 2	0.0	4.2	0.12	.189	.211	.125		
	TOE 4	0.0	-4.3	0.03	.127	.203	.125		

+   See Fig. 3-11.

*   F denotes a site causing fatigue failure.
I denotes a site initiating a fatigue crack but not involved in the final fatigue failure.

Table 3-10

Loading Condition and Weld Geometry for the Modified
Specimens of Structural Detail No. 20.

Spec. No.	Site	Applied Mean Stress (ksi)	Induced Grip Stress (ksi)	Bending Factor (x)	Geometry[+] L1	L2	c (in.)	Failure Sites[*]	Fatigue Life (Blocks)
C-1	IJP 1-3	0.0	4.2	0.19	.675	.768	.500	F	739
	TOE 1	0.0	-3.6	-0.05	.630	.905	.500		
	TOE 3	0.0	4.2	0.19	.675	.768	.500	F	
	IJP 2-4	0.0	-3.8	-0.17	.774	.748	.500		
	TOE 2	0.0	-3.8	-0.17	.774	.748	.500		
	TOE 4	0.0	4.0	0.03	.583	.748	.500		
C-2	IJP 1-3	0.0	11.1	0.16	.711	.777	.500		326
	TOE 1	0.0	-10.9	-0.05	.680	.807	.500		
	TOE 3	0.0	11.1	0.16	.711	.777	.500		
	IJP 2-4	0.0	-9.60	-0.10	.705	.847	.500	F	
	TOE 2	0.0	-9.60	-0.10	.705	.847	.500	F	
	TOE 4	0.0	10.1	0.13	.575	.881	.500	F	
C-3	IJP 1-3	0.0	29.7	-0.18	.331	.413	.250		252
	TOE 1	0.0	-29.2	0.20	.372	.433	.250		
	TOE 3	0.0	29.7	-0.18	.331	.413	.250		
	IJP 2-4	0.0	-29.5	-0.10	.359	.453	.250	F	
	TOE 2	0.0	-29.5	-0.10	.359	.453	.250		
	TOE 4	0.0	29.6	0.21	.333	.472	.250	F	
C-4	IJP 1-3	0.0	-24.6	0.27	.383	.394	.250	F	320
	TOE 1	0.0	-24.6	0.27	.383	.394	.250		
	TOE 3	0.0	24.3	0.02	.336	.492	.250	F	
	IJP 2-4	0.0	20.2	0.30	.385	.453	.250		
	TOE 2	0.0	-20.5	-0.19	.391	.453	.250		
	TOE 4	0.0	20.2	0.30	.385	.453	.250		
C-5	IJP 1-3	0.0	-8.4	0.01	.160	.188	.125	F	338
	TOE 1	0.0	8.3	0.15	.161	.219	.125	F	
	TOE 3	0.0	-8.4	0.01	.160	.188	.125		
	IJP 2-4	0.0	7.9	0.00	.164	.203	.125		
	TOE 2	0.0	7.9	0.00	.164	.203	.125		
	TOE 4	0.0	-7.3	-0.24	.161	.203	.125		

+ See Fig. 3-11.

* F denotes a site causing fatigue failure.
I denotes a site initiating a fatigue crack but not involved in the final fatigue failure.

61

Table 3-10 (Continued)

Spec. No.	Site	Applied Mean Stress (ksi)	Induced Grip Stress (ksi)	Bending Factor (x)	Geometry[+] L1	L2	c (in.)	Failure Sites[*]	Fatigue Life (Blocks)
C-6	IJP 1-3	0.0	15.0	0.17	.185	.203	.125	F	497
	TOE 1	0.0	15.0	0.17	.185	.203	.125	I	
	TOE 3	0.0	-14.5	0.04	.188	.297	.125		
	IJP 2-4	0.0	15.7	0.15	.160	.219	.125		
	TOE 2	0.0	15.7	0.15	.160	.219	.125		
	TOE 4	0.0	-15.5	0.05	.161	.234	.125		

+ See Fig. 3-11.

* F denotes a site causing fatigue failure.
  I denotes a site initiating a fatigue crack but not involved in the final fatigue failure.

Table 3-11

Loading Conditions and Weld Geometry for the 12.7 mm
(1/2-in.) Secimens of Cruciform Joint.

Spec. No.	Site	Applied Mean Stress (ksi)	Induced Grip Stress (ksi)	Bending Factor (x)	Geometry[+] L1	L2	c (in.)	Failure Sites[*]	Fatigue Life (Blocks)
M-1	IJP 1-3	12.3	5.23	0.15	.472	.354	.068	F	110
	TOE 1	12.3	5.23	0.15	.472	.354	.068		
	TOE 3	12.3	-1.13	0.12	.511	.394	.068		
	IJP 2-4	12.3	4.9	0.15	.472	.315	.038		
	TOE 2	12.3	4.9	0.15	.472	.315	.038		
	TOE 4	12.3	-0.08	0.11	.492	.354	.038		
M-2	IJP 1-3	9.0	3.43	0.16	.413	.295	.036		258
	TOE 1	9.0	3.43	0.16	.413	.295	.036		
	TOE 3	9.0	-1.87	0.13	.492	.315	.036		
	IJP 2-4	9.0	0.10	0.03	.413	.315	.056	F	
	TOE 2	9.0	1.40	0.06	.519	.335	.056		
	TOE 4	9.0	0.10	0.03	.413	.315	.056		
M-3	IJP 1-3	6.3	3.88	0.15	.394	.315	.042		345
	TOE 1	6.3	3.88	0.15	.394	.315	.042		
	TOE 3	6.3	-1.63	0.00	.472	.315	.042		
	IJP 2-4	6.3	1.80	0.07	.492	.295	.040	F	
	TOE 2	6.3	1.80	0.07	.492	.295	.040		
	TOE 4	6.3	0.23	0.17	.433	.315	.040		
M-4	IJP 1-3	3.0	2.30	0.18	.394	.276	.045		302
	TOE 1	3.0	2.30	0.18	.394	.276	.045		
	TOE 3	3.0	-1.30	-0.04	.413	.315	.045		
	IJP 2-4	3.0	1.10	0.03	.472	.276	.045	F	
	TOE 2	3.0	1.10	0.03	.472	.276	.045		
	TOE 4	3.0	-0.20	-0.12	.433	.354	.045		
M-5	IJP 1-3	0.0	1.27	0.09	.416	.295	.058		(stopped
	TOE 1	0.0	1.27	0.09	.416	.295	.058		by power
	TOE 3	0.0	-1.13	0.09	.472	.315	.058		failure
	IJP 2-4	0.0	2.67	0.08	.506	.275	.030	I	at 299
	TOE 2	0.0	2.67	0.08	.506	.275	.030		blocks)
	TOE 4	0.0	-2.43	0.03	.504	.315	.030		

+   See Fig. 3-11.

*   F denotes a site causing fatigue failure.
    I denotes a site initiating a fatigue crack but not involved in the
    final fatigue failure.

63
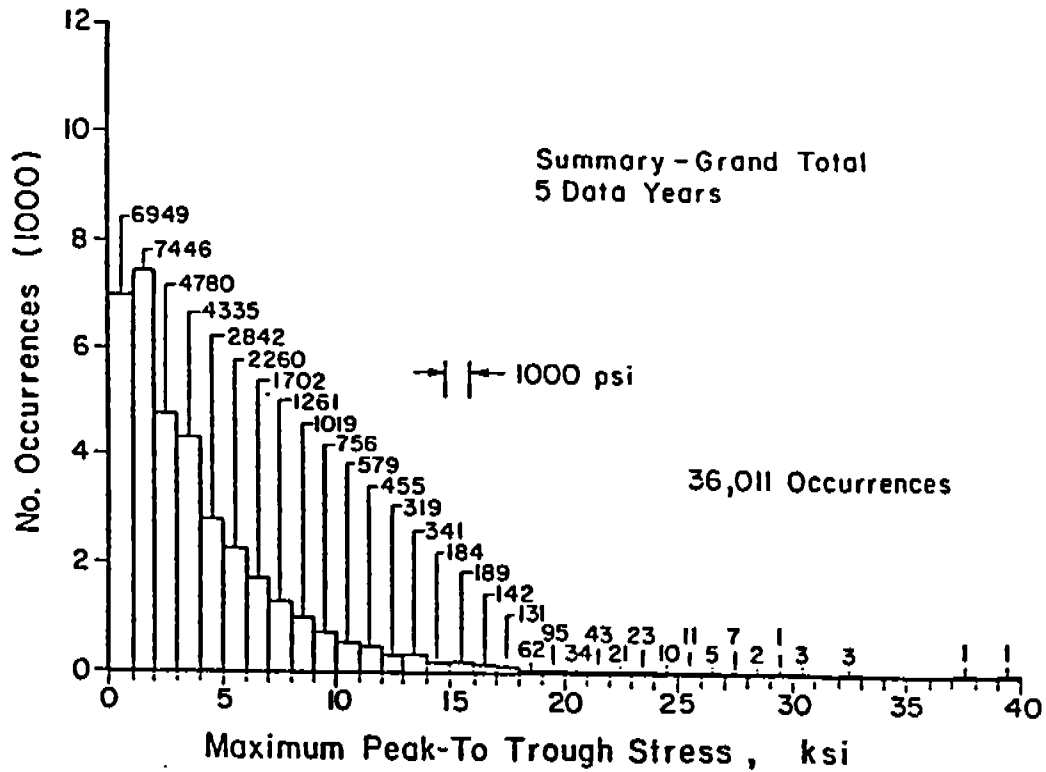
Fig. 3-1 Histogram from the SL-7 container ship scratch gauge data. The
number of occurances during a five year history is plotted as a
function of maximum peak-to-trough stress range [3-1].
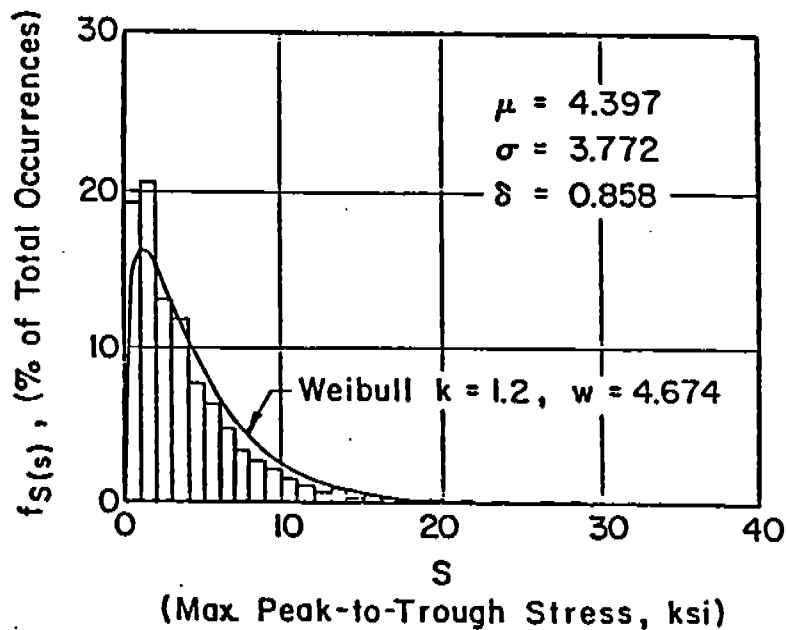
Fig. 3-2 Histogram from the SL-7 container ship scratch gauge data
fitted with a Weibull distribution [1-4].

Log Stress Range

S-N Curve (In Air)
With Fatigue Limit

BS 5400

1
m+2

Extended Line

10^7

Log N_f, cycles
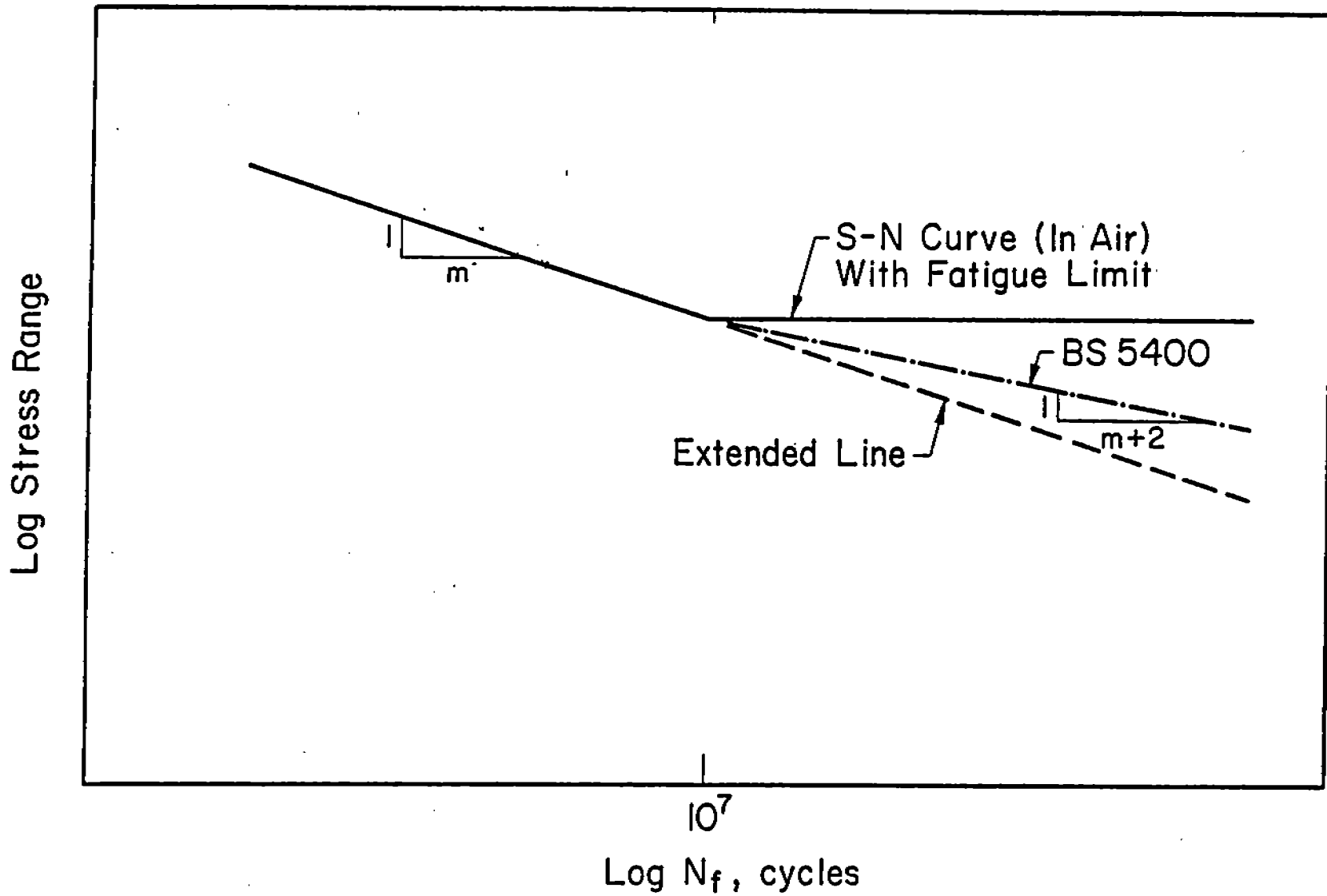
Fig. 3-3 Three suggested shapes of the S-N diagram in the long-life regieme.
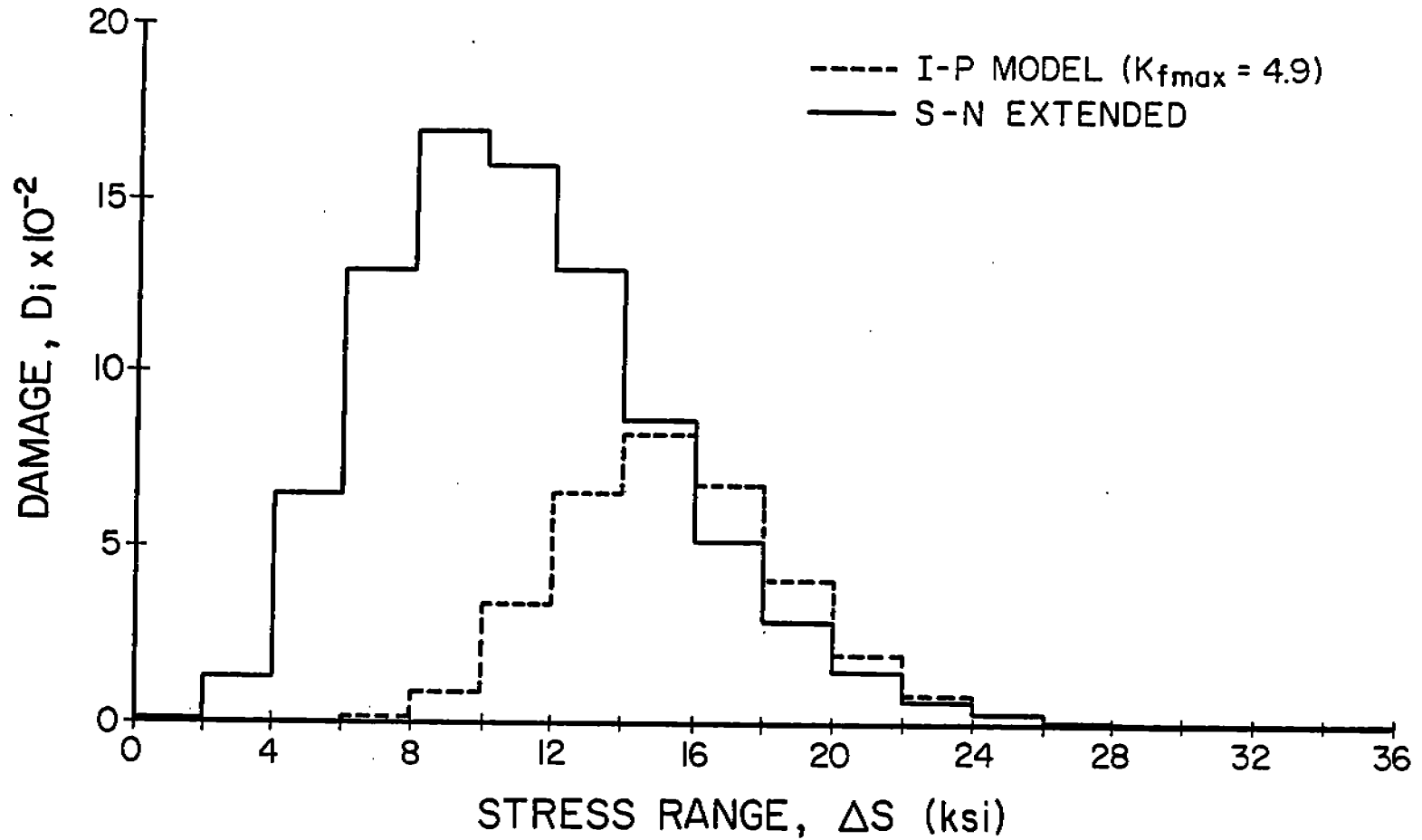
Fig. 3-4 Calculated damage attributable to each stress range interval for a Weibull distribution based on the 10^8 cycle SL-7 container ship history [1-4]. Damage was calculated using both the extended S-N curve and the I-P model as shown. The damage estimates depend upon the assumed shape of the S-N diagram in the high cycle region as well as the severity of the stress concentration K_{fmax}. K_{fmax} value was assumed as 4.9 at the IJP sites of Detail No. 20.
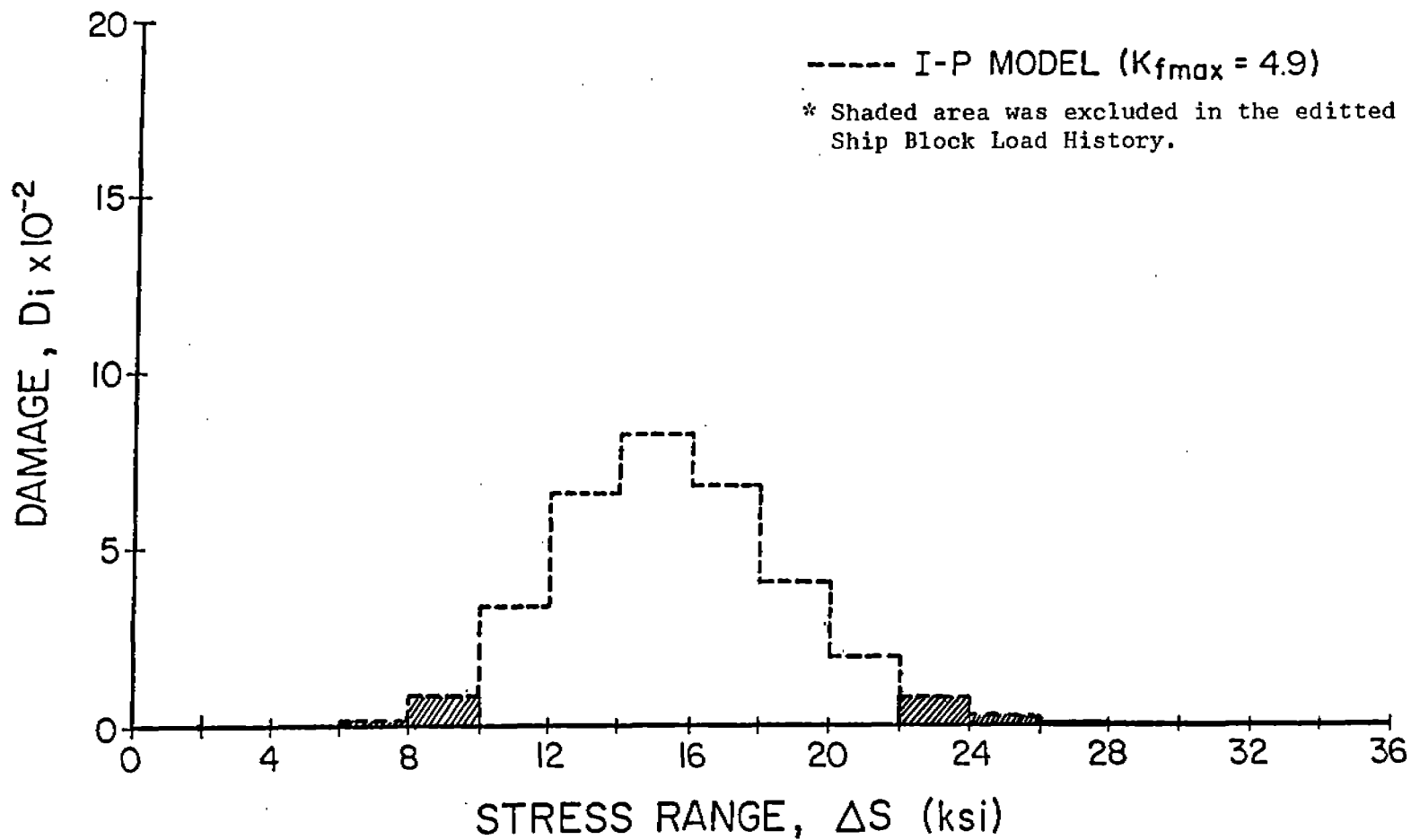
Fig. 3-5   Editing used to exclude unimportant small and large cycles. Stresses above 22 and
below 10 ksi were excluded. The developed 5,047 cycle block represents 92.8% of
the damage imparted during one month of the SL-7 ship history. K_{fmax} value was
assumed as 4.9 at the IJP sites of Detail No. 20.
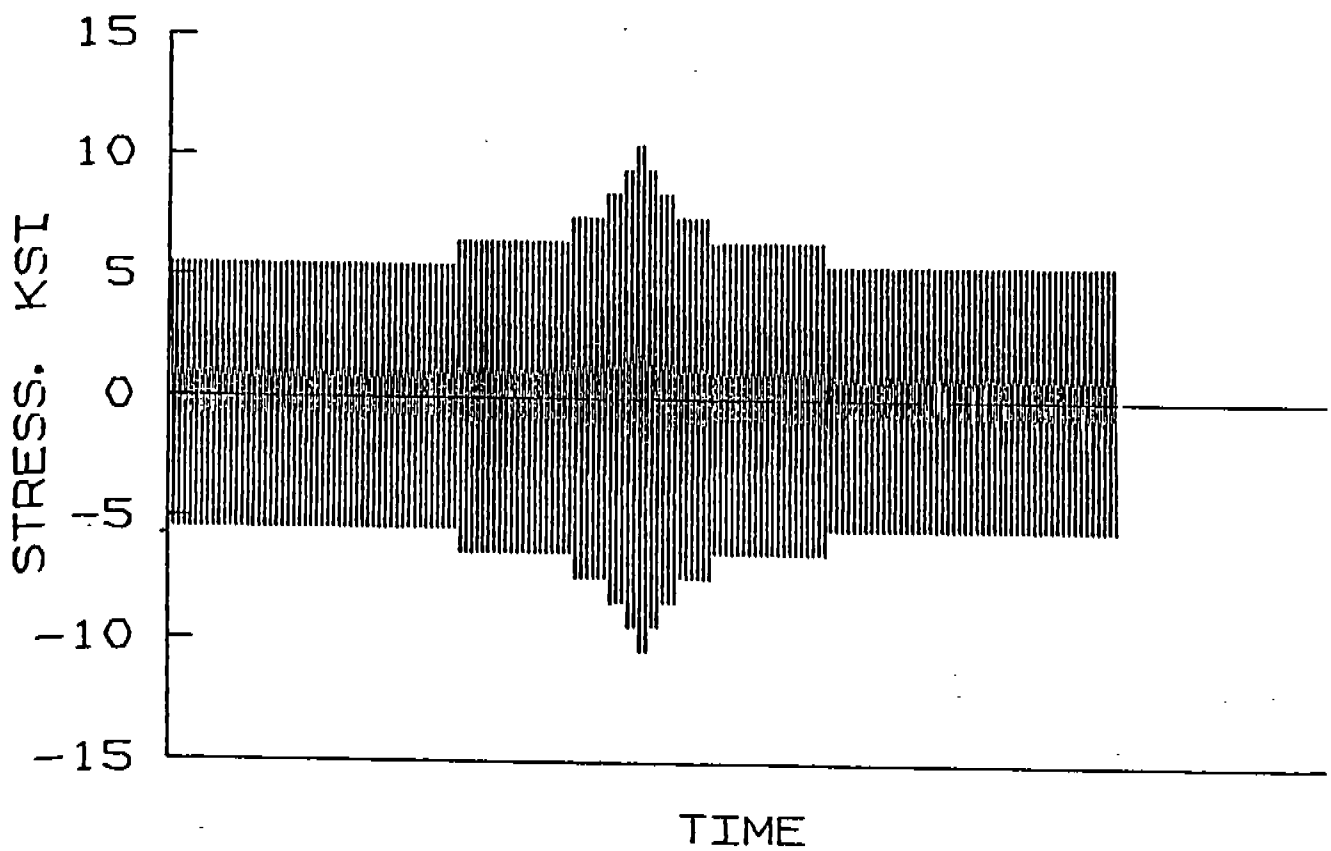
Fig. 3-6 Plot of one block of -the constructed ship history having the 92.8% of the
SL-7 container ship history damage. The central portion of the history
represents a period of severe weather.
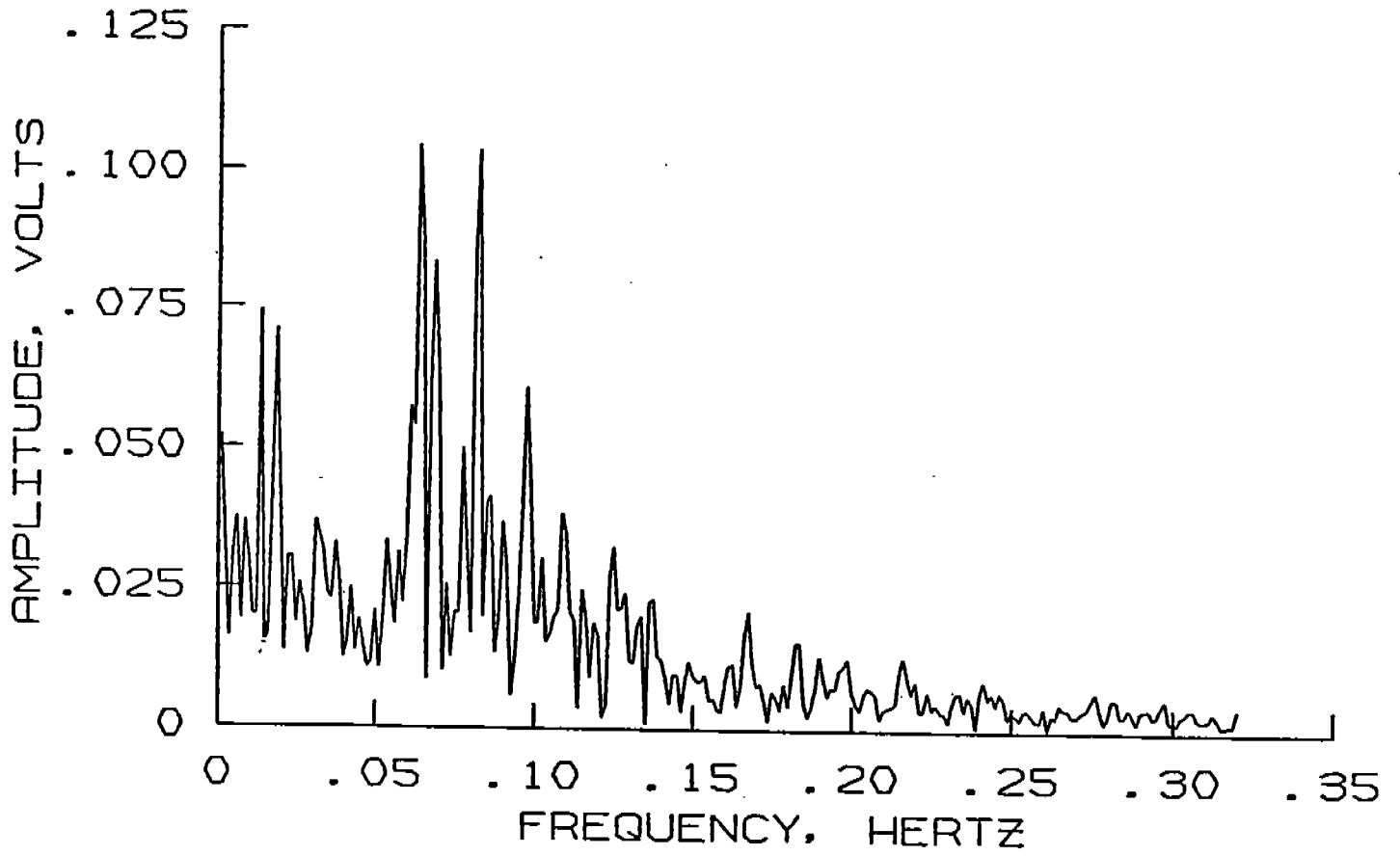
Fig. 3-7 Spectrum with redefined resolution and range of frequency.

69
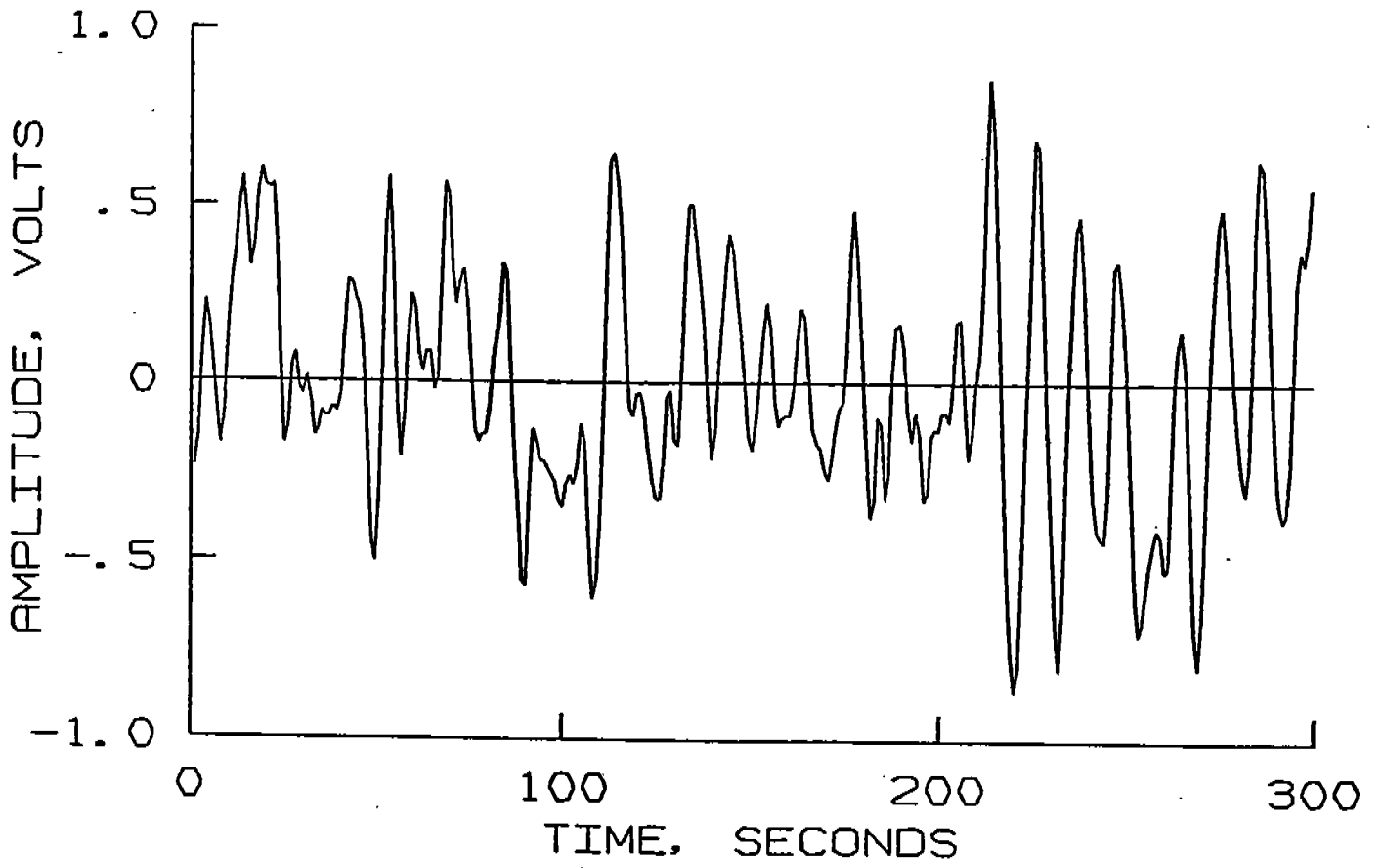
Fig. 3-8   Simulated stress-history corresponding to spectrum.

178 x 102 x 15.9

w = 9.5

203 x 76 x 12.7

203 x 76 x 12.7

50.8

76

178

50.8

15.9

203

203
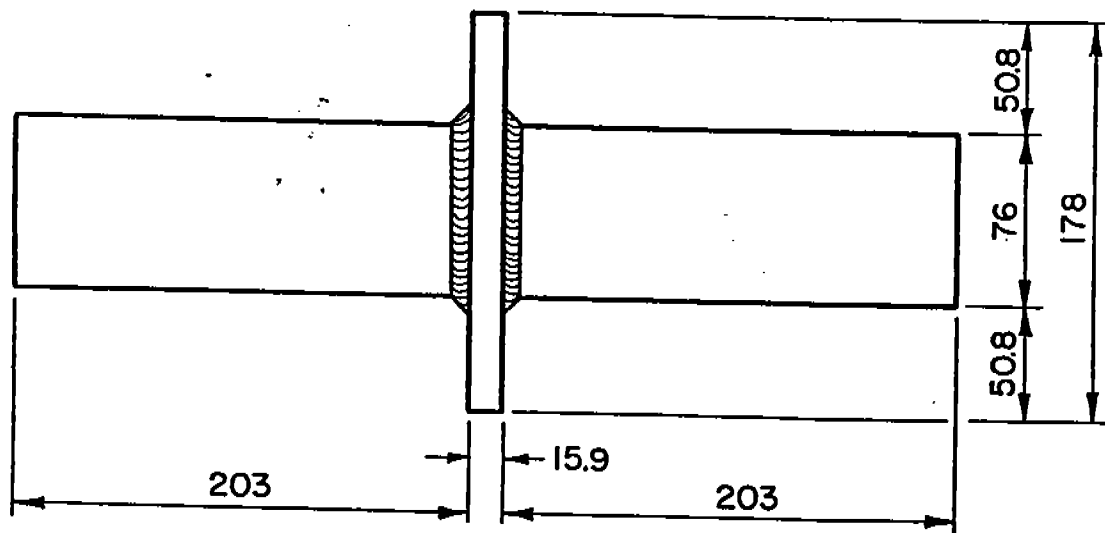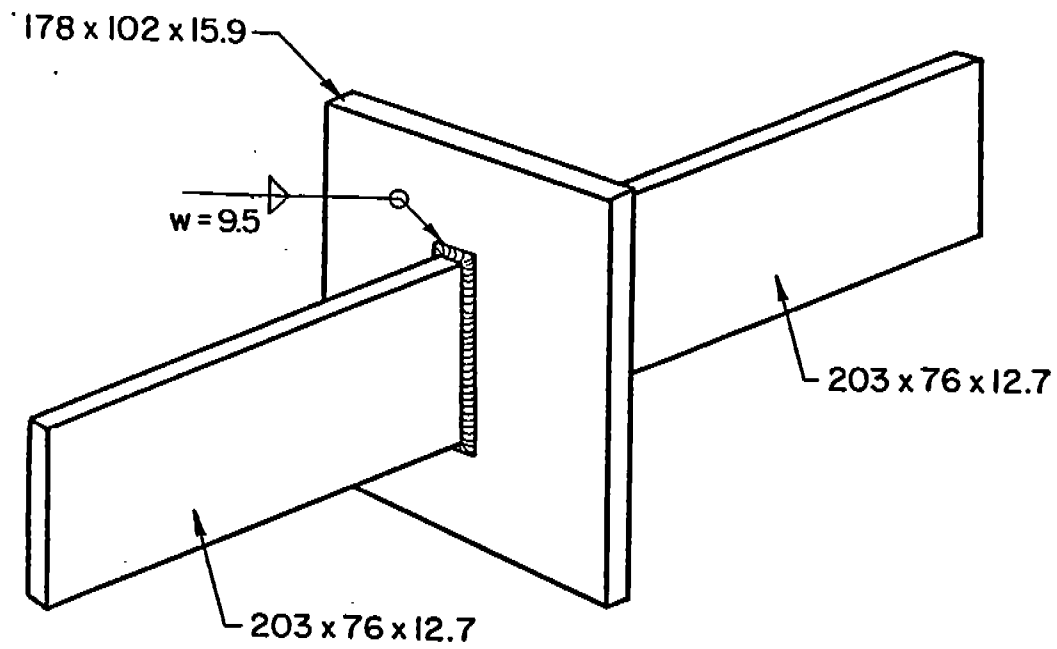
Fig. 3-9   Geometry and dimensions for testpieces of detail no. 20.
(Dimensions in mm.)

71
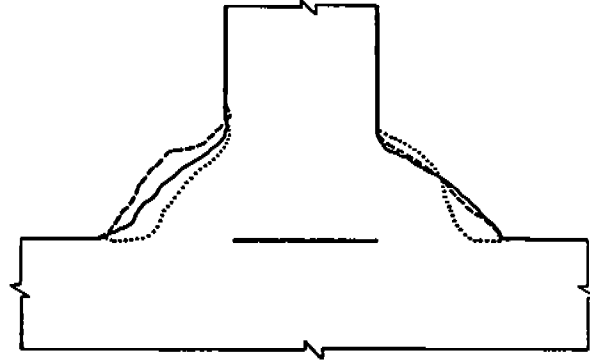
Schematic Comparison of the Actual Weld Configuration
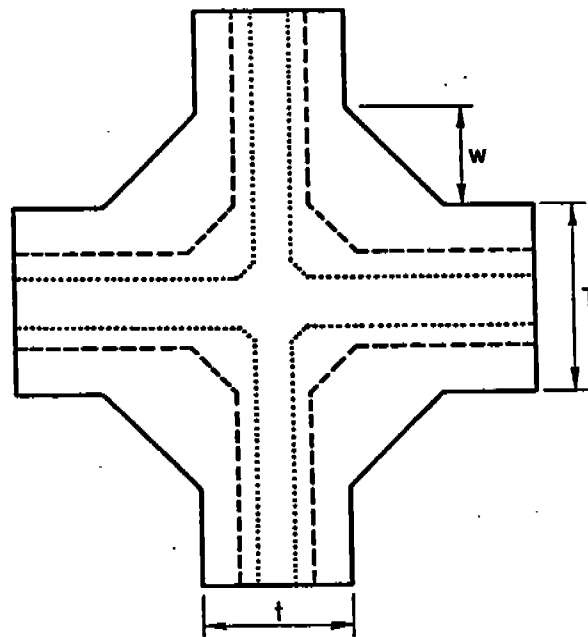
	T	t	w
———	31.8	25.4	19.1
– – –	15.9	12.7	9.5
···········	7.94	6.35	4.76

Design of the Geometric Similitude

Fig. 3-10 A comparison of weld shapes and relative dimensions for testpieces used in the thickness effect studies (Task 4). (Dimensions in mm.)

Fig. 3-11 Schematic description of possible crack
initiation locations and geometric parameters
of weldment.
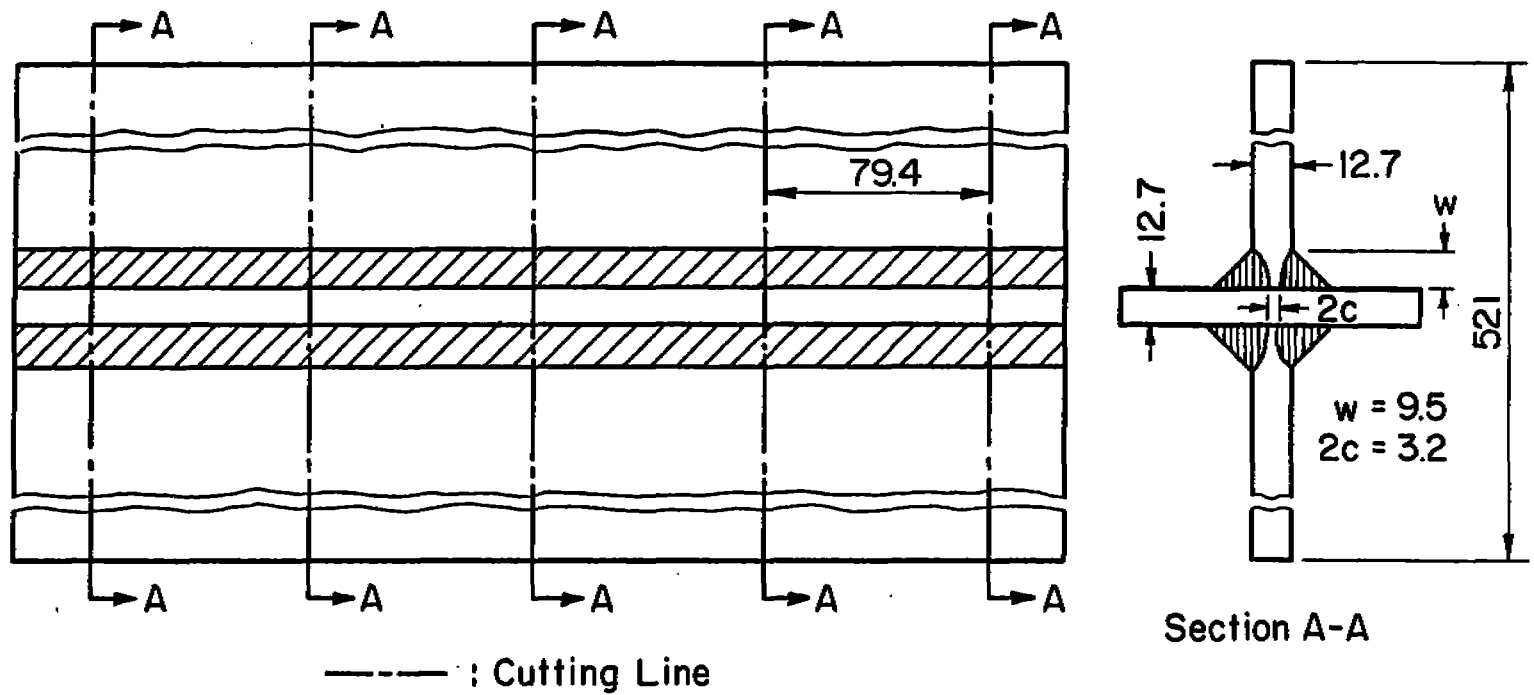
Fig. 3-12   Specimen details of cruciform joints for the   study   of mean stress effects.
(Dimensions in mm.)

— — — — : Cutting Line

* Materials at the Outside of the Cutting Lines
Were Removed.

Fig. 3-13   Conversion of 12.7mm thick testpieces of detail no. 20 to cruciform testpieces.
(Dimensions in mm.)
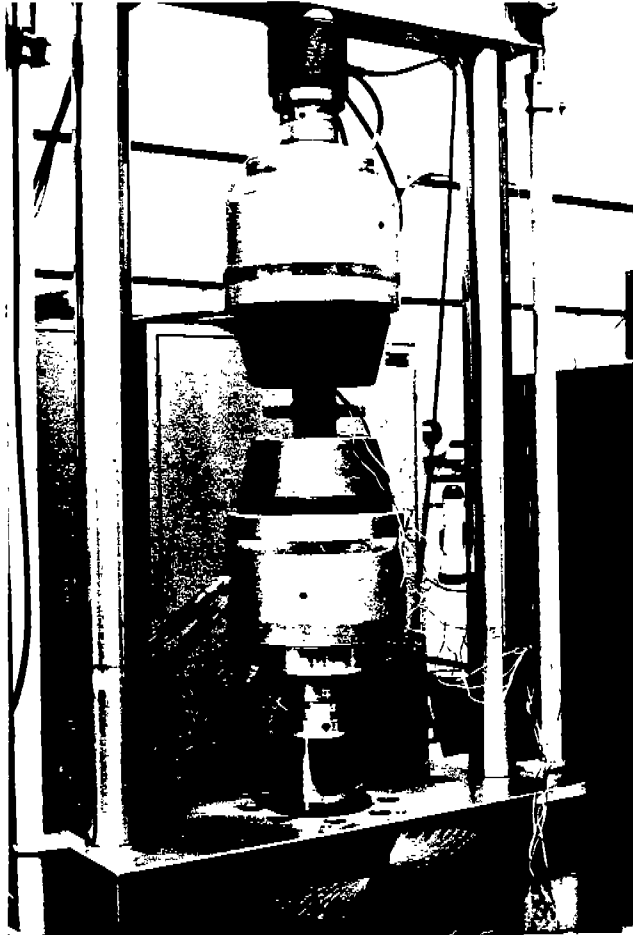
Fig. 3-14 A 12.7 mm thick testpiece of Detail No. 20 mounted
for testing in the 100 kip MTS frame.
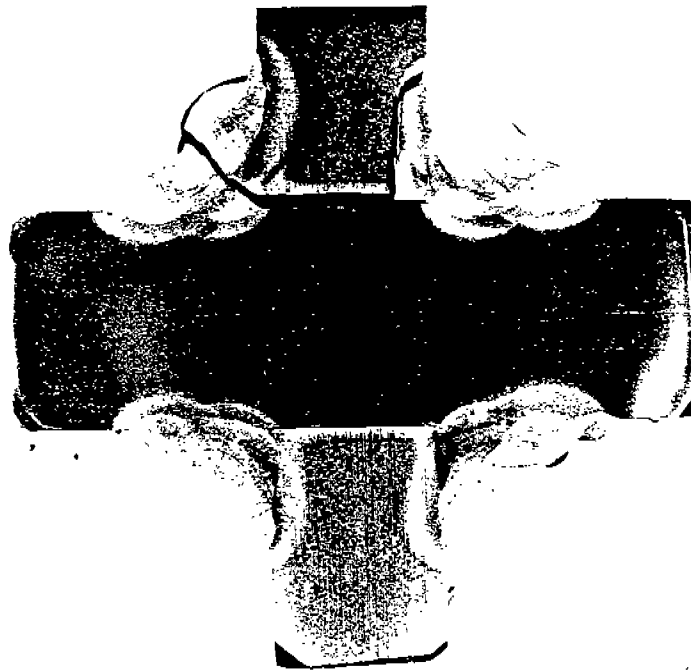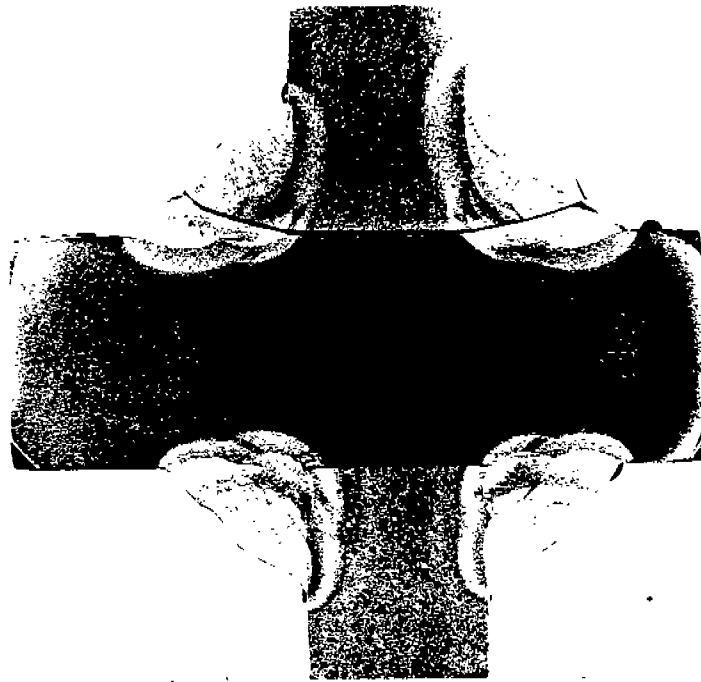
Fig. 3-15 Polished and etched section through two failed specimens of
Detail No. 20. Photo above shows the simpler pattern of
failure also sketched in Fig. 3-16 in which a fatigue crack
initiated at the IJP and propagated through the throat of
the fillet welds. The lower photo shows the more complex
pattern of failure also sketched in Fig. 3-17 in which a
fatigue crack initiated at the toe links with the IJP.
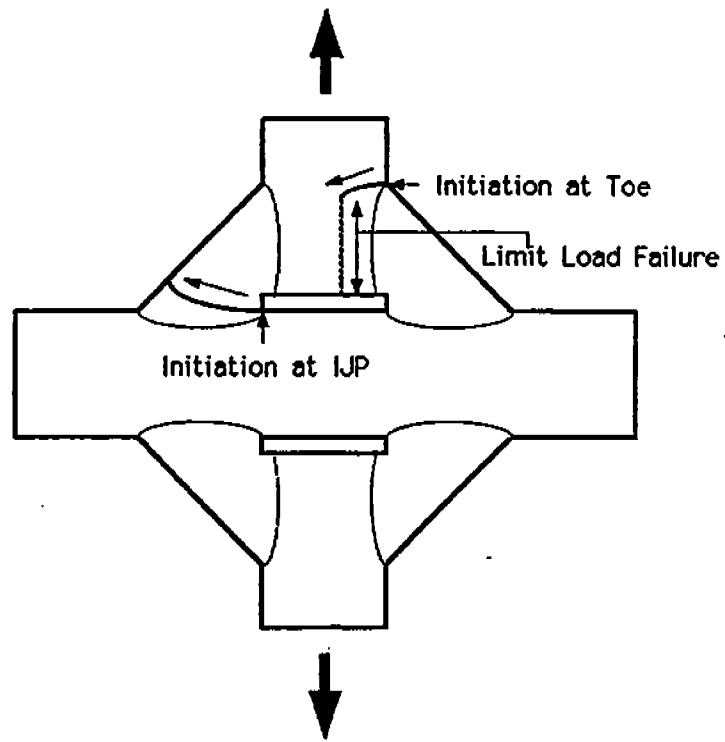
Fig. 3-16 Schematic description of fatigue failure
mode at the IJP sites.
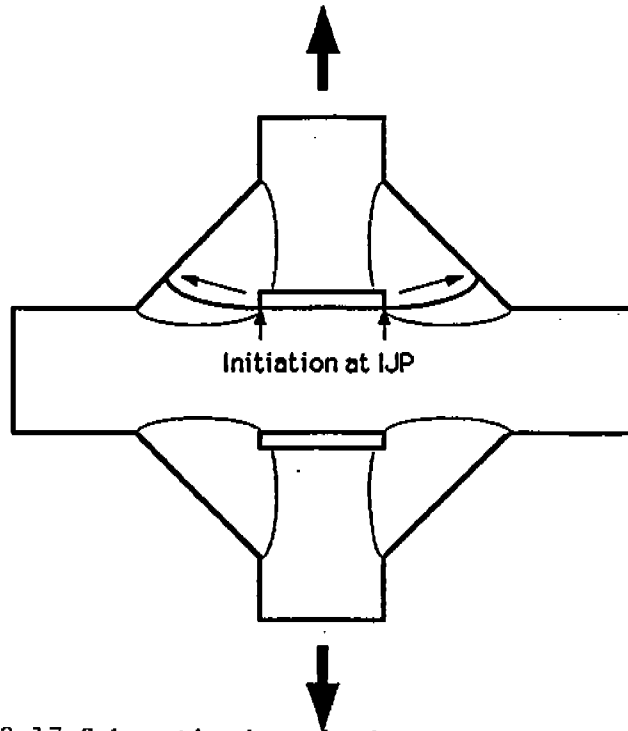
Fig. 3-17 Schematic description of combined fatigue
failure mode at the Toe sites and IJP sites.
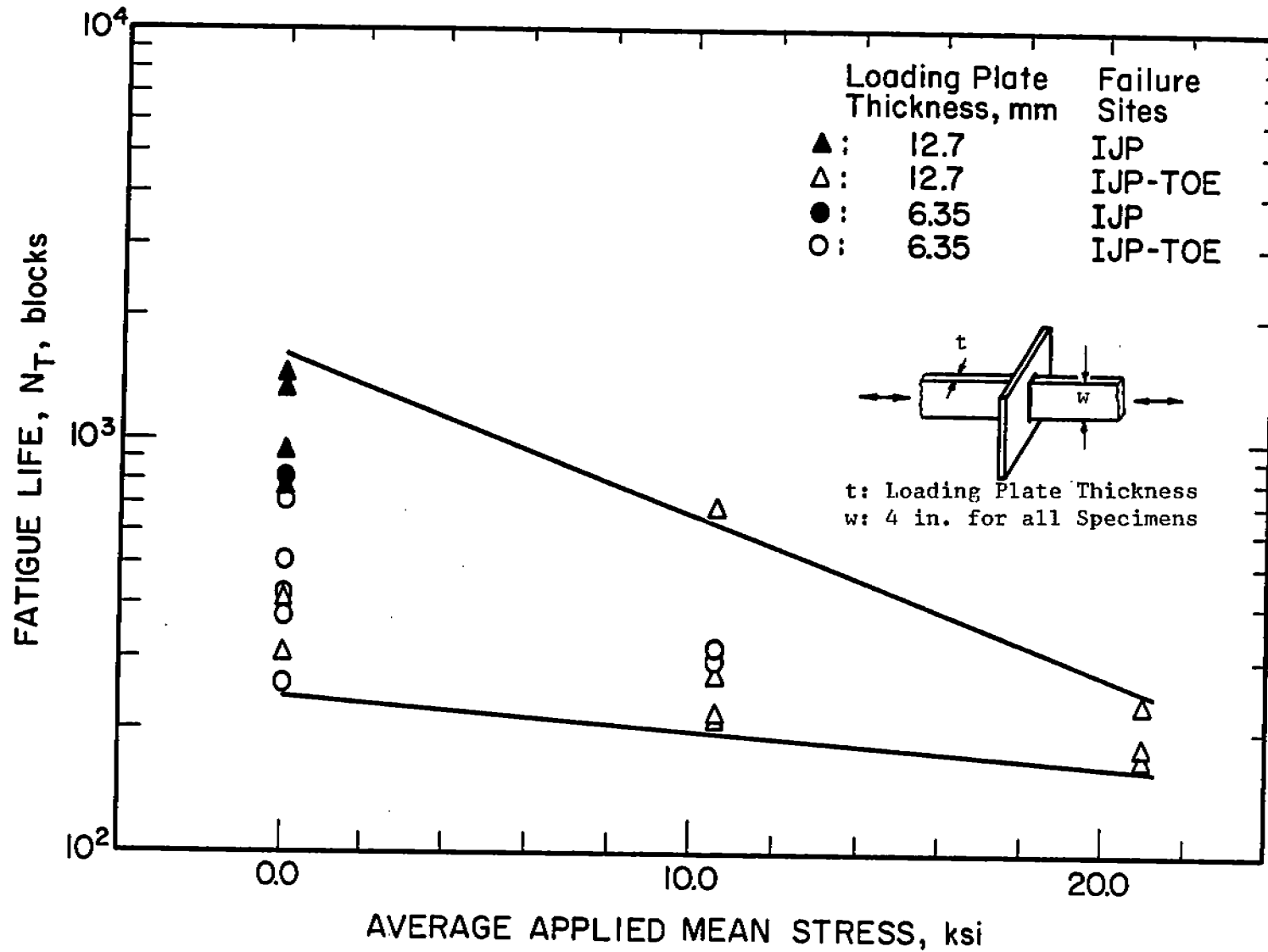
Fig. 3-18 Total fatigue life (blocks) versus the applied mean stress (ksi).
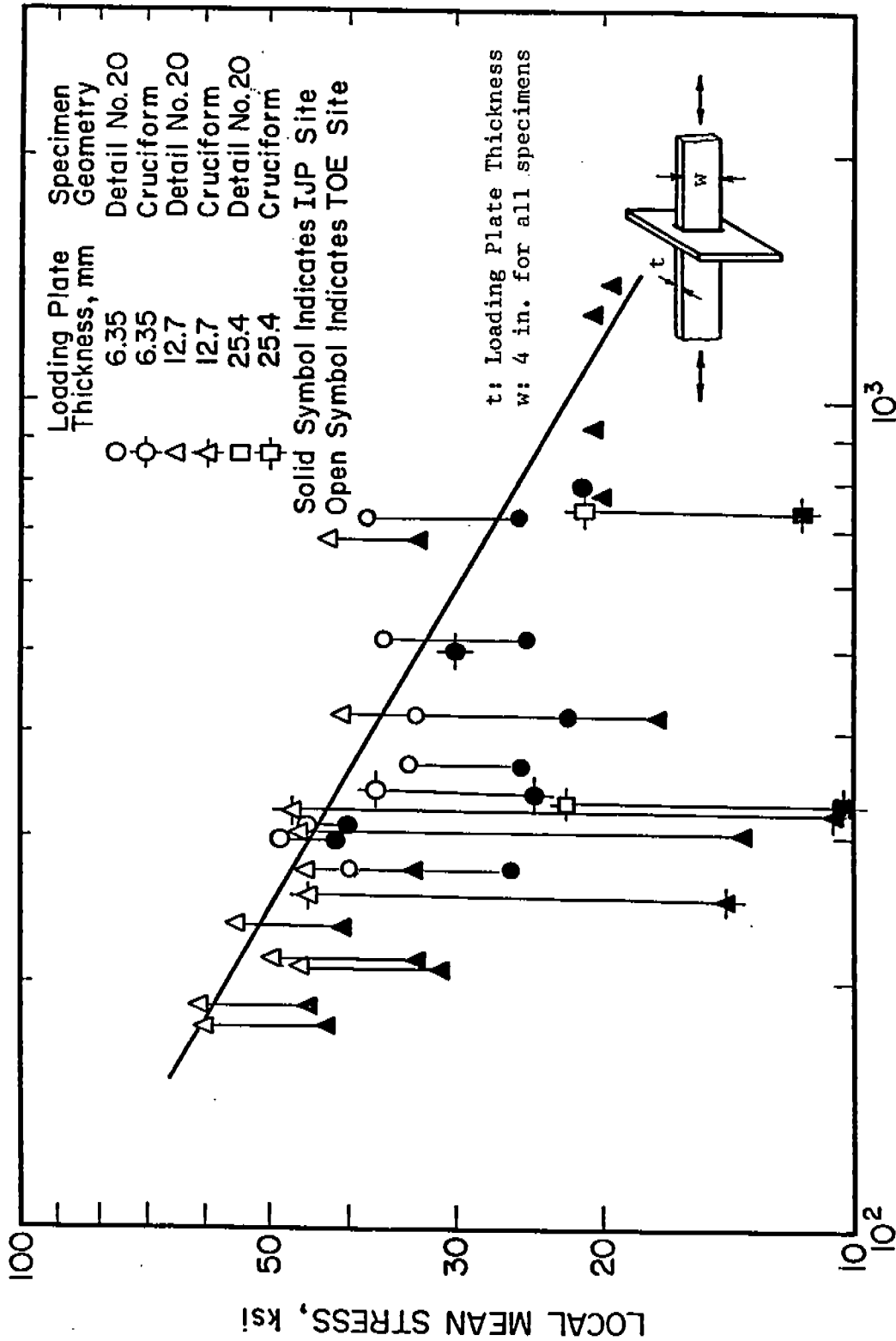
FATIGUE LIFE, N_T, blocks

Fig. 3-19 Local mean stress (ksi) versus total fatigue life in blocks. The tie-lines connect the values of
local mean stress for the IJP and toe of a given specimen in those cases in which both sites were
active. Specimens having short lives had high bending stresses, and the toe was the critical location.
Specimens having low bending stresses exhibited long lives, and the IJP was the critical location.
The best fit line is taken from Fig. 3-20.
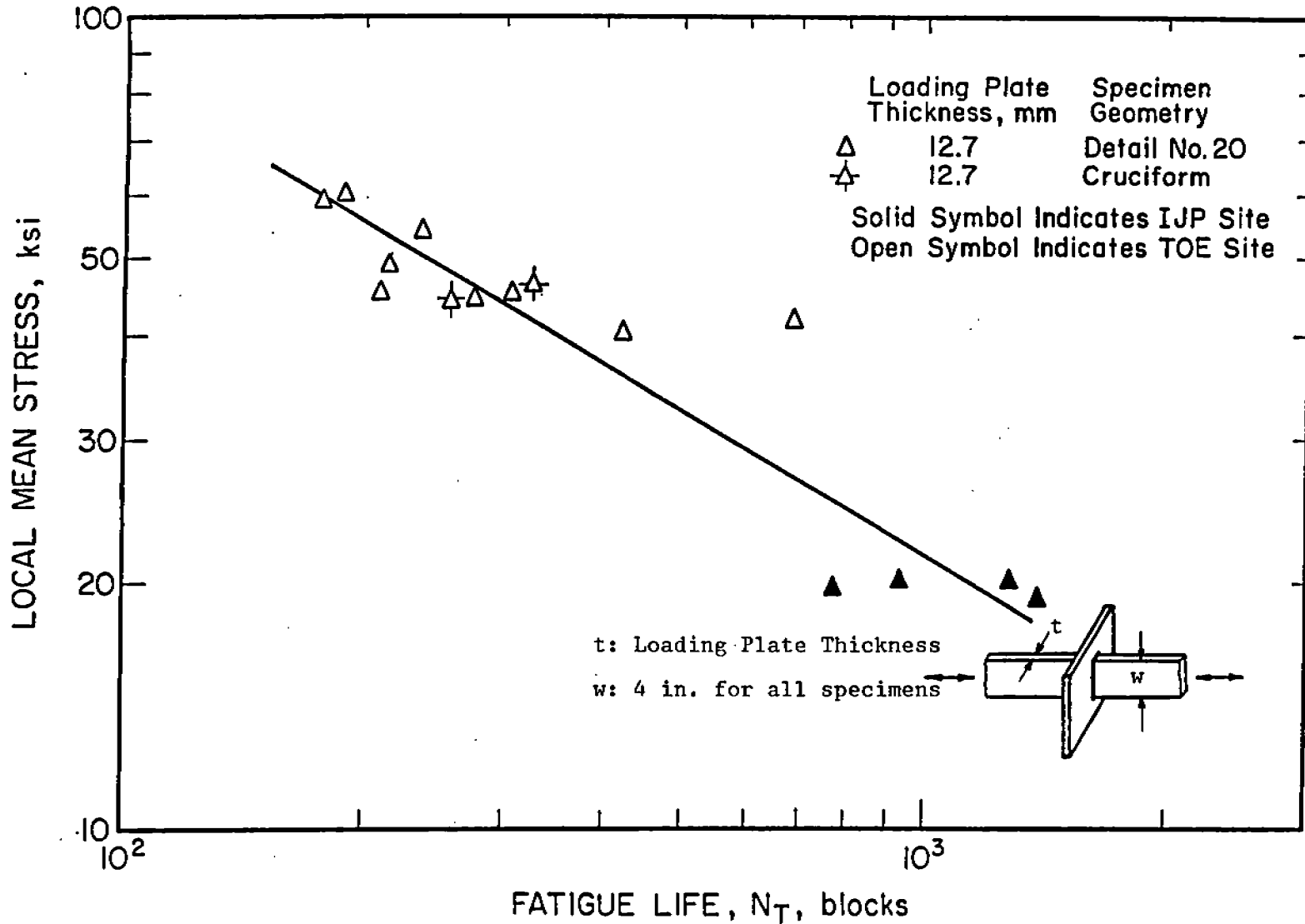
Fig. 3-20 Local mean stress (ksi) versus total fatigue life in blocks. Location having lower values of local mean stress have been excluded from this plot. There is a definite correlation between local mean stress and total fatigue life.
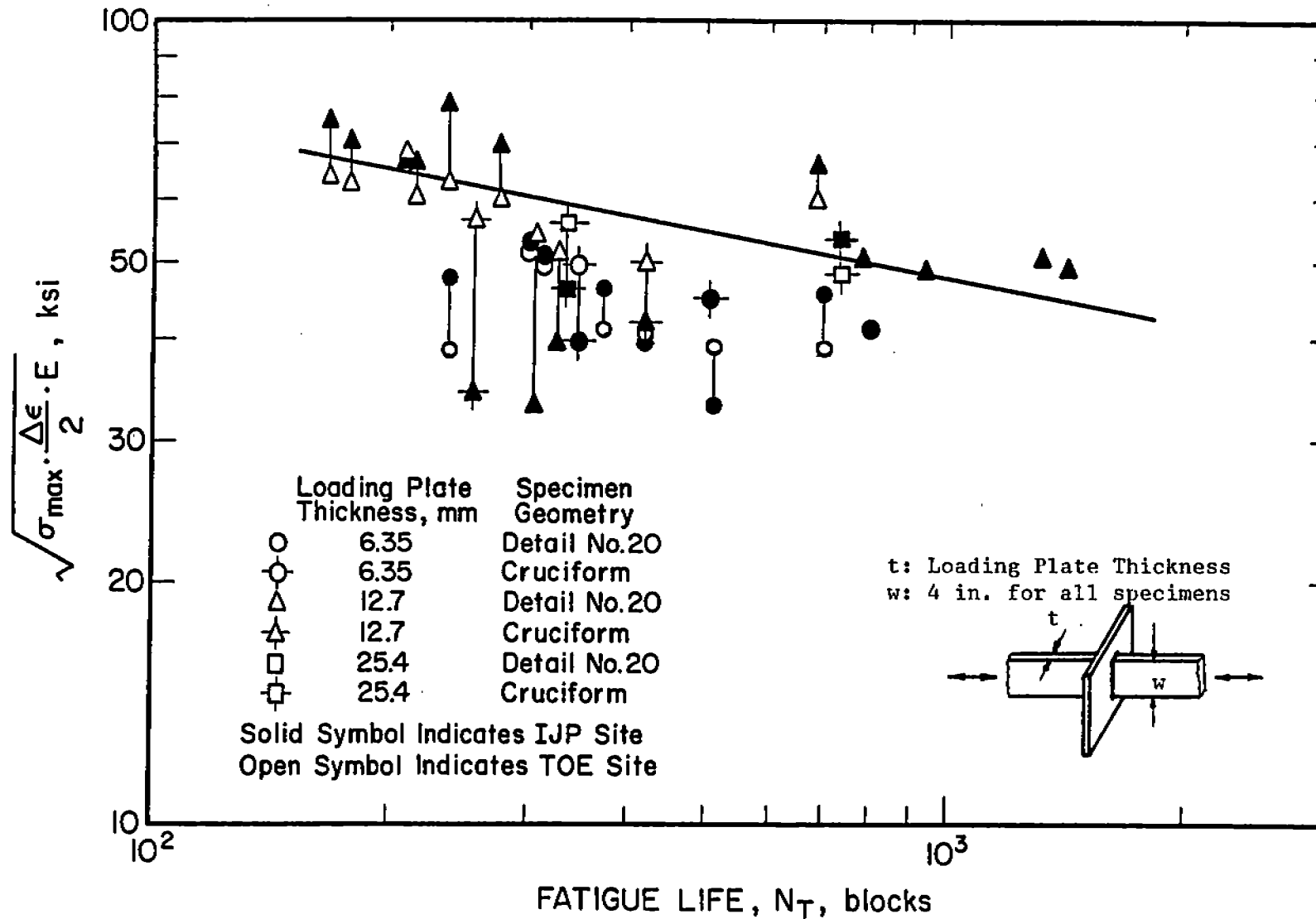
Fig. 3-21 The Smith-Watson-Topper (SWT) parameter versus total fatigue life in blocks. The SWT parameter reflects both the local mean stress and the range in local strain. The tie-lines connect the values of local mean stress for the IJP and toe of a given specimen in those cases in which both sites were active. The test-fit line is taken from Fig. 3-22.
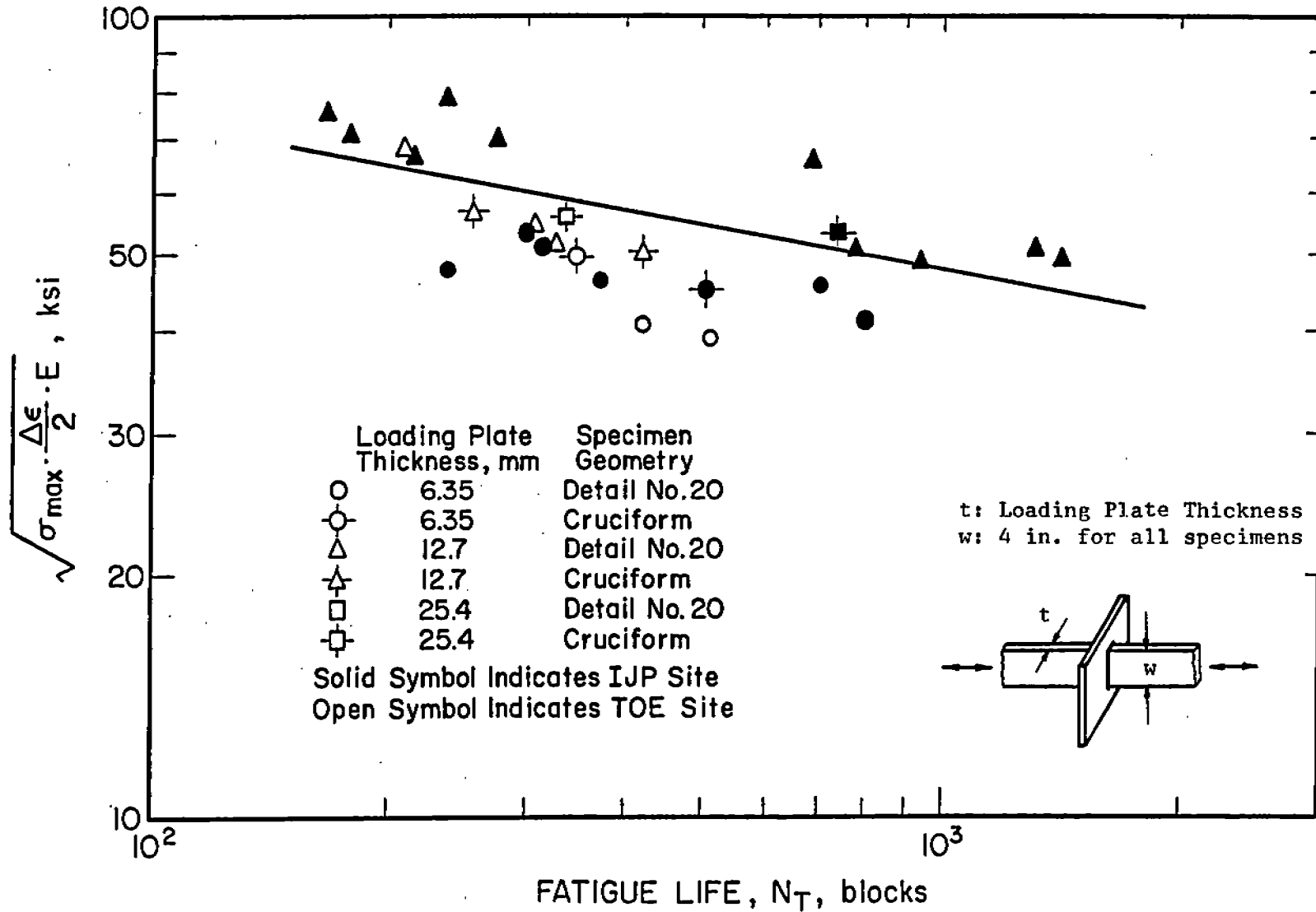
Fig. 3-22 The Smith-Watson-Topper (SWT) parameter versus total fatigue life in blocks. Only the location having the highest values of SWT parameter are plotted.
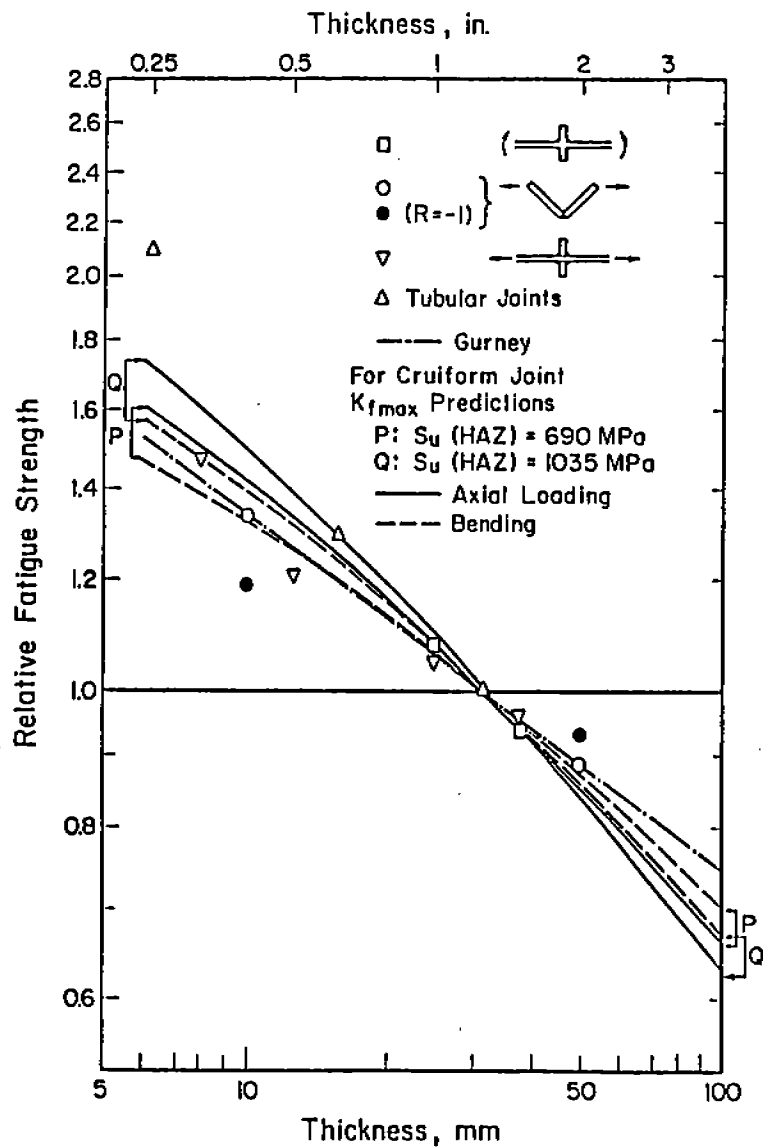
Fig. 3-23 Influence of plate thickness on fatigue
Strength (normalized to a thickness of
32 mm, all tests at R=0 except where
stated [3-6].
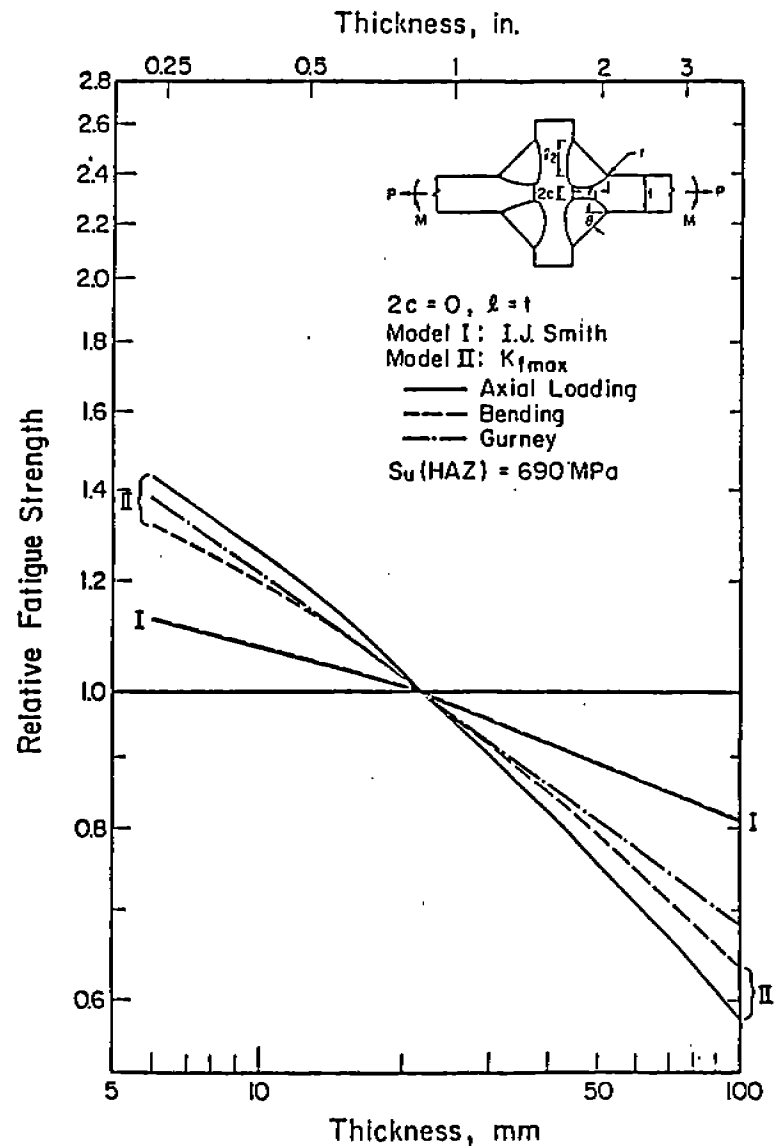
Fig. 3-24 The variation of predicted relative
Fatigue strength with plate thickness
(normalized to a thickness of 22 mm).
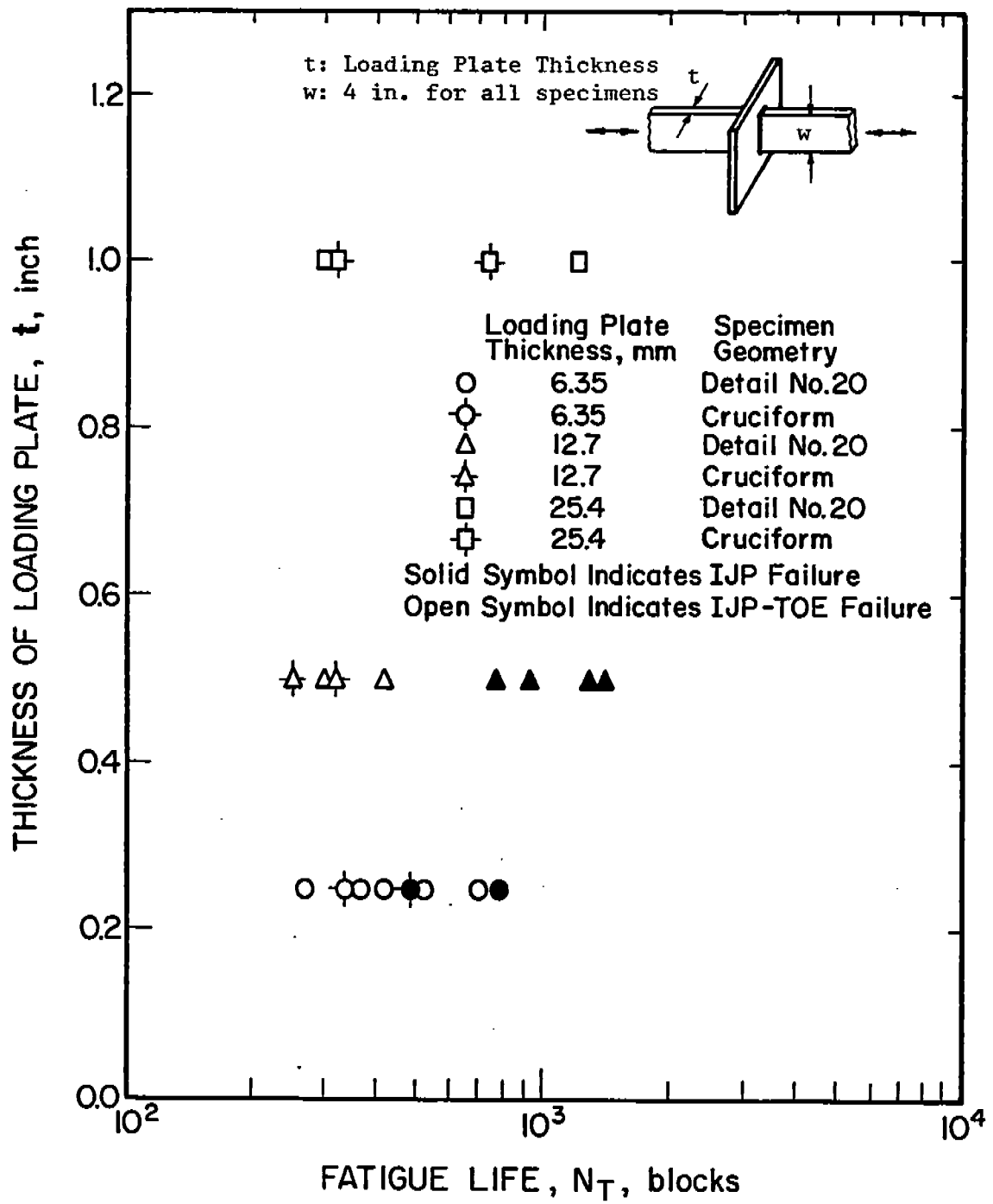
Fig. 3-25 Total fatigue life (blocks) versus the thickness
of the loading plate.

4. FATIGUE LIFE PREDICTION (TASK 6)

4.1 Predictions of the Test Results Using the MFDP

The Munse Fatigue Design Procedure (MFDP) was used to predict the expected mean fatigue life under variable load histories as shown in Sections 1.5 and 2. A comparison of the fatigue test results for Detail No. 20 tested under the ship block load history (see Section 3.1) and the predictions of the MFDP based on constant amplitude S-N diagram data for Detail No. 20 reported in [1-4] are shown in Fig. 4-1. The lower line is predicted by the MFDP for the edited history (S_{max} = 145 MPa (21 ksi)). The upper line is the prediction of the MFDP for the unedited history (S_{max} = 235 MPa (34.1 ksi)). The MFDP predicts an expected life of 610 blocks for the edited history and an expected life of 290 blocks for the unedited (actual) history. The difference between the edited and unedited history predictions is due to the sensitivity of the MFDP to the large and small cycles removed by editing. The MFDP estimates damage using the extended constant-amplitude S-N diagram. There is good agreement between the predictions of the MFDP for the edited history and the results obtained for Detail No. 20 tested under that history as shown in Fig. 4-2.

The MFDP does not take mean stresses into account. It is usually difficult to know what the mean stresses are in most practical situations. However, in comparing the MFDP predictions with the test data for which the level of applied mean stresses are known, it would be interesting to modify the MFDP to take account of the applied mean stresses to see if such modifications would improve the predictive abilities of the MFDP. As seen in Fig. 2-4, the MFDP can be in error for histories such as the SAE Transmission history which has a net tensile mean stress. To take mean stresses into account, an additional mean stress factor was incorporated into the MFDP (see Appendix B)

$$\Delta S_{D_m} = (\Delta S_{N(-1)})(1 - 2S_m C^{-1/m})(\xi)(R_F) \tag{B-6}$$

where: S_m is the average applied mean stress. It is assumed that the $\Delta S_{N(-1)}$ data are collected under reversed loadings. As seen in Fig. 4-3, the mean stress correction of Eq. B-6 above improves the correlation of the

86

MFDP with the test data of Detail No. 20. It is suggested that this correction be used whenever feasible.

4.2 Predictions of the Test Results Using the I-P Model

The test results for all specimens were predicted using the I-P model which was compared with the MFDP in Section 2 and which is described in detail in Appendix A. The I-P model differs from the MFDP principally in that the I-P model predicts the total fatigue life of weldments based solely on the applied stresses, calculated geometry effects and estimated material properties (Tables 3-5 and 3-6). No tests of the weldment itself are required. Tables 4-1 and 4-4 are derived from Tables 3-7 through 3-11 and are arranged in the same format. Included in Tables 4-1 to 4-4 are the estimated fatigue notch factors (K^A_{fmax} and K^B_{fmax}) for the two IJP and four toe locations in each specimen. Also contained in these tables are estimated initiation lives (N_I), propagation lives (N_p) and total lives (N_T) for each potential failure site in each specimen.

The predictions for the fatigue crack initiation and propagation lives were made using the procedures outlined in Appendix A and take into account the applied and induced bending mean stresses as well as the applied and induced cyclic axial and bending stresses. The least predicted value is the predicted total life for each joint, and this value should be compared with the actual life also listed in these tables. Figure 4-4 compares the predictions made using the I-P model with the observed total fatigue lives. The predictions for the 6.35 mm (1/4-in.) specimens were unconservative by more than a factor of four. This is not considered a good result.

Considerable effort was expended in trying to improve the predictions for the 6.35 mm (1/4-in.) specimens. There are three possible explanations which can be put forward for the really poor agreement between the predictions and observed total fatigue lives: The first is that the size correction of the I-P model is incorrect or at least too large (see Section 3.9). Indeed, the results of this study do not confirm the existence of a size effect of the magnitude suggested by Gurney [3-6] and Smith [3-7]. A second explanation is that both the 25.4 mm (1-in.) and the 6.35 mm (1/4-in.) specimens had lives different than expected because they experienced loading histories different than that of the 12.7 mm (1/2-in.) specimens by

reason of differences in K_f values (1-in. $K_f \approx 6.5$, 1/2-in. $K_f \approx 5.5$, 1/4-in. $K_f \approx 4.0$: see Section 3.5). The third and most likely explanation is experimental difficulties with the 6.35 mm (1/4-in.) specimens.

In short, it is likely that the welding control of the 6.35 mm (1/4-in.) specimens was not sufficiently good. For 6.35 mm (1/4-in.) specimens, care was exercised in maintaining geometric similitude in the shape of the weld bead and the size and height of the IJP. However, the fillet welds for the 6.35 mm (1/4-in.) specimens were irregular, and the root penetration of the welds varied considerably so that the width of the IJP varied along the length of any specimen and in some locations was greater than the plate width due to incomplete fusion particularly in the vicinity of the tack welds. It was decided during the course of the study to use these specimens despite their poor quality to provide a realistic and severe test of the I-P model.

In general, the Detail No. 20 welded using SMA welding procedures and containing an IJP provided a difficult test for this model. The presence of the IJP greatly complicated the analysis of the test results. Midway through the program, the advisory committee questioned whether Detail No. 20 should actually have contained an IJP. The committee had understood Detail No. 20 to be full penetration. The investigators had interpreted the diagram for Detail No. 20 literally and incorporated the IJP evident in that diagram: see Fig. 5-1. Moreover, Munse in the previous study [1-4] had incorporated an IJP in Detail No. 20. The program would have been much simpler if full penetration welds had been used; but at a time six months prior to the end of the program (April 1986), it was not possible to repeat the tests of Tasks 2-4 with full penetration weldments.

The predictions for only the 12.7 mm (1/2-in.) specimens and their observed total lives are compared in Fig. 4-5. The predictions and the total life data agree within a factor of four.

4.3 Modeling the Fatigue Resistance of Weldments

The I-P model usually predicts the life of weldments within a factor of two for constant amplitude loadings and within a factor of three for the variable load histories studied previously. The experience with the 6.35 mm (1/4-in.) weldments in this study provides the poorest coorelation to date

and no satisfactory explanation for the discrepancy between the predictions and the observed total lives is available at this time. Nonetheless, the I-P model is still one of the best available and can be used as a design tool and as a means for understanding the behavior of weldments.

As outlined in Appendix A, for long lives and constant amplitude loading conditions, the notch root stresses are mostly elastic and the residual stresses can be considered not to relax. Under these conditions the Basquin equation (Eq. A-12) can be used to estimate the total fatigue life:

$$S_a K_f = (\sigma_f' - K_f S_m - \sigma_r) \ (2N_I)^b \qquad (A\text{-}12)$$

where σ_f' is the fatigue strength coefficient ($\sigma_f' \approx S_u + 50$ (ksi. units)), S_m is the remotely applied mean stress, σ_r is the notch-root residual stress and K_f is the appropriate fatigue notch factor. Expanding the mean stress (S_m) to include both (applied or induced) axial and bending mean stresses (S_m^A and S_m^B), and considering both applied and induced cyclic axial and bending stresses through Eq. A-7:

$$K_{f\ max}^{eff} = (1\text{-}x) \ K_{f\ max}^A + x \ K_{f\ max}^B; \qquad x = S_a^B / S_a^T \qquad (A\text{-}7)$$

where: K_{fmax}^A and K_{fmax}^B are the worst-case-notch fatigue notch factor for axial and bending load conditions, respectively; S_a^B and S_a^T are the bending stress and the total stress amplitude, respectively. From Eq. A-12 and A-7 above, one can derive an expression for the fatigue strength of a weldment subjected to axial and bending mean and constant-amplitude cyclic stresses:

$$S_a^T = [\frac{(1/K_{fmax}^A)(\sigma_f' - \sigma_r) - S_m - XS_m^B}{1 - x \ (1 - X)}] \ (2N_I)^b = S_F \ (2N_I)^b \qquad (4\text{-}2)$$

where X is the ratio of K_{fmax}^B to K_{fmax}^A. If the assumptions of the I-P model are valid, then this expression should predict the constant amplitude fatigue strength at long lives ($N_T > 2 \times 10^6$ cycles) for which initiation is thought to dominate the total fatigue life. Figure 4-6 shows the mean S-N

89

curve for Detail No. 20 from the UIUC Fatigue Data Bank. Also shown in Fig. 4-6 is the long-life behavior of the toe and IJP of Detail No. 20 predicted by Eq. 4-2 assuming no mean stress, no induced bending stresses and full tensile residual stresses (as-welded condition). As can be seen in Fig. 4-6, the agreement is very good and lends credence to the idea that Eq. 4-2 (as well as Eq. A-15) does quite well at predicting the constant amplitude fatigue strength at long lives. The use of the I-P model as a design aid is presented and discussed in Appendix A.

If Eqs. B-6 and A-15 stand further tests as design tools, they may prove useful as such. However, Eq. 4-2 can also be used to create a stochastic model for the fatigue strength of weldments and provide an analytical means of estimating Ω_c in the MFDP (see Section 1.5) as is shown below.

The variables in Eq. 4-2 can be divided into either constants (X), known quantities (S_m^A, S_m^B, $2N_I$), and random variables (σ_f', σ_r, K_{fmax}^A, x). Of the random variable K_{fmax}^A and x will be considered here as determining the variation in the fatigue strength. Both material properties, the fatigue strength coefficient (σ_f') which is proportional to the UTS and the residual stress (σ_r) which is equal to the base metal yield strength (S_y), do not vary greatly for one material and welding process.

The fatigue notch factors (K_{fmax}^A and K_{fmax}^B) for each of the weld toes and IJPs of the 32 weldments of Detail No. 20 the cruciform weldments are estimated in Tables 4-1 and 4-4. The bending factor (x) was also calculated for each of the above mentioned locations. The values of K_f and x were plotted on normal probability basis and found to be normally distributed: see Figs. 4-7 to 4-9. The mean (μ) and standard deviation (σ) for each condition are given in these figures.

Since the two main random variables were normally distributed it was possible to estimate the mean and standard deviation of the constant S_F in the basic fatigue relation (Eq. 4-2) using a simple computer simulation.

$$S_a^T - S_F \ (2N)^b \qquad\qquad (4-3)$$

The results of two simulations for the 12.7 mm (1/2-in.) and 6.35 mm (1/4-in.) specimens of Detail No. 20 are given in Figs. 4-10 to 4-13. In one

simulation, both positive and negative values of x were permitted to model the situation in which the weld distortions can induce either tensile (damaging) or compressive (favorable) bending stresses at the critical location of a weldment (weld toe or IJP). In the second simulation, only positive values of bending factor were permitted to model the situation of symmetrical weldments such as the double-V butt weld or Detail No. 20 in which distortions induce both tensile and compressive bending stresses so that the fatigue life of one site is always reduced.

As can be seen in these figures, the constant S_F is normally distributed. The standard deviation of S_F was found to depend more upon the dispersion in the bending factor (x) than on the dispersion in the fatigue notch factor K_f (the effects of geometry); although both were nearly equal.

The MFDP idealizes the detail S-N diagrams using Eq. 2-2. It is interesting to relate the distribution calculated for S_F, the intercept of the S-N diagram (slope b) on the stress axis, with that of the constant C in Eq. 2-2, the intercept of the S-N diagram (slope 1/m) on the life axis.

$$N = \frac{C}{(\Delta S_N)^m} \qquad\qquad (2\text{-}2)$$

Munse reported average values of log C for Detail No. 20 as 11.57 with a COV of .4. Average values of log C and COV were calculated using Eqs. 4-3 and 2-2 from values of S_F simulated using the I-P model (Eq. 4-2). For the 12.7 mm specimens, simulated toe failures gave an average log C value of 11.35 and a COV of .020; and simulated IJP failures gave an average log C value of 12.12 and a COV of .019. The agreement in the calculated average values of log C is also reflected in the agreement between the experimental and predicted S-N curves shown in Fig. 4-6.

Thus, the simulation using Eq. 4-2 predicted the experimental average value of log C but predicted an order of magnitude less variation (that is scatter in the S-N diagram). This difference in scatter between the experimental S-N diagrams and the simulation which considers the effects of geometry and induced bending stresses may reflect the unavoidable variation in results inherent in the fatigue testing of weldments, but it may also reflect the penalty in uncertainty paid for our current inability to

91

quantify and control the effects of residual stress, mean stress, induced secondary member stresses, and specimen size as well as differences in testing between laboratories.

Table 4-1

Life Prediction for 12.7 mm (1/2-in.) Specimens of Structural
Detail No. 20 under the Ship Block Load History.

Spec. No.	Sites	Mean Stress (ksi)	K^A_{fmax}	K^B_{fmax}	Actual Life (Blocks)	Predicted Life		
						N_I	N_p (Blocks)	N_T
H-1	IJP 1-3	0.0	5.36	0.92	926	599	301	900
	TOE 1	0.0	4.24	2.08		7794	1110	8904
	TOE 3	0.0	3.49	2.01		25651	941	26591
	IJP 2-4	0.0	5.48	0.82		495	356	851
	TOE 2	0.0	3.49	2.01		25828	707	26535
	TOE 4	0.0	3.49	2.02		181399	1630	183029
H-2	IJP 1-3	0.0	5.75	0.80	769	342	255	597
	TOE 1	0.0	3.93	2.03		7386	756	8142
	TOE 3	0.0	3.81	2.02		38693	1050	39743
	IJP 2-4	0.0	5.59	0.80		438	353	791
	TOE 2	0.0	3.30	1.98		95384	1120	96504
	TOE 4	0.0	3.74	2.04		1961889	7480	1969369
H-3	IJP 1-3	0.0	5.54	0.90	1291	457	310	767
	TOE 1	0.0	3.34	2.00		377630	1410	379040
	TOE 3	0.0	3.70	2.03		7769	629	8398
	IJP 2-4	0.0	5.55	0.79		465	341	806
	TOE 2	0.0	3.32	1.98		209061	1120	210181
	TOE 4	0.0	3.89	2.07		16059	1150	17209
H-4	IJP 1-3	0.0	5.21	0.77	1414	766	371	1140
	TOE 1	0.0	3.87	2.06		17500	1210	18710
	TOE 3	0.0	3.95	2.06		250528	4810	255338
	IJP 2-4	0.0	5.77	0.98		337	301	638
	TOE 2	0.0	3.49	2.01		42595	913	43508
	TOE 4	0.0	3.53	2.00		68587	1040	69627
H-5	IJP 1-3	0.0	5.13	0.71	416	896	390	1286
	TOE 1	0.0	3.81	2.06		2090380	1110	2091490
	TOE 3	0.0	3.77	2.06		4112	687	4799
	IJP 2-4	0.0	5.24	0.79		777	348	1125
	TOE 2	0.0	3.90	2.06		1228444	1120	1229564
	TOE 4	0.0	3.86	2.08		4660	761	5431
H-6	IJP 1-3	0.0	5.45	0.86	303	493	318	811
	TOE 1	0.0	3.73	2.03		1675	535	2210
	TOE 3	0.0	3.92	2.08		3319125	1330	3320455
	IJP 2-4	0.0	5.01	0.82		1118	348	1466
	TOE 2	0.0	4.02	2.11		1772	757	2529
	TOE 4	0.0	4.79	2.14		186802	1250	188052

Table 4-1 (continued)

Spec. No.	Sites	Mean Stress (ksi)	K^A_{fmax}	K^B_{fmax}	Actual Life (Blocks)	N_I	N_P (Blocks)	N_T
H-7	IJP 1-3	10.5	5.41	0.69	269	189	56	235
	TOE 1	10.5	3.75	2.05		3851	87	4938
	TOE 3	10.5	3.15	1.97		109193	160	109353
	IJP 2-4	10.5	5.25	0.65		256	56	312
	TOE 2	10.5	3.27	2.00		17867	93	17760
	TOE 4	10.5	3.61	2.04		24103	173	24276
H-8	IJP 1-3	10.5	5.45	0.97	207	177	48	225
	TOE 1	10.5	3.81	2.07		4803	69	4872
	TOE 3	10.5	3.42	2.00		14412	150	14562
	IJP 2-4	10.5	5.20	0.64		264	64	330
	TOE 2	10.5	3.25	2.00		86120	106	86226
	TOE 4	10.5	3.66	2.07		383	34	417
H-9	IJP 1-3	10.5	5.18	0.77	678	275	45	320
	TOE 1	10.5	4.09	2.10		12928	348	13276
	TOE 3	10.5	3.99	2.07		4523	118	4641
	IJP 2-4	10.5	5.23	0.70		258	54	312
	TOE 2	10.5	3.66	2.06		6317	108	6425
	TOE 4	10.5	3.49	2.02		37953	161	38114
H-10	IJP 1-3	10.5	5.05	0.60	211	346	62	408
	TOE 1	10.5	3.43	2.03		21030	104	21134
	TOE 3	10.5	3.89	2.09		6130	156	6286
	IJP 2-4	10.5	5.58	0.97		151	37	188
	TOE 2	10.5	3.90	2.04		10115	136	10251
	TOE 4	10.5	3.91	2.10		3243	123	3366
H-11	IJP 1-3	21.0	5.64	0.96	232	60	37	97
	TOE 1	21.0	3.74	2.02		2030	96	2126
	TOE 3	21.0	3.62	2.01		7736	151	7887
	IJP 2-4	21.0	5.51	0.89		73	39	112
	TOE 2	21.0	3.73	2.03		3245	120	3365
	TOE 4	21.0	4.05	2.07		2656	188	2844
H-12	IJP 1-3	21.0	5.56	0.83	184	69	42	111
	TOE 1	21.0	3.85	2.07		1870	142	2012
	TOE 3	21.0	3.41	2.00		9928	92	10020
	IJP 2-4	21.0	5.87	0.94		44	35	79
	TOE 2	21.0	3.50	2.00		9719	87	9806
	TOE 4	21.0	3.30	1.97		56597	205	56802
H-13	IJP 1-3	21.0	5.39	0.84	173	87	45	132
	TOE 1	21.0	3.92	2.09		1832	85	1917
	TOE 3	21.0	3.72	2.04		1710	108	1818
	IJP 2-4	21.0	5.24	0.71		119	53	172
	TOE 2	21.0	3.51	2.03		1760	56	1816
	TOE 4	21.0	3.97	2.09		957	99	1056

Table 4-2

Life Prediction for 6.35 mm (1/4-in.) Specimens of Structural
Detail No. 20   under the Ship Block Load History.

Spec. No.	Sites	Mean Stress (ksi)	K^A_{fmax}	K^B_{fmax}	Actual Life (Blocks)	Predicted Life N_I	N_P (Blocks)	N_T
Q-1	IJP 1-3	10.5	4.38	0.75	306	1116	57	1173
	TOE 1	10.5	3.42	1.75		2338	70	2408
	TOE 3	10.5	2.76	1.66		116380	96	116476
	IJP 2-4	10.5	4.62	0.89		641	38	679
	TOE 2	10.5	2.74	1.65		24281	78	24355
	TOE 4	10.5	2.80	1.68		50684	77	50761
Q-2	IJP 1-3	10.5	4.34	0.92	292	1120	29	1149
	TOE 1	10.5	3.05	1.68		14128901	190	14129091
	TOE 3	10.5	3.74	1.72		912	79	991
	IJP 2-4	10.5	3.72	0.50		5102	95	5197
	TOE 2	10.5	3.24	1.74		109901	152	110053
	TOE 4	10.5	3.19	1.75		5433	93	5526
Q-3	IJP 1-3	0.0	4.56	0.90	787	2040	366	2406
	TOE 1	0.0	2.87	1.67		47118	691	47809
	TOE 3	0.0	3.00	1.70		124540	733	125273
	IJP 2-4	0.0	4.68	0.88		1710	309	2019
	TOE 2	0.0	2.75	1.66		41981	524	42505
	TOE 4	0.0	2.64	1.64		785075	975	786050
Q-4	IJP 1-3	0.0	4.56	0.90	415	2100	366	2466
	TOE 1	0.0	2.87	1.67		266881	972	267853
	TOE 3	0.0	2.81	1.67		38074	1090	19164
	IJP 2-4	0.0	4.41	0.74		2873	453	3326
	TOE 2	0.0	2.70	1.66		172104	580	172684
	TOE 4	0.0	2.74	1.69		16433	353	16786
Q-5	IJP 1-3	0.0	4.43	0.74	708	2738	367	3105
	TOE 1	0.0	2.66	1.65		42309	487	42796
	TOE 3	0.0	3.00	1.70		240662	1020	241682
	IJP 2-4	0.0	4.23	0.64		4111	543	4654
	TOE 2	0.0	2.68	1.66		84236	694	84930
	TOE 4	0.0	3.11	1.72		191131	1030	192161
Q-6	IJP 1-3	0.0	4.09	0.54	369	5560	507	6067
	TOE 1	0.0	3.16	1.72		80148	691	80839
	TOE 3	0.0	2.61	1.66		176802	876	177678
	IJP 2-4	0.0	4.45	0.84		2537	279	2816
	TOE 2	0.0	3.87	1.75		24746	1410	26156
	TOE 4	0.0	3.06	1.68		14875	504	15379

Table 4-2 (continued)

Spec. No.	Sites	Mean Stress (ksi)	K_{fmax}^A	K_{fmax}^B	Actual Life (Blocks)	Predicted Life		
						N_I	N_P (Blocks)	N_T
Q-7	IJP 1-3	0.0	4.53	0.84	267	2332	392	2724
	TOE 1	0.0	2.71	1.67		117203	748	117951
	TOE 3	0.0	2.74	1.68		785480	1240	786720
	IJP 2-4	0.0	4.63	0.83		1776	392	2168
	TOE 2	0.0	2.58	1.64		72605	547	73152
	TOE 4	0.0	2.97	1.68		359151	1100	360251
Q-8	IJP 1-3	0.0	4.20	0.64	506	4645	543	5188
	TOE 1	0.0	2.75	1.68		49290	571	49861
	TOE 3	0.0	2.75	1.67		924094	1230	925324
	IJP 2-4	0.0	4.10	0.59		5478	595	6073
	TOE 2	0.0	2.61	1.70		95957	718	96675
	TOE 4	0.0	3.26	1.78		24238	971	25209

Table 4-3

Fatigue Life Prediction for the Modified Specimens
of Structural Detail No. 20.

Spec. No.	Sites	Mean Stress (ksi)	K^A_{fmax}	K^B_{fmax}	Actual Life (Blocks)	Predicted Life		
						N_I	N_P (Blocks)	N_T
C-1	IJP 1-3	0.0	6.56	1.19	739	52	116	168
	TOE 1	0.0	5.17	2.42		1359	1200	2559
	TOE 3	0.0	4.76	2.34		565	560	1125
	IJP 2-4	0.0	6.84	1.23		42	93	135
	TOE 2	0.0	4.32	2.29		17236	1760	18996
	TOE 4	0.0	5.29	2.38		510	969	1479
C-2	IJP 1-3	0.0	6.57	1.20	326	52	101	153
	TOE 1	0.0	4.74	2.38		18525	871	19396
	TOE 3	0.0	4.60	2.33		602	604	1206
	IJP 2-4	0.0	6.19	0.98		82	124	206
	TOE 2	0.0	4.70	2.36		146073	1350	147423
	TOE 4	0.0	5.53	2.47		189	728	917
C-3	IJP 1-3	0.0	5.36	0.87	252	650	378	968
	TOE 1	0.0	3.75	2.04		831918	598	832516
	TOE 3	0.0	4.01	2.06		9809	2220	12029
	IJP 2-4	0.0	5.11	0.72		955	390	1345
	TOE 2	0.0	3.86	2.06		6817787	1530	6819317
	TOE 4	0.0	4.09	2.10		920	592	1512
C-4	IJP 1-3	0.0	5.66	0.94	320	397	290	687
	TOE 1	0.0	3.62	2.01		483354	458	483812
	TOE 3	0.0	4.10	2.10		3146	1090	4236
	IJP 2-4	0.0	5.17	0.71		788	390	1178
	TOE 2	0.0	3.67	2.04		24051043	2260	24053303
	TOE 4	0.0	3.70	2.05		1690	419	2109
C-5	IJP 1-3	0.0	4.29	0.76	338	3782	453	4235
	TOE 1	0.0	3.06	1.71		24288	656	24944
	TOE 3	0.0	3.00	1.69		213261	989	214250
	IJP 2-4	0.0	4.11	0.65		5406	543	5949
	TOE 2	0.0	2.99	1.70		77761	1010	78771
	TOE 4	0.0	3.02	1.70		971657	2240	973897
C-6	IJP 1-3	0.0	4.18	0.64	497	4590	543	5133
	TOE 1	0.0	2.79	1.68		36497	612	37109
	TOE 3	0.0	2.94	1.74		8111241	912	8112153
	IJP 2-4	0.0	3.91	0.56		8290	650	8940
	TOE 2	0.0	3.07	1.72		16645	656	17301
	TOE 4	0.0	3.10	1.73		4415649	900	4416549

Table 4-4

Fatigue Life Prediction of the Specimens of
Cruciform Joints by GMAW Process.

Spec. No.	Sites	Mean Stress (ksi)	K^A_{fmax}	K^B_{fmax}	Actual Life (Blocks)	Predicted Life		
						N_I	N_P (Blocks)	N_T
M-1	IJP 1-3	12.3	4.37	0.25	110	10	34	44
	TOE 1	12.3	2.68	1.95		167	10	177
	TOE 3	12.3	2.68	1.95		276	12	288
	IJP 2-4	12.3	3.93	0.16		22	50	72
	TOE 2	12.3	2.59	1.92		231	10	241
	TOE 4	12.3	2.62	1.94		351	12	363
M-2	IJP 1-3	9.0	3.94	0.17	258	23	96	119
	TOE 1	9.0	2.62	1.94		245	14	259
	TOE 3	9.0	2.57	1.91		442	15	457
	IJP 2-4	9.0	4.33	0.25		13	50	63
	TOE 2	9.0	2.59	1.91		749	20	769
	TOE 4	9.0	2.68	1.95		433	19	452
M-3	IJP 1-3	6.3	3.94	0.18	345	23	96	119
	TOE 1	6.3	2.68	1.96		151	18	169
	TOE 3	6.3	2.59	1.92		1081	33	1111
	IJP 2-4	6.3	4.18	0.19		19	93	109
	TOE 2	6.3	2.55	1.90		740	27	767
	TOE 4	6.3	2.63	1.94		271	20	291
M-4	IJP 1-3	3.0	4.36	0.24	302	17	140	157
	TOE 1	3.0	2.63	1.93		280	35	315
	TOE 3	3.0	2.66	1.95		1364	66	1430
	IJP 2-4	3.0	4.49	0.24		15	140	155
	TOE 2	3.0	2.55	1.89		1133	54	1187
	TOE 4	3.0	2.69	1.97		2245	85	2330
M-5	IJP 1-3	0.0	4.57	0.29	(stopped	16	226	242
	TOE 1	0.0	2.65	1.93	by power	660	88	748
	TOE 3	0.0	2.62	1.92	failure	790	88	878
	IJP 2-4	0.0	4.01	0.15	at 299	39	372	411
	TOE 2	0.0	2.50	1.90	blocks)	1048	87	1135
	TOE 4	0.0	2.55	1.90		1617	102	1719
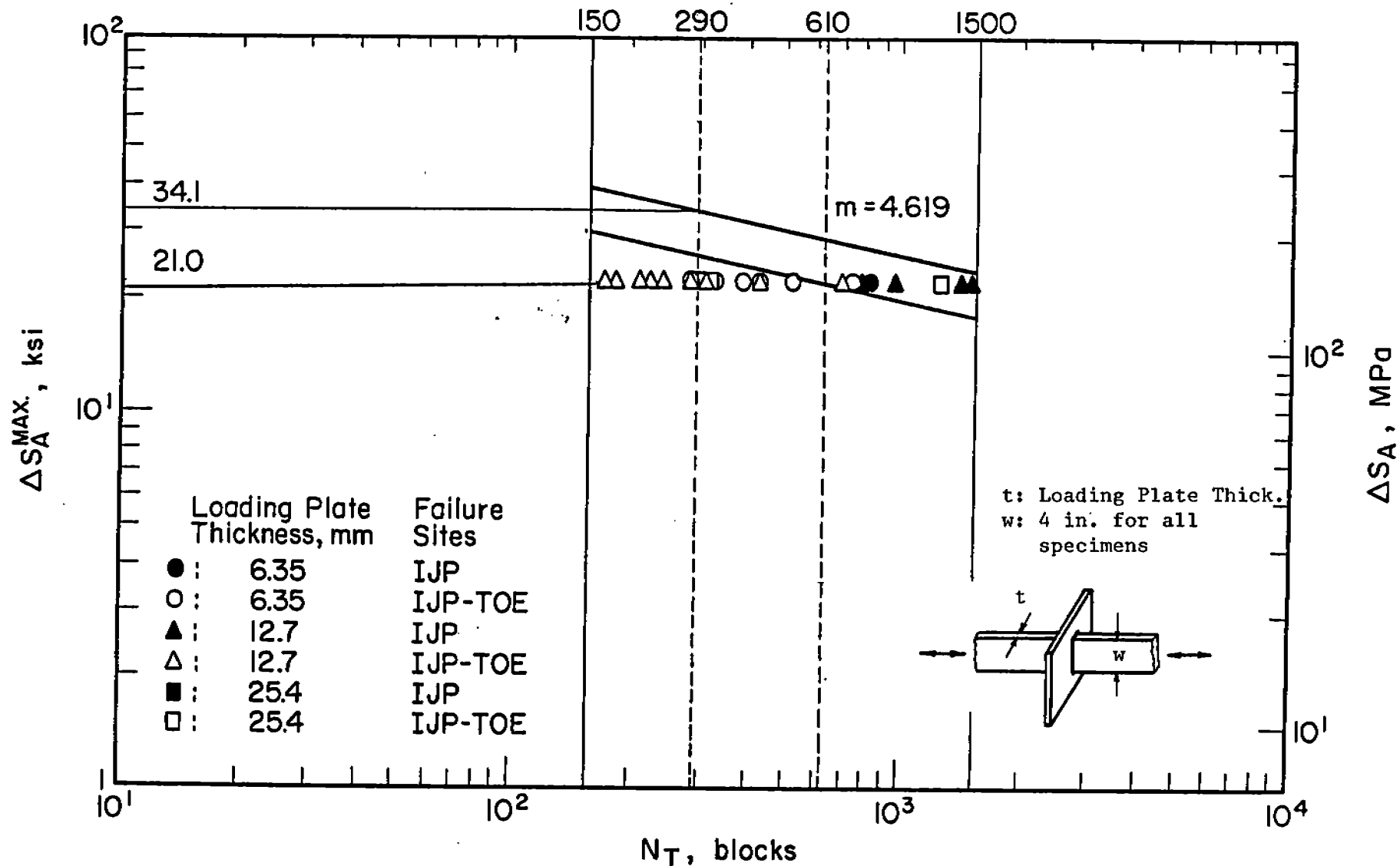
Fig. 4-1 Test data compared with the predictions of the Munse Fatigue Design Procedure. The sloped lower solid line is the prediction for the edited history. The sloped top solid line is the prediction for the full SL-7 history. The Munse Fatigue Design Procedure is based on the extended S-N diagram and therefore predicts a large influence for the small cycles absent in edited history. S_A^{max} is the biggest stress range in the load history.
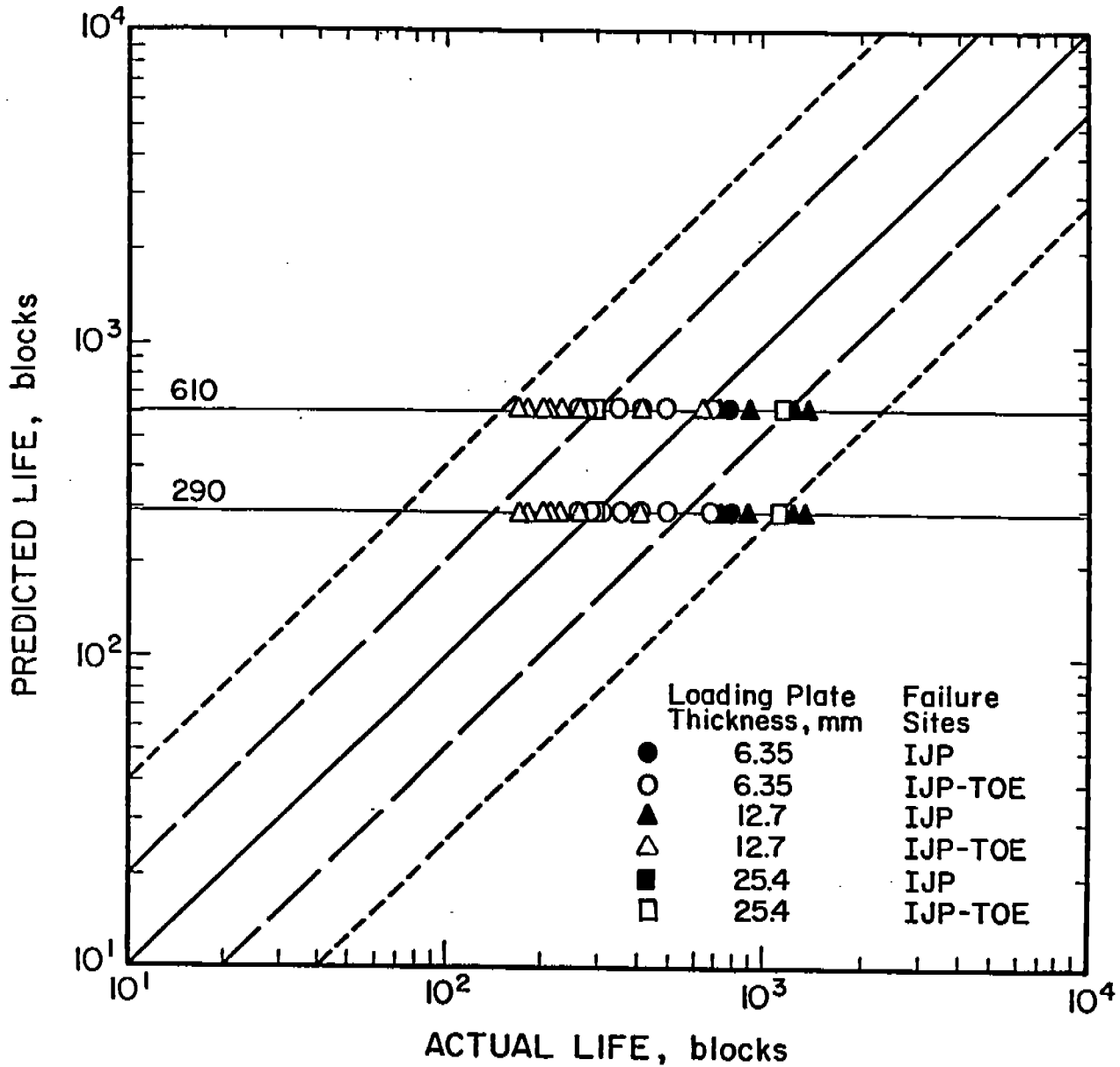
Fig. 4-2 Actual total fatigue lives (blocks) compared with total
fatigue lives predicted using the Munse Fatigue Design
Procedure. The top solid line is the prediction for the
edited history. "The lower solid line is the prediction
for the full SL-7 history. The dashed lines represent
factors of two and four departures from perfect agreement.
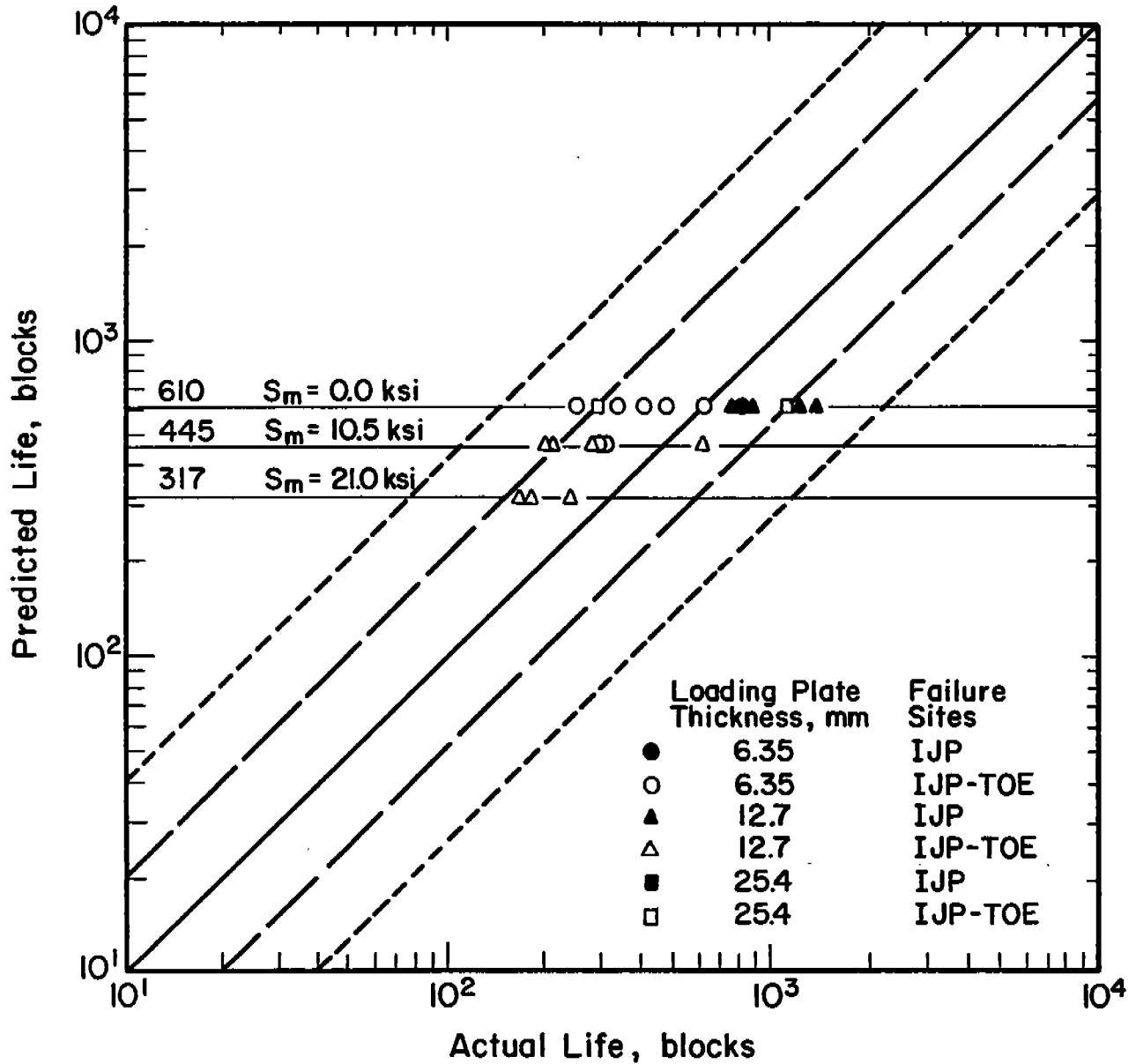
Fig. 4-3 Comparison of observed total lives with prediction of the
Munse Fatigue Design Procedure modified to include the effects
of mean stress. See Eq. 4-1. The horizontal solid lines are
predictions for different levels of applied mean stress. The
dashed line represent factors of two and four departures
from perfect agreement.
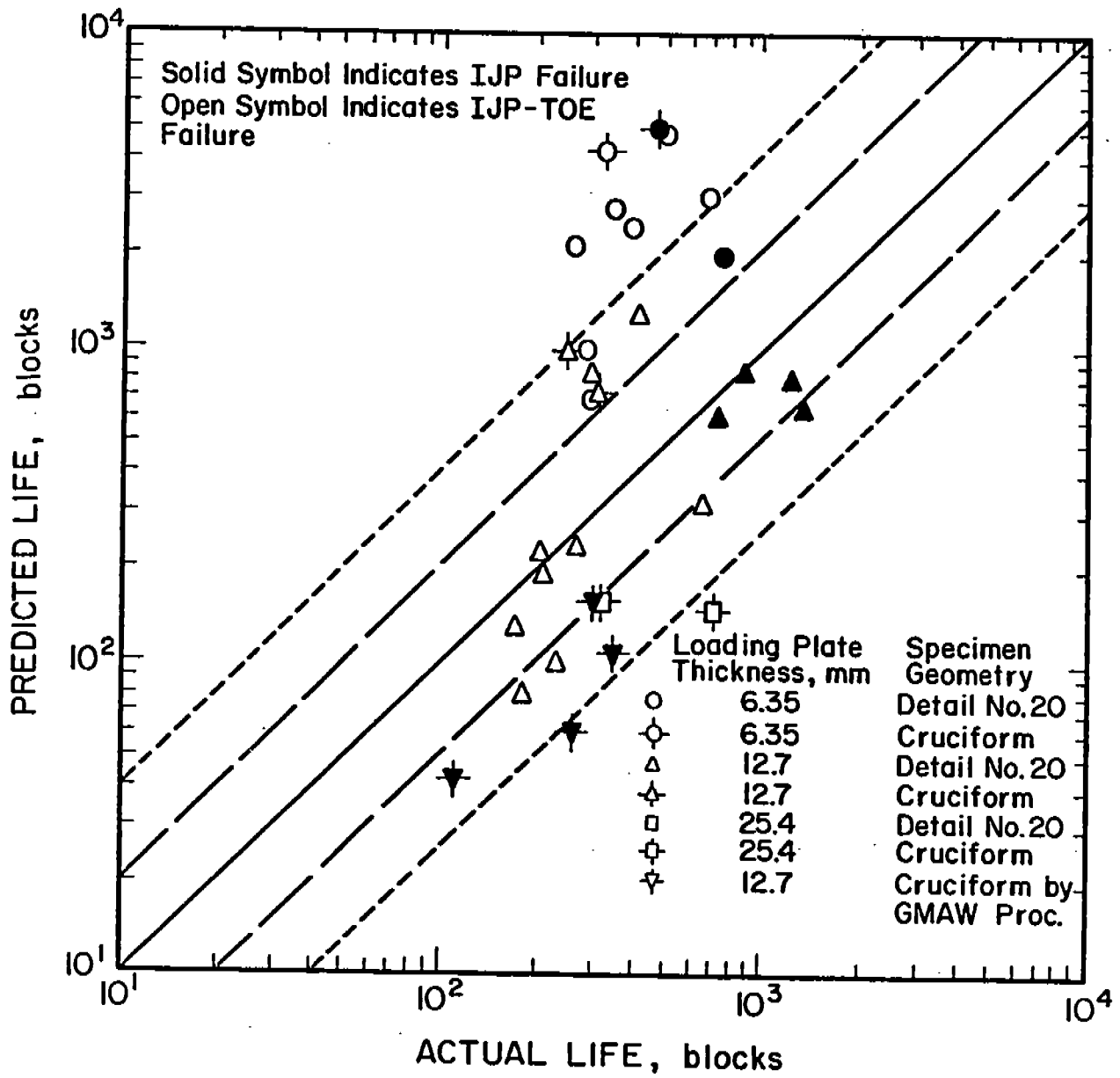
Fig. 4-4 Actual Total Fatigue lives (blocks) compared with total fatigue
lives predicted using the initiation-propagation (IP) model.
The predictions for all specimens are included in this figure.
The dashed lines represent factors of two and four departures
from perfect agreement.
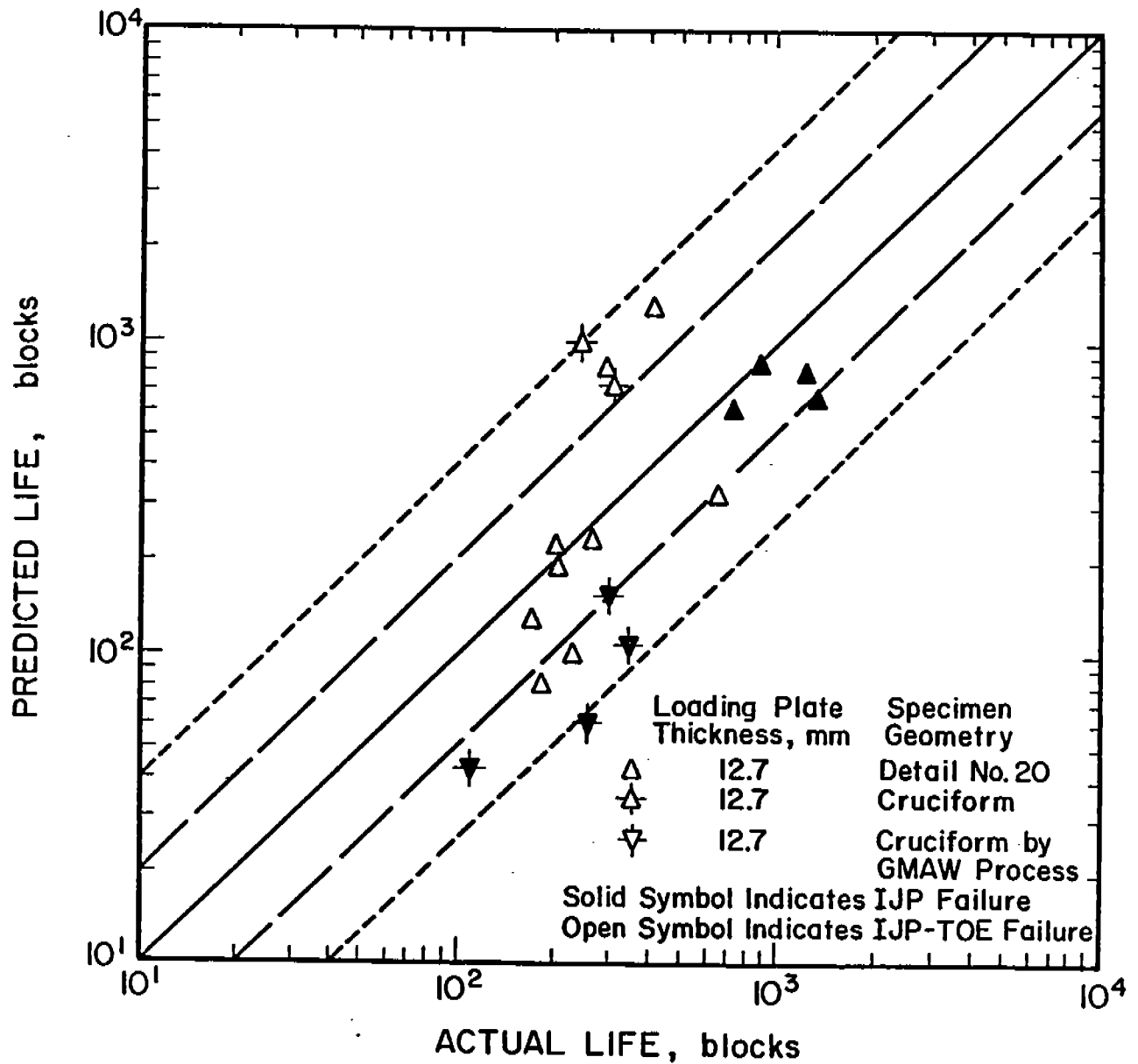
Fig. 4-5   Actual total fatigue lives (blocks) compared with total
fatigue lives predicted using the initiation-propagation
model. The predictions are only for the 12.7 mm thick
specimens. The dashed lines represent factors of two and
four departures from perfect agreement.
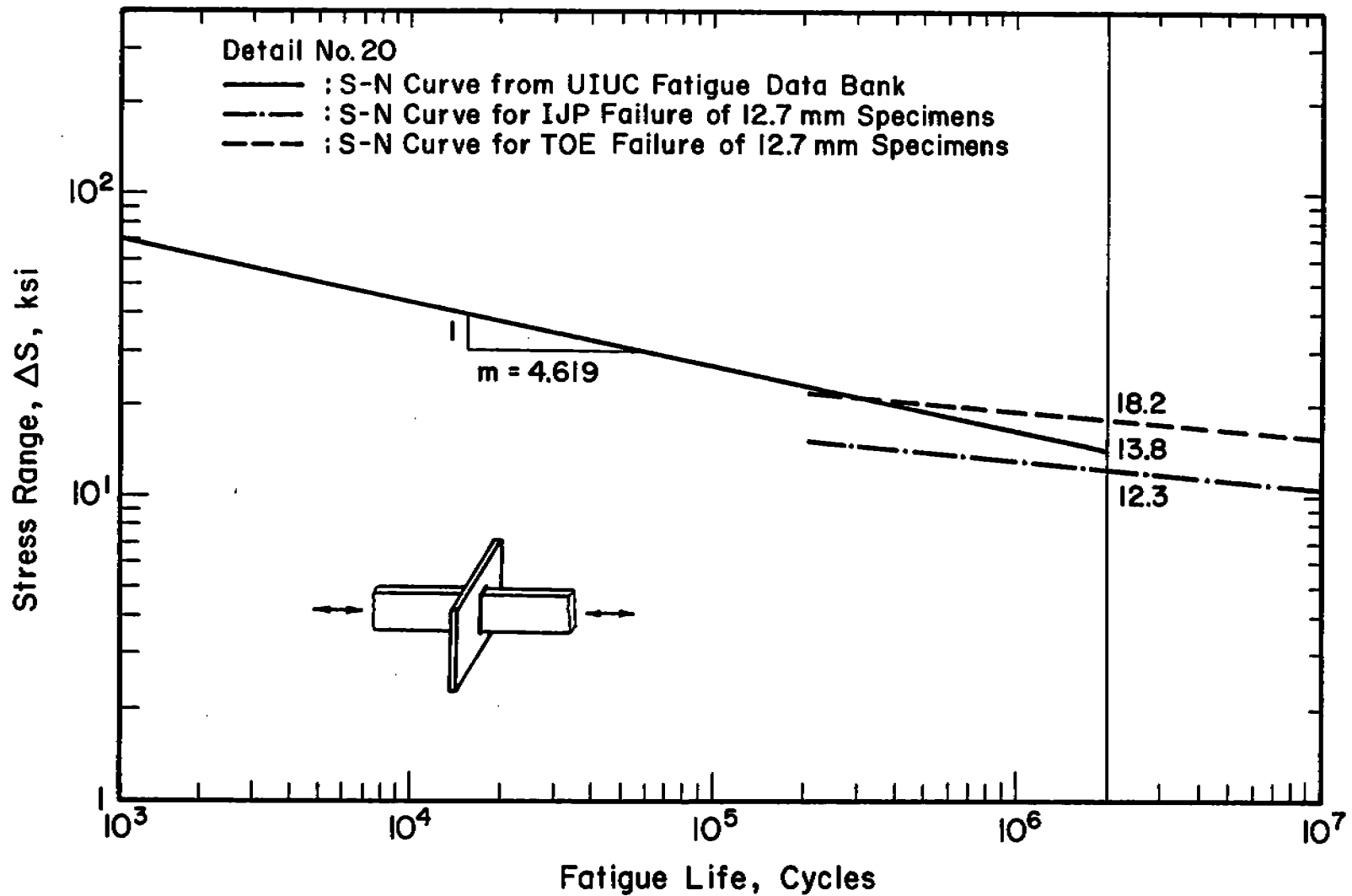
Fig. 4-6 Comparison of the S-N curve for detail No. 20 taken from the UIUC fatigue data bank with the long life behavior predicted by the I-P model. See Eq. 4-2.
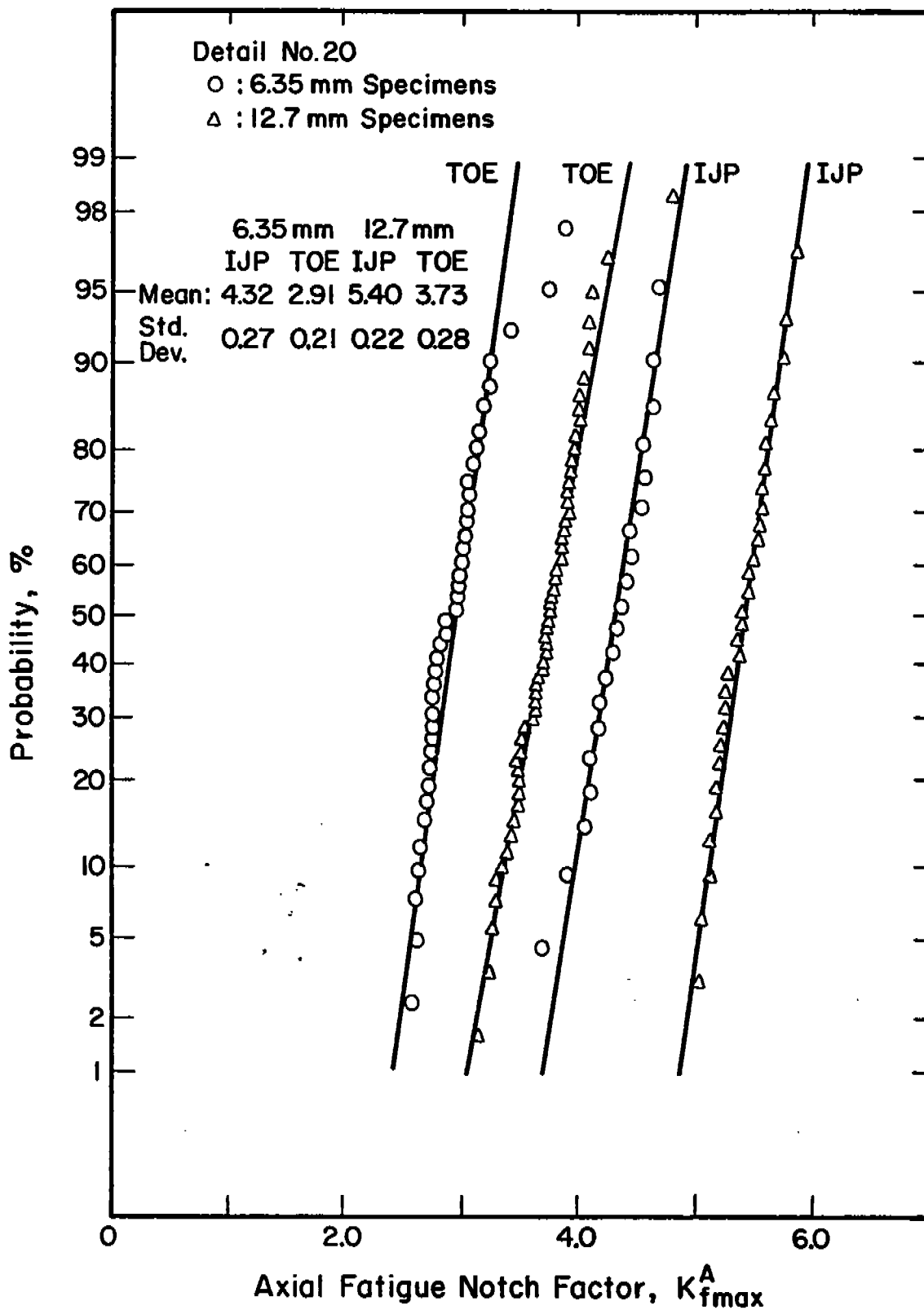
Fig. 4-7 A plot of the cumulative probability of the axial fatigue notch factor (K_{fmax}^{A}) on the normal probability paper which shows that K_{fmax}^{A} is normally distributed.

105
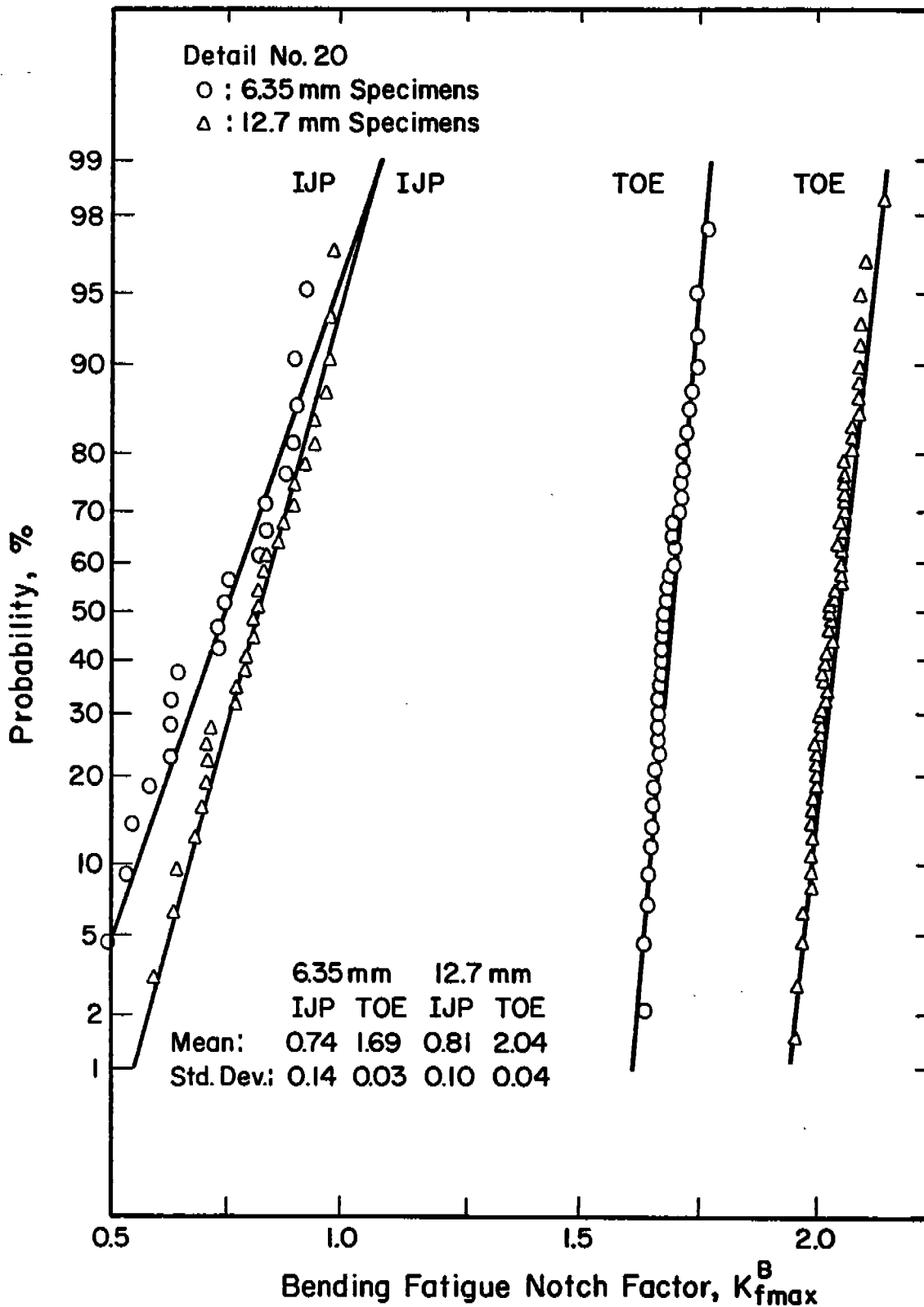
Fig. 4-8 A plot of the cumulative probability of the bending fatigue notch factor (K^B_{fmax}) on the normal probability paper which shows that the K^B_{fmax} can be described by the normal probability distribution.

106
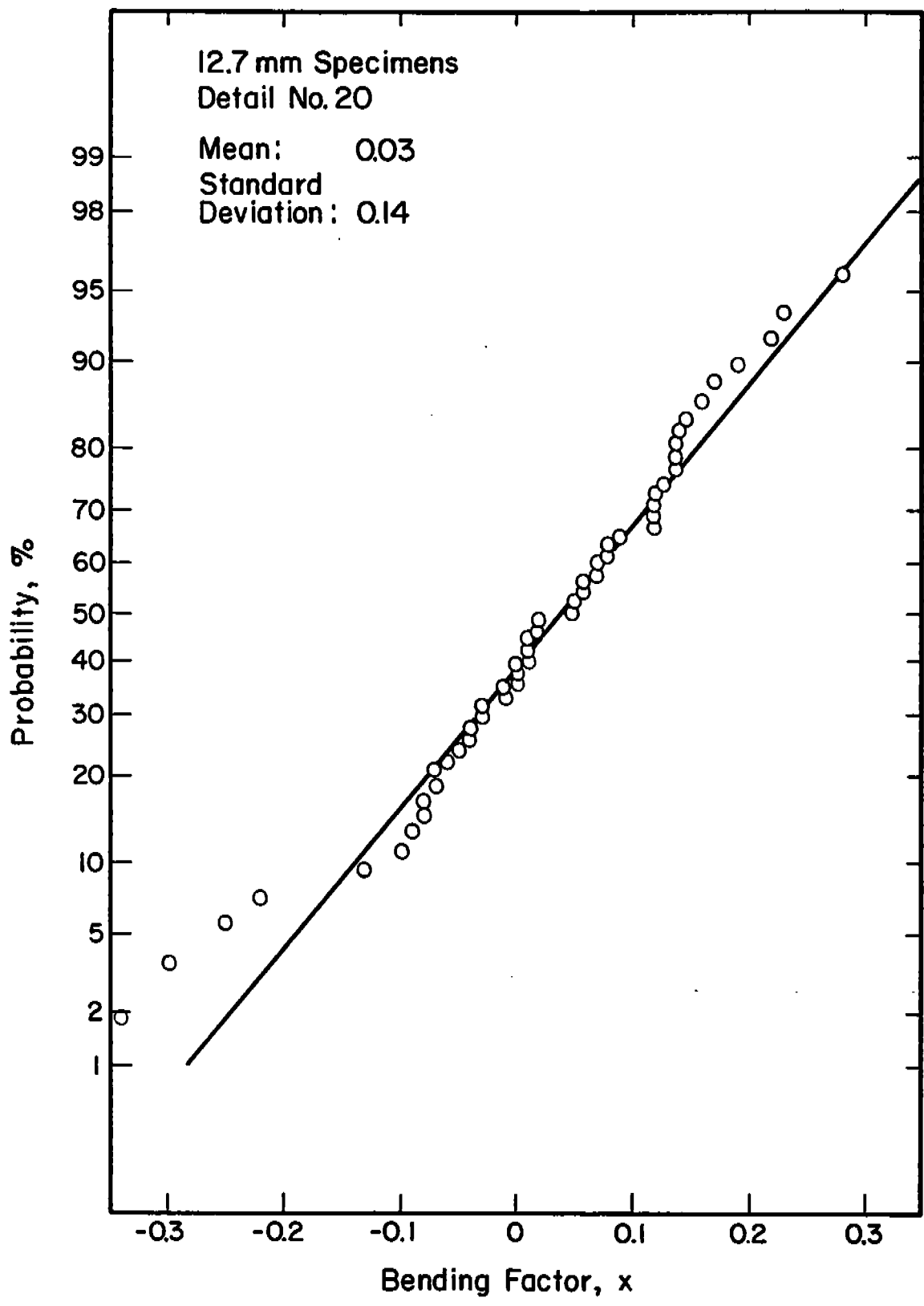
Fig. 4-9 A plot of the cumulative probability of the bending factor
x on the normal probability paper which shows that x can be
described by the normal probability distribution.
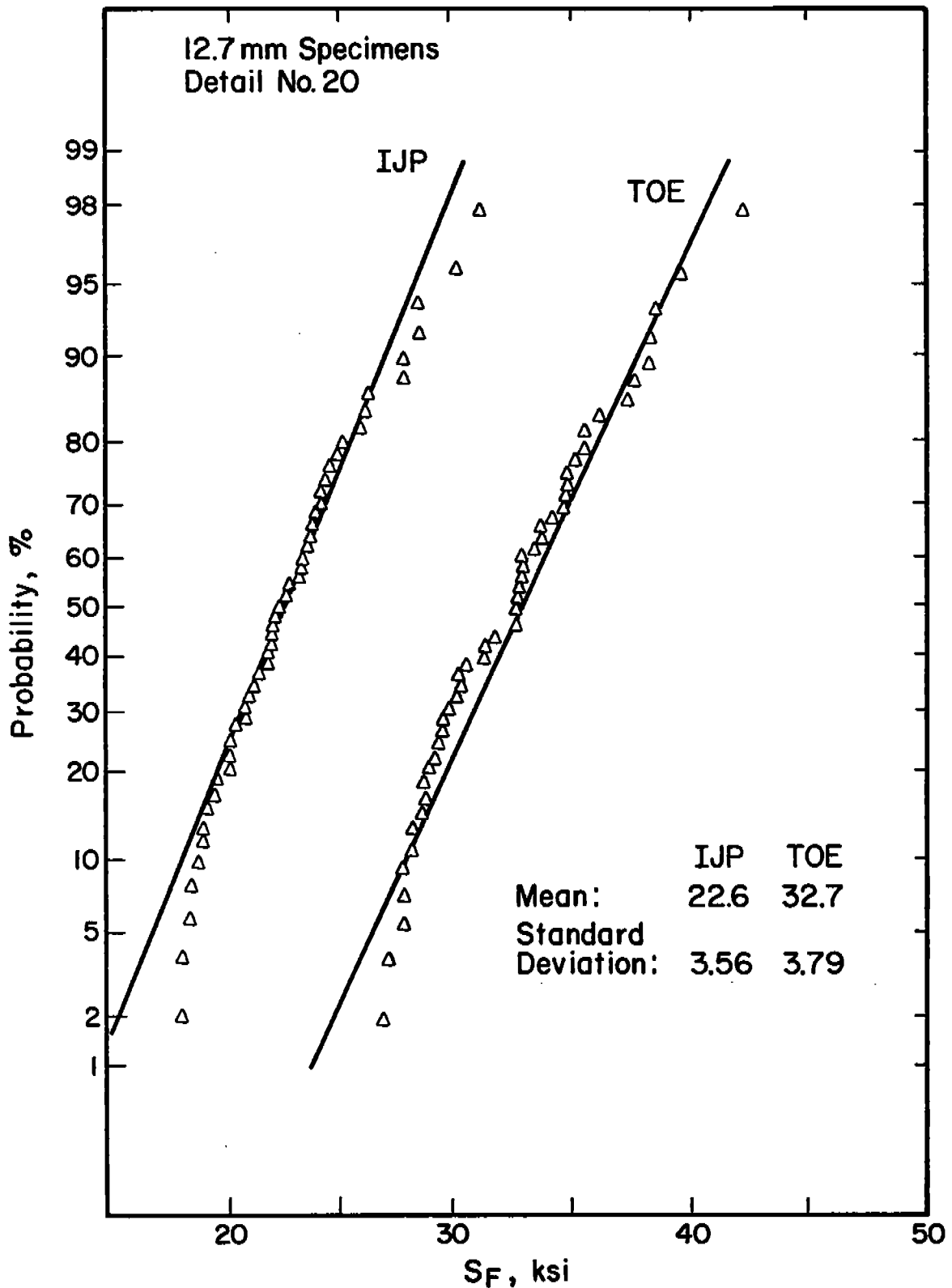
Fig. 4-10 A plot of the cumulative probability of the constant S_F for values of x (-1 x 1) for 12.7 mm specimens. This simulates the situation in which the bending stresses can only increase or decrease the cyclic stress and hence increase or decrease the fatigue life.

108
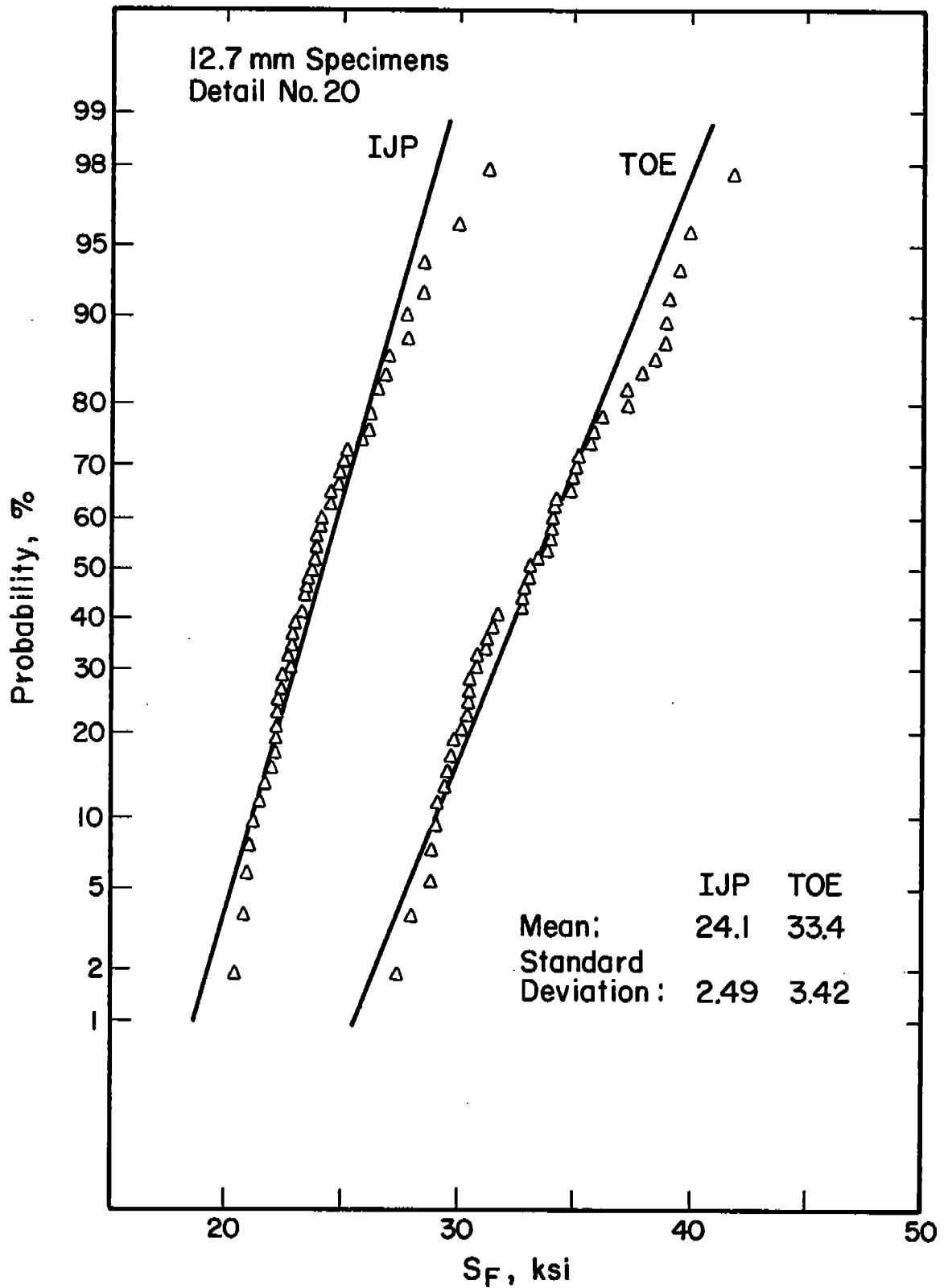
Fig. 4-11 A plot of the cumulative probability of the constant S_F for values of x (0 x 1) for 12.7 mm specimens. This simulates the situation in which the induced bending stresses can only increase or decrease the cyclic stress at some location in the weldment and hence only reduce the fatigue life.
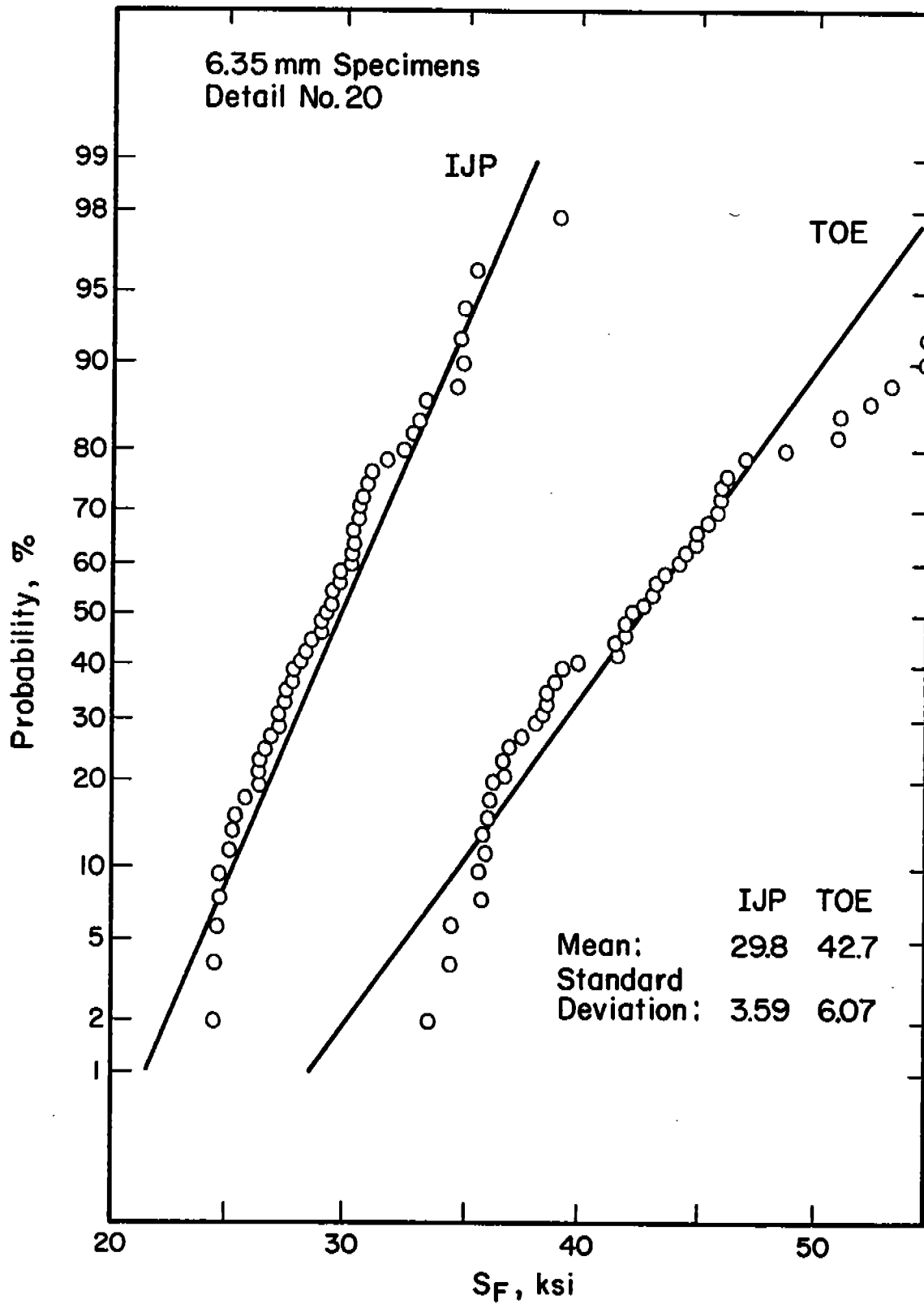
Fig. 4-12 A plot of the cumulative probability of the constant S_F for values of x (-1 x 1) for 6.35 mm specimens. This simulates the situation in which the induced bending stresses can either increase or decrease the cyclic stress and hence increase or reduce the fatigue life.

110
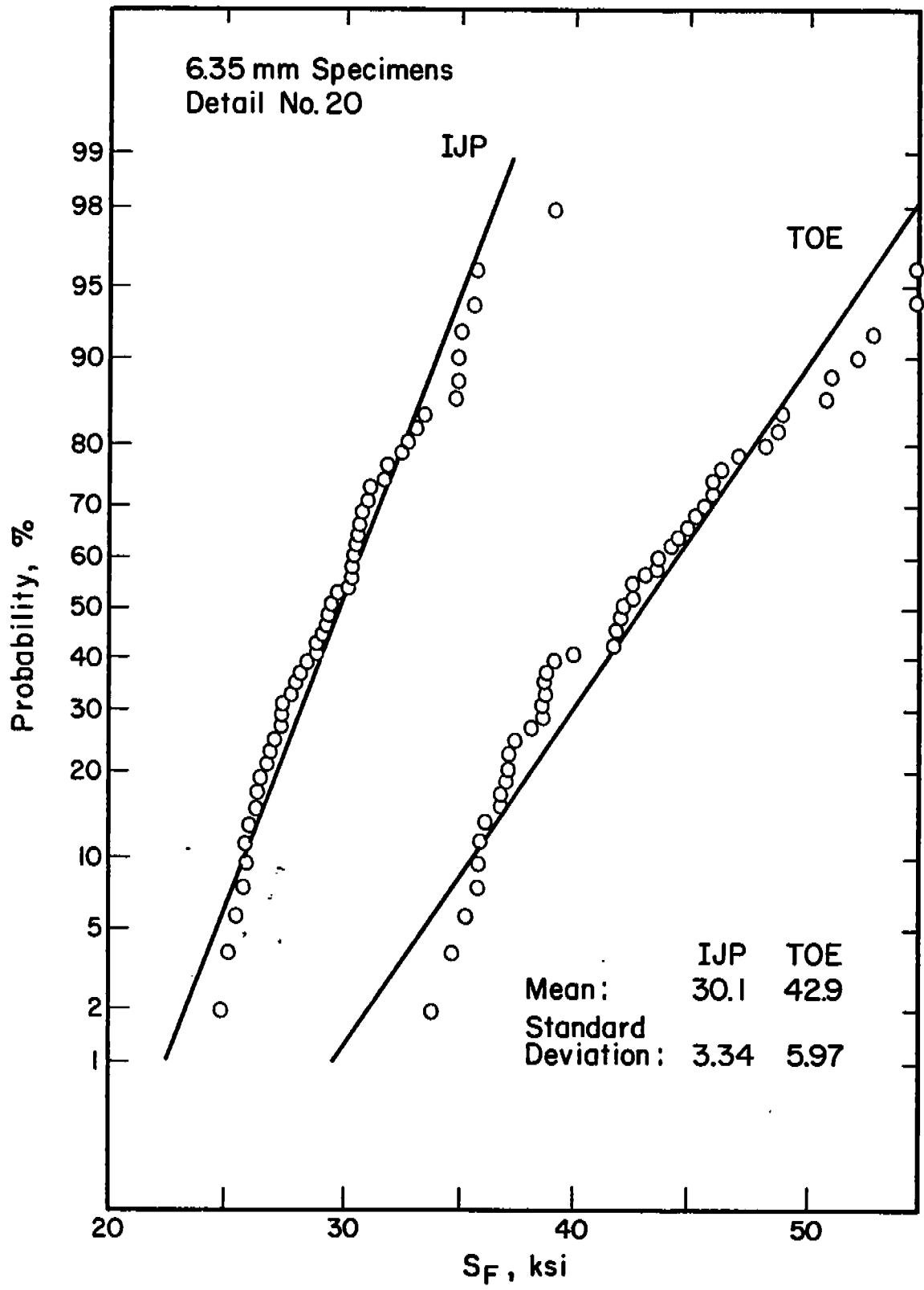
Fig. 4-13 A plot of the cumulative probability of the constant S_F for values of x (0 x 1) for 6.35 mm specimens. This simulates the situation in which the induced bending stresses can only increase or decrease the cyclic stress at some location in the weldment and hence only reduce the fatigue life.

111

5. FATIGUE TESTING OF SHIP STRUCTURAL DETAILS
UNDER CONSTANT AMPLITUDE LOADING (TASK 7)

Munse categorized 53 ship structural weld details shown in Fig. 4-1. Five details (Details No. 34, 39-A, 43, 44 and 47) were selected from this collection and fatigue tested to establish the constant amplitude S-N diagram. Details were selected based on the greatest need for data and upon recommendations of the project advisory committee (Table 3-2).

5.1 Materials and Welding Process

Table 3-3 lists the mechanical and chemical properties of the steels used in this study. The properties of these steels are within the specifications for ASTM A-36 steel and the specifications for ASTM A131 ship plate Grade A. To reduce possible scatter in the test data, materials having nearly identical mechanical properties were selected. The range of yield strength was restricted to 284 to 335 MPa (41.2 to 48.6 ksi), and the range of ultimate tensile strength was restricted to 441 to 489 MPa (64 to 71 ksi).

The specimens were welded using the shielded-metal-arc-welding (SMAW) process and E7018 electrodes described earlier in Section 3.4. The welding parameters were 17 to 22 volts and 125 to 230 amperes; no preheat or interpass temperatures were used. Welding was carried out in the flat or horizontal position.

5.2 Specimen Preparation, Testing Conditions and Test Results
5.2.1 Detail No. 34 - A Fillet Welded Lap Joint.

Detail No. 34 is a lap joint with fillet welds on both sides as shown in Fig. 5-2. Two 12.7 mm (1/2-in.) thick plates were welded to a 15.9 mm (5/8-in.) thick center plate. The leg size of the weld (w) was 6.35 mm (1/4-in.), and the length of the weld on each side was 241 mm (9.5-in.). To induce pure bending moment at the expected crack initiation sites, a fixture for the four-point-bending shown in Fig. 5-3 was designed. All specimens were tested in a 223 kN (50 kip) MTS machine with zero-to-maximum load cycle (R $\doteq$ 0).

Table 5-1 lists the test results, and Fig. 5-4 shows the S-N curve for Detail No. 34. The S-N curve had an intercept (log C) of 16.96 and a slope (m) of 7.41: see Table 5-6. Figure 5-5 shows a schematic drawing of the failure mode for this detail. Cracks initiated in the strap plate at the end of the weld as shown in Fig. 5-5 and propagated perpendicular to the maximum principal stresses to final rupture. Fig. 5-6 shows a typical fracture surface including the initiation site, propagation path and the final ductile rupture surface.

5.2.2 Detail No. 39-A - A Fillet Welded I-Beam with a Center Plate Intersecting the Web and One Flange.

As shown in Fig. 5-7, Detail No. 39-A is fillet-welded I-beam structure. Plates 12.7 mm (1/2-in.) thick were used for both the web and flange plates. The leg size of the welds (w) was nominally 6.35 mm (1/4-in.) for all of the weldments. A separate loading fixture, shown in Fig. 5-8, was made to induce pure bending. A 2670 kN (600 kip) capacity MTS machine was used, and Fig. 5-9a shows a specimen mounted in the test frame. All specimens were tested using a zero-to-maximum load cycle (R - 0).

Table 5-2 lists the fatigue data, and Fig. 5-10 shows the S-N curve for the Detail No. 39-A. The best fit curve to the test data had an intercept (log C) of 12.60 and a slope (m) of 5.87: see Table 5-6. Cracks initiated at the weld toe and the incomplete joint penetration (IJP) sites in the tensile stressed zone as shown in Fig. 5-9b. Figure 5-11 shows the fracture surface and failure mode observed in low cycle regime. In the lower cycle regime, cracks initiated in the flange at the weld toe and the IJP sites and became connected during the final failure as the crack progressed through the weld joining the web and center plates. The two specimens which failed at lives over 400,000 cycles had cracks which initiated at the IJP site and propagated to the surface of the weld at the flange plates along the critical throat of the weld. As was observed in the lower cycle regime, the cracks propagated through the weld joining the web and center plate to final rupture. Figure 5-12 shows the fracture surface and failure mode of a specimen which was tested using a 94 MPa (13.6 ksi) stress range and failed after 700,000 cycles.

113

5.2.3 Detail No. 43 - A Partial-Penetration Butt Weld

Figure 5-13 shows the geometry and dimensions of the specimen of Detail No. 34, a partial penetration butt-welded joint which was tested in pure bending. Plates 15.9 mm (5/8-in.) thick were used as the base plates. The four-point bending fixture was used for the testing of Detail No. 34 (Fig. 5.3). A 223 kN (50 kip) MTS machine was used. Figure 5-14a shows a mounted specimen. All specimens were tested with zero-to-maximum load cycle (R = 0).

Table 5-3 lists the fatigue data, and Fig. 5-15 shows the S-N curve for Detail No. 43. The best-fit curve had an intercept (log C) and slope (m) of 13.47 and 5.13, respectively, see Table 5-6. Cracks initiated at the tensile IJP sites and propagated perpendicular to the maximum tensile stress direction as shown in Fig. 5-16. Figure 5-14b shows a typical failure of a specimen including the fracture surface and the crack propagation path.

5.2.4 Detail No. 44 - Tubular Cantilever Beam

As shown in Fig. 5-17 Detail No. 44 is a tubular cantilever beam welded to a plate using a circumferential fillet weld. A 4.8 mm (3/16-in.) thick tube with 50.8 mm (2-in.) outer diameter was welded to a 12.7 mm (1/2-in.) thick plate by fillet weld having a 6.35 mm (1/4-in.) leg length. This detail was subjected to a cantilever bending load using the load fixture shown in Fig. 5-18. A back-up plate was used to increase the rigidity of the base plate. A 89 kN (20 kip) MTS machine was used, and Fig. 5-19a shows the specimen mounted in the test machine. All specimens were tested using a zero-to-maximum load cycle (R = 0).

Table 5-4 lists the test results and Fig. 5-20 shows the S-N curve for Detail No. 44. The best-fit curve had an intercept (log C) and slope (m) of 13.14 and 5.66, respectively (Table 5-6). With the back-up plate as shown in Fig. 5-18, the crack initiated at the weld toe on the tube (Fig. 5-21-Type B). However, without the back-up plate), the crack initiated at the weld toe on the plate as shown in Fig. 5-21 - Type A. Figure 5-19b shows a broken specimen with the crack initiated at the weld toe on the tube.

5.2.5 Detail No. 47 - A Fillet-Welded Tubular Penetration

As Fig. 5-22 shows, Detail No. 47 was a 65 mm length tube inserted into a plate and fillet welded. The 3.8 mm (0.15-in.) wall thickness tube had a with 50.8 mm (2-in.) outer diameter; 12.7 mm (1/2-in.) thick plates were used. The leg size of the weld was 6.35 mm (1/4-in.). The specimen was axially loaded and directly gripped and tested in 445 kN (100 kips) or 2670 kN (600 kips) capacity MTS machines. To study the effects of width on the stress concentration factor of the fatigue initiation site, two testpiece widths were used: 101.6 mm (4-in.) wide specimens were tested in the 445 kN MTS machine and 197 mm (7-3/4-in.) wide specimens were tested in a 2670 kN MTS machine. Fig. 5-23a shows the 102 mm (4-in.) specimen equipped in the 445 kN MTS machine. All the specimens were tested using a zero-to-maximum load cycle (R=0).

Table 5-5 presents the fatigue data and Figs. 5-24 and 5-25 show the S-N curves for Detail No. 47. As mentioned above, this detail had two geometries with two different plate widths. On the basis of the nominal gross-section plate stress range, the two different width specimens showed a difference in fatigue life. As shown in Table 5-6: the 101.6 mm width specimens had an intercept (log C) of 10.80 and a slope (m) of 4.16; whereas, 197 mm width specimens had an intercept and slope of 11.45 and 4.26.

Utilizing net section stress range in the plate at the expected initiation site (which was the mid-point of quarter-circular arc), the results from these two different geometries can be made coincident as shown in Fig. 5-25. Figure 5-26 schematically shows the fatigue crack initiation site and the failure paths. Two opposite paths are possible. The initiation of a crack at about 45 degrees above and below the horizontal at the weld toe is due to the fact that this location has the greatest component of stress normal to the weld toe. In contrast, at the point 0 in Fig. 5-26, there is only a small normal stress due to the nearby presence of a free surface; at point P, the stress is parallel to the weld toe. After initiation, the fatigue crack propagated along the weld toe to the point where it changed its direction and turned normal to the maximum tensile stress, Fig. 5-23b shows a broken specimen, and Fig. 5-27 shows a typical fracture surface for this detail.

115

Table 5-1

Fatigue Data for The Ship Structural Detail No.34 under Constant Amplitude Loading, R=0.

Spec. No.	(a) Stress Cycle, Mpa (ksi)			Load Cycle, kN (kips)			Cycles to Failure
	min.	max.		min.	max.		
34-1	0.0	331	(48.0)	0.0	89	(20.0)	49,510
34-2	0.0	290	(42.0)	0.0	78	(17.5)	143,660
34-3	0.0	269	(39.0)	0.0	73	(16.3)	239,910
34-4	0.0	248	(36.0)	0.0	67	(15.0)	707,670
34-5	0.0	221	(32.0)	0.0	59	(13.3)	229,130
34-6	0.0	207	(30.0)	0.0	56	(12.5)	279,870

(a) ; Nominal bending stress at the cross-section A in Fig. 5-2.

Table 5-2

Fatigue data for the Ship Structural Detail No. 39-A
under Constant Amplitude Loading, R=0.

Spec. No.	(a) Stress Cycle, Mpa (ksi)			Load Cycle, kN (kips)			Cycles to Failure
	min.	max.		min.	max.		
39-A-1	0.0	250	(36.2)	0.0	356	(80.0)	2,300
39-A-2	0.0	187	(27.1)	0.0	267	(60.0)	24,870
39-A-3	0.0	150	(21.7)	0.0	214	(48.0)	52,820
39-A-4	0.0	125	(18.1)	0.0	178	(40.0)	304,620
39-A-5	0.0	94	(13.6)	0.0	133	(30.0)	441,010
39-A-6	0.0	94	(13.6)	0.0	133	(30.0)	706,460

(a) ; Nominal bending stresses at the cross-section A in Fig. 5-7.

Table 5-3

Fatigue Data for the Ship Structural Detail No.43
under Constant Amplitude Loading, R=0.

Spec. No.	(a) Stress Cycles, Mpa (ksi)			Load Cycles, kN (kips)			Cycles to Failure
	min.	max.		min.	max.		
43-1	0.0	362	(52.5)	0.0	133	(30.0)	64,050
43-2	0.0	302	(43.8)	0.0	111	(25.0)	99,990
43-3	0.0	241	(35.0)	0.0	89	(20.0)	208,490
43-4	0.0	241	(35.0)	0.0	89	(20.0)	902,490
43-5	0.0	181	(26.3)	0.0	67	(15.0)	1,069,690
43-6	0.0	181	(26.3)	0.0	67	(15.0)	1,178,270

(a) ; Nominal bending stress at the cross-section of the center of the weldment including the Incomplete Joint Penetration and two weld reinforcements whose average size is 2 mm for each.

Table 5-4

Fatigue Data for The Ship Structural Detail No.44
under Constant Amplitude Loading, R=0.

Spec. No.	(a) Stress Cycle, Mpa (ksi)			Load Cycle, kN (kips)			Cycles to Failure
	min.	max.		min.	max.		
44-1	0.0	242	(35.1)	0.0	8.90	(2.0)	44,750
44-2	0.0	181	(26.3)	0.0	6.07	(1.5)	79,510
44-3	0.0	145	(21.1)	0.0	5.34	(1.2)	279,780
44-4	0.0	121	(17.6)	0.0	4.45	(1.0)	1,255,870
44-5	0.0	121	(17.6)	0.0	4.45	(1.0)	1,922,560
44-6	0.0	99	(14.1)	0.0	3.56	(0.8)	3,722,000

(a) ; Nominal stress at the cross-section of the tube including the toe of the fillet weldment.

Table 5-5

Fatigue Data for The Ship StructuralDetail No. 47
under Constant Amplitude Loading, R=0.

Spec. No.(a)	Stress Cycle, Mpa (ksi) min.	max.1(b)	max.2(c)	Load Cycle, kN (kips) min.	max.		Cycles to Failure
47-1	0.0	207 (30.0)	319 (46.3)	0.0	267	(60.0)	48,950
47-2	0.0	130 (20.0)	192 (30.9)	0.0	178	(40.0)	329,930
47-3	0.0	121 (17.5)	186 (27.0)	0.0	156	(35.0)	486,040
47-4	0.0	103 (15.0)	160 (23.2)	0.0	133	(30.0)	993,360
47-5	0.0	90 (13.0)	139 (20.1)	0.0	116	(26.0)	1,457,970
47-6	0.0	130 (20.0)	170 (24.6)	0.0	347	(78.0)	752,180
47-7	0.0	173 (25.1)	211 (30.7)	0.0	433	(97.3)	357,770
47-8	0.0	207 (30.0)	253 (36.7)	0.0	517	(116.3)	138,350

(a) ; Specimen No. 1 to 5 had 101.6 mm width, and Specimen No.
6 to 8 had 197 mm width.
(b) ; Max.1 indicates the maximum nominal stress at the cross-
section A-A.
(c) ; Max.2 indicates the maximum nominal stress at the cross-
section N-N.

Table 5-6

Values of Intercept ($\log_{10}C$) and Slope (m) of
The S-N Curves Fitted by Linear Regression
Analysis for Stress Given Life.

Detail No.	Log C	m
34	16.960	7.407
39-A	12.596	5.873
43	13.471	5.129
44	13.140	5.663
47 *1	10.858	4.157
*2	11.452	4.257
*3	11.721	4.217

*1 : S-N Curve with Nominal Stress Range at the Cross-Section A-A
for the 101.6 mm Width Specimens.
*2 : S-N Curve with Nominal Stress Range at the Cross-section A-A
for the 197 mm Width Specimens.
*3 : S-N Curve with Nominal Stress Range at the Cross-section N-N
for the 101.6 and 197 mm Width Specimens.
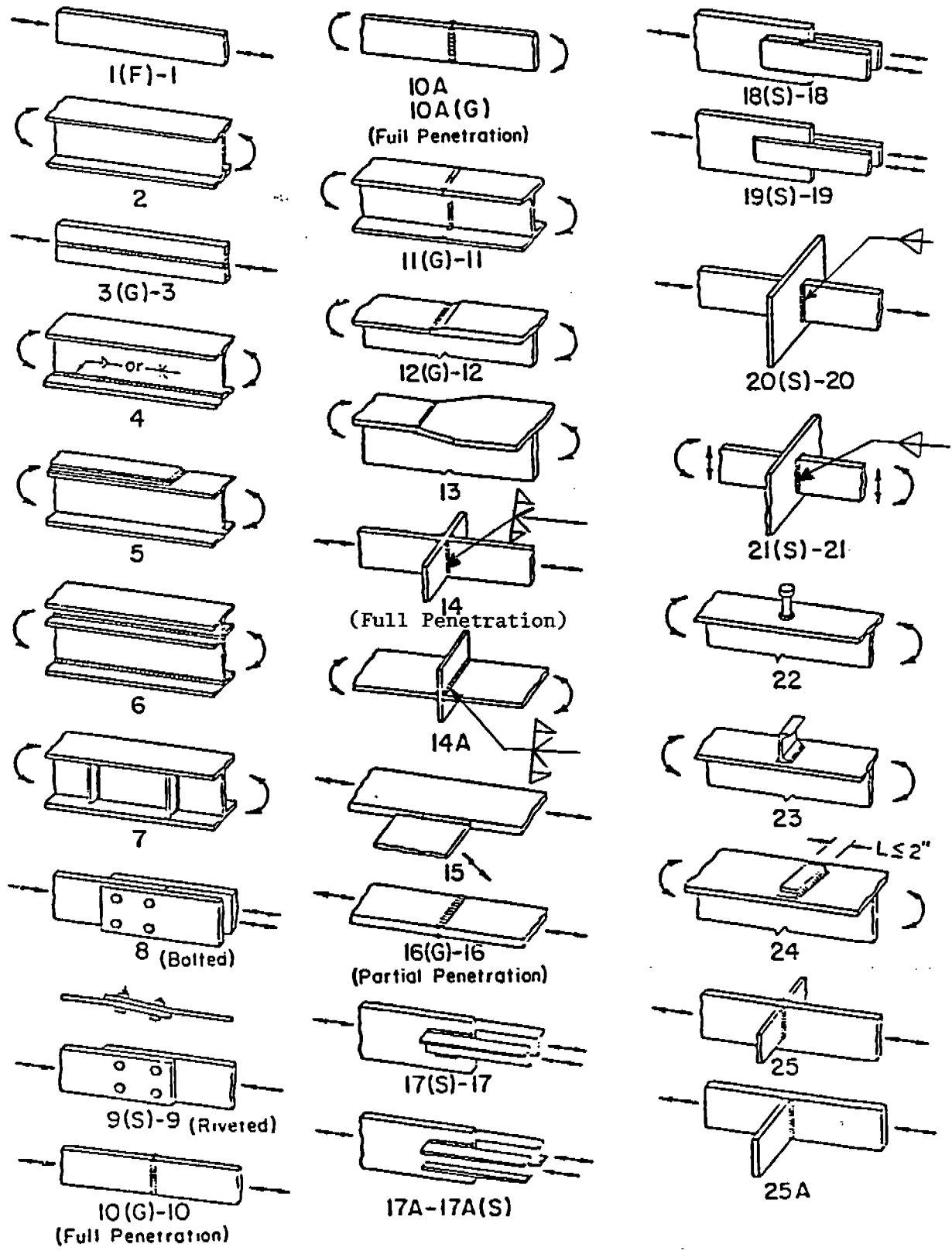
121

Fig. 5-1   Ship structural details [1-4].   Detail No. 20 was tested under the variable ship block load history and Details No. 34, 39-A, 43, 44 and 47 were tested under constant amplitude loading in this study. ---Continued.

122

25B

26

27(S)-27
(Slot or Plug Welds)

28(F)-28

29(F)-29
29R1 (Radius = 1/4" to 1/2")
29R2 (Radius = 1/2" to 1")

30

30A

31

31A

32

32A

32B

32C

33(S)-33

34(S)-34

35

36

36A

37(S)-37

38(S)-38

39

39A

39B

40

41

42

Fig. 5-1 Ship structural details [1-4]. Detail No. 20 was tested under the variable ship block load history and Details no. 34, 39-A, 43, 44 and 47 were tested under constant amplitude loading in this study. ---Continued.

123

43
(Partial Penetration)

43A

44

45

46

47

47A

48-48R

49

50

51

52

53

(G) - Designates a ground surface
(S) - Designates shear on weld or
fastener
(F) - Designates flame-cut edges for
comparison with machined edges

Fig. 5-1 Ship structural details [1-4]. Detail No. 20 was tested under the variable ship block load history and Details No. 34, 39-A, 43, 44 and 47 were tested under constant amplitude loading in this study.

124

508

254

88.9

63.5

101.6

A   B C

6.35

15.9

12.7   12.7
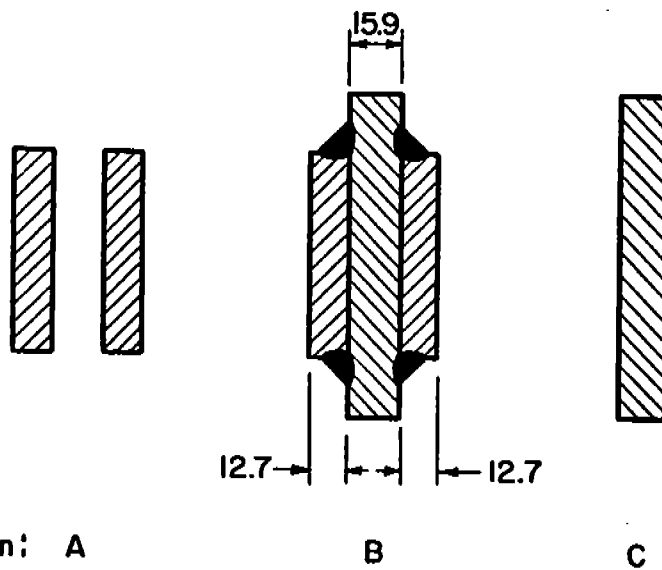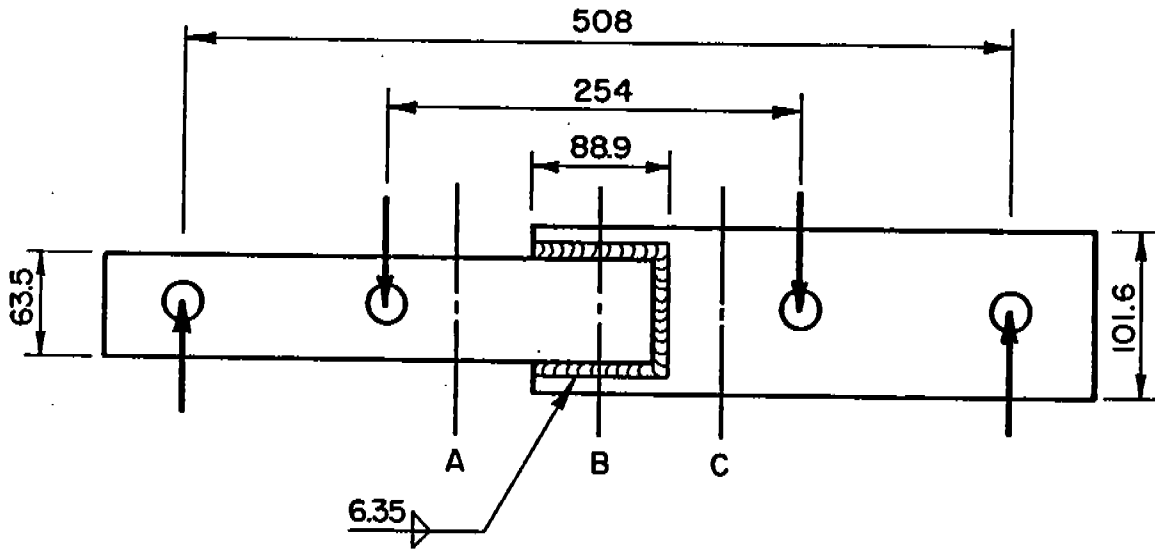
Cross-Section: A   B   C

Fig. 5-2 Testpiece dimensions and loading conditions for detail no. 34 --
          a fillet welded lap joint. (Dimensions in mm.)

125
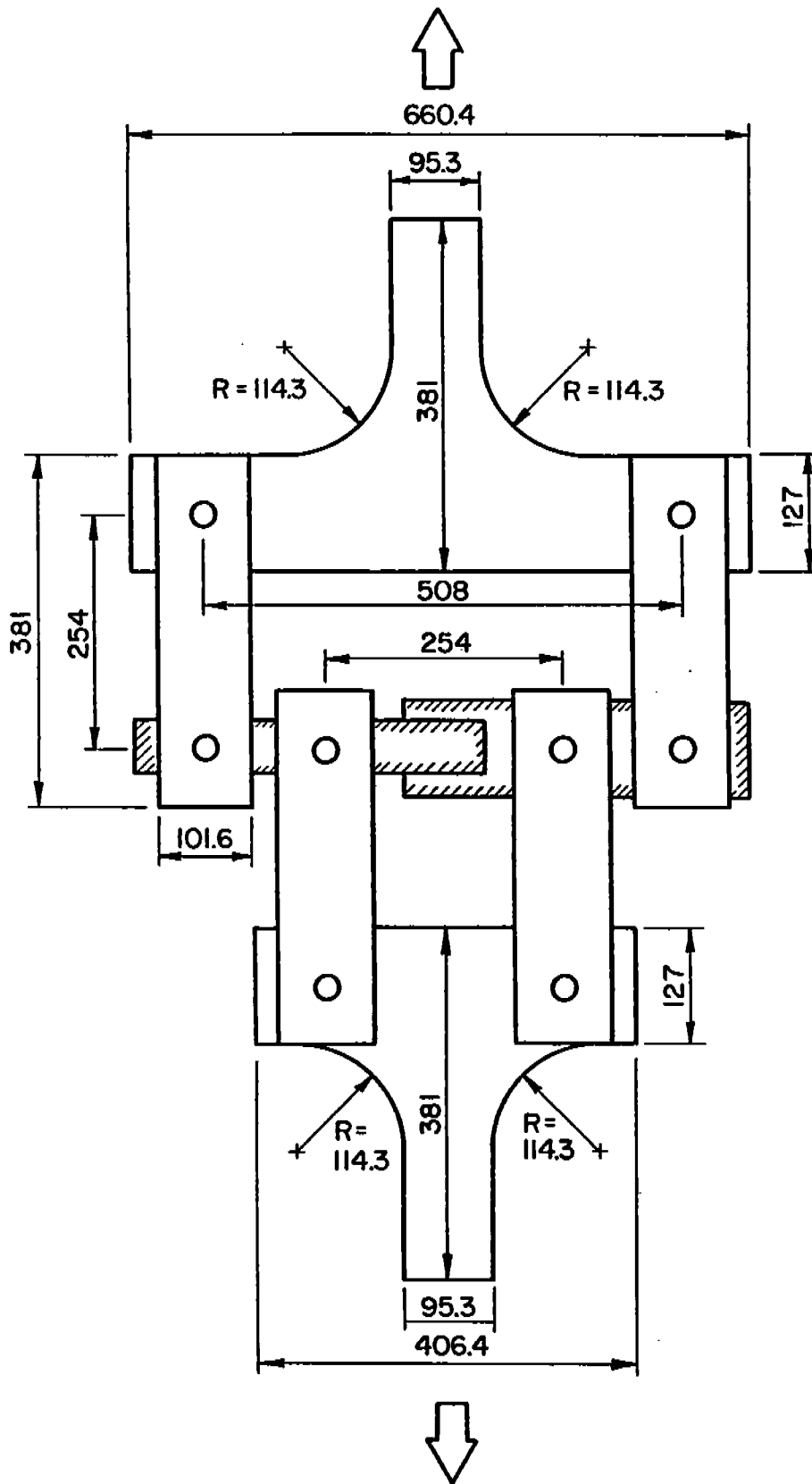
Fig. 5-3 Loading fixture design for detail no. 34.
(Dimensions in mm.)
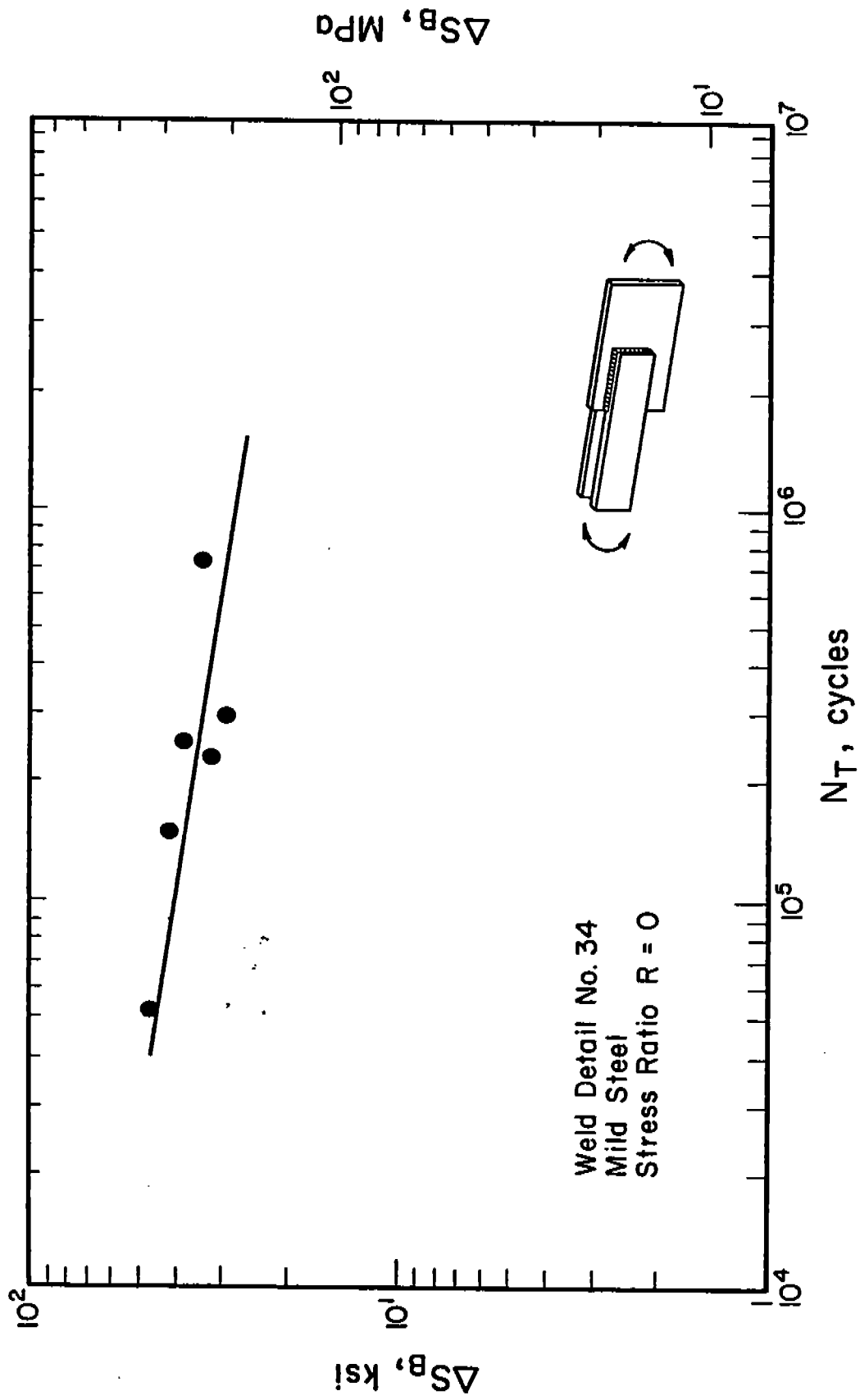
Fig. 5-4 Constant amplitude fatigue test results for detail no. 34.
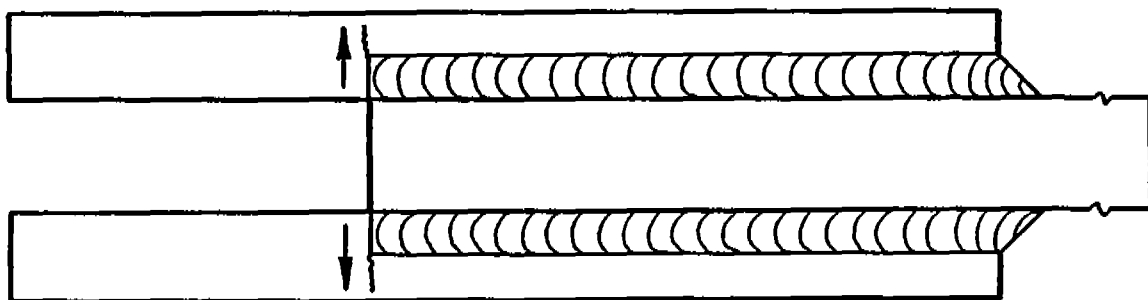
TOP VIEW
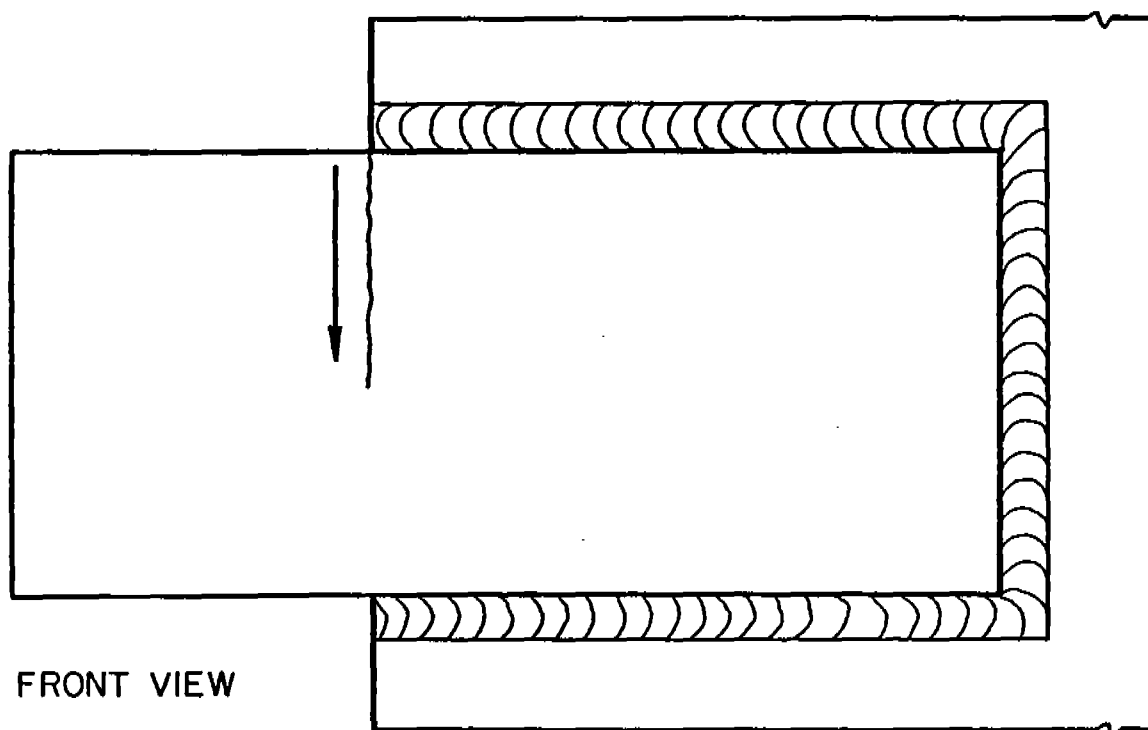
FRONT VIEW

Fig. 5-5 Pattern of fatigue crack initiation and growth for
          Detail No. 34.

Fig. 5-6 A typical failure and fatigue fracture surface for Detail
No. 34.

129
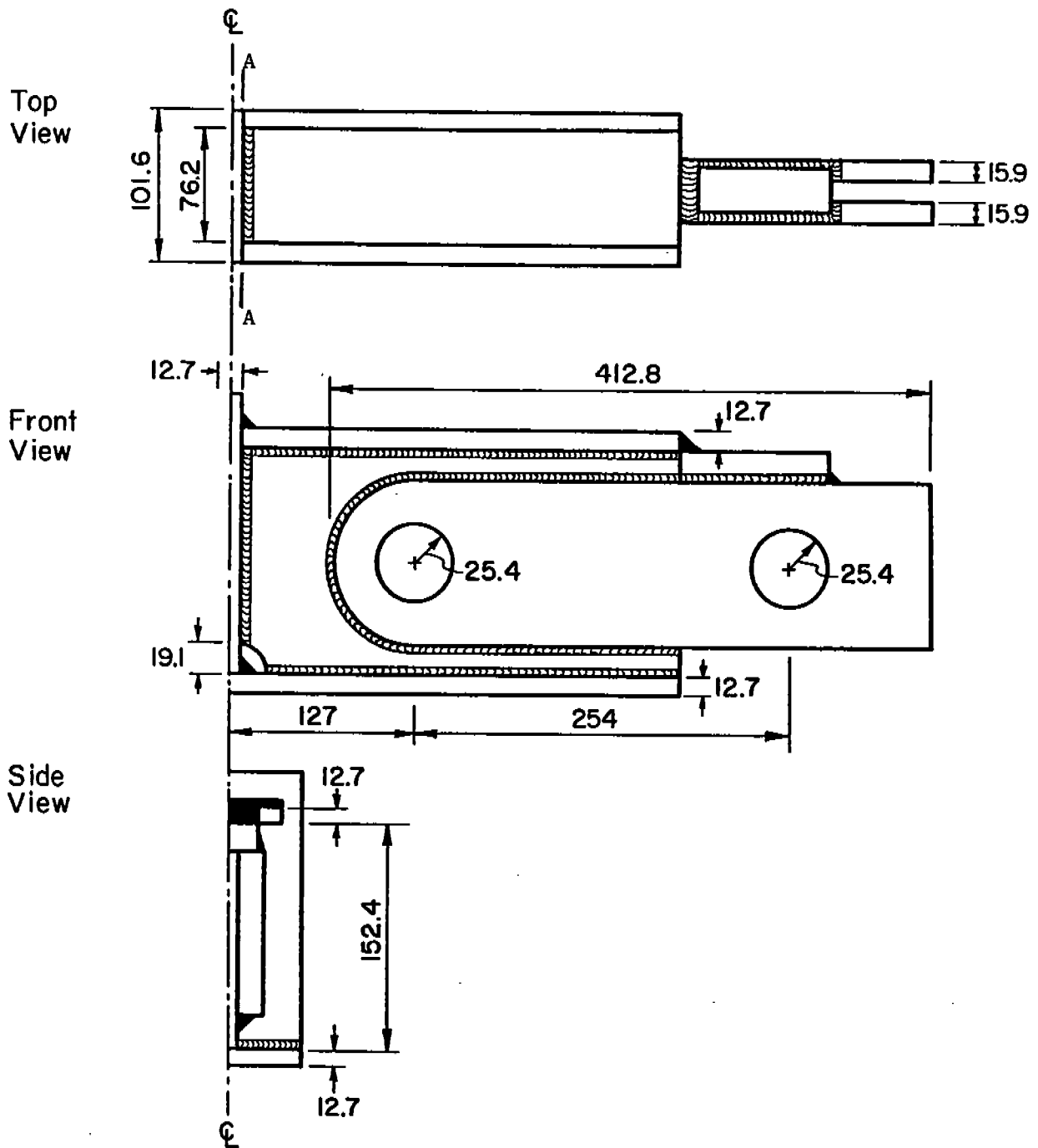
Fig. 5-7 Testpiece dimensions for detail no. 39A - a fillet welded I-beam,
with a center plate intersecting the web and one flange.
(Dimensions in mm.)

130
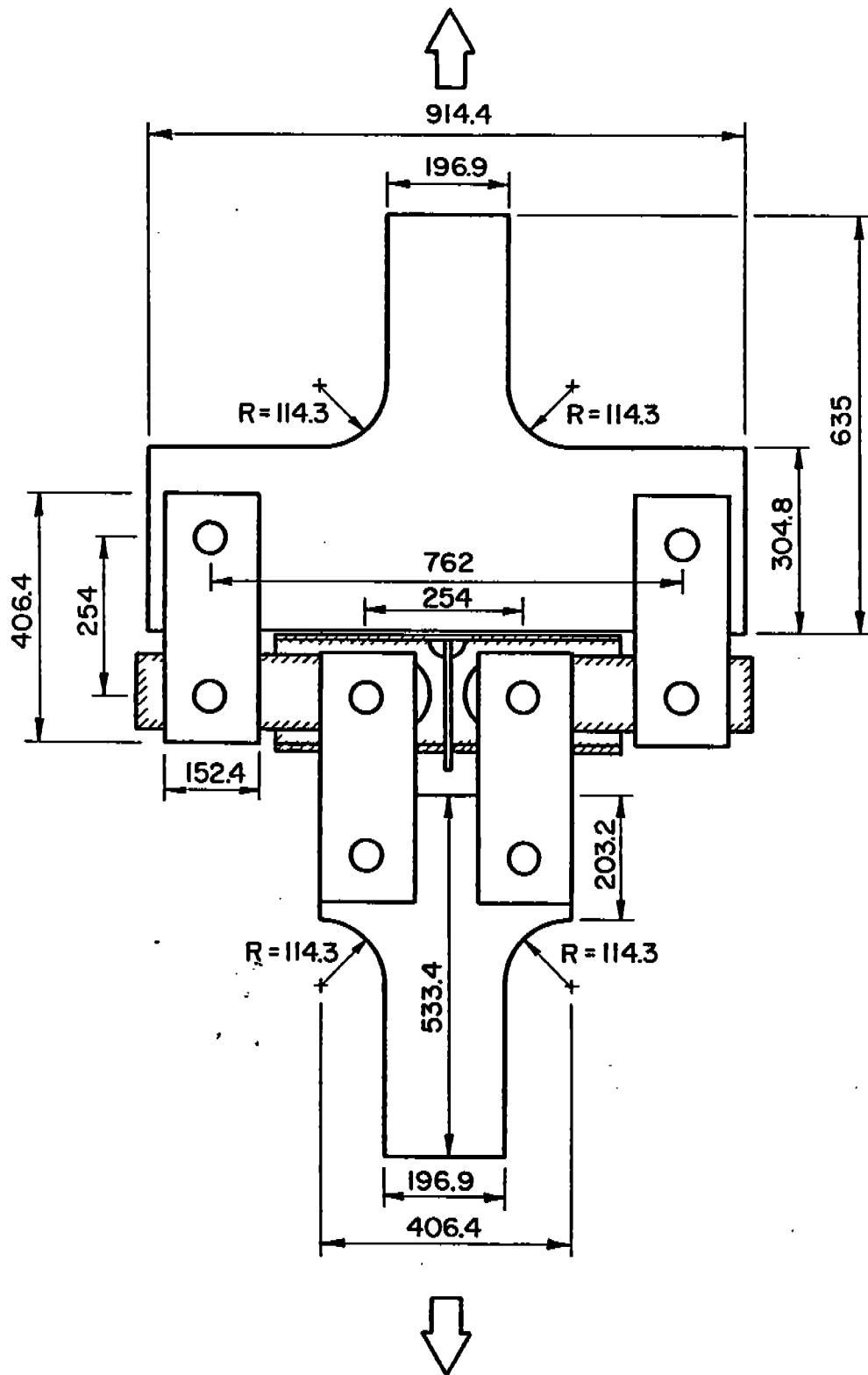
Fig. 5-8 Loading fixture design and loading conditions for detail no. 39A. (Dimensions in mm.)

Fig. 5-9 Photograph of loading fixture and a failed testpieces of
Detail No. 39-A.

132
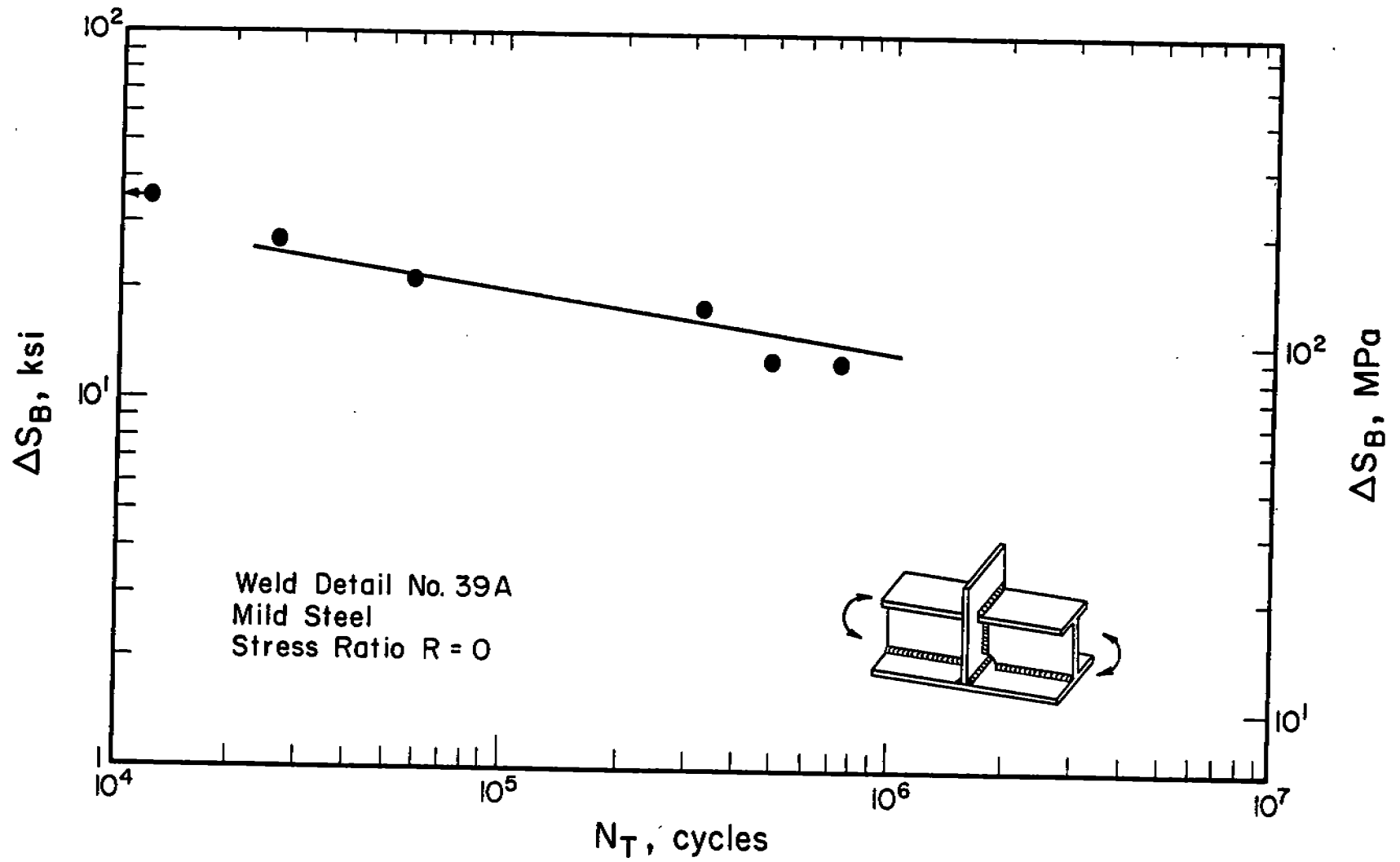
Fig. 5-10 Constant amplitude fatigue test results for detail no. 39A.
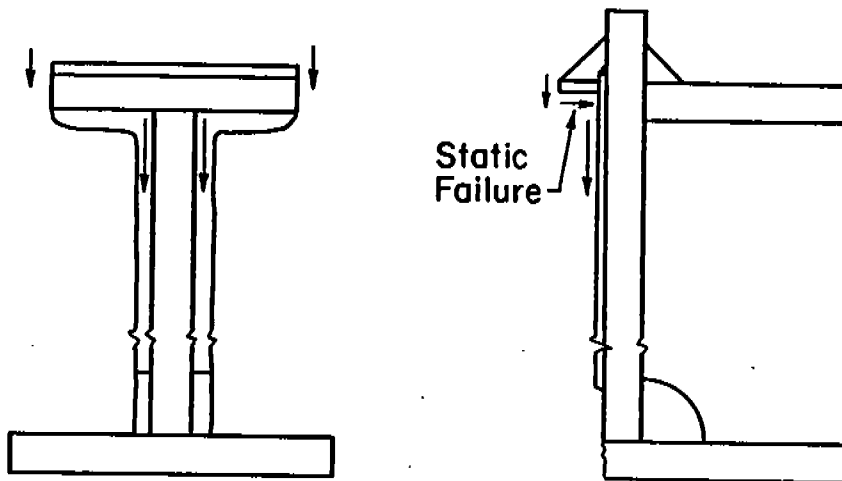
Fig. 5-11 A fatigue fracture surface and a schematic diagram of the failure mode of testpiece 39-A-4. The two fatigue crack initiation sites (one at the toe of the top flange plate, the other at the IJP of the fillet weld on the web) were connected by a shear failure. Testpieces 39-A-1 to 39-A-4 exhibited this type of behavior.

134
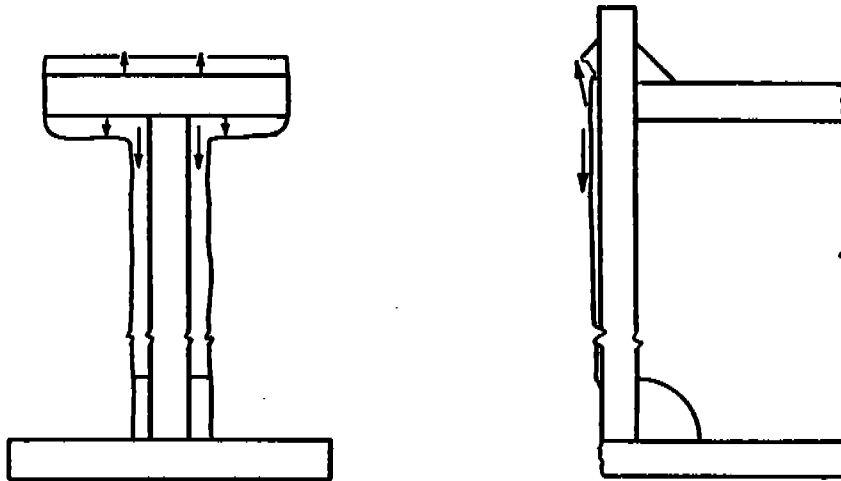
Fig. 5-12 A fatigue fracture surface and a schematic diagram of the failure mode
of testpiece 39-A-5. There were two fatigue crack initiation sites:
one at the IJP of the fillet weld of the top flange, the other at the
IJP of the fillet weld on the web. Both propagated independently to
failure. Testpieces 39-A-5 and 39-A-6 exhibited this type of behavior.

135
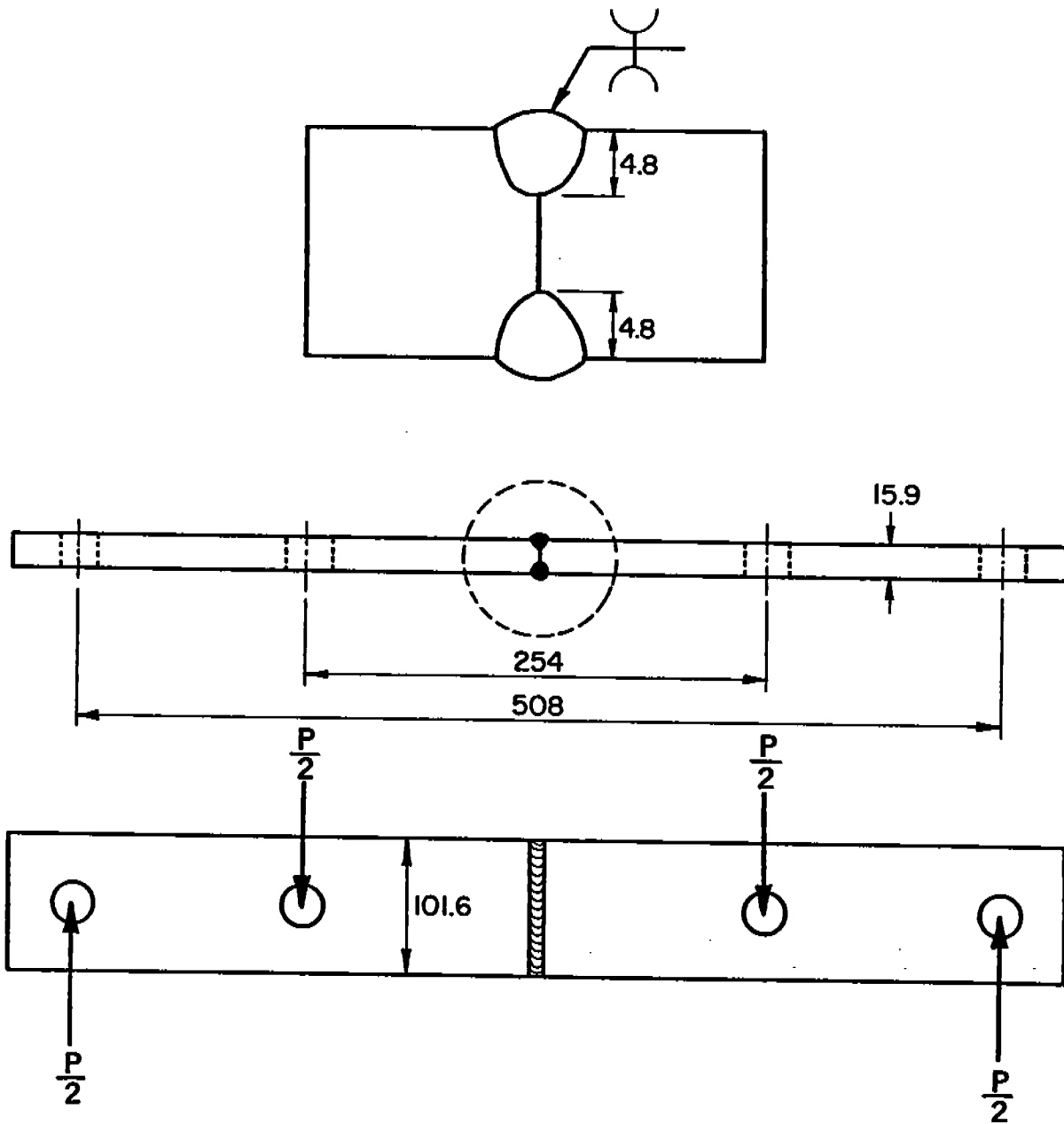
Fig. 5-13 Testpiece dimensions and loading conditions for detail no. 43 -
a partial-penetration butt weld. (Dimensions in mm.)

136

(b)

(a)
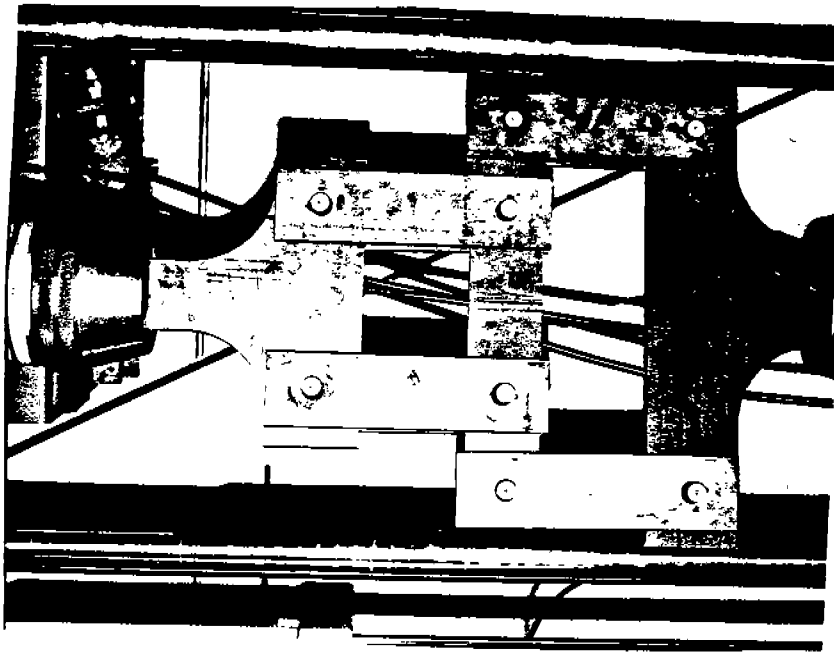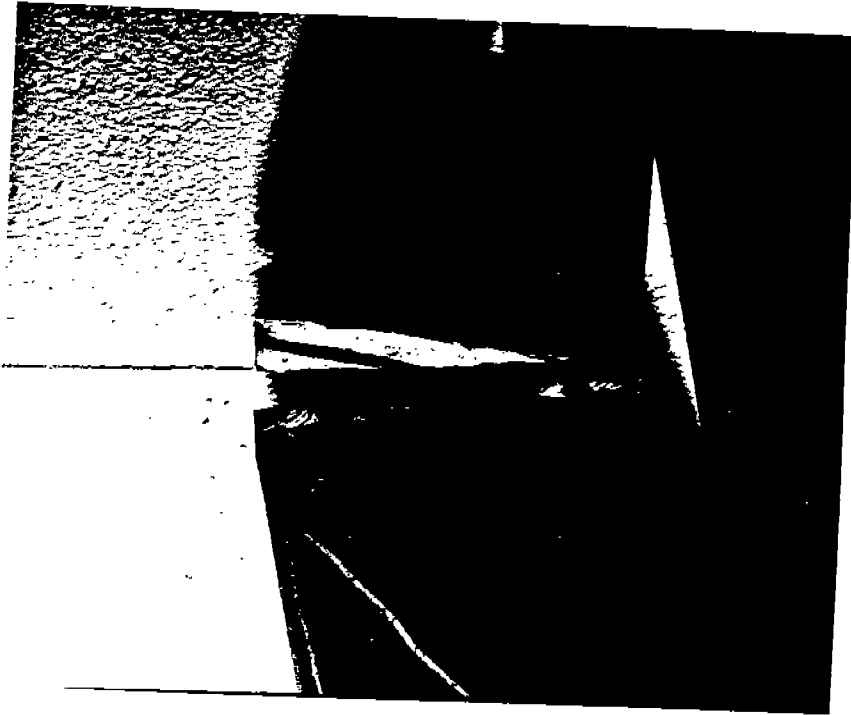
Fig. 5-14 Photograph of loading fixture and a failed testpiece of Detail No. 43.

137
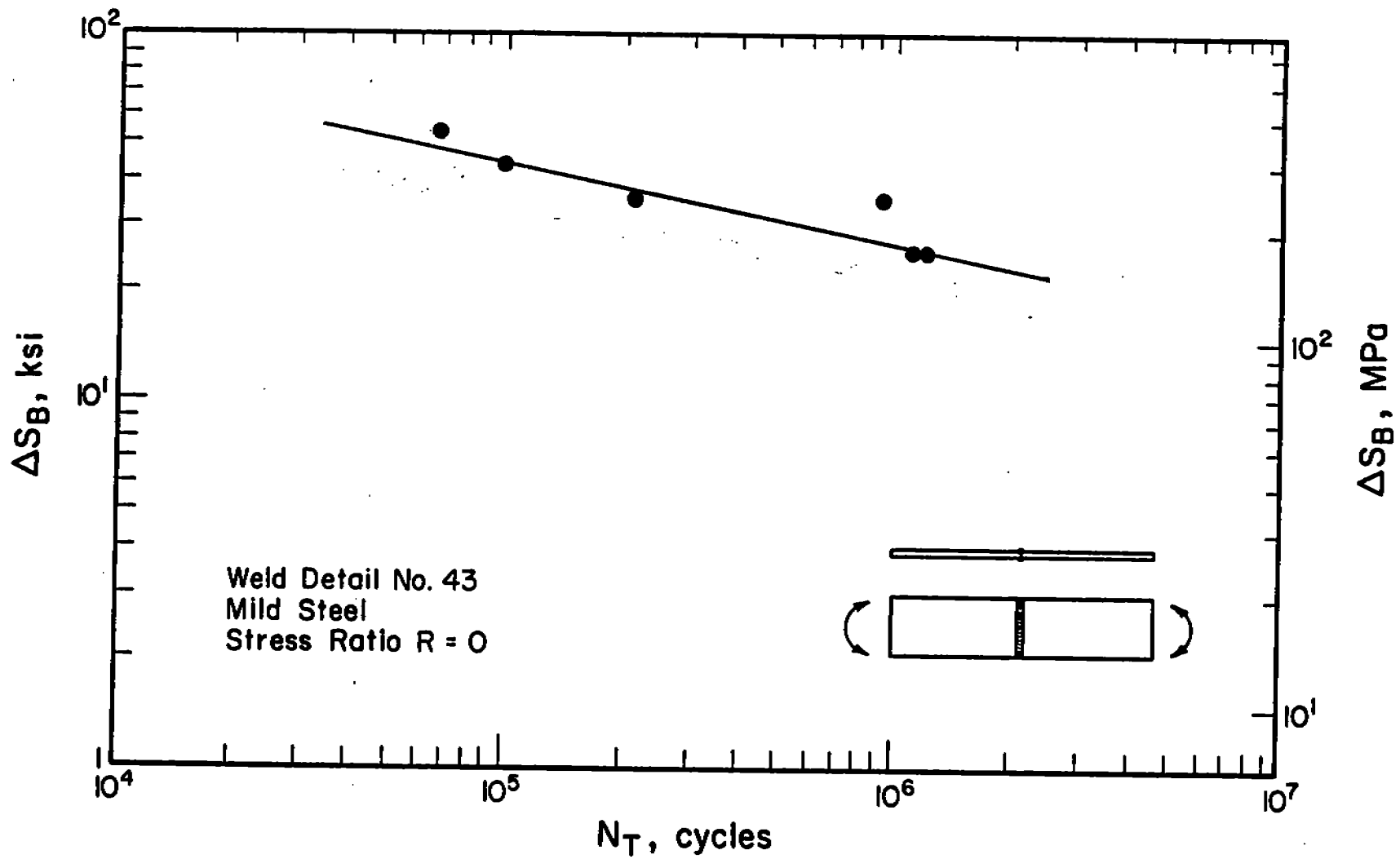
Fig. 5-15 Constant amplitude fatigue test results for detail no. 43.
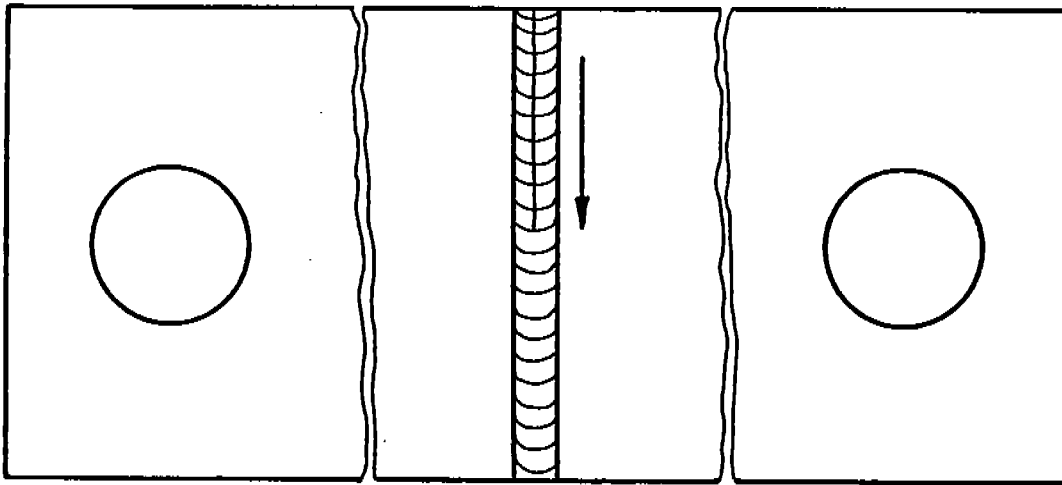
Fig. 5-16 Pattern of fatigue crack initiation and growth for detail no. 43.
The fatigue crack initiated at the IJP of the extreme fiber of
the specimen and propagated normal to the maximum principal stress.

139
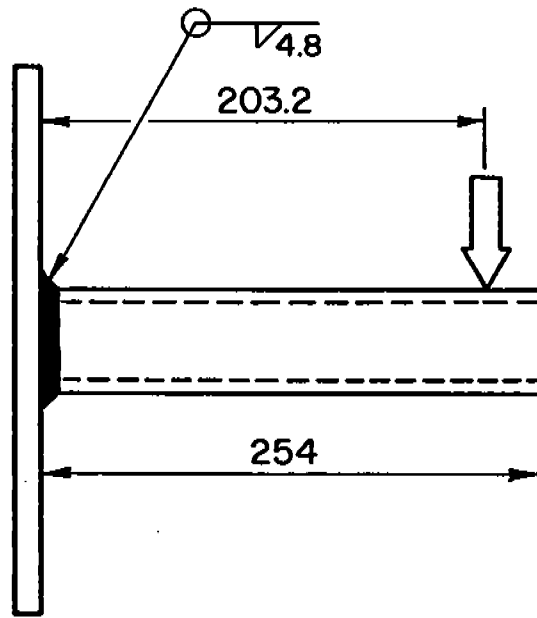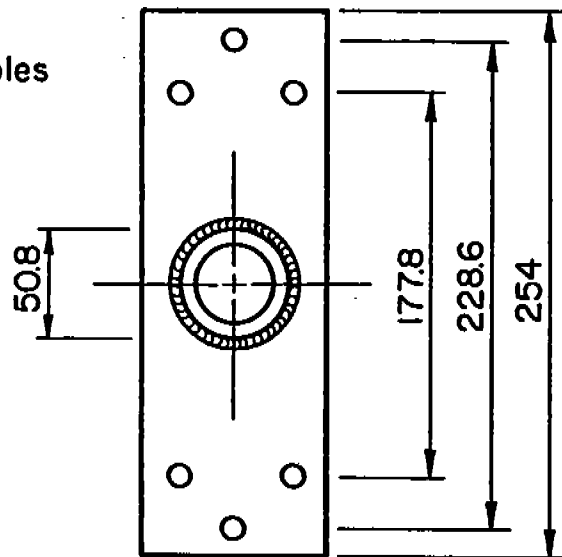
Fig. 5-17   Testpiece dimensions and loading conditions for detail no. 44
— a tubular cantilever beam.   (Dimensions in mm.)
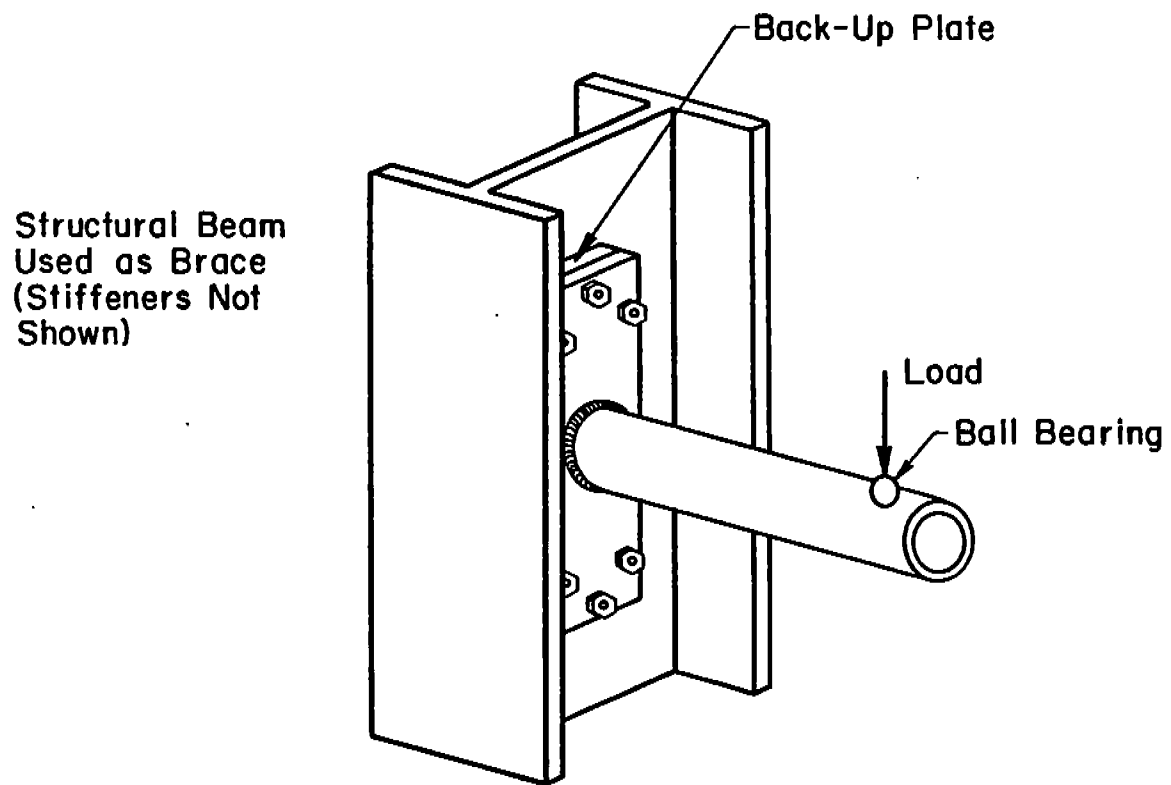
Fig. 5-18 Loading fixture design and loading conditions for detail no. 44.
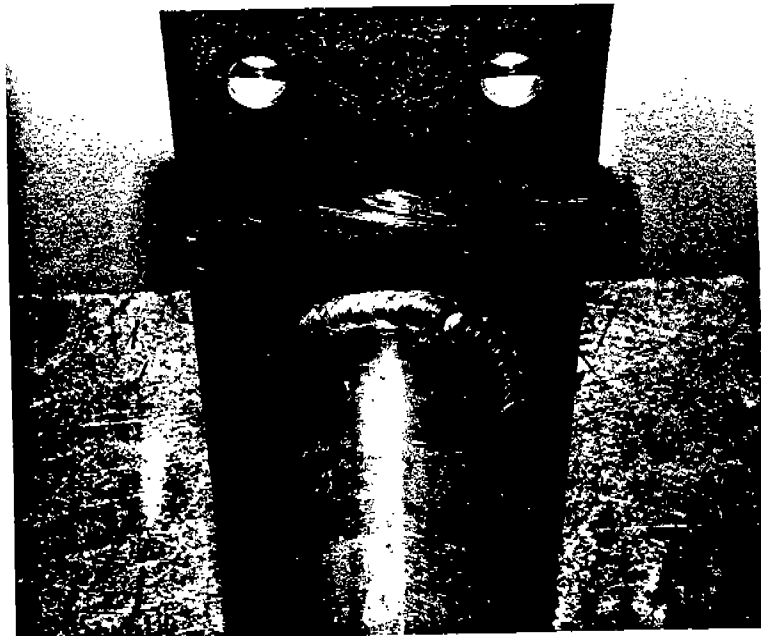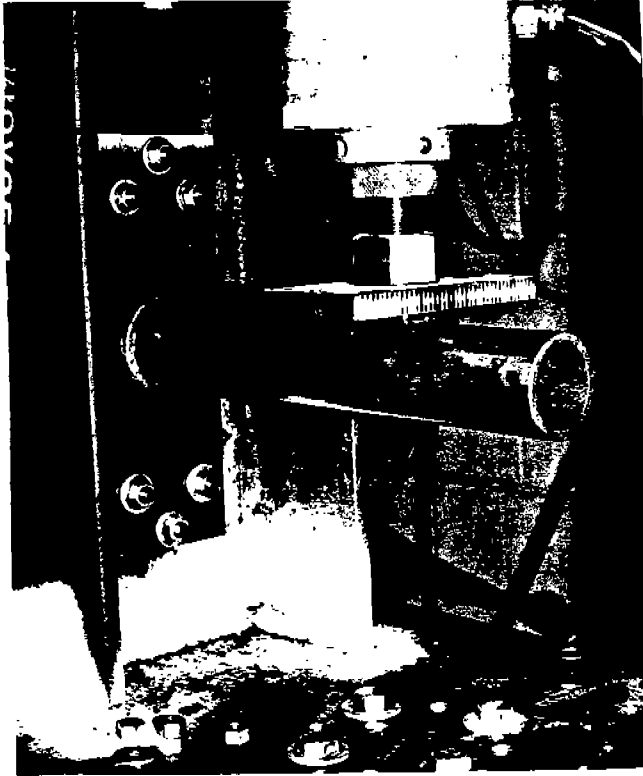
Fig. 5-19 Photograph of loading fixture and a failed testpiece of
Detail No. 44.
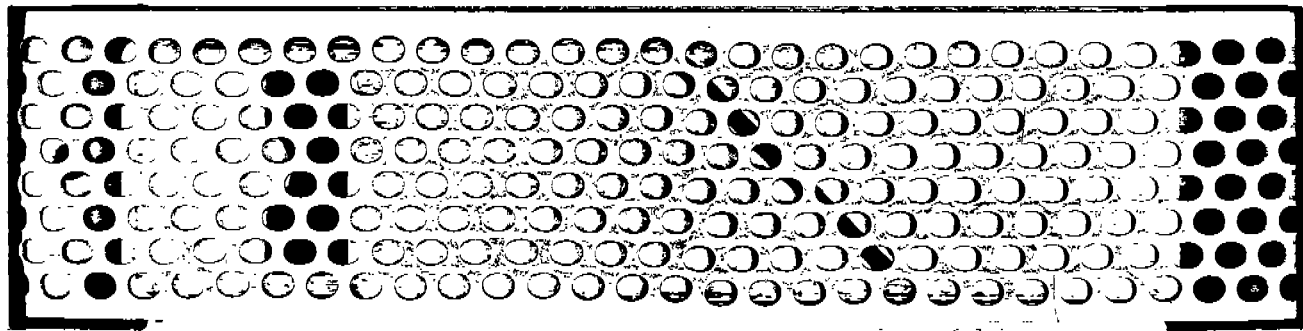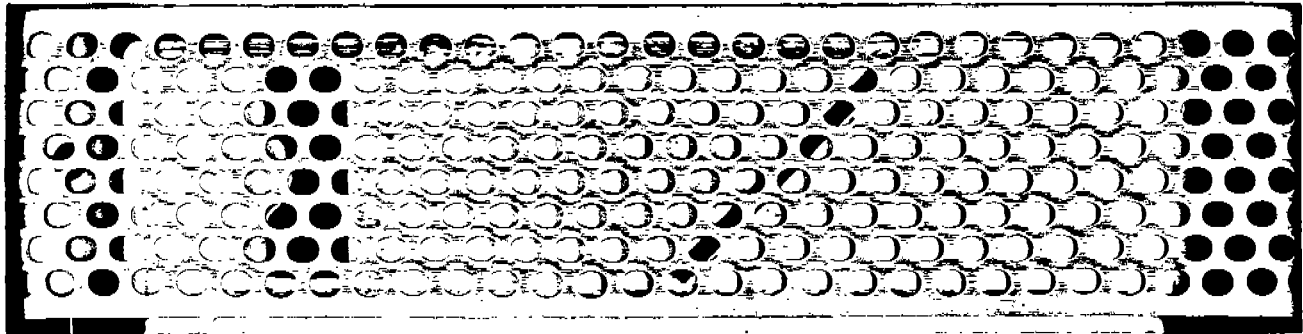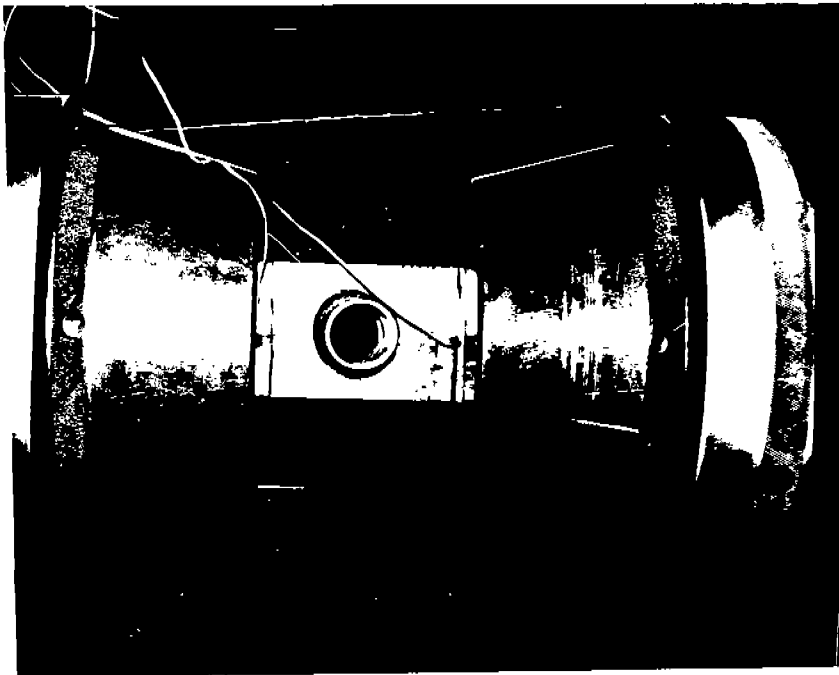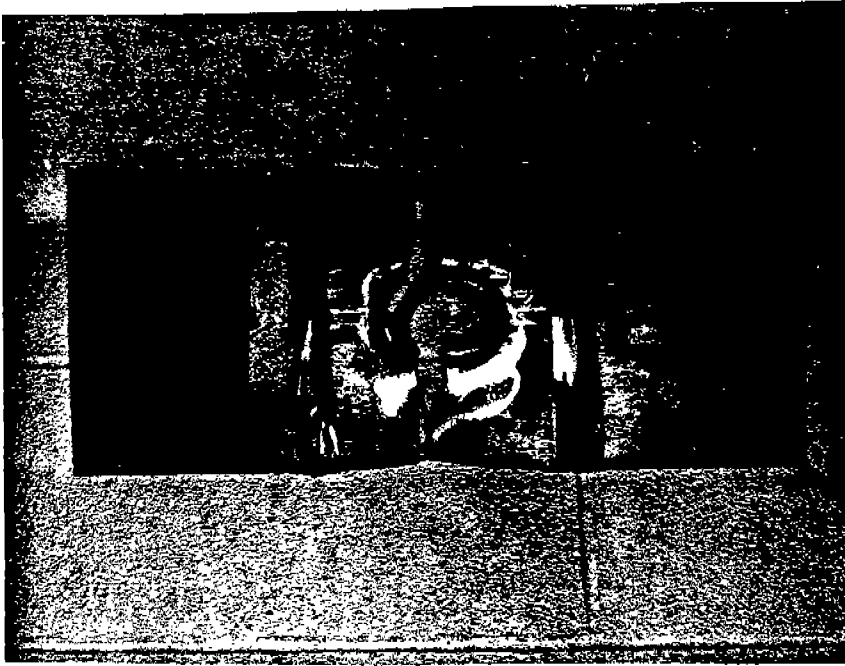
Fig. 5-23 Photograph of loading fixture and a failed testpieces of detail No. 47.

146
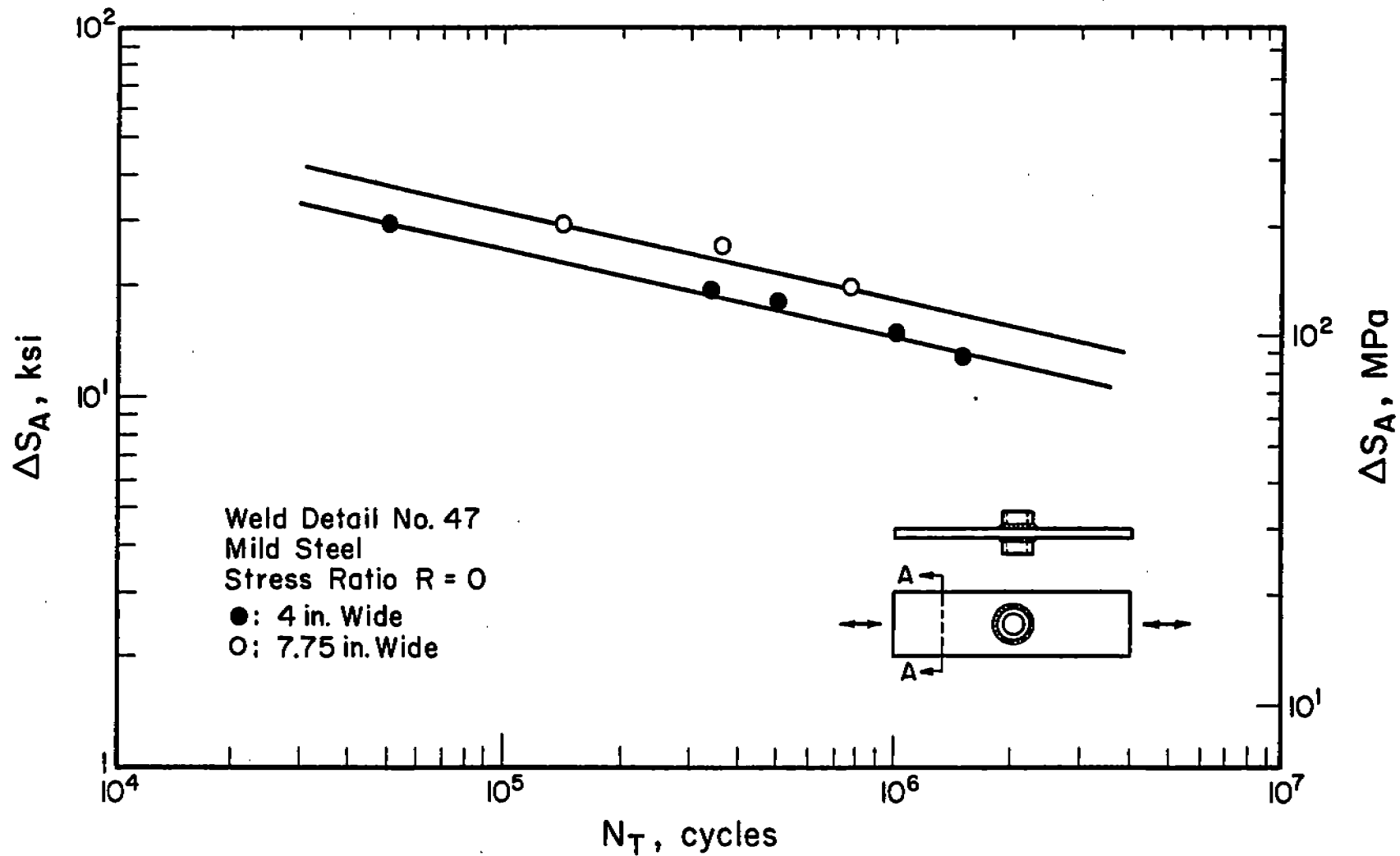
Fig. 5-24   Constant amplitude fatigue test results for detail no. 47.   The nominal stress
range was calculated at the section A-A.
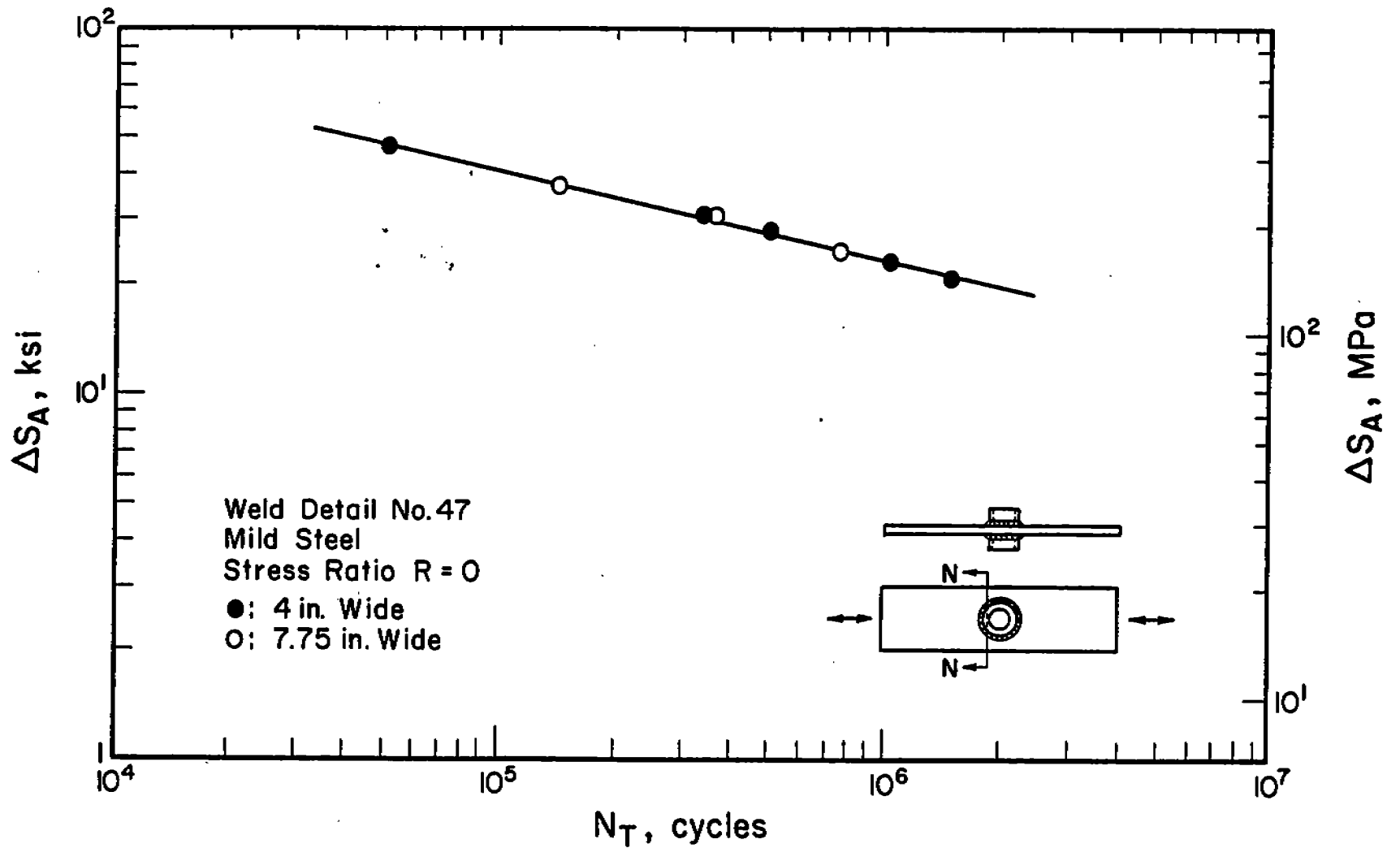
Fig. 5-25   Constant amplitude fatigue test results for detail no. 47.   The net stress range
was calculated at the section N-N.
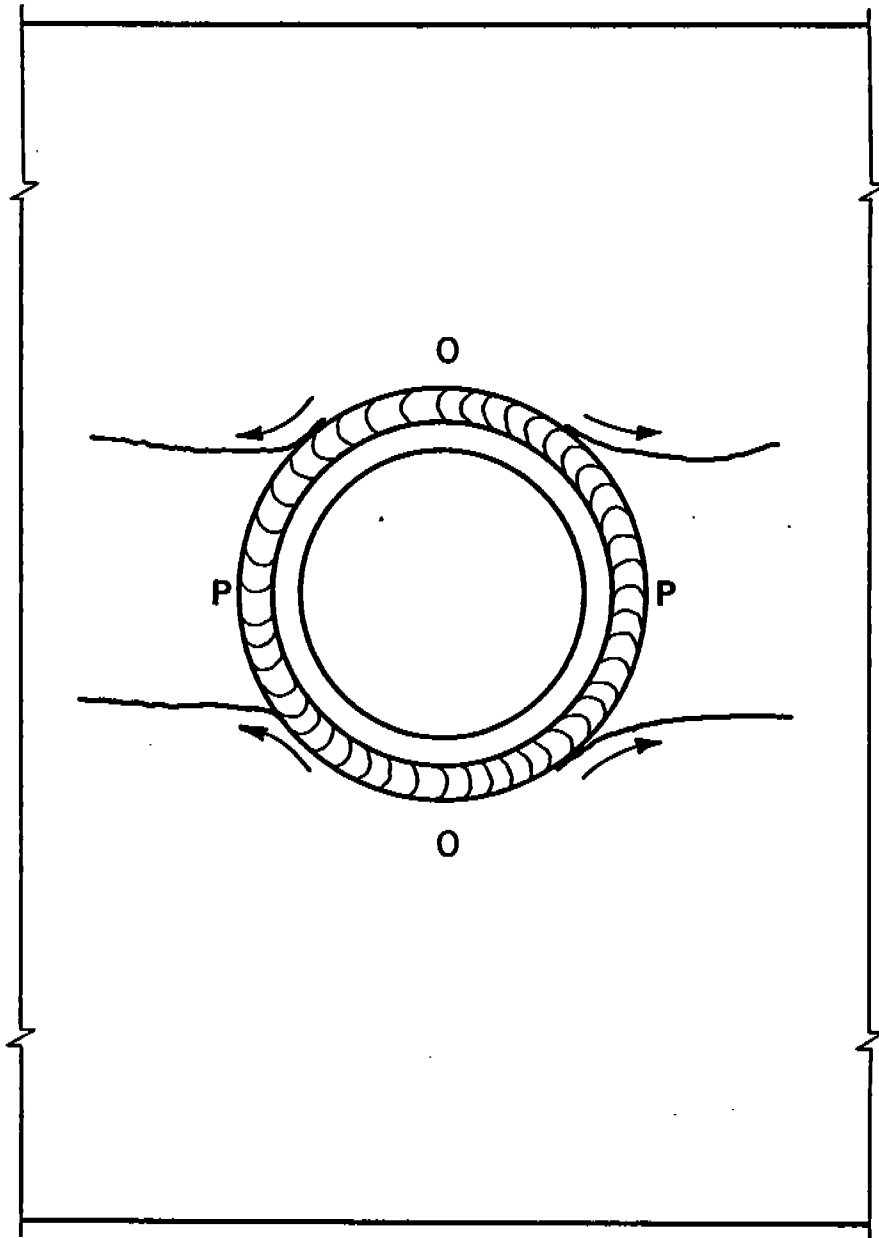
Fig. 5-26 Pattern of fatigue crack initiation and growth for detail no. 47.
Fatigue cracks initiated at either of the two opposite locations
mid-way between O and P and propagated through the plate normal
to the principal stress.

Fig. 5-27 Photograph of a typical fracture surface for Detail No. 47.

6. SUMMARY AND CONCLUSIONS

6.1 Evaluation of the Munse Fatigue Design Procedure (Task 1)

The Munse Fatigue Design Procedure (MFDP) was described in Sect. 1.5 and compared with other fatigue design and analysis models in Sect. 2. The experimental test results for Detail No. 20 were predicted with good agreement using the MFDP and constant amplitude fatigue data. From these two results it can be said that the MFDP works as well as any model based on linear cumulative damage assessment. The MFDP has the advantage of simplicity and the ability to incorporate required levels of structural reliability into the calculation of a maximum design stress range. As with other models based upon S-N diagrams and simple damage models, the MFDP in its original form neglects the effects of mean stress, detail size, and load sequence effects. In the case of tensile mean stresses the MFDP gives non-conservative predictions. The omission of a mean stress correction particularly can lead to incorrect predictions for variable load histories having significant average mean stresses.

Additional terms for the MFDP are suggested in Appendix B which take into account the mean stress of both the constant amplitude baseline data and any net mean stress of the applied variable load history and the effect of detail size. While the use of these additional terms may not be warranted in most circumstances, occasional design situations may occur in which these corrections could prove useful:

$$\Delta S_{Dm} = (\Delta S_{N(-1)}) \; (1 - 2 S_m C^{-1/m}) \; (t_s^n / t_2^n)(\xi)(R_F) \qquad (B-9)$$

where:

S_{Dm} = The maximum design stress range (see Fig. 1-9).

$(\Delta S_{N(-1)})$ = Mean fatigue strength at the design life from detail S-N diagram for R = -1 testing conditions, i.e. zero mean stress.

$(1 - 2 S_m C^{-1/m})$ = Mean stress correction for the average mean stress of the applied variable load history. S_m is the applied mean stress and C and m are the constants characterizing the constant amplitude detail S-N diagram: see Fig. 1-3.

151

(t_s^n/t_2^n) = Suggested thickness correction after Smith, Gurney or the predictions of the I-P model: see Sect. 3.9. The value of the exponent n is not well established. Gurney suggested a value of 1/4 based on experimental results. t_s and t_2 are the standard ($\approx$12.7 mm) and nonstandard weldment plate thicknesses, respectively.

(ξ) = The random load factor: see Eqs. 1-2 and 2-3 and Table 2.1.

(R_F) = The reliability factor: see Eqs. 1-1, 1-2, 2-3 and 2-4.

6.2 The Use of Linear Cumulative Damage (Task 2)

The MFDP was thought to take a conservative approach in estimating damage using the extended S-N diagram thereby giving greater weight to the damage resulting from the stress ranges at or below the "endurance limit". Neither the tests and comparisons of Sect. 2 nor the edited ship history used in this study provide a critical test of this problem. Furthermore, recent studies [2-1, 2-7] have shown that certain variable load histories in which most of the damage results from stress ranges near the endurance limit may cause failure at lives as much as four times shorter than predicted using linear cumulative damage and the extended S-N diagram. It is difficult and time consuming to study this phenomenon for ship details at normal testing frequencies. However, there remains serious concern that linear cumulative damage assessments may be unconservative in some situations. The results of this study did not uncover any difficulty in the use of linear cumulative damage either for MFDP of I-P model predictions, however the ship history was edited to eliminate stress ranges below 69 MPa (10 ksi) and above 152 MPa (22 ksi) or notch root stress ranges below about 276 MPa (40 ksi). While this level of editing may seem imprudent, it should be recalled that the lives obtained with this edited history required 1.7 to 17 days for Detail No. 20. These specimen failure lives were believed to represent actual service lives of 12 to 120 years (see Sects. 3.3 and 3.5).

6.3 The Effects of Mean Stress (Task 3)

Task 3 of this study showed that mean stresses have a secondary but sometimes important influence on the fatigue life of a welded detail. When

feasible, mean stresses should be taken into account. Correction factors for the MFDP were suggested in Eq. B-9 above. Comparison with the test data of this study shows that these corrections improved the life predictions made using the MFDP (Eq. B-9): see Figs. 4-2 and 4-3. The factors dealing with mean stresses in the I-P model were rewritten to include the effects of both applied or induced axial and bending mean stresses:

$$S_a^T = [\frac{(1/K_{fmax}^A)(\sigma_f' - \sigma_r) - S_m^A - XS_m^B}{1 - x(1 - X)}] (2N_I)^b \qquad (4-2)$$

The use of the set-up cycle and the Smith-Watson-Topper (SWT) parameter showed that the fatigue life of the Detail No. 20 correlated well with that parameter. The SWT parameter takes both mean and cyclic notch root (local) stresses into account. The reasonably good correlation of the total fatigue lives with this parameter underscores the correctness of the local strain concept in dealing with the fatigue phenomenon in structural weldments its utility as a useful aid in future design methods for weldments based on a local stress strain approach.

6.4 Size Effect (Task 4)

Because of experimental difficulties with the smallest (6.35 mm) specimens of Detail No. 20, no effect of weldment size on the fatigue life of these details could be discerned from the results of this study. However, other recent studies of the effect have shown that very large weldments do give shorter than expected fatigue lives [2-1, 2-7]. A size correction for the MFDP is suggested after Gurney [3-6] and Smith [3-7]. Further studies should be performed to determine the proper value of the exponent or in the size correction factor: see Eq. B-9.

6.5 Use of the I-P Model as a Stochastic Model (Task 6)

The I-P model was used as a means of understanding the variable nature of weldment fatigue resistance, that is, the uncertainty Ω_c in Eq. 1.1. According to the I-P model (see Eq. A-15 and 4-2), the major variables are the fatigue strength coefficient (σ_f'), the notch-root residual stress (σ_r), the mean stresses $(S_m^A$ and $S_m^B)$, the bending factor (x), the fatigue notch

153

factor (K^A_{fmax}), and the ratio of the bending and axial fatigue notch factors (X). The variables with the greatest dispersion were found to be the fatigue notch factors K^A_{fmax} and K^B_{fmax} which describes the basic geometry of the particular weldment and the bending factor (x) which is related to the distortions and the consequent induced secondary bending stresses in the member. Both of these random variables were found to be normally distributed and the sensitivity of the constants S_F and C to each was studied using a computer simulation. The constants S_F and C was found to follow a normal distribution and the disperson in the values of S_F and C were most influenced by the bending factor x for the Detail No. 20 studied here.

6.6 Baseline Data for Ship Details (Task 7)

Additional constant-amplitude baseline fatigue data was collected for five ship details: Nos. 34, 39a, 43, 44, and 47 (see Fig. 5-1). The results of these test series are described in Sect. 5. No attempt was made to model the fatigue behavior of these weldments using the I-P model since this task would have been time consuming and was deleted from the program at the outset. Despite the more complex appearance of the ship details studied in this part of the program, the patterns of fatigue crack initiation and growth observed were generally simpler than those observed for Detail No. 20 with an IJP. The results for Detail No. 47 were complex: see Figs. 5-22 to 5-27.

The results of all the baseline tests of Sect. 5 will be added to the UIUC fatigue data bank.

6.7 Conclusions

The results of this study have shown that linear cumulative damage provides reasonable estimates of fatigue life under the variable load history employed in this study. Mean stress was found to have a moderate influence on fatigue life under variable load history. Specimen size or thickness had little influence on the test results.

The test pieces used in this study had realistic variations in distortion and weld geometry. Indeed, the scatter in the fatigue test results observed is attributed to these causes. The test results of the smallest size test pieces studied are not understood; and the behavior of thin gauge

weldments bears further study, although such weldments may not be encountered in ship construction.

At the conclusion of this study, one is left with a heightened appreciation of the complexity of the fatigue design of weldments. Even weldments of the same type may differ in their behavior due to variations in geometry and distortions. Consequently, a given load history may have differing effects on weldments of different geometry because the notch root history controlling the accumulation of damage there depends both upon the history itself and upon the fatigue notch factor. A corollary is that editing a history to remove the small cycles will differently affect weldments of high and low fatigue notch factor.

Despite these complexities, steady progress has been made in models such as the I-P model which can analytically predict the weldments just as well as a full scale laboratory investigation of the detail. Indeed, laboratory tests for structural details fatigued under certain long-term histories containing many small cycles are often not feasible.

In its current state of development, the I-P model can provide accurate estimates of the long-life fatigue strength and can therefore be used as a design aid or to estimate the average fatigue strength required in the Munse Fatigue Design Procedure. At present, computer modeling of weldments is restricted to reasonably simply details, but future reductions in the cost of finite element computations and increases in the size of problems which can be analyzed promise the possibility of studying ever more complex weldments.

An interesting development of this study was the introduction of stochastic modeling of the fatigue variables in the I-P model. Further work in determining the possible variation of each of the variables is needed, but the approach seems very promising and applicable to design.

The Munse Fatigue Design Procedure (MFDP) remains a practical method for the fatigue design of ship details in those circumstances in which constant amplitude S-N diagrams are available or can be reasonably estimated. Modifications to the MFDP for thickness and mean stress suggested in this study may allow better estimates of the allowable design stresses. No tests of the reliability aspects of the MFDP were undertaken in this study and this aspect of the MFDP requires further study.

155

7. SUGGESTIONS FOR FUTURE STUDY

Several major questions remain unanswered: There continues to be uncertainty regarding the adequacy of linear cumulative damage in dealing with the low amplitude stress cycles in long term ship histories. Further studies focused on this problem alone and devoted to very long term tests should help reduce the uncertainty. One experimental approach would be to apply either the block history or the random history to a ship detail such as No. 20 (preferably GMA welded or the variation in test results due to geometry and distortion alone will mask the results) with different levels of stress cycle editing. One could systematically edit out cycles smaller than 69 MPa (10 ksi), 55 MPa (8 ksi), 41 MPa (6 ksi) to show the effect of the small cycles. One experimental difficulty which should be recalled is the fact that stress concentrators such as weldments magnify the applied stress history. Consequently, a weldment with a high stress concentration should react differently to a given applied history than one with a low stress concentration.

Additional analytical modeling of weldments is needed if either initiation or propagation based life prediction models are to be more widely used. Although the modeling of weldment fatigue life by fatigue crack propagation is the accepted analytical method of prediction, in fact, the modeling of fatigue crack growth in weldments is more difficult than obtaining good estimates of K_t and K_f for the calculation of fatigue crack initiation life. Much more analytical work is needed to model the fatigue crack propagation patterns.

In summary, weldments are very complex, and their behavior is really difficult to understand without careful studies of their actual behavior using the most recent and advanced methods (FEM analyses, etc.). For example, it was shown in the present study that the uncertainty in the fatigue behavior of Detail No. 20 was due more to distortions and the consequent induced bending stresses than to variation in the weld geometry per se. A clear understanding of the role of each of the variables influencing the fatigue resistance of weldments will ultimately reduce the uncertainty that now surrounds their response to fatigue loadings and lead to improved design methods.

156

Appendix A

ESTIMATING THE FATIGUE LIFE OF WELDMENTS USING THE IP MODEL

A-1 Introduction

The authors and their coworkers have developed a model for the fatigue life of weldments which can be applied quite generally to estimate the fatigue resistance of notched components [A-1]. This model considers the total fatigue life (N_T) to be comprised of a period devoted to crack initiation and early growth (N_I) and a period devoted to the growth of a dominant crack (N_p):

$$N_T = N_I + N_P \tag{A-1}$$

While the total life is the sum of these two periods, at long lives, N_I dominates [A-1, A-2] and the fatigue life or fatigue strength of a notched member can be estimated by considering only crack initiation and early growth through the Basquin equation with the Morrow mean stress correction:

$$\sigma_a = (\sigma_f' - \sigma_m)(2N_I)^b \tag{A-2}$$

where σ_a is the stress amplitude, σ_f' is the fatigue strength coefficient, σ_m is the mean stress which includes the residual and local mean stress after the first cycle of load (set-up cycle), $2N_I$ is the reversals devoted to crack initiation and early growth (one cycle equals two reversals) and b is the fatigue strength coefficient.

The general scheme for estimating N_I is diagrammed in Fig. A-1. Estimates of the total fatigue life (N_T) can be obtained by adding the crack propagation life (N_p) to these estimates of N_I. Sections A2 to A4 give a step-by-step summary of the method of estimating the fatigue crack initiation life N_I using the schematic diagram of Fig. A-1 as a guide. The methods calculating the fatigue crack propagation life is summarized in Section A-5.

A-2. Estimating the Fatigue Crack Initiation Life (N_I)

The steps in the estimation of the fatigue crack initiation life (N_I) are diagrammed in Fig. A-1. Each step in the analysis is numbered in the approximate sequence in which it is carried out. At the left are four main types of information which must be collected, estimated (or guessed) to permit the calculation of the long life fatigue strength or fatigue crack initiation life (N_I): one requires information about the service history, notch and loading geometry, residual stresses, and notch-root material properties. The accuracy of the predictions to be made depends most sensitively upon the level and nature of the applied stresses (Task 1). The effects of geometry can be calculated with considerable accuracy (Task 2) and the appropriate values for the residual stresses (Task 3) and particularly the material properties (Tasks 4-6) can usually be roughly estimated without greatly diminishing the accuracy of the calculation.

Having collected this information and used it to estimate the fatigue notch factor (Task 7) and, if necessary, the stress relaxation constant (Task 9), two main analyses are then carried out: the Set-up Cycle analysis (Task 8) and the Damage Summation analysis (Task 10).

A-2.1 Defining the Stress History (Task 1)

The most important step in the estimation of N_I is determining the nominal stresses in the vicinity of the critical notch (Task 1). Indeed, the entire analysis depends on identifying the critical notch or notches and determining the stresses in their vicinity. In the case of weldments, one applies strain gauges near the weldment and measures the nominal axial and bending strains (Fig. A-2). It is important to partition the bending and axial stresses since the elastic stress concentration factors, K_t (Task 2) and consequently K_f determined in Task 7 are different for these two types of stresses.

Proper gauge placement may require a stress analysis of the notch and its vicinity to identify areas in which the global stresses can be measured without entering the stress field of the notch itself and consequently making the measured strains an essentially unknown function of gauge placement. Global stress analyses which give strain-gauge accuracy should

158

provide adequate information in the absence of a prototype and the possibility of measuring strain directly.

In bi-axial loading cases, the nominal maximum principal stresses should be determined [A-3]. If the load history cannot be considered to be constant amplitude, then the load history must be recorded and edited for subsequent use in Tasks 8 and 10.

A-2.2 Determining the Effects of Geometry (Task 2)

The fatigue process usually occurs at notches. Thus, it is necessary to quantify the severity of the critical notch using a parameter which describes the intensification of stress at the notch root during the set-up and subsequent cycles, the fatigue notch factor K_f. The fatigue notch factor is equal to or less than the elastic stress concentration factor K_t. The factor K_t can be analytically determined using finite element stress analysis methods (Task 2) and can be used to estimate K_f (Task 7) using Peterson's equation:

$$K_f = 1 + (K_t - 1)/(1 + a/r) \qquad (A-2)$$

The K_t of many notches have been collected by Peterson [A-4]. The stress concentration factor of complex notches can be estimated using finite element stress analysis methods. Such stress analyses determine both the notch-root stresses (which control the crack initiation and early growth phenomena) and the variation of stresses along the crack path away from the notch root (which determines the variation of stress intensity factor (ΔK_I) with crack depth and hence the rate of fatigue crack propagation or N_p: see the Appendix).

Our practice has been to establish a definite radius at the notch root and to refine the element size to an order of magnitude less than this radius: see Fig. A-3. Values of K_t for radii smaller or larger than that used in the analysis can be estimated in many cases by the expression:

$$K_t = 1 + a(t/r)^{1/2} \qquad (A-4)$$

where a is a coefficient which describes the severity of the notch, r is the notch root radius and t is a measure of the size of the component (plate thickness or shaft diameter, etc.). Because the stress concentration factor for purely axial loads is different and usually greater than that for pure bending, finite element analyses must be carried out for both the axial and bending cases, and values of K_t and a must be determined for each. A summary of axial and bending K_t values for common weld shapes is given in [A-5].

A-2.3 Estimating the Residual Stresses (Task 3)

After the magnitude of the applied stress, the notch-root residual stresses are the most influential factor in determining the fatigue resistance of notched components of a given material. The notch root residual stresses are generally unknown and difficult to measure; consequently, estimating the value of the notch root residual stresses is very important. Fortunately, obtaining estimates of sufficient accuracy is facilitated by several facts: first, the level of notch-root residual stress is often greatly altered during the set-up cycle (Task 8) so that the value of the notch-root residual stress may not depend too heavily upon its initial value prior to the set-up cycle but rather upon the set-up cycle itself; secondly, under high strain amplitudes, the notch-root residual stresses may quickly relax or shake down to negligible values; thirdly, the initial value of residual stress can often be bounded by the ability of the material to sustain residual stresses, so that, as in the case of weldments, one can adopt the pessimistic view that the residual stresses are as large as possible, that is, limited only by the yield strength of the (base) metal.

We therefore customarily assume that the initial value of residual stress is:

$$\sigma_r = S_y \qquad \text{for weldments in the as welded state, etc.}$$
$$\sigma_r = 0 \qquad \text{for stress-relieved or residual stress free conditions}$$
$$\sigma_r = -S_y \qquad \text{for peened or over-stressed notches}$$

where S_y is the yield point of the material limiting the level of the residual stresses, that is, the base metal yield in the case of weldments or the yield point of peened material in the case of shot peening.

160

The residual stresses on the surface of peened mild steel weldments were found to be 50-60% of S_u of the heat-affected-zone before peening as is commonly assumed for mild steels [A-6]. The peening induced residual stresses in the higher strength steels were found to follow the relationship [A-6]: $\sigma_r = -(0.21 \ S_u + 551)$ MPa. While one usually assumes that stress relieving reduces the residual stresses to zero, in fact, the residuals are reduced only to the value of the yield strength of the material at the stress relief temperature which is not necessarily zero.

A-2.4 Material Properties (Tasks 4 - 6)

Determining the fatigue crack initiation life requires measured or estimated values of many material properties. Surprisingly, the estimated fatigue crack initiation life and long life fatigue strength are rather insensitive to material properties, and small changes in properties usually do not cause large changes in the estimated results. In fact, a major role of yield (or ultimate) strength is limiting the maximum value of residual stress which can be sustained. The properties required in Tasks 8 and 10 are tabulated below:

Set-up Cycle Analysis (Task 8):

Young's Modulus	E
Yield Strength*	S_y
Ultimate Strength	S_u
Peterson's Material Constant*	a
Monotonic Stress-strain properties	K,n
Cyclic stress-strain properties	K',n'

Damage Analysis (Task 10):

Fatigue strength coefficient*	σ'_f
Fatigue strength exponent*	b
Stress relaxation exponent	k
Ultimate Strength	S_u

These properties can be measured using the tensile test (Task 4), cyclic stress-strain studies (Task 5), and cyclic stress relaxation tests (Task 6).

161

Since performing these tests is time consuming, expensive, and in some cases nearly impossible, it is useful to establish correlations of these required properties with ultimate strength or hardness of the notch-root material. Each of the material properties above denoted with an asterisk (*) can be correlated with ultimate strength which in turn is related to hardness. Thus, using the hardness of the notch-root material, it is possible to estimate the material properties needed in the analysis using the expressions below (MPa-mm units) (see also Figs. A-4 and A-5) [A-7]:

Yield strength of hot-rolled steel	$S_y \approx 5/9\ S_u$
Yield strength of normalized steel	$S_y \approx 7/9\ S_u - 138$
Yield strength of quenched and tempered steel	$S_y \approx 1.2\ S_u - 345$
Peterson's material constant for steel	$a \approx 1.087 \times 10^5 S_u^{-2}$
Fatigue strength coefficient for steel	$\sigma_f' \approx 345 + S_u$
Fatigue strength exponent for steel	$b \approx -1/6 \log[2(1+345/S_u)]$

The monotonic stress-strain properties (K,n) are best estimated directly from tensile test data and the cyclic stress properties (K',n') are best estimated from cyclic test data; although the set-up cycle can often be performed using only the monotonic and elastic properties.

The cyclic stress relaxation exponent (k) depends both upon the material and the applied strain. A reasonable correlation, the relaxation exponent (k) has been found to be related to the notch-root plastic strain amplitude (ε_{pa}):

$$k \propto \varepsilon_{pa} \qquad\qquad (A-5)$$

The available data for the relaxation exponent are plotted in Fig. A-6 [A-1, A-8].

Two other facts are worth noting. The elevation of hardness for peened mild steel has been found to be 1.2 times the original hardness for structural steels (see Fig. A-7 [A-9]). Secondly, the hardness of grain coarsened heat-affected-zones of weldments has been found to vary systematically with base metal hardness; and for fusion welding processes typical of struc-

tural welding, the hardness of the grain coarsened heat-affected-zone is generally 1.5 times the hardness of the base metal (see Fig. A-8). These two observa- tions facilitate the estimation of fatigue life and strength for peened and welded components.

A-2.5 Estimating the Fatigue Notch Factor (Task 7)

In cases in which the elastic stress concentration factor (K_t) and the notch-root radius are known and defined, one can calculate the fatigue notch factor (K_f) using Peterson's equation (Eq. A-3) and estimated or measured values of the material parameter (a). There have been many efforts to give physical significance to K_f [A-10], and a useful concept is that K_f represents the intensification of stress at the most distant region from the notch tip at which the initiation and early crack growth phenomena are the dominant fatigue mechanisms. Thus, K_f is generally less than K_t except for very large notch-root radii.

For many engineering notches, the notch-root radius is highly variable. Examples of such notches are weld toes or simple notches such as circular holes which have been exposed to corrosion. It is difficult to determine K_f for such notches because their notch-root radii are generally unknown, difficult to measure and highly variable. To cope with the variable nature of such notches, we have developed the concept of the "worst-case notch" in which a radius giving the highest possible value of fatigue notch factor is presumed to occur somewhere at the notch root. Our experience with the notch size effect for steels has led us to conclude that Peterson's equation correctly interrelates the fatigue notch and elastic stress concentration factors. The worst-case notch value of the fatigue notch factor, K_{fmax}, can be found by substituting Eq. A-4 into Eq. A-3 and differentiating with respect to r to find the value of notch-root radius for which the fatigue notch factor is maximum. Because the exponent in Eq. A-4 is usually 1/2, K_{fmax} occurs at notch-root radii numerically equal to Peterson's parameter a.

The concept of the worst-case notch and a graphical representation of the K_{fmax} concept are shown in Fig. A-9. The value of K_{fmax} depends upon: the nature of the remote stresses (axial or bending) and the geometry of the joint through the constant (a), the ultimate strength of the material at the

notch root (S_u) and the absolute size of the weldment through the dimension (t). The use of the worst-case notch concept leads to predictions that the fatigue strength of a notched component depends upon its size as well as its shape, material properties and manner of loading.

$$K_{fmax}^A = 1 + 0.0015\alpha_A S_u t^{1/2}$$

$$(A-6)$$

$$K_{fmax}^B = 1 + 0.0015\alpha_B S_u t^{1/2}$$

when both axial and bending stresses occur in an application K_{fmax} becomes a weighted average of K_{fmax}^A and K_{fmax}^B or K_{fmax}^{eff}:

$$K_{fmax}^{eff} = (1 - x) \ K_{fmax}^A + x \ K_{fmax}^B \qquad (A-7)$$

where $x = S_a^B/S_a^T$; $S_a^T = S_a^A + S_a^B$. A and B represent the axial and bending loading conditions, respectively.

A-3. The Set-up Cycle (Task 8)

The notch-root stress amplitude (σ_a) and mean stress (σ_m) which prevail during the fatigue life of a notched component are established during the first few reversals of loading. If no notch-root yielding occurs during this time, one can skip over the set-up cycle analysis and assume elastic notch- root conditions. If notch-root yielding does occur during the first few applications of load, then a set-up cycle analysis should be performed, and failure to do so could lead to mistaken estimates of the notch-root conditions during fatigue.

The notch root stress ($\Delta\sigma$) can be related to the remote stresses (ΔS) through Neuber's rule:

$$\Delta\sigma\Delta\varepsilon = (K_f \Delta S)^2/E \qquad (A-8)$$

where $\Delta\sigma$ and $\Delta\varepsilon$ are the notch root stresses and strain ranges, respectively and ΔS is the remote stress range which is within the elastic region. For the more complex but more general case involving both axial, bending and

164

residual stresses, the notch-root stress-strain response for the first application of load (that is, the first reversal {0-1} as shown in Fig. A-10) is limited by Neuber's rule modified for combined states of stress:

$$\Delta\sigma\Delta\varepsilon = (K_f^A \Delta S_{0-1}^A + K_f^B \Delta S_{0-1}^B + \sigma_r)^2/E \tag{A-9}$$

where the superscript A is for the axial and the superscript B is for the bending loading conditions. The notch root stresses and strains at the end of the first reversal can be obtained by solving Eq. 8 above either analytically or graphically as shown in Fig. 10 using the monotonic stress-strain properties (K,n) and the power law relation:

$$\Delta\varepsilon = \frac{\Delta\sigma}{E} + z(\frac{\Delta\sigma}{zK})^{\frac{1}{n}} \tag{A-10}$$

where z equals 1 for the first reversal and equals 2 for subsequent reversals.

The notch-root stresses and strains at the end of the second {1-2} and subsequent reversals can be found in a similar manner using the cyclic stress-strain properties (K',n') and the expression below:

$$\Delta\sigma\Delta\varepsilon = (K_f^A \Delta S_{1-2}^A + K_f^B \Delta S_{1-2}^B)^2/E \tag{A-11}$$

At the end of the first full cycle of the load history (2 or 3 reversals), one can determine the (stabilized) notch-root stress amplitude (σ_a) and mean stress (σ_m). It is assumed in this analysis that the material does not strain harden or soften and at the end of the first full cycle of the load history (2 or 3 reversals), one can determine the (stabilized) notch-root stress amplitude (σ_a) and mean stress (σ_m). It is further assumed that the stress amplitude and mean stress after the set-up cycle remain unchanged except for the possibility that the notch-root mean stress may relax with continued cycling.

Several interesting consequences of the set-up cycle analysis are shown in Figs. A-10-A-12. In Fig. A-11 [A-11] one can see that the role of resid-

ual stress depends greatly upon the amount of plasticity in the first cycle. Very ductile materials may wash-out any notch-root residual stress during the set-up cycle. Figures A-10 and A-12 show that the initial value of notch- root residual stress may be greatly altered and even be changed in sign from tension to compression or from compression to tension by the set-up cycle.

In the case of variable load histories, one customarily assumes that the history begins with the largest stress or strain event, and it is this series of reversals which is dealt with in the set-up cycle analysis.

A-4 The Damage Analysis (Task 10)

A-4.1 Predicting the Fatigue Behavior Under Constant Amplitude Loading With No Notch-Root Yielding or Mean-Stress Relaxation

Under the simplest conditions, the fatigue strength (S_a) of a notched component at given long lives can be estimated using the expression below:

$$\Delta S_a K_f = (\sigma'_f - K_f S_m - \sigma_r)(2N_I)^b \qquad (A-12)$$

where S_a is the remote stress amplitude, σ_r is the notch-root residual stress and S_m is the applied mean stress or the global residual stress in the structure near the notch. A simple expression for the fatigue strength of notched members at long lives can be obtained from the expression above.

$$S = \left(\frac{\sigma'_f - \sigma_r}{K_f}\right)\left(\frac{(2N_I)^b}{1 + \frac{1 + R}{1 - R}(2N_I)^b}\right) \qquad (A-13)$$

since $S_m = S_a(1+R/1-R)$. The above expression can be used only in the simplest case: at long lives (in quasi-elastic notch root conditions), when the K_f of the notch is known, when the residual stresses do not relax, when the loads are either purely axial or pure bending, and when the load history is constant amplitude.

Eq. A-13 which is rewritten below to incorporate the concept of K_{fmax}^{eff}:

166

$$S_a^T = \frac{(\sigma_f' - \sigma_r)(2N_I)^b}{K_{fmax}^{eff}[1 + \frac{1 + R}{1 - R}(2N_I)^b]} \qquad (A\text{-}14)$$

where

$$K_{fmax}^{eff} = (1 - x)K_{fmax}^A + xK_{fmax}^B \qquad (A\text{-}7)$$

$$x = S_a^B/S_a^T = \frac{S_a^B}{S_a^A + S_a^B}$$

A comparison of fatigue strength predictions made using Eq. A-14 and experimental data for both as-welded and post-weld treated steel weldments [A-9] is given in Fig. A-14. The fatigue strength S_a^T predicted by Eq. A-14 can be plotted in a manner similar to K_{fmax} for a weldment of a given material and post-weld treatment. Since the fatigue strength coefficient (σ_f'), the fatigue strength exponent (b), the residual stress (σ_r), and K_{fmax} all depend upon or can be correlated with hardness or ultimate strength of the base metal, Eq. A-14 can be expressed as a function of the ultimate strength and constants which depend upon ultimate strength and the type of post-weld treatment:

$$S_a^T = \frac{AS_u + B}{C(K_{fmax}^{eff} - 1) + 1} \cdot \frac{(2N_I)^b}{1 + \frac{1 + R}{1 - R}(2N_I)^b} \qquad (A\text{-}15)$$

where:

S_u = tensile strength of base metal

$b = -1/6 \log[2(1 + D/S_u)]$

K_{fmax}^{eff} is calculated using the ultimate strength of base metal (see Eq. A-14)

A,B,C,D = coefficients given in Table A-1 and below

$AS_u + B = CS_u + 344 + \sigma_r$

$\sigma_r = \pm S_y(BM) = 5/9 \; S_u$ Hot rolled

$= 7/9 \; S_u - 138$ Normalized

$= 1.2 \; S_u - 345$ Quenched and tempered

$\sigma_r = 0$ Stress relieved

$C = 1$ Plain plate

   $= 1.5$ HAZ (stress relief might reduce this value)

   $= 1.5 \times 1.2 = 1.8$ Peened HAZ

$D = 344/C$

TABLE A-1

Coefficients of equation (A-15) for each post-weld treatment
and base metal heat treatment

	Post-weld treatment	Base metal heat-treatment	A	B	C	D
1.	Plain plate	-	· 1	345	1.0	345
2.	As-welded	Hot-rolled	0.94	345	1.5	230
		Normalized	0.72	483	1.5	230
		Q&T	0.30	690	1.5	230
3.	Stress-relief	-	1.50	345	1.5	230
4.	Over-stressed	Hot-rolled	2.06	345	1.5	230
		Normalized	2.28	207	1.5	230
		Q&T	2.70	0	1.5	230
5.	Shot-peening	S_u(HAZ) <862 Mpa	2.12	896	1.8	191
		S_u(HAZ) >862 Mpa	2.12	896	1.8	191

Units: t(mm); S_u(MPa).

Figure A-14 gives an example of the graphical determination of the fatigue strength of weldments based upon Eq. 14 for as-welded ASTM A36 steel. Comparison of the conditions described by lines A→A''' and B→B''' show that welds with more favorable geometries (A→A''') may have lower fatigue strengths than weldments having worse geometries but smaller thicknesses, having smaller flank angles, and having a smaller R ratio. Comparison of line B→B''' with line C→C''' shows that weldments subjected to bending (C→C''') give higher fatigue lives than smaller weldments subjected to more nearly axial loading conditions (B→B''').

Figures A-15 and A-16 give similar graphical aids for ASTM A36 in the post- weld treated (stress-relieved and shot-peened) conditions, respectively. These design aids are based entirely upon Eq. A-15 above. Nomographs

for other steels and other notch geometries can be constructed in a similar way.

The accuracy of predictions based on Eq. A-15 requires further study, but comparison of predictions made using Eq. A-15 and available test data is given in Fig. A-13. If one discounts the data for stress-relieved and hammer-peened weldments (treatments which may not be as effective as hoped), then Eq. A-15 would seem to predict the fatigue strength of steel weldments with an accuracy of roughly 25%.

A-4.2 Predicting the Fatigue Behavior Under Constant Amplitude Loading With Notch-Root Yielding and No Mean-Stress Relaxation

When the notch-root conditions are not quasi-elastic and substantial plastic deformation occurs during the set-up cycle (Task 8,) the simple expressions developed in the preceding section cannot be used. When there is notch-root yielding during the set-up cycle but no mean-stress relaxation during subsequent cycling, the notch-root stress amplitude (σ_a) and mean stress (σ_m) determined in the set-up cycle can be substituted into Eq. A-2 to estimate (the long life) fatigue strength or fatigue crack initiation life (N_I).

A-4.3 Predicting the Fatigue Crack Initiation Life Under Constant Amplitude Loading With Notch-Root Yielding and Mean-Stress Relaxation

In general, there are several possible outcomes which may result from the notch-root residual stresses which exist prior to the set-up cycle: There may be substantial notch-root mean stresses after the set-up cycle or there may be none; subsequent to the set-up cycle, any non-zero notch-root mean stress may persist for the duration of the fatigue life or it may relax. The outcome in which notch-root mean stresses exist after the set-up cycle but relax during fatigue cycling requires a special analysis.

If the mean stress established during the set-up cycle relaxes during cycling, the current value of mean stress $(\sigma_{m,2N})$ can be predicted using a power function (see also Fig. A-17):

$$\sigma_{m,2N} = \sigma_{m,i}(2N-1)^k \qquad \text{(A-15)}$$

where k is the relaxation exponent determined in Task 9 using the material properties describing stress relaxation (Task 6) and the notch-root stresses and strains determined in the set-up cycle analysis (Task 8); $\sigma_{m,i}$ is the notch-root mean stress after the set-up cycle; and 2N is the elapsed reversals. Larger plastic strain amplitudes and higher mean stresses cause a more rapid relaxation of notch-root mean stress. Using the above expression for the current value of notch-root mean stress and the Basquin equation (Eq. A-2), one can solve for the fatigue crack initiation life ($2N_I$) as the upper limit of integration of the equation below:

$$\int_{1}^{2N_I} \{(\sigma'_f/\sigma_a)(1 - (\sigma_{m,i}/\sigma'_f)(2N_i)^k)\}^{1/b} \ dN_i = 1 \qquad \text{(A-16)}$$

Typical behavior of Eq. A-16 above is shown in Fig. A-18.

A-4.4 **Predicting the Fatigue Crack Initiation Life**
       Under Variable Load Histories Without Mean Stress Relaxation

For variable amplitude load histories the linear cumulative damage rule is used to sum up the fatigue damage rate (D_i) of each closed hysteresis loop in one block of the load history ignoring the possibility of notch root mean stress relaxation [A-12]:

$$D_{block} = \sum D_i = \sum_i [\frac{\sigma'_f - \sigma_m}{\Delta\sigma/2}]^{1/b} \qquad \text{(A-17)}$$

then N_I is the reciprocal of D_{block}

$$N_I = 1/D_{block}$$

Although many cycle counting methods have been proposed in the past years, the 'vector method' concept developed by Dowling and Socie [A-13] is considered to be the most effective and easier to program for a digital computer. For a notched member without bending stresses and residual stresses, the load history is rearranged in such a manner that the largest value of $(K^A_{fmax}$

171

$S_i^A + K_{fmax}^B \, S_{i+\sigma_r}^B$) as the first and last values while performing the cycle counting.

A-5. Estimating the Fatigue Life Devoted to Crack Propagation (N_p)

The fatigue crack propagation life N_p for constant amplitude loading can be computed by integrating Paris' equation [A-14] from the initial crack length a_i to the final crack length a_f:

$$da/dN - C \, (\Delta K)^n \qquad\qquad\qquad (A-18)$$

$$N - \int_{a_i}^{a_f} da \; /[C(\Delta K)^n] $$

where C and n are material constants, ΔK is the stress intensity factor range:

$$\Delta K - YS(\pi a)^{1/2} \qquad\qquad\qquad (A-19)$$

where Y is the geometry factor.

Mean stress effect on crack propagation rate can be accounted for by substituting effective stress intensity factor range ΔK_{eff} [A-15] into Eq. A-18. For a given shape of weld, Y can be expressed conveniently by super-position of several geometry effects [A-16]:

$$Y - M_s M_t M_k/\phi_o \qquad\qquad\qquad (A-20)$$

in which M_s accounts for the effect of free front surface; M_t for the finite plate width w; ϕ_o for the crack shape; M_k for nonuniform stress gradient due to the stress concentration of weld discontinuity.

When a weld is subjected to combined loading of axial, induced bending and residual stress, the total stress intensity factor range ΔK_T can be obtained by a superposition method:

$$\Delta K_T - \Delta K_A + \Delta K_B + K_r \qquad \text{(A-21)}$$

$$K_r - F\sigma_r(\pi a)^{1/2} \qquad \text{(A-22)}$$

where ΔK_A and ΔK_B are the stress intensity factors for tension and bending respectively, and K_r is the stress intensity factor due to residual stress and F is a function of residual stress distribution. When a crack is subjected to a distributed residual stress $\sigma_r(x)$, the stress intensity factor K_r is calculated by the integral:

$$K_r - \frac{2\sqrt{a}}{\sqrt{\pi}} \int_0^a \frac{\sigma_r(x)}{(a^2-x^2)^{1/2}} \, dx \qquad \text{(A-23)}$$

Tada and Paris [A-17] derived the stress intensity factor for a crack perpendicular to a weld bead using Eq. A-23. The stress intensity factor caused by the residual stresses was expressed in a simple form shown in Fig. A19. It has been shown [A-19] that compressive residual stress has an influence on the fatigue crack propagation behaviour in hammer-peened welds. The ability of notch compressive residual stresses to regard fatigue crack growth depends on the distribution in depth of both the residual stresses and the local stresses, and the relaxation of the residual streses in depth [A-20]. Figure A-20 shows the typical residual stress distribution for shot-peened specimens, and two hypothetical notch residual stress fields and their corresponding stress intensity factors [A-21, A-22]. Calculation of N_p is carried out by substituting ΔK_T into Eq. A-18.

The fatigue crack propagation life N for a weld under variable amplitude loading can be estimated using a method developed by Socie [A-23] and modified by Ho [A-9]. The crack growth rate per block $\Delta a/\Delta B$, is calculated by considering the crack length as being fixed at the initial crack size and summing the incremental crack extension for each cycle:

$$\Delta a/\Delta B - \sum_i \Delta a_i \qquad \text{(A-24)}$$

Combining Eqs. A-18, A-21, A-22, Eq. A-24 becomes

$$\Delta a/\Delta B = C \ (\pi a)^{n/2} \sum (Y_A \Delta S_A + Y_B \Delta S_B + F\sigma_r)^n \qquad \text{(A-25)}$$

Then, the crack propagation life N_p (in blocks) is

$$N_p = \int_{a_i}^{a_f} (\Delta B/\Delta a) \ da \qquad \text{(A-26)}$$

Appendix A References

A-1. Lawrence, F.V., Jr., Mattos, R.J., Higashida, Y. and Burk, J.D. (1978) "Estimation of Fatigue Initiation Life of Weld." ASTM STP 684, 134-158.

A-2. Lawrence, F.V., Jr., Ho, N.-J. and Mazumdar, P.K. (1980) "Predicting the Fatigue Resistance of Welds." FCP Report No. 36, University of Illinois at Urbana-Champaign.

A-3. Yung, J.-Y. and Lawrence, F.V., Jr. (1985) "Fatigue of Weldments Under Combined Bending and Torsion." Spring conference on experimental mechanics, Society for Experimental Mechanics, 646-648.

A-4. Peterson, R.E. (1974) Stress concentration factors. John Wiley & Sons, Inc.

A-5. Yung, J.-Y. and Lawrence, F.V., Jr. (1985) "Analytical and Graphical Aids for the Fatigue Design of Weldments." Accepted for publication in Fatigue and Fracture of Engineering Materials and Structures.

A-6. Cichlar, D. (1980) Private Communication, Metal Improvement Company, Chicago, Illinois.

A-7. McMahon, J.C. and Lawrence, F.V., Jr. (1984) "Predicting Fatigue Properties through Hardness Measurements." FCP Report No. 105, University of Illinois at Urbana-Champaign.

A-8. Prine, D.W., Malin, V.D., Yung, J.-Y., McMahon, J. and Lawrence, F.V., Jr. (1982) "Improved Fabrication and Inspection of Welded Connections in Bridge Structures." U.S. Department of Transportation, Report No. FHWA/RD-83/006.

A-9. Chang, S.T. and Lawrence, F.V., Jr. (1983). "Improvement of Weld Fatigue Resistance." FCP Report No. 46, University of Illinois at Urbana-Champaign.

A-10. Chen, W.-C. and Lawrence, F.V., Jr. (1979). "A Model for Joining the Fatigue Crack Initiation and Propagation Analysis." FCP Report No. 32, University of Illinois at Urbana-Champaign.

A-11. Burk, J.D. and Lawrence, F.V., Jr. (1978) "Effect of Residual Stresses on Weld Fatigue Life." Ph.D. Thesis, University of Illinois at Urbana-Champaign.

A-12. Ho, N.-J. and Lawrence, F.V., Jr. (1984) "Constant Amplitude and Variable Load History Fatigue Test Results and Predictions for Cruciform and Lap Welds." Theoretical and Applied Fracture Mechanics 1, 3-21.

A-13. Dowling, S.D. and Socie, D.F. (1982) "Simple Rainflow Counting Algorithms," International Journal of·Fatigue 4, 31-40.

A-14. Paris, P.C. and Erdogan, F. (1963) "A Critical Analysis of Crack Propagation Law." Journal of Basic Engineering ASME Transaction Ser. D 85, 528-534.

A-15. Elber, W. (1974) "Fracture Toughness Testing and Slow Stable Cracking.' ASTM STP 559, 45-58.

A-16. Maddox, S.J. (1975) "An Analysis of Fatigue Cracks in Fillet Welded Joints." International Journal of Fracture 11, 221-243.

A-17. Tada, H. and Paris, P.C. (1983) "The Stress Intensity Factor for a Crack Perpendicular to the Welding Bead." International Journal of Fracture 21, 279-284.

A-18. Al-Hassani, S.T.S. (1982) "The Shot Peening of Metals - Mechanics and Structures." SAE Report No. 821452.

A-19. Smith, I.F.C. and Smith, R.A. (1983) "Fatigue Crack Growth in a Fillet Welded Joint." Engineering Fracture Mechanics 18, 861-869.

A-20. Nelson, D.V. and Socie, D.F. (1982) "Crack Initiation and Propagation Approaches to Fatigue Analysis." ASTM STP 761, 110-132.

A-21. Throop, J.F. (1983) "Fracture Mechanics Analysis of the Effects of Residual Stress on Fatigue Life." Journal of testing and Evaluation 11, 75-78.

A-22. Elber, W. (1974) "Fracture Toughness Testing and Slow Stable Cracking." ASTM STP 559, 45-58.

A-23. Socie, D.F. (1977) "Estimating Fatigue Crack Initiation and Propagation Lives in Notched Plates Under Variable Loading History." TAM Report No. 417, University of Illinois at Urbana-Champaign.
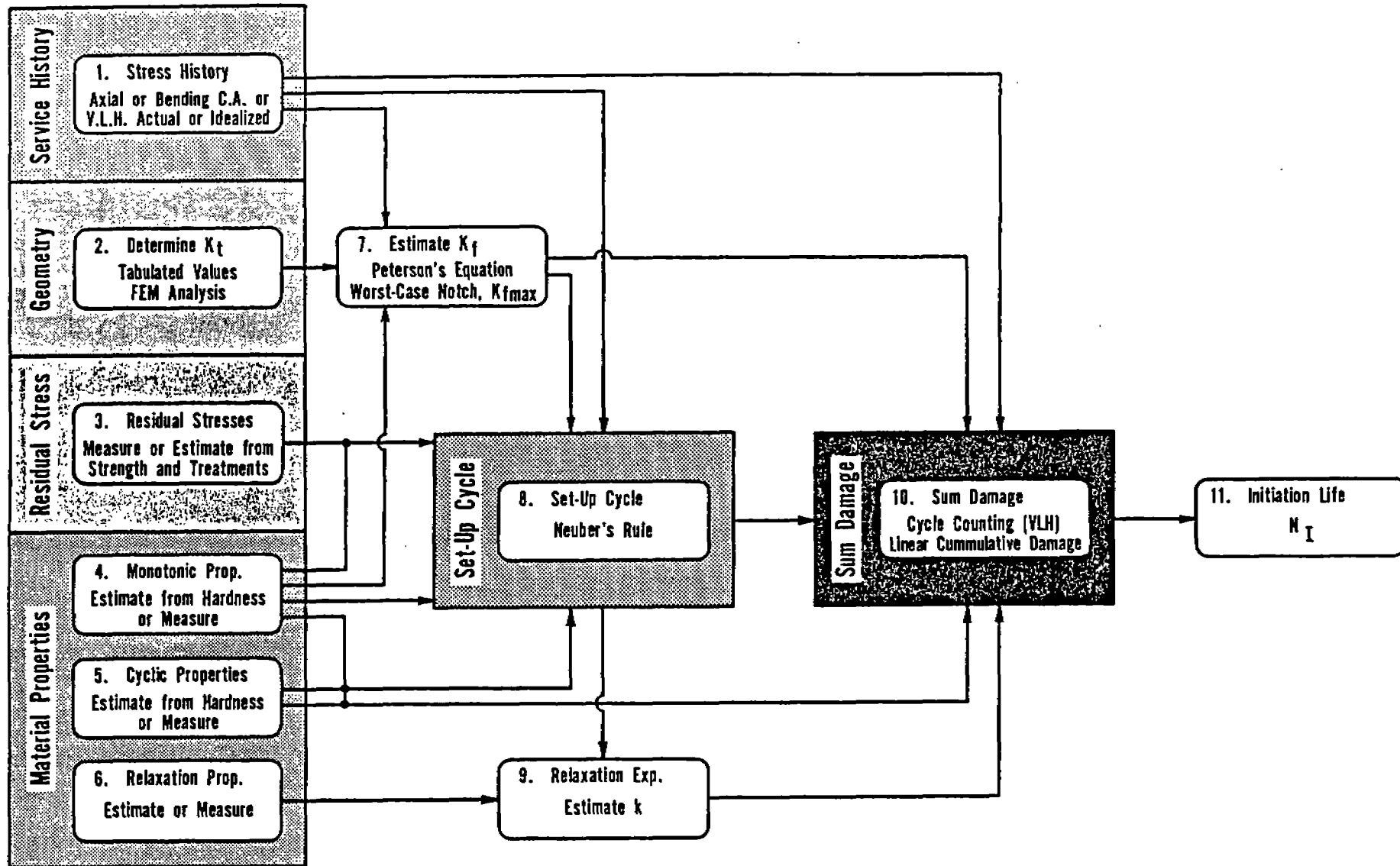
Fig. A-1 Schematic diagram for the fatigue crack initiation life estimation procedure.
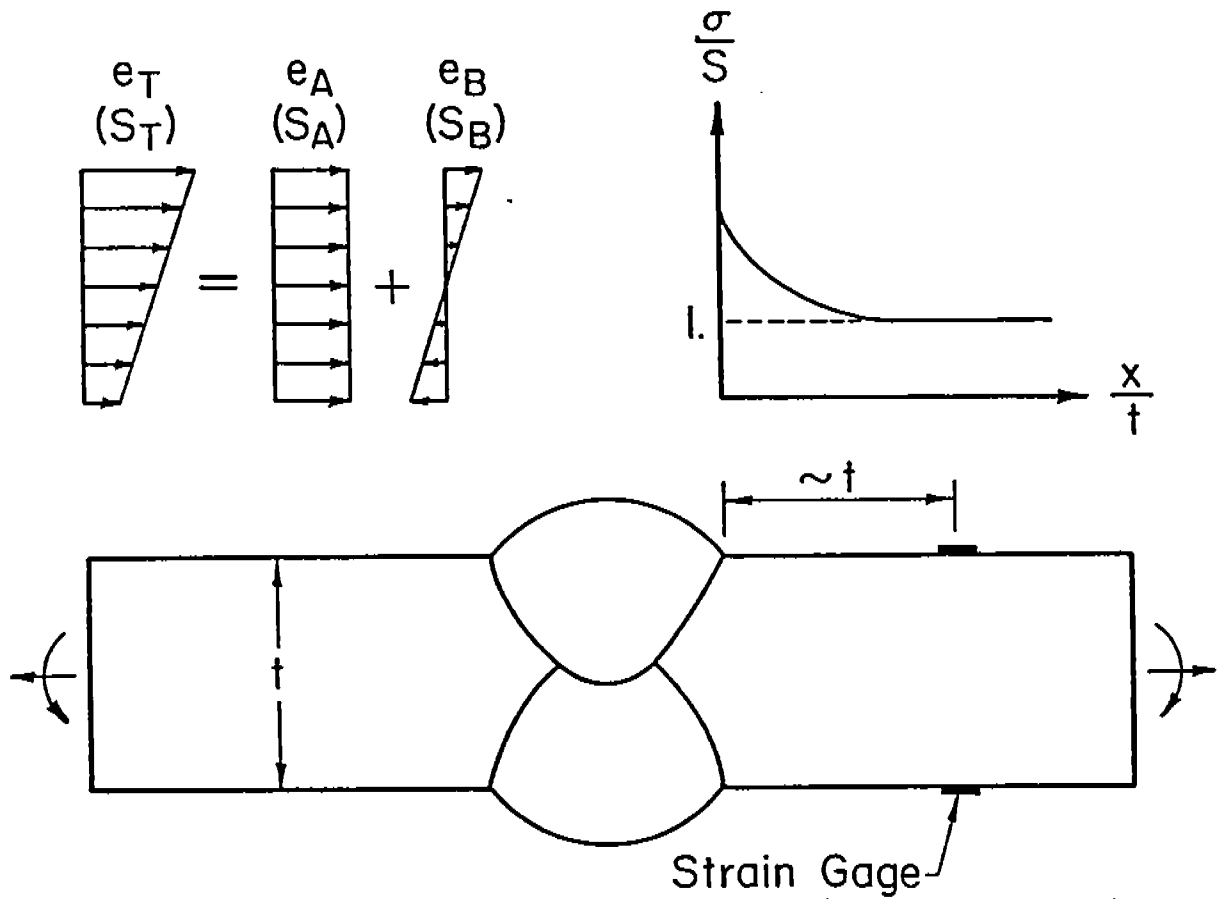
Fig. A-2 The location of strain gauges relative to the notch and the separation of remote axial and bending strains (stresses).
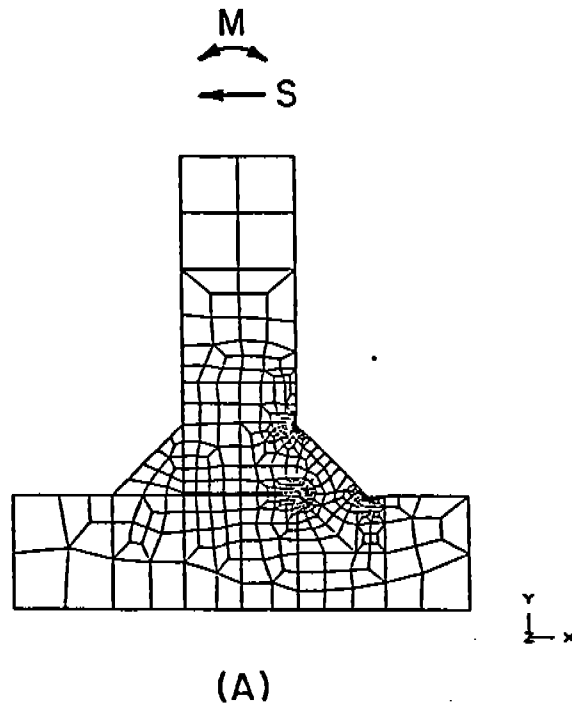
(A)
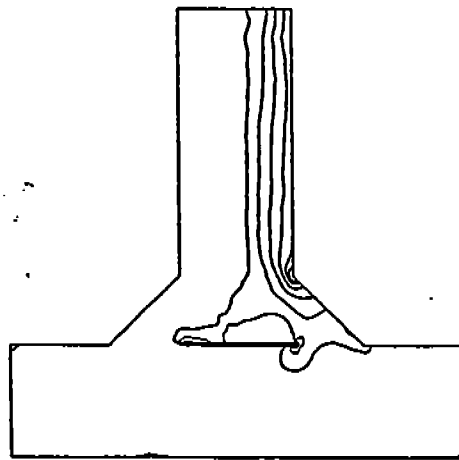
(B)

Fig. A-3 (a) Finite element mesh for T joints
subjected to bending and shear;
(b) Contours of tensile maximum principal
stresses resulting from (a).
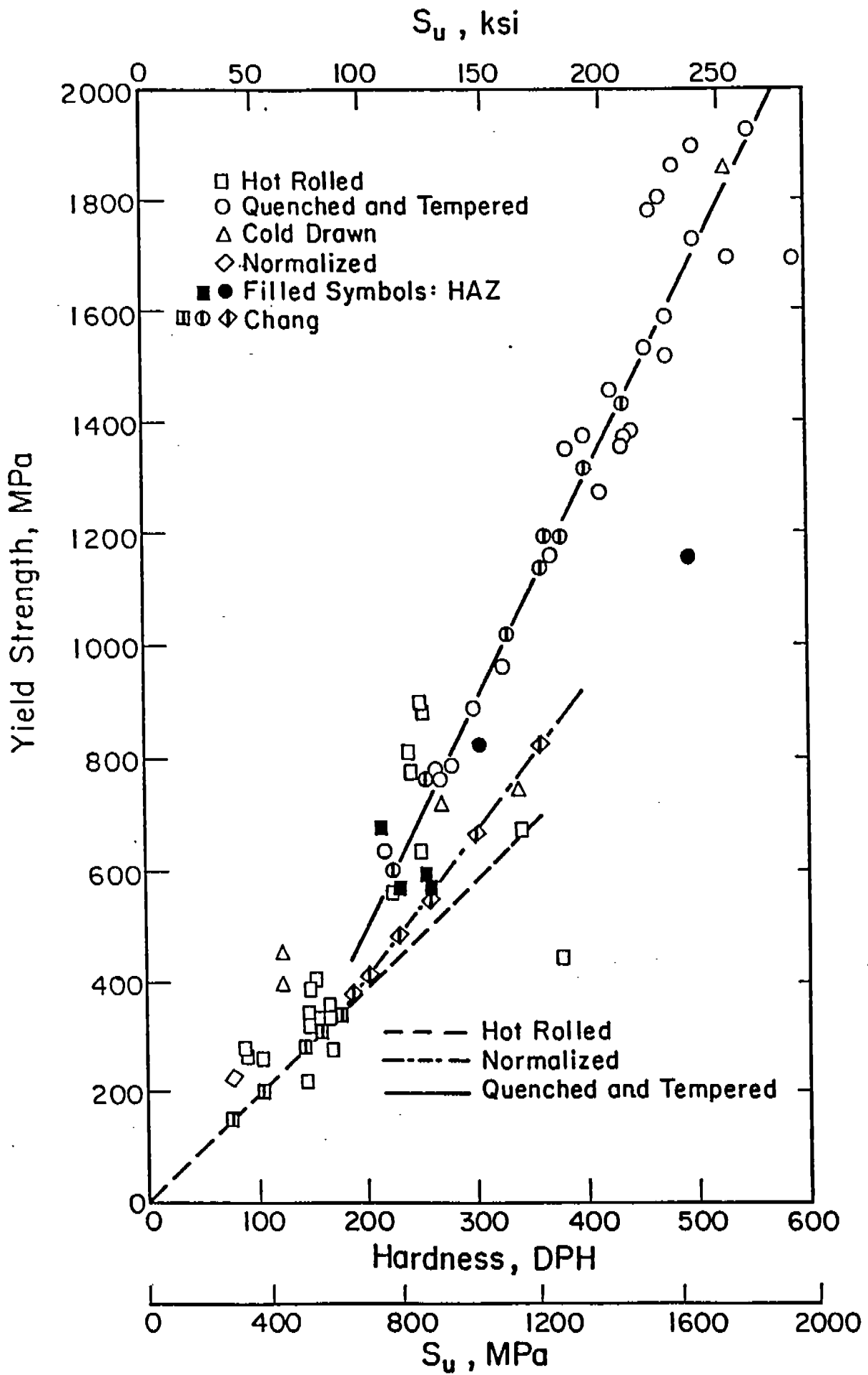
Fig. A-4 Yield strength as a function of ultimate strength and hardness[A-7].

179
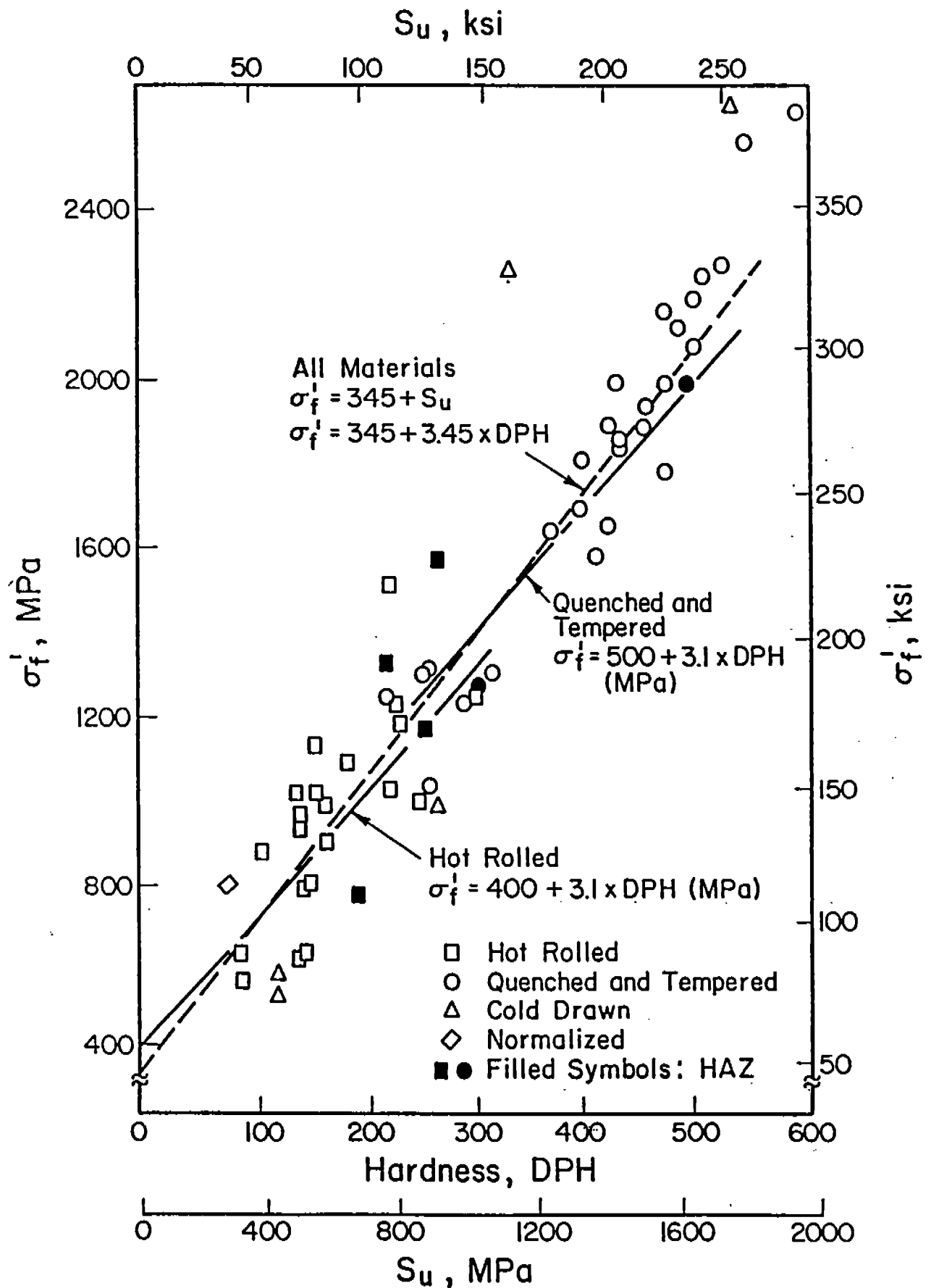
Fig. A-5 Fatigue strength coefficient as a function of ultimate strength
and hardness[A-7].
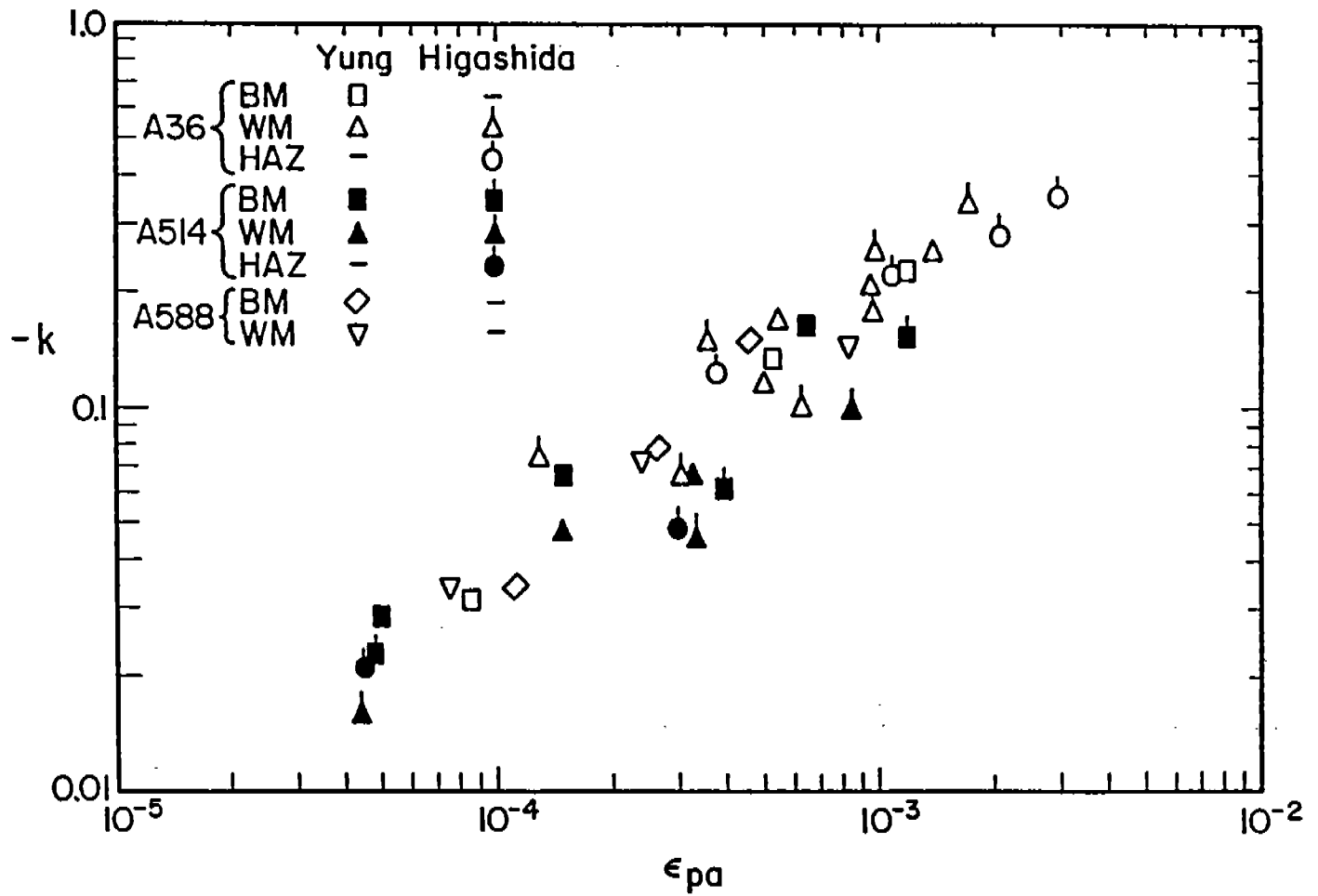
Fig. A-6 Relaxation exponent as a function of plastic strain amplitude
[A-1, A-8].
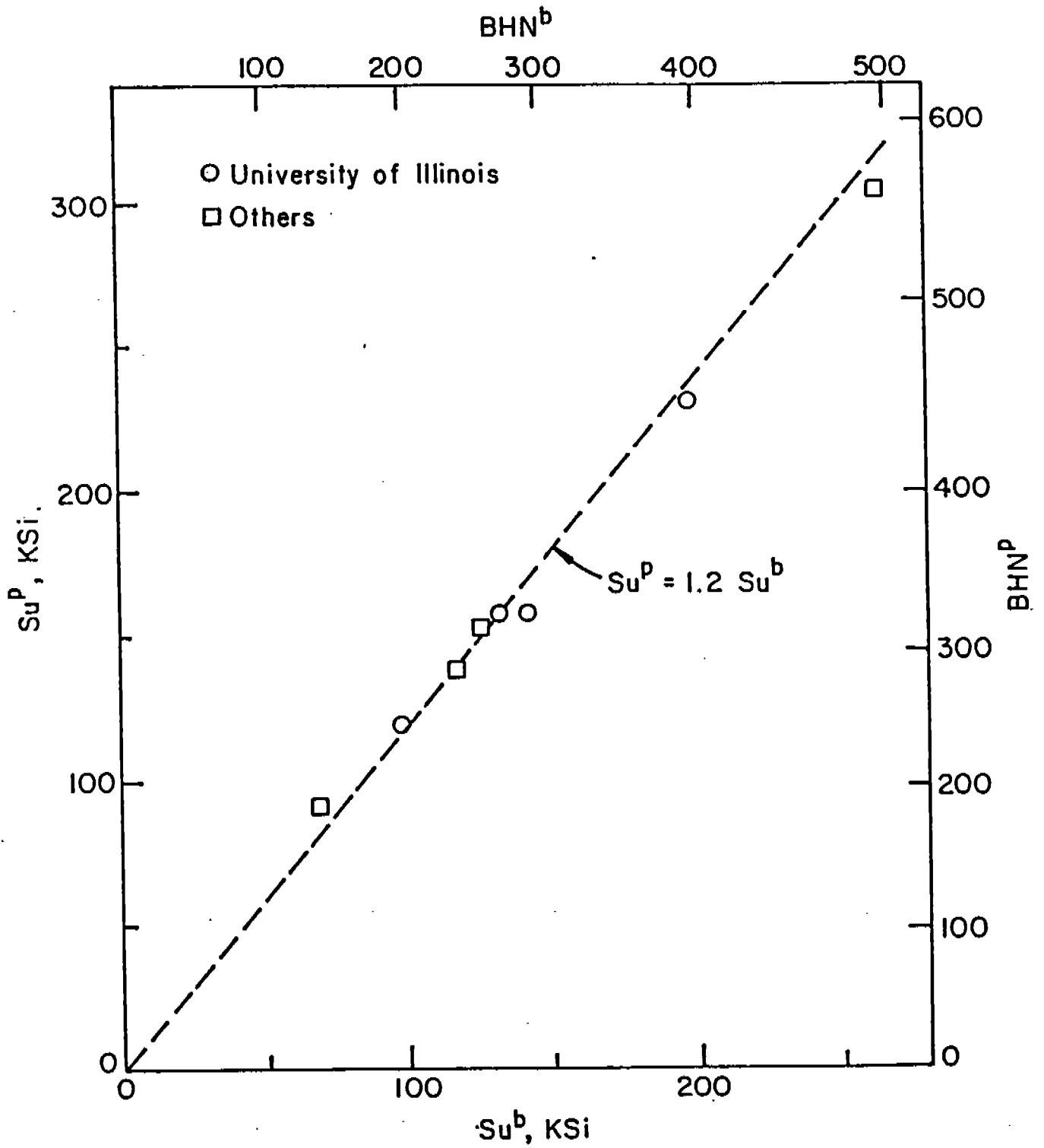
Fig. A-7   Peened material hardness as a function of base metal Hardness
[A-9].
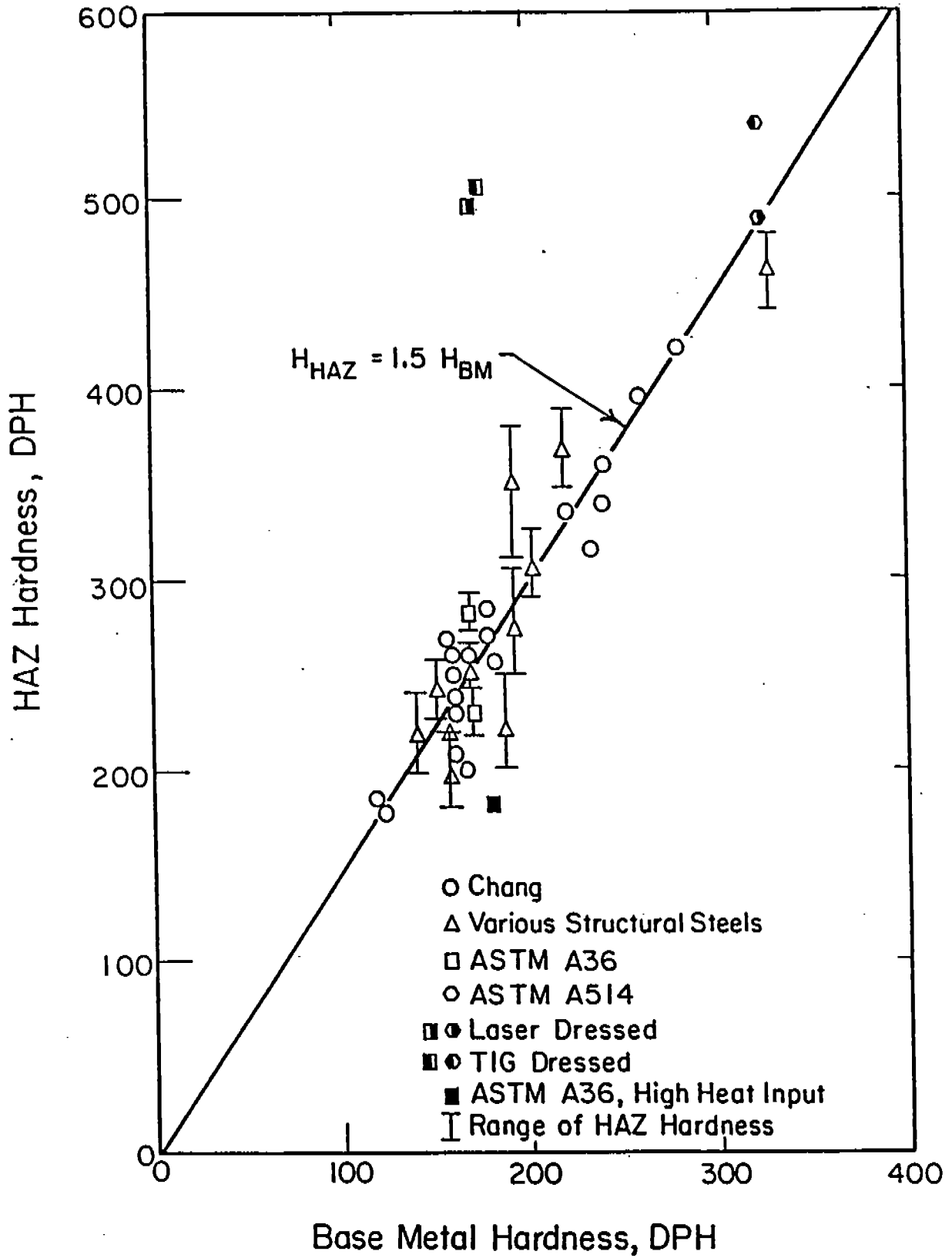
Fig. A-8 Heat-affected-zone hardness as a function of base metal hardness [A-7].
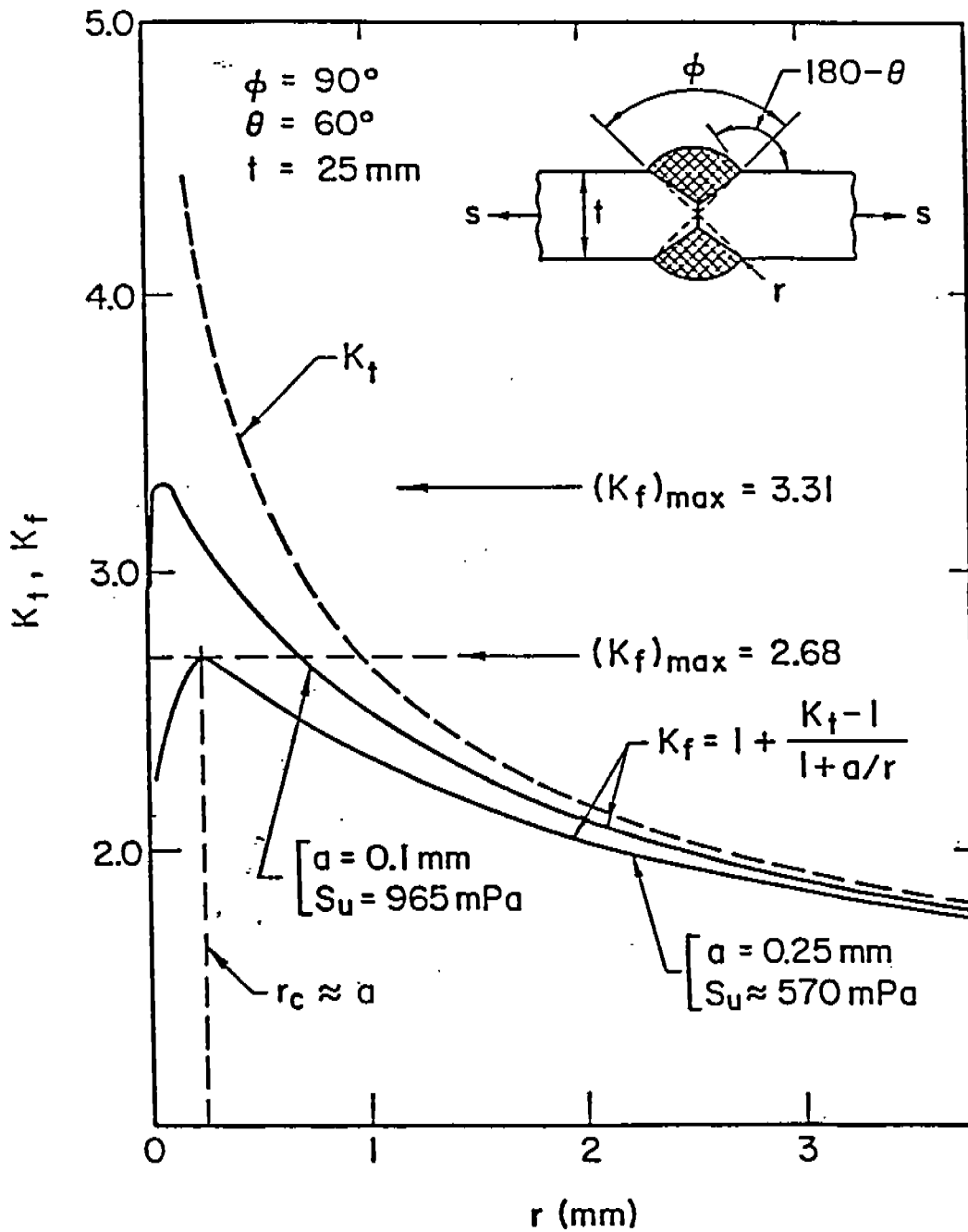
Fig. A-9 Elastic stress concentration factor (K_t) and fatigue notch factor (K_f) as a function of toe root radius. $K_{f_{max}}$ is the "worst case" value of K_f for a given material and geometry.

$$(K_f^A \, \Delta S_A + K_f^B \, \Delta S_B)^2 \, / \, E = \Delta\sigma \, \Delta\epsilon$$

$$(K_f^A S_1^A + K_f^B S_1^B + \sigma_r)^2 \, / \, E = \Delta\sigma\Delta\epsilon$$

$$(K_f^A \Delta S_A + K_f^B \Delta S_B)^2 \, / \, E = \Delta\sigma\Delta\epsilon$$
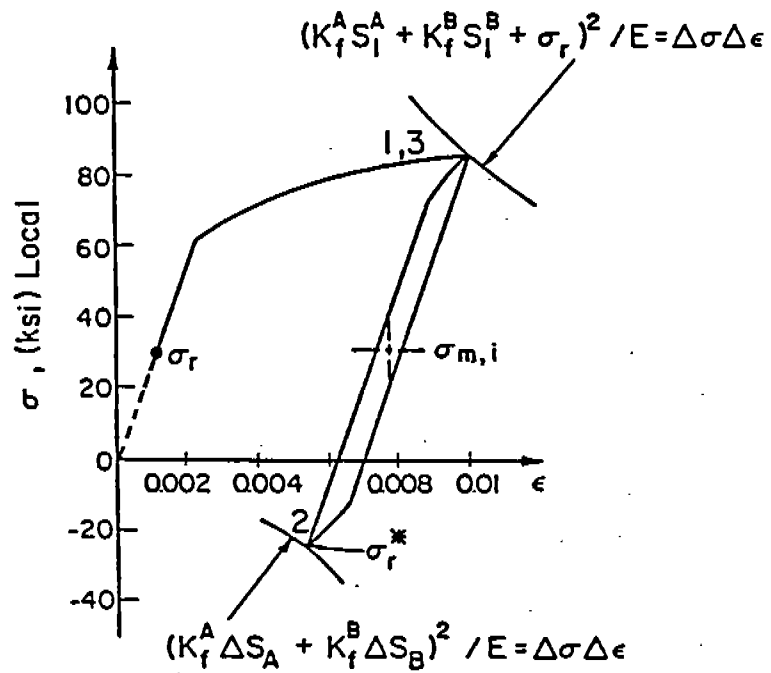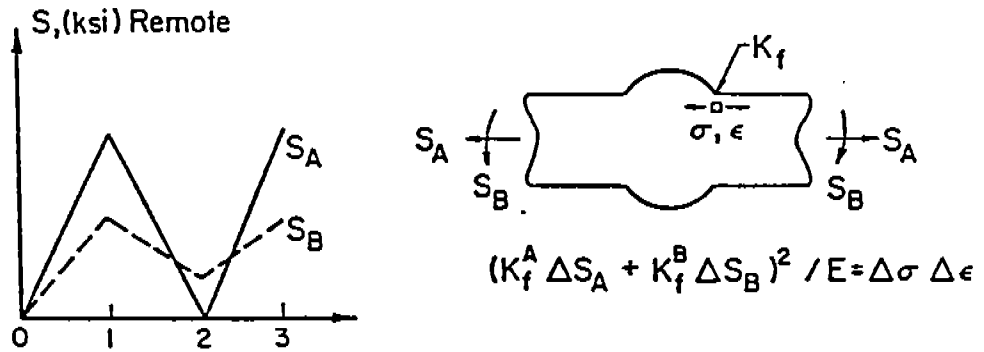
Fig. A-10 Set-up cycle analysis for the weld toe with tensile residual stresses. Note the change of the sign of the notch-root residual stresses after the second reversal of load.
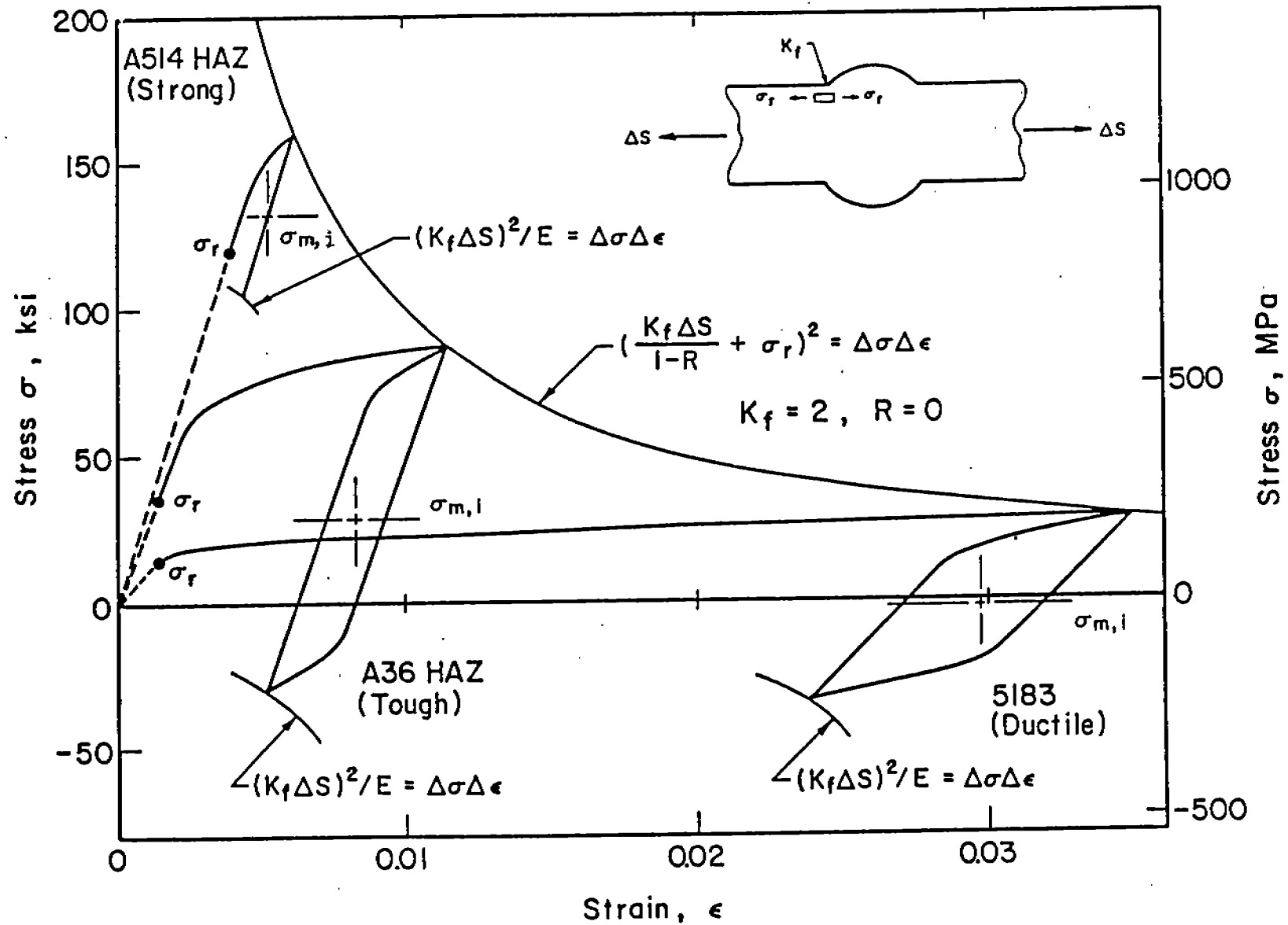
Fig. A-11   Set-up cycle for ASTM A514 HAZ (strong), A36 HAZ (tough) steels, and aluminum alloy 5183 WM (ductile) materials [A-11]. The set-up cycle may eliminate notch-root residual stresses in ductile materials.

S (ksi), Remote

σ (ksi), Local

$(K_f^A \Delta S_A + K_f^B \Delta S_B)^2/E = \Delta\sigma\Delta\epsilon$

$(K_f^A S_I^A + K_f^B S_I^B + \sigma_r)^2 = \Delta\sigma\Delta\epsilon$
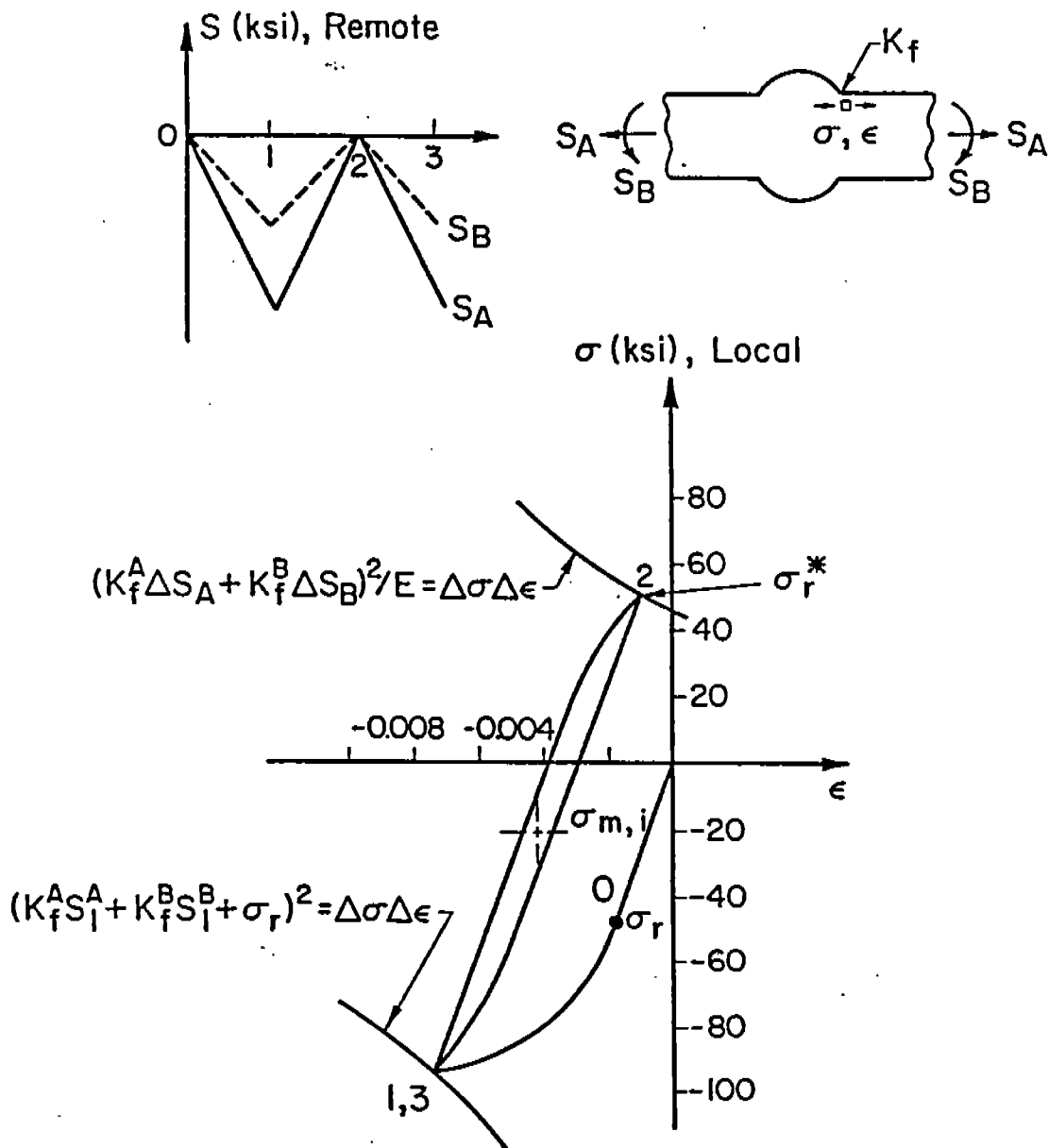
Fig. A-12 Reversal of sign of residual stresses after set-up cycle. An example of compressive loadings and compressive residual stresses.
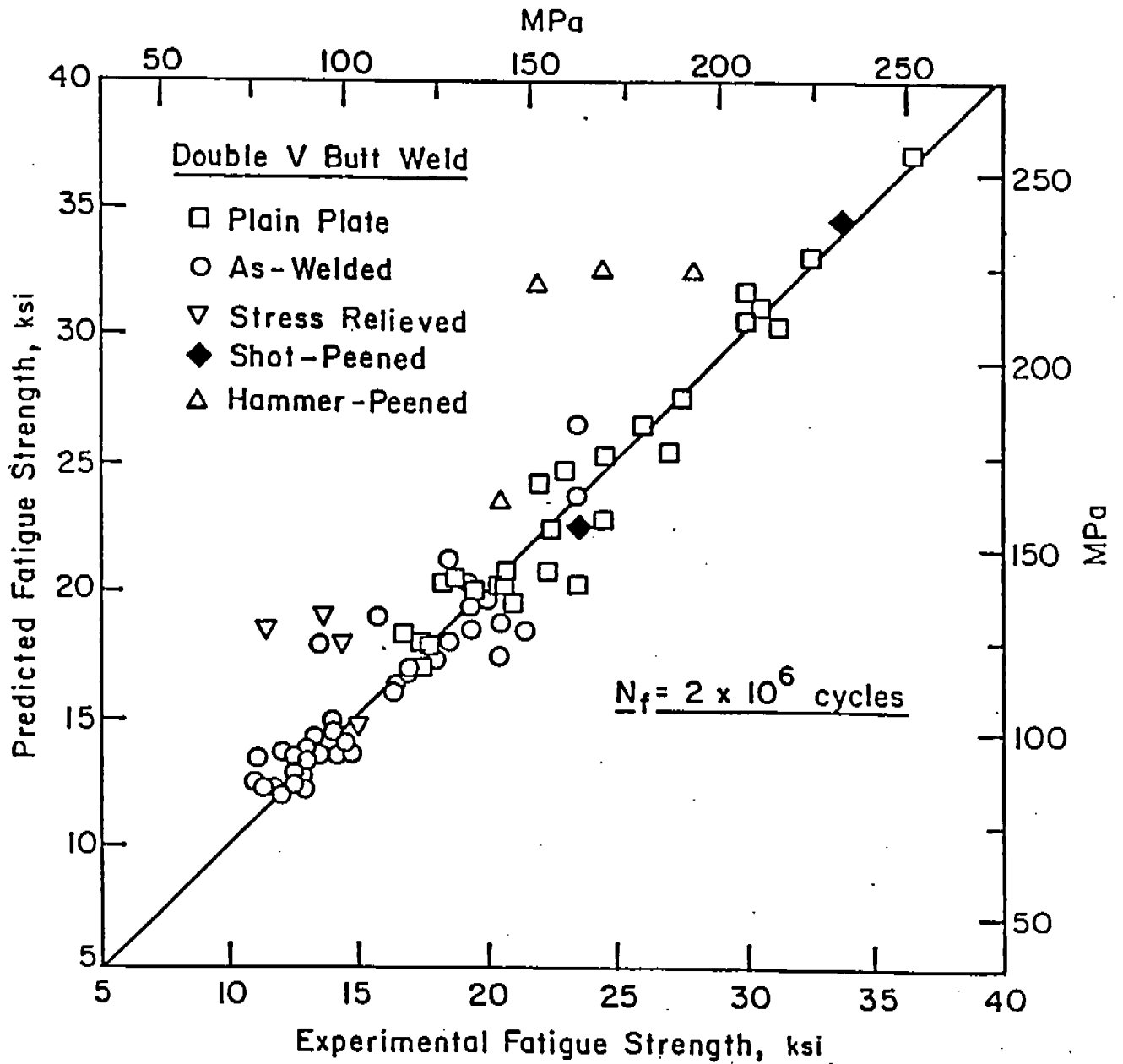
Fig. A-13 Comparison of fatigue strength predicted using Eq. 14 with experimental data [A-9].

ASTM-A36, AS-WELDED

Weld Joint
$\ell = t$

G9

B

G3

C

A

G1

Axial   Bending

Plate Thickness, t : mm (in.)

12.7   25.4   38.1
(0.5)   (1.0)   (1.5)

B'

50.8
(2.0)

C'

A'

0   0.2   0.4   0.6   0.8   1.0

x

S_a^T (at 2×10^6 cycles), MPa

0   100   200   300

0.5   0   -1.0

C'''

B''' C''''

A'''

C''

B''

A''

15°

30°

45°

60°

Stress Ratio, R

Flank Angle, θ: Degrees

0   10   20   30   40   50

S_a^T (at 2×10^6 cycles), ksi
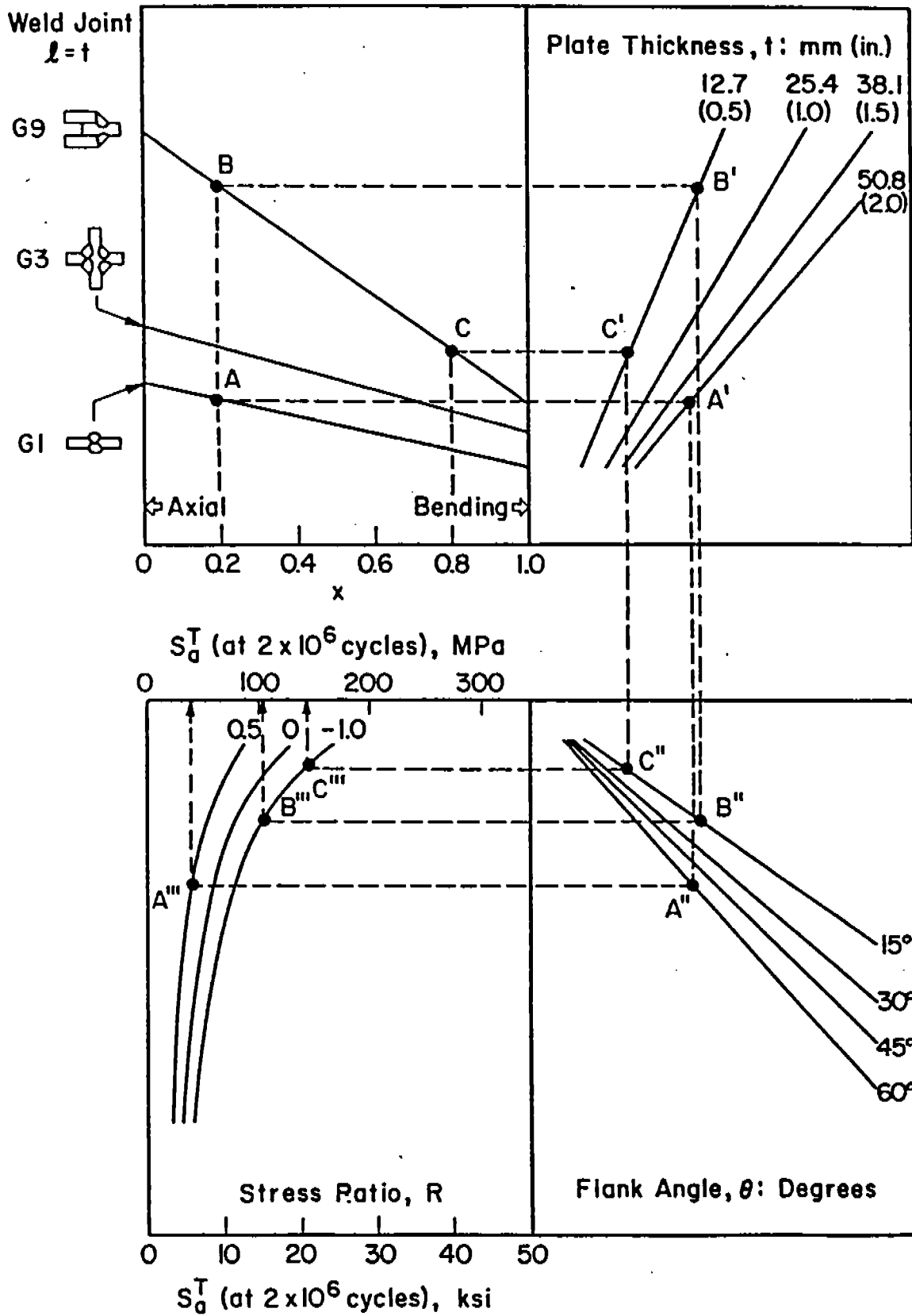
Fig. A-14 Use of the proposed nomograph for the fatigue design of as-
welded ASTM A36 weldments [A-5].

ASTM-A36, STRESS-RELIEVED
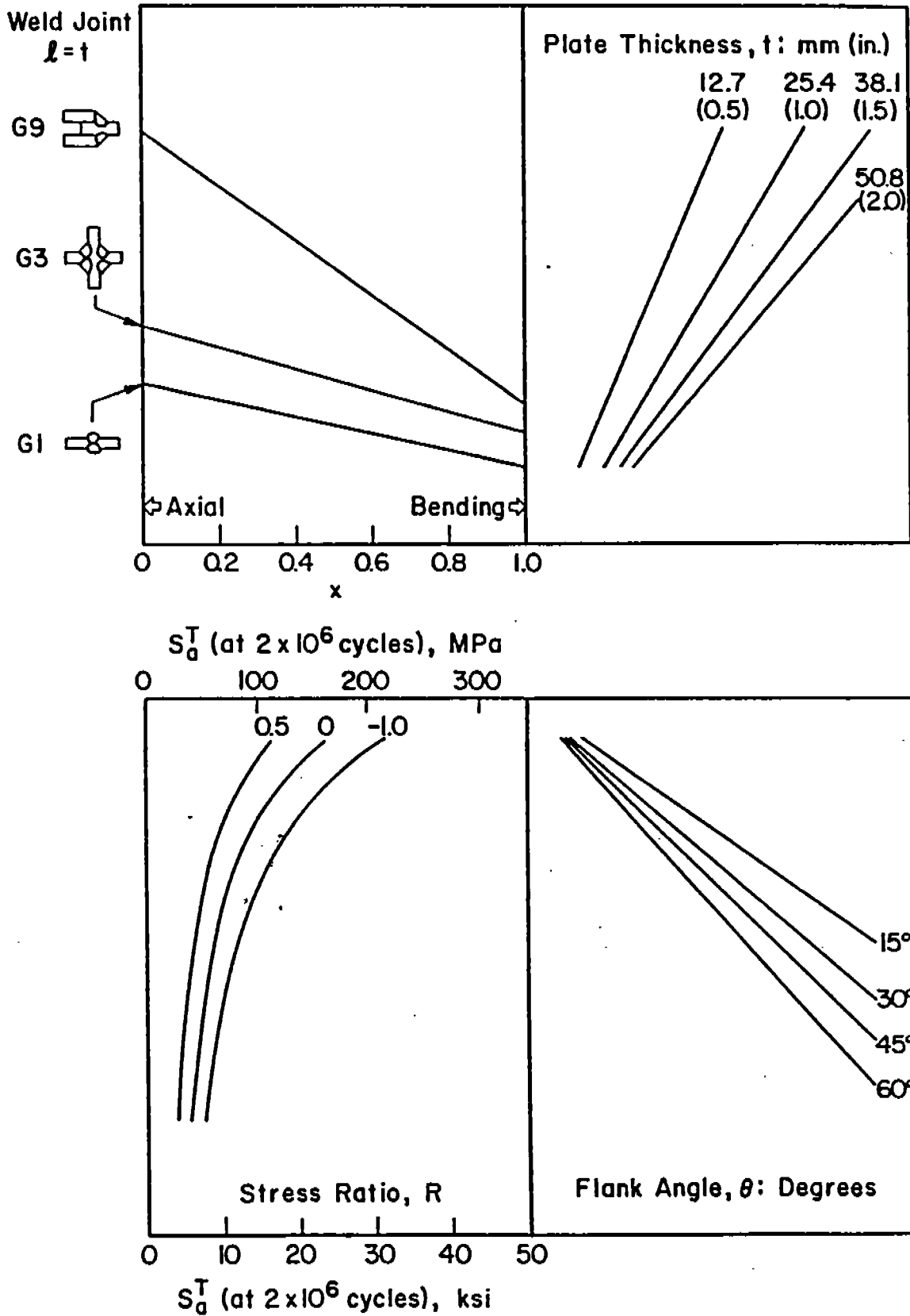
Fig. A-15 Nomograph for the fatigue design of stress relieved ASTM
A36 weldments [A-5].

190

ASTM-A36, SHOT-PEENED

Weld Joint
$\ell = t$

G9

G3

G1

Axial   Bending

0   0.2   0.4   0.6   0.8   1.0
x

Plate Thickness, t : mm (in.)

12.7   25.4   38.1
(0.5)   (1.0) (1.5)

50.8
(2.0)

S_a^T (at 2×10^6 cycles), MPa

0   100   200   300

0.5   0   -1.0

15°

30°

45°

60°

Stress Ratio, R

Flank Angle, θ : Degrees

0   10   20   30   40   50

S_a^T (at 2×10^6 cycles), ksi
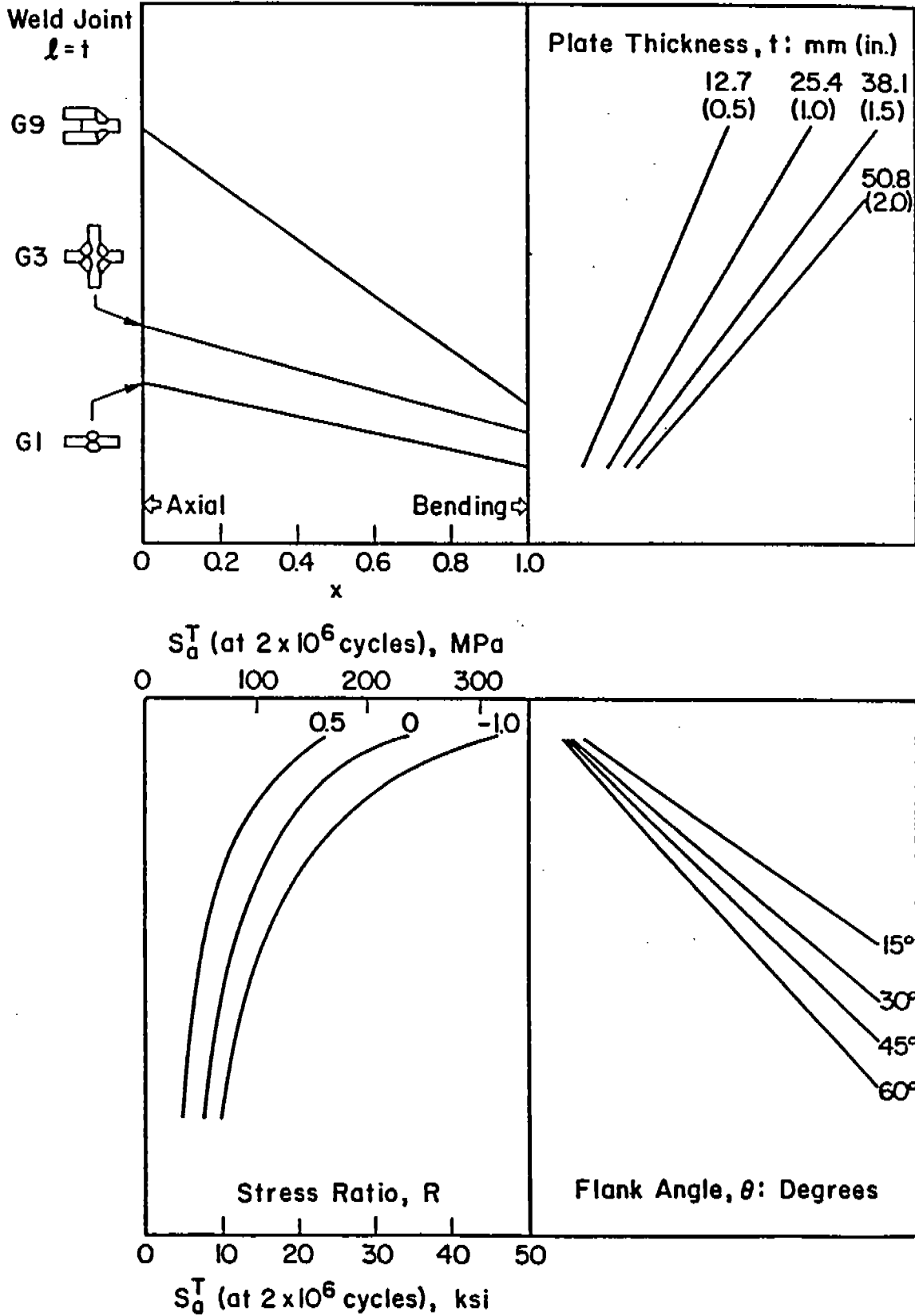
Fig. A-16 Nomograph for the fatigue design of shot-peened ASTM A36
weldments [A-5].

191
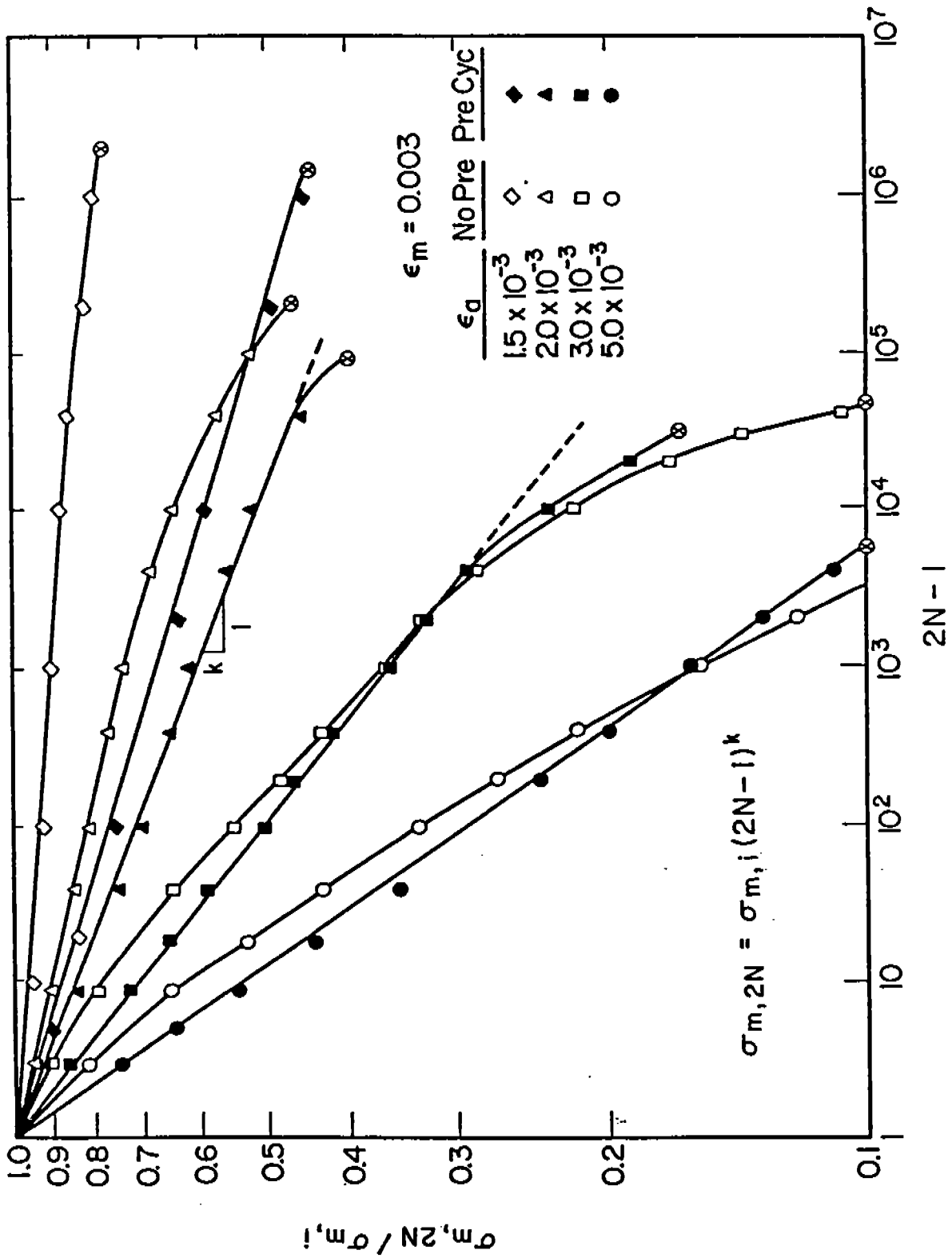
Fig. A-17 Mean stress relaxation behavior as a function of cycles [A-11].
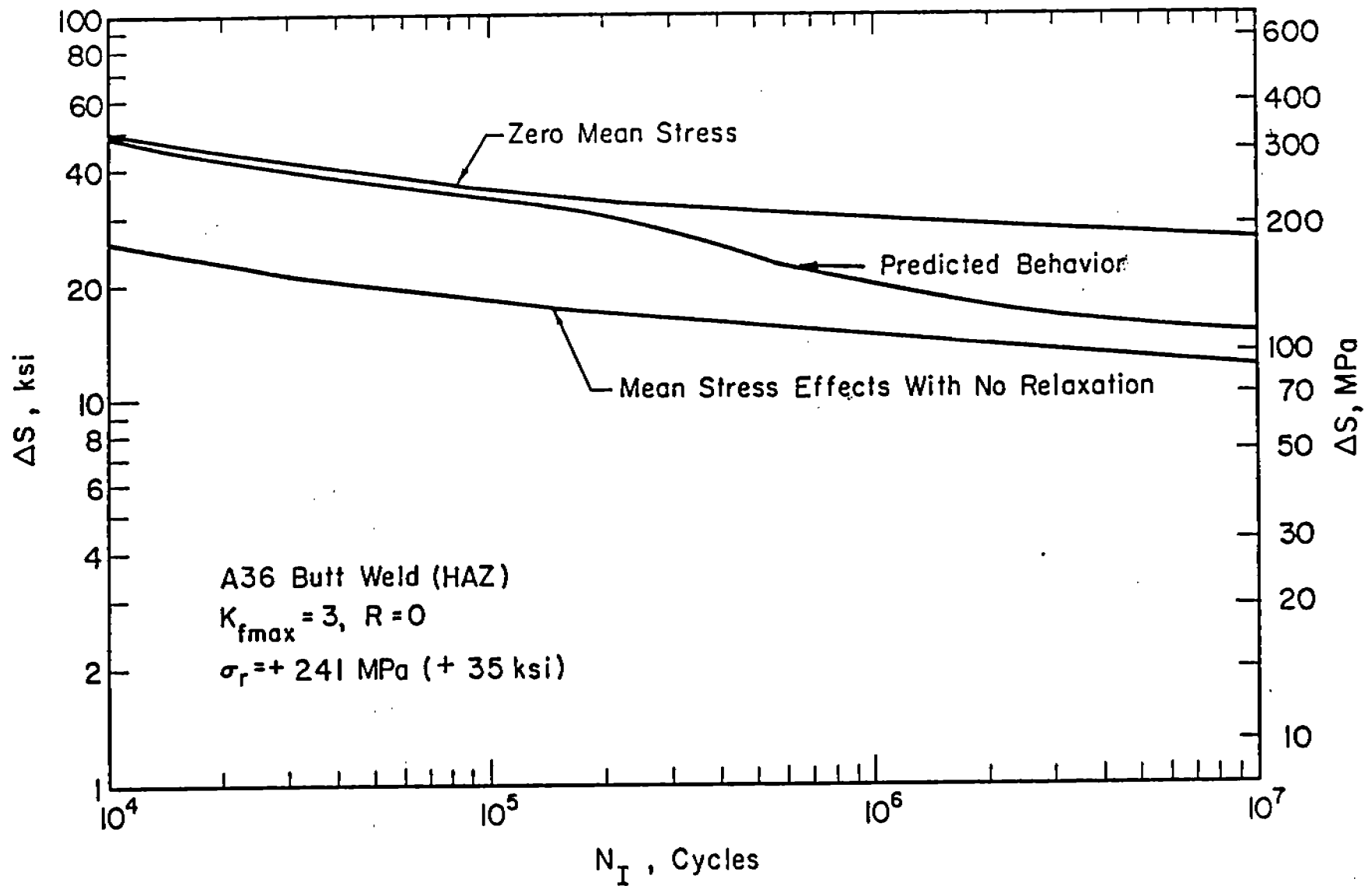
Fig. A-18 Mean stress relaxation influence on the fatigue crack initiation life [A-11].

$$\sigma_{ra}$$

$$\sigma_r(x,0) = \sigma_{ro}f(x/c)$$

$$-c \quad O \quad c \quad x$$

(A)

$$\sigma_r(x,0) = \sigma_{ro}f(x/c)$$

$$K_r = \sigma_{ro}\sqrt{\pi a}\, F(a/c)$$

$$c \quad a \quad O \quad a \quad c \quad x$$
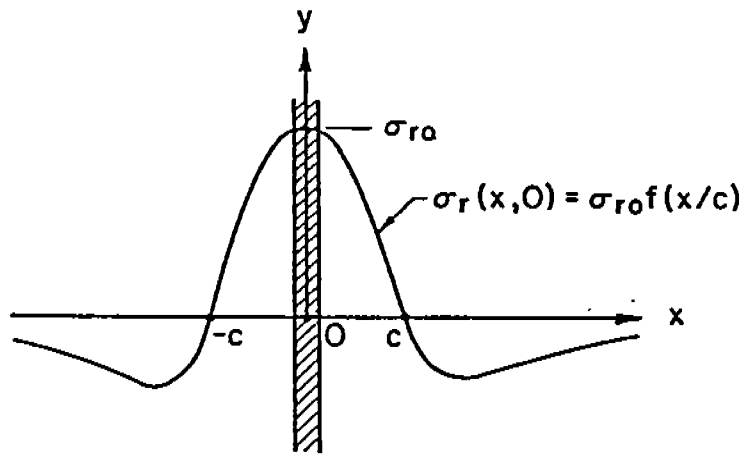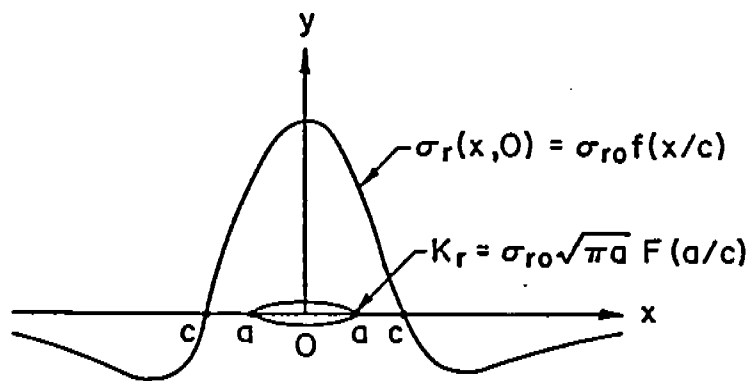
$$F(a/c) = \left\{ \frac{\left[1+(a/c)^4\right]^{1/2} - (a/c)^2}{1+(a/c)^4} \right\}^{1/2}$$

(B)

Fig. A-19 (a) Longitudinal residual stress field due to welding (hatched area: weld metal); (b) Crack in residual stress field [A-17].

194
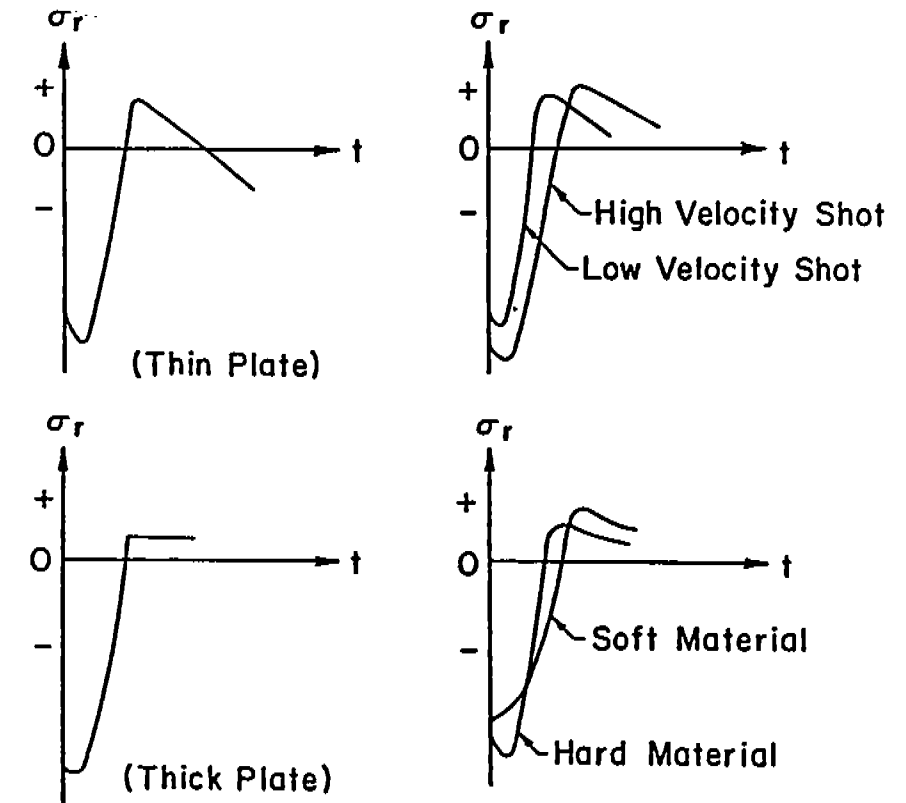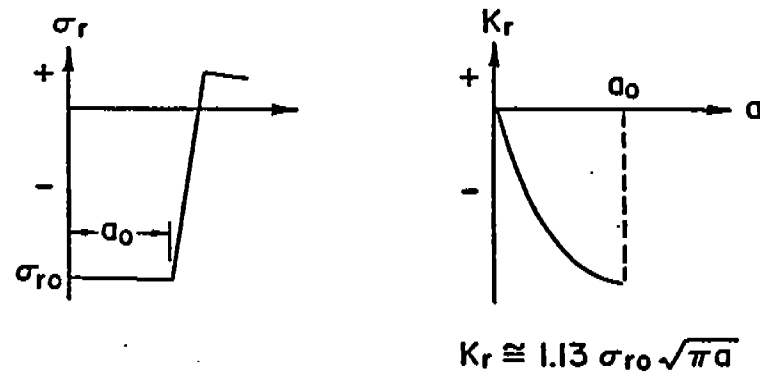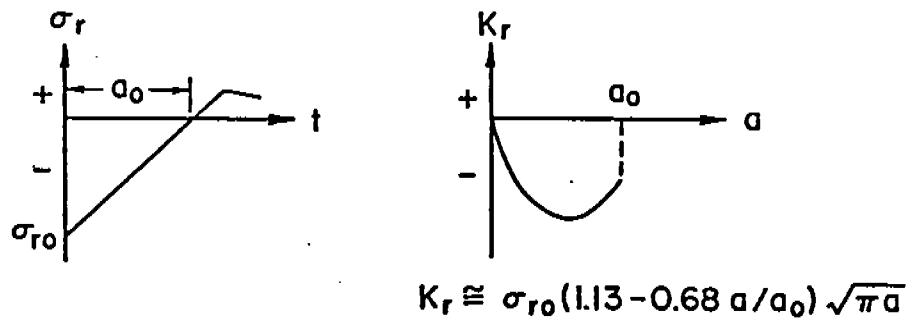
Fig. A-20 (a) Typical residual stress distributions resulting from shot
            peening [A-18]; (b) Hypothetical notch residual distribution
            and corresponding residual stress intensity factor [A-21,22].

Appendix B

DERIVATION OF THE MEAN STRESS AND THICKNESS
CORRECTIONS TO THE MUNSE FATIGUE DESIGN PROCEDURE

The Munse Fatigue Design Procedure (MFDP) estimates the permitted maximum allowable stress range from constant amplitude S-N data for the structural detail in question [1-4]:

$$\Delta S_D = \Delta S_N(\xi)(R_F) \qquad (1\text{-}2)$$

where: ΔS_D — The maximum allowable stress range permitted in the structure during its service history to avoid failure during the design lifetime N

ΔS_N — Average fatigue strength of constant amplitude test results at the design life N

ξ — Random load factor

R_F = Reliability factor

As with most other design methods, the MFDP is based solely on stress range and does not take mean stresses into account. While stress ratio is a convenient measure of mean stresses in constant amplitude testing, the only index of mean stress easily obtained or dealt with for variable load histories is the average mean stress (S_m). To include the effects of average mean stress of the variable load history (S_m), one can introduce a mean stress factor in Eq. 2-3 similar to the Morrow mean stress correction to the Basquin Eq. (Eq. A-2).

$$N = (C/\Delta S_N)^{1/m} \qquad (2\text{-}3)$$
$$\Delta S_N = C^{1/m} N^{-1/m} \qquad (B\text{-}1)$$
$$S_{Na} = \Delta S_N/2 = 1/2 C^{1/m} N^{-1/m} \qquad (B\text{-}2)$$

In a manner similar to the Basquin Equation (Eq. A-2) a mean stress correction can be introduced into Eqs. 2-3 (see Fig. B-1):

$$S_{Na} = (1/2C^{1/m} - S_m) N^{-1/m} \qquad (B\text{-}3)$$

196

$$\Delta S_{Nm} = (C^{1/m} - 2S_m) N^{-1/m} \tag{B-4}$$

$$\Delta S_N = (1 - 2S_m C^{-1/m}) C^{1/m} N^{-1/m} \tag{B-5}$$

$$\Delta S_{Dm} = \Delta S_{N(-1)} (1 - 2S_m C^{-1/m})(\xi)(R_F) \tag{B-6}$$

where: ΔS_{Dm} = The maximum allowable stress range permitted in the structure during its service history to avoid failure during the design lifetime N taking into account the average mean stress of the variable load history ($\dot{S}_m$).

$\Delta S_{N(-1)}$ = Average fatigue strength from R = -1 constant amplitude test results at the design life N.

If the average fatigue strength from baseline S-N curves having no imposed mean stress (R = -1 tests) are unavailable, $\Delta S_{N(-1)}$ can be estimated from the fatigue strength $\Delta S_{N(R)}$ obtained from constant amplitude tests at R ratios other than -1 by a similar correction written in terms of R:

$$\Delta S_{N(-1)} = \Delta S_{N(R)} \left[\frac{1}{1 - \frac{1+R}{1-R} N^{-1/m}} \right] \tag{B-7}$$

Thus the MFDP expression (Eq. 1-2) corrected for both the mean stress effects of the baseline S-N data and the average mean stress of the applied variable load history becomes:

$$\Delta S_{Dm} = \Delta S_{N(R)} \left[\frac{1}{1 - \frac{1+R}{1-R} N^{-1/m}} \right] (1 - 2S_m C^{-1/m})(\xi)(R_F) \tag{B-7}$$

If thicknesses substantially larger or smaller than those used in the baseline data tests are encountered in design, then a thickness correction similar to that of Gurney [3-6] and Smith [3-7] (Eq. 3-5) could also be incorporated:

$$\Delta S_{Dm} = \Delta S_{N(-1)} (1 - 2S_m C^{-1/m}) (t_s^n/t_2^n)(\xi)(R_F) \tag{B-9}$$

where: t_s = The standard baseline test thickness

t_2 = The size or thickness of the detail being designed

n = Exponent $\approx$ 1/4 to 1/2 (see Sect. 3.9)
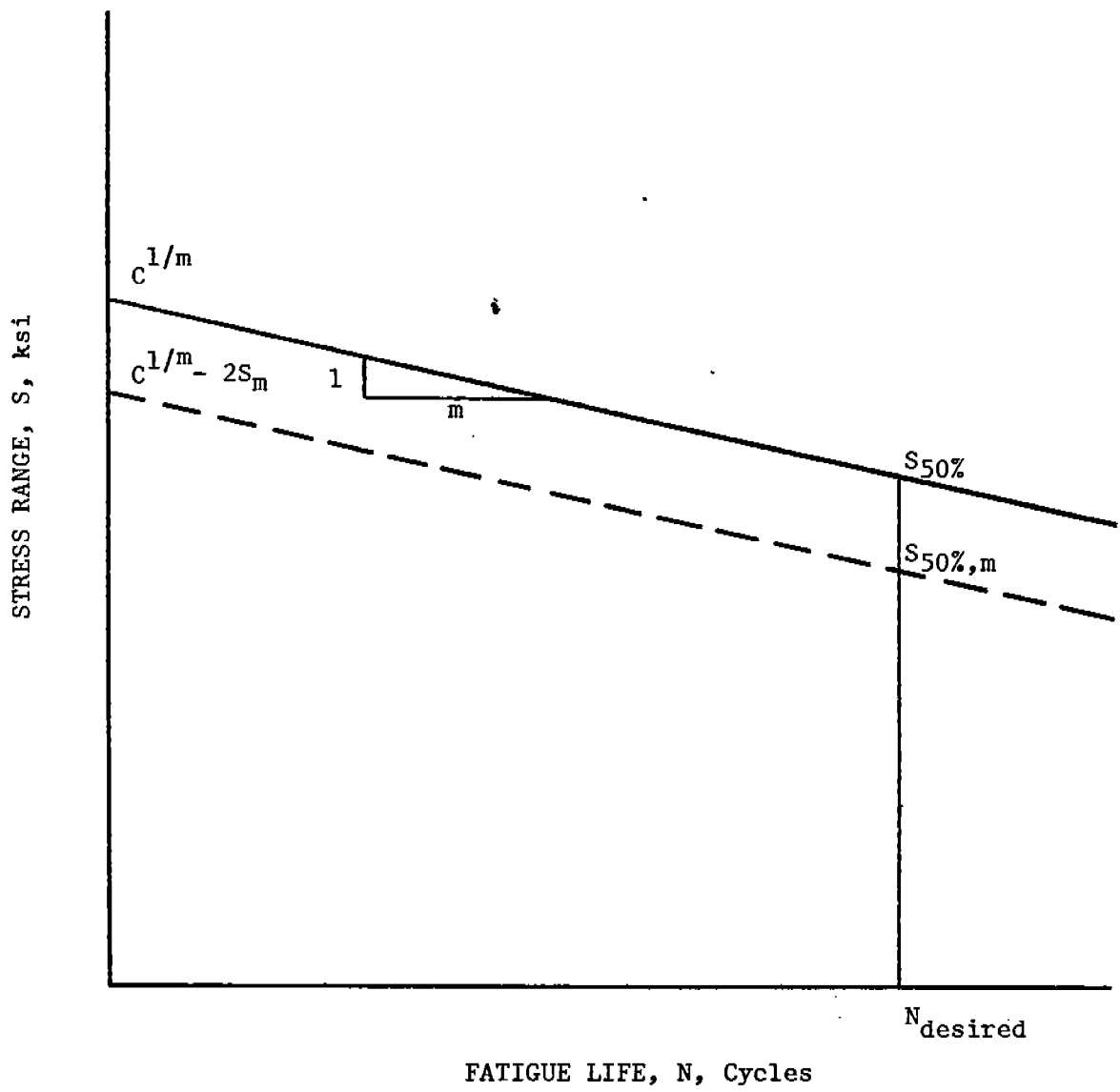
Fig. B-1 Modification of constant amplitude fatigue strength for the effects of applied mean stress.

Appendix C

SCHEMATIC DESCRIPTION OF SAE BRACKET AND
TRANSMISSION VARIABLE LOAD HISTORIES [C-1]

Appendix C Reference

C-1. Wetzel, R. M., Editor, "Fatigue Under Complex Loading: Analysis and
Experiments." Advances in Engineering, Vol. 6, SAE, 1977.
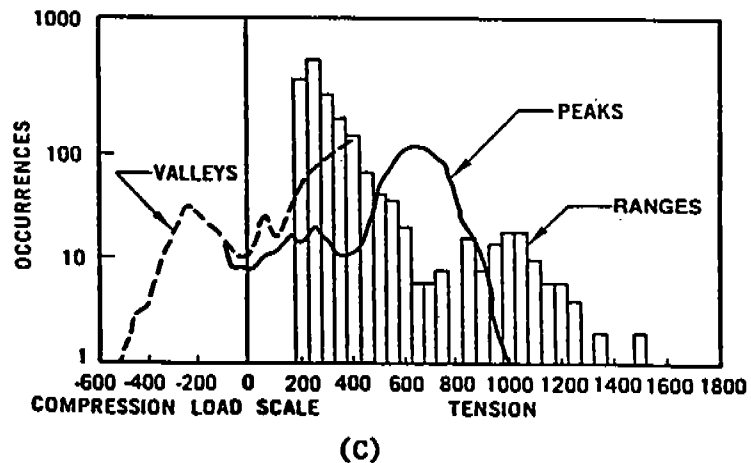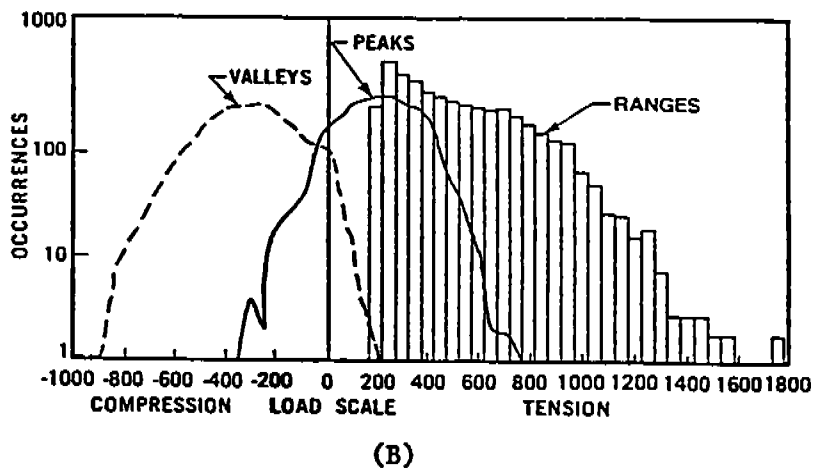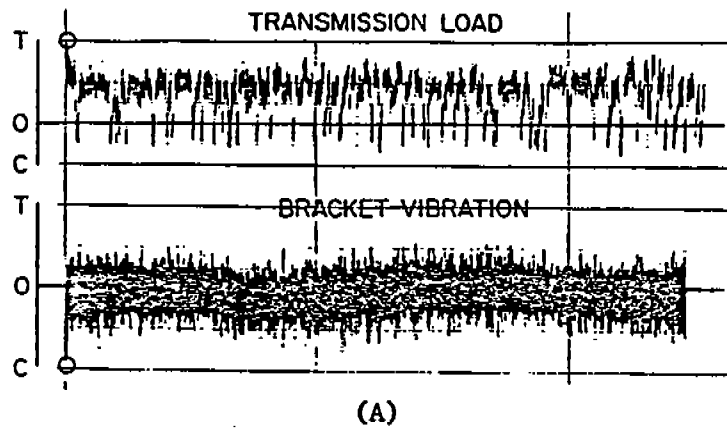
Fig. C-1 (A) Load Amplitude-Time Display of the SAE
Bracket and Transmission Histories.
(B) Bracket Histograms.
(C) Transmission Histograms [27].

201

SHIP STRUCTURE COMMITTEE PUBLICATIONS

SSC-332   Guide for Ship Structural Inspections by Nedret S. Basar & Victor W. Jovino   1985

SSC-333   Advance Methods for Ship Motion and Wave Load Prediction by William J. Walsh, Brian N. Leis, and J. Y. Yung   1989

SSC-334   Influence of Weld Porosity on the Integrity of Marine Structures by William J. Walsh , Brian N. Leis, and J. Y. Yung   1989

SSC-335   Performance of Underwater Weldments by R. J. Dexter, E. B. Norris, W. R. Schick, and P. D. Watson   1986

SSC-336   Liquid Slosh Loading in Slack Ship Tanks; Forces on Internal Structures & Pressures by N. A. Hamlin   1986

SSC-337   Part 1 - Ship Fracture Mechanisms Investigation by Karl A. Stambaugh and William A. Wood   1987

SSC-337   Part 2 - Ship Fracture Mechanisms - A Non-Expert's Guide for Inspecting and Determining the Causes of Significant Ship Fractures by Karl A. Stambaugh and William A. Wood 1987

SSC-338   Fatigue Prediction Analysis Validation from SL-7 Hatch Corner Strain Data by Jen-Wen Chiou and Yung-Kuang Chen 1985

SSC-339   Ice Loads and Ship Response to Ice - A Second Season by C. Daley, J. W. St. John, R. Brown, J. Meyer, and I. Glen 1990

SSC-340   Ice Forces and Ship Response to Ice - Consolidation Report by C. Daley, J. W. St. John, R. Brown, and I. Glen   1990

SSC-341   Global Ice Forces and Ship Response to Ice by P. Minnick, J. W. St. John, B. Cowper, and M. Edgecomb   1990

SSC-342   Global Ice Forces and Ship Response to Ice - Analysis of Ice Ramming Forces by Yung-Kuang Chen, Alfred L. Tunik, and Albert P-Y Chen   1990

SSC-343   Global Ice Forces and Ship Response to Ice - A Second Season by p. Minnick and J. W. St. John   1990

None   Ship Structure Committee Publications - A Special Bibliography   1983